

AN ABSTRACT OF THE THESIS OF

Jacob M. Hartsock for the Master of Science
in Physical Sciences presented on April 14, 2014

Title:

Evaluating the Effectiveness of Pre-remedial LNAPL Recovery Modeling using the
'LNAPL Distribution and Recovery Model' at Two Active Remediation Sites

Abstract approved: _____

Retrospective pre-remedial modeling was conducted at two active remediation sites to evaluate the effectiveness of the LNAPL Distribution and Recovery Model (LDRM) in estimating LNAPL recovery. The two research sites contain petroleum hydrocarbon contamination of shallow subsurface soils and groundwater, which has resulted in LNAPL discharge to surface water receptors and subsequent regulatory action. Vacuum-enhanced recovery, also known as multiphase extraction, has been implemented at each site to recover free-phase LNAPL (i.e., free-product) and to prevent further discharge to adjacent canals. In addition to minimal success in preventing LNAPL discharge, recoverable LNAPL volume at both sites was overestimated by an approximate order-of-magnitude. The objective of this thesis is to determine if a relatively simple analytical modeling software program, readily available at no cost, can predict accurate vacuum-enhanced LNAPL recovery volumes based on commonly available site data.

The LDRM is a semi-analytical model based on steady-state radial flow and is used to estimate LNAPL distribution and recovery for several hydraulic remediation technologies. Input parameters include maximum LNAPL thickness, fluid properties, soil capillary and petrophysical characteristics, and recovery well performance. Maximum LNAPL thickness is corrected by estimating LNAPL hydrogeologic condition using diagnostic gauge plots and hydrostratigraphs. Additional inputs are determined through site-specific data and estimated based on empirically derived values for matching fluids and soils. In order to account for potential error, an input value range was established for each LDRM parameter and designed to simulate maximum and minimum LNAPL recovery. The results of the maximum and minimum LDRM simulations were compared with actual LNAPL recovered at each research site. The results for each of the four simulations were within an error factor of five of the actual recovered LNAPL. The results indicate that the LDRM can be utilized to prevent order-of-magnitude errors in vacuum-enhanced LNAPL recovery volumes with commonly available site data.

Keywords: LNAPL Distribution and Recovery Model, LDRM, petroleum hydrocarbons, remediation, vacuum, multiphase, extraction, recovery, MPE, diagnostic gauge plots, hydrostratigraphs

**Evaluating the Effectiveness of Pre-remedial LNAPL Recovery Modeling using the
'LNAPL Distribution and Recovery Model' at Two Active Remediation Sites**

A Thesis

Presented to

The Departments of Physical Sciences

EMPORIA STATE UNIVERSITY

In Partial Fulfillment

of the Requirements for the Degree

Master of Science

By

Jacob M. Hartsock

May 2014

Thesis approved by:

Dr. Marcia Schulmeister, Committee Chair

Dr. James Aber, Committee Member

Dr. Eric Trump, Committee Member

Dr. Richard Sleezer, Department Chair

Dr. Kathy Ermler, Dean of the Graduate
School and Distance Education

DEDICATION

This work is dedicated to my wife, Sahar. Without your unquestionable support and constant encouragement, well, this would have been a hell of a lot harder.

ACKNOWLEDGEMENTS

This work could not have been completed without the generous assistance of several people. I would like to extend a special thank you to my thesis advisor, Dr. Marcia Schulmeister, for providing technical assistance, practical advice, and humor throughout the research process and my tenure at Emporia State University. Additionally, I would like to thank Dr. James Aber for serving on my thesis committee and providing insightful comments that have improved this work. As a student of both Dr. Schulmeister and Dr. Aber, I have observed the utmost expertise and professionalism in their teaching of graduate-level course work for the Earth Science Department at Emporia State University. I would also like to thank Dr. Eric Trump for taking the time to serve on my thesis committee outside of his department.

Thank you to AMEC Environment & Infrastructure, Inc. and particularly Tony Dappas for providing the resources and flexibility to conduct this research. Mr. Dappas goes above and beyond the requirements of a manager by continually imparting technical and professional wisdom, as well as fostering a work environment that is conducive to advancement and high morale.

Finally, without the constant love and support of my family, none of this could have been possible. Thank you to Mike and Terry Hartsock, Jan and Brad Fear, Jessica Larson, Karen and Ali Nimrouzi, and Jim and Cheri Powell.

TABLE OF CONTENTS

DEDICATION.....	iii
ACKNOWLEDGEMENTS.....	iv
TABLE OF CONTENTS.....	v
LIST OF TABLES.....	viii
LIST OF FIGURES.....	ix
LIST OF APPENDICES.....	xii
CHAPTER 1: INTRODUCTION.....	1
1.1 Problem Statement and Research Objectives.....	2
1.2 Background and Significance.....	5
1.2.1 Research Site Overview.....	7
CHAPTER 2: LITERATURE REVIEW.....	9
2.1 LNAPL Theories.....	9
2.1.1 Pancake Model.....	9
2.1.2 Exaggerated Thickness Model.....	10
2.1.3 Multiphase Theory.....	12
2.2 LNAPL Hydrogeologic Condition.....	15
2.2.1 Unconfined LNAPL.....	16
2.2.2 Confined LNAPL.....	17
2.2.3 Perched LNAPL.....	21
2.3 Graphical Determination of LNAPL Hydrogeologic Condition.....	22
2.3.1 Diagnostic Gauge Plots.....	22
2.3.2 Hydrostratigraphs.....	26
2.3.3 Discharge versus Drawdown Graphs.....	30
2.4 LNAPL Thickness Corrections and Volume Estimates.....	32
2.5 Hydraulic LNAPL Recovery.....	36
2.5.1 MPE Application.....	39
2.5.2 MPE Advantages.....	40
2.5.3 MPE Limitations.....	40
CHAPTER 3: THE LNAPL DISTRIBUTION AND RECOVERY MODEL.....	44
3.1 LNAPL Distribution.....	45
3.1.1 Porous Media.....	45
3.1.2 Capillary Pressure Curves.....	47
3.1.3 Permeability Models.....	49
3.1.4 Saturation and Residual Saturation.....	50
3.2 LNAPL Mobility.....	52
3.2.1 Darcy’s Law.....	53

3.3	Model Parameters	55
3.4	Model Assumptions	56
3.5	Model Interface	57
3.6	Model Output Options	59
3.6.1	Initial Output	59
3.6.2	Recovery Output	60
3.6.3	Graphical Output	61
CHAPTER 4: RESEARCH SITES		63
4.1	Site A	63
4.1.1	Geology	66
4.1.2	Nature and Extent of Contamination	67
4.1.3	Remediation System	67
4.1.4	LNAPL Estimates and Recovery	68
4.2	Site B	69
4.2.1	Geology	71
4.2.2	Nature and Extent of Contamination	71
4.2.3	Remediation System	72
4.2.4	LNAPL Estimates and Recovery	73
CHAPTER 5: LDRM METHODS		76
5.1	Input Parameter Values	76
5.1.1	Available Data	76
5.1.2	Estimated Data	77
5.1.3	Nominal Input Values	80
5.2	Sensitivity Analysis	84
5.3	Determination of Input Value Range	87
5.3.1	Maximum LNAPL Thickness	88
5.3.2	Radius of Recovery	102
5.3.3	Fluid Parameters	106
5.3.4	Capillary and Petrophysical Parameters	107
5.4	Model Calibration	111
5.5	Specific Model Simulations	112
CHAPTER 6: MODEL RESULTS		116
6.1	Nominal Results	116
6.1.1	Site A	116
6.1.2	Site B	117
6.2	Maximum Recovery Simulation	118
6.2.1	Site A	118
6.2.2	Site B	119
6.3	Minimum Recovery Simulation	120

6.3.1	Site A	120
6.3.2	Site B.....	121
6.4	Graphical Recovery Results.....	123
CHAPTER 7: ANALYSIS and DISCUSSION		124
7.1	LDRM Estimations	124
7.1.1	Site A	125
7.1.2	Site B.....	125
7.2	Error and Uncertainty	125
7.2.1	Actual Recovery Volume.....	126
7.2.2	LNAPL Hydrogeologic Condition.....	127
7.2.3	Input Values Based on Published Results.....	128
7.3	Model Limitations.....	129
7.4	Future Work	130
CHAPTER 8: SUMMARY AND CONCLUSION		131
REFERENCES		134

LIST OF TABLES

Table 1. Pre-remedial estimates and actual LNAPL recovery.....	3
Table 2. Parameters required to estimate LNAPL distribution and recovery.....	55
Table 3. Summary of available site data.....	77
Table 4. LDRM input parameters known with a high degree of accuracy.....	77
Table 5. LDRM input parameters that require estimation.....	78
Table 6. Nominal LDRM input values for Site A.....	81
Table 7. Nominal LDRM input values for Site B.....	82
Table 8. Effect of increasing nominal value by 20% on modeled LNAPL recovery.....	85
Table 9. Parameter sensitivity and relationship to recoverable LNAPL.....	86
Table 10. Uncorrected and corrected monitoring well maximum ANT.....	95
Table 11. Uncorrected and corrected recovery well maximum ANT.....	95
Table 12. Grain-size distribution from samples collected at Site B.....	109
Table 13. LDRM input values for Site A.....	113
Table 14. LDRM input values for Site B.....	114
Table 15. Nominal results for Site A.....	117
Table 16. Nominal results for Site B.....	117
Table 17. Maximum results for Site A.....	119
Table 18. Maximum results for Site B.....	119
Table 19. Minimum results for Site A.....	121
Table 20. Minimum results for Site B.....	122
Table 21. LDRM results as compared to pre-remedial estimates and actual recovery.....	124

LIST OF FIGURES

Figure 1. Sand tank experiment with downward migration and “pancake” LNAPL layer (ITRC, 2013a, modified from Schwille, 1988).....	10
Figure 2. Conceptualization of the exaggerated thickness model for a typical unconfined aquifer (Ballesteros et al., 1994).	11
Figure 3. Characteristic shark fin LNAPL saturation distribution for unconfined gasoline at vertical equilibrium (ITRC, 2013a).	12
Figure 4. Field results of Huntley et al. (1994) and modeled predictions of Lenhard and Parker (1990) (ITRC, 2013b).....	13
Figure 5. Sand tank experiment showing a soil core and monitoring well under ultraviolet light (ITRC, 2013b).	14
Figure 6. Conceptualized cross-sections displaying unconfined and confined LNAPL (Hawthorne, 2012).	18
Figure 7. Sand tank exhibiting confined LNAPL and exaggerated apparent NAPL thickness (Illangasekare, 1995).....	19
Figure 8. Photograph of fine-grained soil with matrix blocks and dendritic macropore network (Colin Johnston via ITRC, 2013a).....	20
Figure 9. Conceptualized cross-section illustrating perched LNAPL (H2A, 2011d).	21
Figure 10. Unconfined LNAPL diagnostic gauge plot trend (adapted from Hawthorne, 2012).	23
Figure 11. Confined LNAPL diagnostic gauge plot trend (adapted from Hawthorne, 2012).	23
Figure 12. Perched LNAPL diagnostic gauge plot trend in an example setting composed of slag and sand (Hawthorne et al., 2011).	24
Figure 13. Theoretical basis for diagnostic gauge plot trends (H2A, 2011b).....	25
Figure 14. Hydrostratigraph exhibiting unconfined LNAPL at Site B.	26
Figure 15. Hydrostratigraph exhibiting confined and perched LNAPL at Site A.	28
Figure 16. Hydrostratigraph exhibiting confined LNAPL at Site B.	29
Figure 17. Discharge versus drawdown graphs for unconfined and confined LNAPL (Muthu and Hawthorne, 2013).....	31
Figure 18. Diagnostic gauge plot exhibiting perched LNAPL (Kirkman et al., 2012).	33
Figure 19. Corresponding discharge versus drawdown graph for conditions discussed in Figure 18 (Kirkman et al., 2012).	33
Figure 20. Cross-section depicting “true LNAPL thickness” for confined LNAPL (H2A, 2011a).	35
Figure 21. LNAPL specific volume (adapted from ITRC, 2013a).	35

Figure 22. Diagrammatic depiction of vacuum influence on an aquifer (Charbeneau, 2007a).	38
Figure 23. Recovery well construction diagram for a standard vacuum-enhanced well (adapted from EPA, 1999).	38
Figure 24. Typical recovery trend for hydraulic recovery of LNAPL (ITRC, 2013b).	43
Figure 25. LNAPL recovery trend for Site A (AMEC 2013).	43
Figure 26. Wetting and non-wetting phase contact angle (Charbeneau, 2007a).	46
Figure 27. Pore-scale photo of wetting and non-wetting fluids (ITRC, 2013a).	46
Figure 28. Lab produced capillary pressure curve showing the drainage and imbibitions curves (Charbeneau, 2007a).	49
Figure 29. Residual LNAPL saturation as a function of pore size (Charbeneau, 2007a)	51
Figure 30. Characteristic LNAPL saturation distribution curve depicting residual and recoverable LNAPL (ITRC, 2013b).	52
Figure 31. Illustration of LNAPL entering adjacent pore (adapted from ITRC, 2013b).	53
Figure 32. Project Setup window for the LDRM.	57
Figure 33. Primary “Data Input” window for the LDRM.	58
Figure 34. Well Recovery Systems window.	58
Figure 35. Initial output window.	59
Figure 36. Advanced LDRM recovery output window.	60
Figure 37. LDRM graphical output: specific volume, recovery, transmissivity.	61
Figure 38. LDRM graphical output: saturation profiles.	62
Figure 39. LDRM graphical output: LNAPL recovery rate.	62
Figure 40. Site A remediation area.	65
Figure 41. Site B site map.	70
Figure 42. Site B LNAPL recovery rate from June 2001 to January 2014.	73
Figure 43. Site A maximum LNAPL thickness plume map with (a) uncorrected and (b) corrected maximum apparent NAPL thickness.	89
Figure 44. Representative diagnostic gauge plot at Site A exhibiting confined LNAPL trend.	91
Figure 45. Representative diagnostic gauge plot at Site A exhibiting perched LNAPL trend.	91
Figure 46. Hydrostratigraph for confined LNAPL at Site A.	93
Figure 47. Hydrostratigraph for perched LNAPL at Site A.	93
Figure 48. Plume map of monitoring well maximum apparent NAPL thickness at Site B.	96

Figure 49. Characteristic diagnostic gauge plot at Site B exhibiting unconfined LNAPL trend	97
Figure 50. Characteristic hydrostratigraph at Site B exhibiting unconfined LNAPL trend. ..	98
Figure 51. Diagnostic gauge plot exhibiting confined LNAPL trend at Site B.....	100
Figure 52. Hydrostratigraph exhibiting confined LNAPL at Site B.....	100
Figure 53. Hydrostratigraph exhibiting perched LNAPL trend at Site B.....	101
Figure 54. Diagnostic gauge plot exhibiting perched LNAPL at Site B.	101
Figure 55. Water table map displaying 1-foot contour intervals for Site A.	104
Figure 56. Water table map for Site A during vacuum operation.....	105
Figure 57. API Parameter Database summary for well-graded sand sample #162.	110
Figure 58. Graphical recovery results for Site A.	123
Figure 59. Graphical recovery results for Site B.	123

LIST OF APPENDICES

Appendix A. Monitoring and Recovery Well Location Maps.....	143
Appendix B. Diagnostic Gauge Plots	147
Appendix C. Hydrostratigraphs	160
Appendix D. Soil Boring Logs and Grain-size Data	172

CHAPTER 1: INTRODUCTION

Petroleum hydrocarbon contamination in subsurface soils and groundwater poses a major environmental and human health concern. Certain petroleum hydrocarbons are classified as Light Non-Aqueous Phase Liquids (LNAPL), which are less dense and generally immiscible with water. Despite low solubility, certain constituents of LNAPL, many of which are known carcinogens, are capable of dissolving into groundwater and volatilizing within the vadose zone. An estimated 200,000 known LNAPL-contaminated sites existed in the United States in 1999 (EPA, 1999). A 2004 EPA report estimated that up to 350,000 sites contaminated with petroleum products and other hazardous waste would require cleanup over the next 30 years (EPA, 2004).

Operations that utilize or produce petroleum products are frequently located near waterways as a means of shipping and receiving petroleum product. This proximity to waterways poses a unique hazard since regional groundwater flow is commonly toward surface water receptors. LNAPL subsurface contamination ultimately migrates in the direction of regional groundwater flow. Migrating LNAPL is known to discharge into surface water receptors in both free (i.e., LNAPL) and dissolved phases. Additionally, vapor phase discharge of volatilized LNAPL is known to migrate through the vadose zone and into subsurface structures and buildings (Huntley and Becket, 2002). This not only poses a serious risk to human health and aquatic ecology, but can also create major financial liability through exorbitant regulatory fines and costly remediation efforts.

Vacuum-enhanced hydraulic recovery is a commonly used technology for LNAPL remediation. Vacuum-enhanced recovery, which is also referred to as multiphase extraction (MPE), simultaneously removes soil vapor, groundwater, and NAPL (EPA,

1999). MPE systems utilize negative pressures at extraction points to recover impacted groundwater and LNAPL, and are frequently designed and implemented under generalized site assumptions with limited preliminary modeling. The resulting implications for remediation systems are often overstated capabilities leading to prolonged recovery efforts with exacerbated financial and regulatory burdens. Limited financial resources and restrictive project deadlines can limit the subsurface investigations necessary to develop accurate plume models and recovery estimates. Comprehensive data sets allow for the development of a more accurate understanding of site-wide processes. However, this does not guarantee accurate models and realistic LNAPL recovery estimates. Complex numerical models, which typically require extensive data and specialized users, are exceedingly expensive, time consuming, and not always more accurate than simpler modeling techniques.

1.1 PROBLEM STATEMENT AND RESEARCH OBJECTIVES

The objective of this thesis is to determine if a relatively simple analytical modeling software program, readily available at no cost, can predict accurate LNAPL recovery volumes based on commonly available site data. In order to achieve this objective, the following hypothesis is being tested: *The 'LNAPL Distribution and Recovery Model' (LDRM) can be implemented retrospectively at two active remediation sites to estimate recoverable LNAPL volume.*

Basic site assumptions and a misunderstanding of contemporary LNAPL theory have resulted in approximate order-of-magnitude errors in pre-remedial recoverable LNAPL when compared to actual recovery at the two research sites. Previous LDRM studies, such as Kahraman (2013), have utilized more advanced data sets to analyze LNAPL

recovery for water-enhanced LNAPL recovery. The objective of this thesis is to determine the accuracy of LDRM results for vacuum-enhanced LNAPL recovery with site data that is generally limited to monitoring well gauging, soil boring logs, and basic recovery observations. Thus, the LDRM as a viable indicator of LNAPL extent and potential vacuum-enhanced recovery in light of realistic financial and site data limitations is investigated. Regardless, the underperformance of MPE systems at the two research sites provides the initiating basis for this research. Therefore, while focusing on the efficacy of the LDRM, this research intends to highlight the issues facing vacuum-enhanced hydraulic recovery of LNAPL from varying soil conditions near surface water receptors.

To test the hypothesis that the LDRM can be used as a predictive tool, site data are analyzed from the two research sites that have experienced approximate order-of-magnitude errors in recoverable LNAPL. Historical site data are used to estimate LNAPL hydrogeologic conditions (i.e., unconfined, confined, perched) and to determine LDRM input parameter values. The hypothesis is tested by comparing the actual recovered LNAPL, as reported in Table 1, to the modeled recoverable LNAPL. The hypothesis will be supported if modeled recoverable LNAPL is within pre-remedial estimates by a maximum factor of five.

TABLE 1. PRE-REMEDIAL ESTIMATES AND ACTUAL LNAPL RECOVERY

Research Site	LNAPL Recovery	
	Pre-remedial Estimate	Actual
Site A	15,000 gal	1,500 gal
Site B	123,000 gal	15,000 gal

While the LDRM is a semi-analytical model based on several underlying assumptions, it has been demonstrated to reliably estimate LNAPL recovery within an order-of-magnitude (Charbeneau and Adamski, 2008a). Furthermore, experienced application using sufficient data and good judgment frequently results in recovered LNAPL volumes within a factor of two or three of modeled estimates (Charbeneau and Adamski, 2008a). The rationale for choosing a factor of five as a metric for testing the hypothesis is a result of realistic LDRM capabilities, site-specific conditions, and general regulatory requirements. Order-of-magnitude estimates are not within an acceptable range of accuracy for many LNAPL recovery operations. For example, 150,000 gallons of recoverable LNAPL at a site would likely result in significantly different management strategies than 15,000 gallons of recoverable LNAPL. This is particularly relevant within current regulatory framework that promotes the vague notion of free-product removal to the maximum extent practicable (Huntley and Beckett, 2002). If the removal of 150,000 gallons is deemed practicable and there are only 15,000 gallons of recoverable LNAPL present, regulatory site closure is not feasible. Alternatively, a factor of two represents a best case modeling scenario with sufficient site data and expert knowledge of the LDRM. Therefore, a factor of five represents a middle ground that assumes basic site data and a limited means for advanced model calibration, of which both conditions are consistent with the two research sites and many other LNAPL sites.

It is important to note that, independent of confirming the hypothesis, the LDRM results within this thesis speak only to the methodology as applied to the research sites. There is inherent uncertainty in any model, and the LDRM is no exception, particularly with the nature of its purpose within this research, which is to provide accurate recovery

estimations in lieu of extensive site data and expensive or complex numerical models.

The stated hypothesis is meant to provide a quantitative basis for comparison only. The actual accuracy of the LDRM ultimately lies within a range of probabilities derived from replicated use under relatively controlled conditions.

1.2 BACKGROUND AND SIGNIFICANCE

Attempting to estimate the volume of total free LNAPL (i.e., mobile free-product) or recoverable LNAPL (i.e., mobile, but specific to one or more recovery wells) at a site without the context of contemporary LNAPL theory or understanding LNAPL hydrogeologic conditions can result in significant remediation system underperformance. For example, out-dated LNAPL theories postulated that subsequent to downward vertical migration under gravitational forces, an oil release would form a nearly 100% saturated oil layer on the water table. In this scenario, measured or gauged oil thickness in a monitoring well – henceforth known as apparent NAPL thickness (ANT) – corresponds directly to the oil in the surrounding formation. Total free LNAPL was then calculated by integrating ANT across the surface area of a monitoring well network while factoring effective porosity. However, contemporary LNAPL theory has thoroughly validated that maximum LNAPL saturations rarely exceed 70%, let alone come close to 100%. Using this specific difference between past and present LNAPL theory alone – there are many more – it is apparent that assuming 100% oil saturation will greatly overestimate free-product and hence, recoverable LNAPL.

Another former theory postulated that once a downward migrating LNAPL mass reaches the capillary fringe, it is prevented from further downward movement. Therefore, if a monitoring well was screened across this interval, it would act as conduit and fill with

LNAPL at an interval well below the capillary fringe and water table. As a result, this theory asserted a 75 to 90% reduction in the formation oil thickness relative to ANT. For example, if the ANT in a monitoring well was observed to be 10 feet, then it could be reasonably assumed that the formation NAPL thickness (FNT) was 1.0 to 2.5 feet thick. This method is known for underestimating total free-product across a site when the “corrected” ANT (e.g., $ANT \times 0.1$) is integrated across a monitoring well network.

Contemporary LNAPL theory – multiphase theory – accounts for a vertical LNAPL saturation distribution that peaks well below 100% and is often observed to extend beneath the groundwater surface. Additional relatively new concepts within multiphase theory, such as LNAPL hydrogeologic condition (i.e., unconfined, confined, perched), have shown to factor greatly in estimating free and recoverable product. For instance, historical assumptions viewed LNAPL within an unconfined sand aquifer to be unconfined as well. However, it is frequently observed that LNAPL in unconfined aquifers is actually confined or perched, of which both conditions are capable of greatly exaggerating ANT relative to FNT. This introduces the important concept of factoring ANT for estimations only under unconfined conditions at vertical equilibrium. Or alternatively, the presence of confined and perched LNAPL requires a correction to redefine the saturation distribution and mobile LNAPL interval. These concepts are described in further detail throughout subsequent sections.

While this research focuses on issues related to incorrect LNAPL assumptions emphasized above, the primary objective is to determine – or corroborate – the accuracy of the LDRM in estimating recoverable LNAPL for vacuum-enhanced systems. In addition to being a free and relatively simple analytical model with a user-friendly,

Windows interface, the LDRM is based on the most up-to-date concepts of LNAPL theory. For these reasons, the model has been chosen to evaluate the approximate order-of-magnitude errors in recoverable LNAPL at the research sites. If the hypothesis is supported, it provides evidence that the LDRM has the potential to serve as an effective tool in developing accurate conceptual site models and ultimately, successful LNAPL recovery operations.

1.2.1 Research Site Overview

The two research sites being studied are both undergoing vacuum-enhanced hydraulic recovery of LNAPL, also known as multiphase extraction (MPE). Site A is an active railroad maintenance yard that has undergone the MPE of diesel fuel since January 2009. Site B is an active bulk oil storage facility that has undergone the MPE of diesel fuel and gasoline since June 2001. The sites are located within approximately 25 miles of each other in a Midwestern urban center and both sites are bound to shipping canals by vertical steel sheet pilings. This setting poses a unique remediation challenge since the aquifer surface at both sites is situated approximately 8 to 12 feet above the canal surface, resulting in steep hydraulic gradients at both locations. The remediation concern stems from the fact that, while LNAPL recovery at both sites has been asymptotically low (i.e., essentially zero) for several years, both sites continue to experience regular oily sheen within sorbent boom containment areas on respective canals, albeit in significantly less frequency and extent than pre-remedial levels. This may be a direct result of the steep gradients along the canals inducing LNAPL migration, and may also indicate that the MPE is providing insufficient hydraulic control of migrating LNAPL. Despite similar hydraulic conditions and remediation technologies, the sites differ in their subsurface

features. Site A consists of extremely heterogeneous fill, underlain by silty clay, while Site B consists of sandy fill, underlain by relatively homogenous well-graded sand. It is an intention of this research to illustrate the possible differences in model outcomes at two geologically different sites. The research sites are discussed in further detail throughout Chapter 4. Detailed site figures including monitoring and recovery well designations and locations are presented in Appendix A.

CHAPTER 2: LITERATURE REVIEW

This chapter provides an overview of historical and current LNAPL theories, the importance of identifying LNAPL hydrogeologic conditions, and introduces methods of hydraulic recovery of LNAPL. The most recent and most valid LNAPL theory, which has been referred to as multiphase theory (Farr et al., 1990; Lenhard and Parker, 1990; Beckett and Lundegard, 1997; Charbeneau, 2007a) and the vertical equilibrium model (Kirkman et al., 2012), has been tested through numerous field and laboratory studies. Recent advancements in subsurface site characterization, including geotechnical engineering techniques with sensor attachments such as direct-push cone penetration testing with laser-induced fluorescence, have added further evidence in support of multiphase theory (EPA, 2005). Understanding the concepts of multiphase theory is necessary to accurately characterize a site with LNAPL contamination.

2.1 LNAPL THEORIES

2.1.1 Pancake Model

Early theories postulated that an LNAPL mass released into subsurface soil would migrate vertically under the force of gravity until reaching the water table. If sufficient volume reached the water table, the LNAPL would form a “pancake” and spread laterally above the saturated zone. The pancake model assumed a nearly 100% oil-saturated layer in the formation that corresponded directly with apparent NAPL thickness (ANT) in a monitoring well (Gruszczenski, 1987; Munzar, 2009). Conceptualizations of these theories gave rise to the “pancake model,” since LNAPL was thought to spread and form a pancake once it reached the water table, and in later theories the capillary fringe. Since the LNAPL floating on the water table and capillary fringe was viewed as an

interconnected uniform mass, it was thought that LNAPL pore saturations neared 100%. Figure 1 displays time-series photographs for a downward migrating LNAPL mass in a sand tank. Based on this perspective, it appears that the LNAPL mass forms a nearly saturated, uniform layer on the water table.

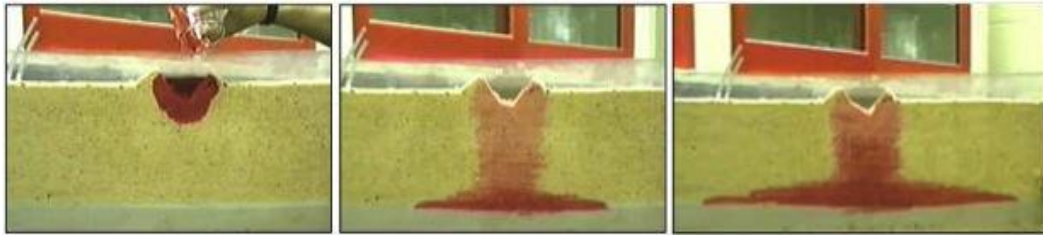


Figure 1. Sand tank experiment with downward migration and “pancake” LNAPL layer (ITRC, 2013a, modified from Schwille, 1988).

Gruszczenski (1987) developed two type curves intended to indicate the relationship between ANT and FNT. The type curves were based on hydrocarbon baildown tests conducted in monitoring wells. One type curve indicated a 1:1 ratio of ANT to FNT; the other type curve suggested a 75 to 90% reduction of the FNT relative to the ANT. Gruszczenski observed that upon bailing the hydrocarbon, the oil-water interface would rise to a particular level before declining due to the originally displaced LNAPL flowing back into the well. This level became known as an inflection point that supposedly represented the “true” hydrocarbon thickness in the formation, for which the type curves were based. However, as noted by Huntley (2000), Gruszczenski’s inflection point and “true” hydrocarbon thickness were without theoretical or physical basis.

2.1.2 Exaggerated Thickness Model

As discussed by Beckett and Lundegard (1997), later versions of the pancake model came to be known as the “exaggerated thickness” model. This model stated that an

LNAPL layer would sit on the capillary fringe and described a situation whereby a monitoring well would act as a giant soil pore with lower capillary pressure than the surrounding formation, inducing LNAPL migration into the monitoring well. Ballesteros et al. (1994) stated that the “apparent free-product thickness indicated in a standard monitoring well is typically much greater than the actual free-product thickness in the surrounding soil.” In Figure 2, where t is the ANT and t_a is the FNT, the monitoring well acts as a conduit for the LNAPL layer vertically restricted by the capillary fringe. However, this model does not account for density differences and the LNAPL mass displacing water throughout the capillary fringe and water table, such a condition is analogous to an iceberg being 90% submerged below the ocean surface (Beckett and Lundegard, 1997).

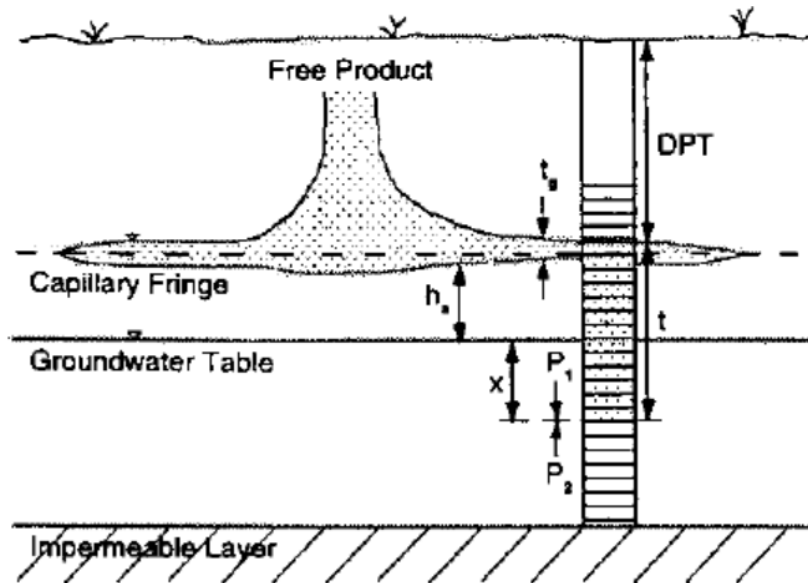


Figure 2. Conceptualization of the exaggerated thickness model for a typical unconfined aquifer (Ballesteros et al., 1994).

2.1.3 Multiphase Theory

Similar and nearly simultaneous papers by Lenhard and Parker (1990) and Farr et al. (1990) described conditions whereby air, water, and LNAPL exist in the capillary fringe, at the water table, and to varying degrees within the saturated zone (Adamski et al., 2005). This more recent theory, which accounts for multiple phases, not only contradicted the so-called pancake model, but also described an LNAPL saturation distribution that was a function of capillary pressure and fluid properties. In multiphase theory under unconfined conditions at vertical equilibrium, LNAPL, air, and water coexist in a vertical soil profile to varying degrees such that LNAPL saturation increases with depth in the capillary fringe, peaks well below 100% at the water table, and decreases again in the saturated zone (Charbeneau, 2007a). This observation has given rise to the characteristic “shark fin” curve of LNAPL saturation with depth (Farr et al., 1990; Lenhard and Parker, 1990; Adamski et al., 2005; ITRC, 2013a). Figure 3 illustrates the gasoline pore-saturation differences between the pancake model and the updated multiphase theory at vertical equilibrium.

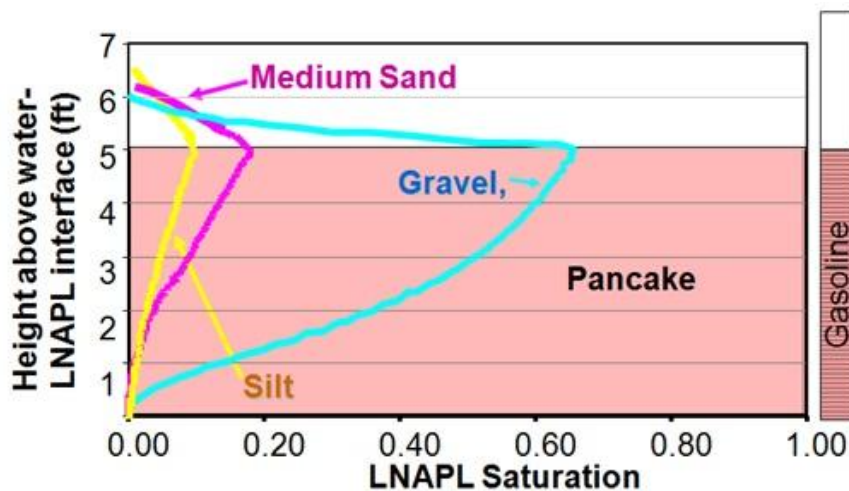


Figure 3. Characteristic shark fin LNAPL saturation distribution for unconfined gasoline at vertical equilibrium (ITRC, 2013a).

Among the wide-ranging significance of the original papers by Lenhard and Parker (1990) and Farr et al. (1990) was the idea that maximum LNAPL saturations rarely ever approached 100%. Both papers demonstrated, as stated in Lenhard and Parker 1990, that “oil-saturated pancakes do not develop in the vast majority of soils and aquifers” (p. 57). Huntley et al. (1994) established a strong agreement between field measurements and the predictions established by Lenhard and Parker (1990), as illustrated in Figure 4. These findings have been replicated in numerous field and laboratory studies since the two papers in 1990, highlighting that LNAPL does not exist as a single coherent mass, but rather as a saturation distribution of coexisting phases of air, water and LNAPL.

Figure 5 is a sand tank monitoring well and a soil core under ultraviolet light. The LNAPL appears yellowish-green and generally follows the predicted saturation distribution. The orange arrows indicate relative LNAPL conductivity suggesting a positive relationship with LNAPL saturation.

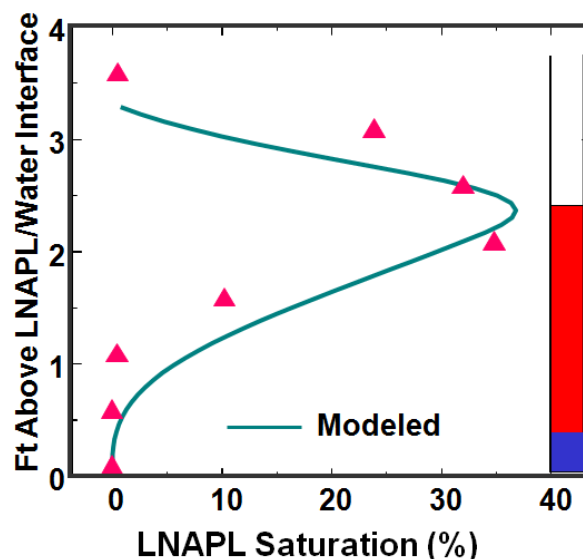


Figure 4. Field results of Huntley et al. (1994) and modeled predictions of Lenhard and Parker (1990) (ITRC, 2013b).

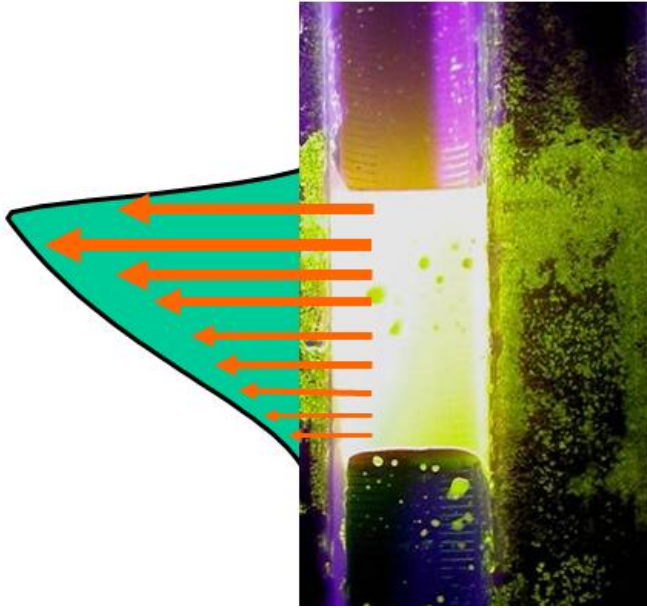


Figure 5. Sand tank experiment showing a soil core and monitoring well under ultraviolet light (ITRC, 2013b).

An analysis of 212 LNAPL-impacted soils resulted in maximum LNAPL saturation of 2 to 5% for fine-grained soils, and 10 to 56% for coarse-grained soils (RTDF, 2006). The ITRC (2013a) indicates that maximum LNAPL saturation in sand is typically 5 to 30%. Multiphase theory incorporates these much lower field saturations while using soil and fluid characteristics as the basis for capillary pressure curves, which are introduced in Chapter 3. The primary implication in multiphase theory is that an LNAPL mass is less recoverable than in previous theories, since recoverability is a function of saturation, indicating conversely that the volume of contaminated soil is typically greater than previously thought (Beckett and Lundegard, 1997).

2.2 LNAPL HYDROGEOLOGIC CONDITION

The LNAPL hydrogeologic condition in unconfined aquifers is frequently assumed to be unconfined. However, localized confined and perched LNAPL is now thought to be present in unconfined aquifers at much greater rates than previous LNAPL theories suggested (Charbeneau and Adamski, 2008a). These conditions are the result of subsurface heterogeneities such as a layer of dense fine-grained sand underlain by medium- to coarse-grained sand.

Charbeneau and Adamski (2008b) estimate that 30-50% of LNAPL sites contain confined LNAPL. Furthermore, while gauged LNAPL thicknesses in unconfined conditions at vertical equilibrium approximate the formation LNAPL thickness, gauged thicknesses of confined and perched LNAPL can greatly exaggerate formation LNAPL thickness (H2A, 2011a; ITRC, 2013a). This not only has the potential to overestimate recoverable LNAPL, but also has significant regulatory consequences since relatively low saturations of LNAPL can result in exaggerated gauged LNAPL thicknesses, possibly initiating regulatory action or preventing site closure.

A key factor in the identification of an exaggerated apparent NAPL thickness (ANT) is the hydrogeologic condition of LNAPL in the adjacent formation as unconfined, confined, or perched. Generally speaking, ANT for unconfined LNAPL at vertical equilibrium will approximate the surrounding formation NAPL thickness (FNT). However, uncertain LNAPL hydrogeologic conditions and transient groundwater elevations have significant consequences since the resulting ANT likely does not represent FNT. Without an accurate determination of FNT, recoverable LNAPL estimations are inherently inaccurate.

The concept of a formation NAPL thickness is somewhat misleading since multiphase theory describes a vertical LNAPL saturation distribution. Therefore, FNT actually refers to the vertical interval of the LNAPL saturation distribution. However, LNAPL specific volume, which is the vertically distributed LNAPL volume per unit planimetric area, can be thought of as a corrected FNT. If integrated across the area of a site from several monitoring wells, LNAPL specific volume can be used to estimate recoverable and total LNAPL volume.

2.2.1 Unconfined LNAPL

The idea of an exaggerated LNAPL thickness is erroneous when the formation is at vertical equilibrium (Huntley and Beckett, 2002). ANT for unconfined LNAPL will approximate the FNT under such conditions. The resulting saturation distribution for unconfined ANT at vertical equilibrium will exhibit the characteristic shark fin distribution curve, as indicated by Figures 3, 4, and 5. However, ANT in unconfined conditions is typically inversely proportional to the potentiometric surface elevation (Adamski et al., 2005). A rapidly rising water table causes LNAPL to become submerged and trapped in the saturated zone, which is reflected in a corresponding decrease in ANT. Conversely, the remobilization and migration of previously trapped LNAPL can occur as a result of a falling water table (Beckett and Lundegard, 1997; ITRC, 2013a). This process results in what is known as an LNAPL smear zone, which is the vertical extent of LNAPL distribution that frequently correlates with the interval of historical groundwater fluctuations (EPA, 2005; ITRC, 2013a). This has consequences for predicting recoverable product since most aquifers experience regular groundwater elevation fluctuations. If free-product volume is calculated by the areal integration of ANT across

a monitoring well network, non-vertical equilibrium conditions can result in extensive errors in LNAPL volume and recoverability.

2.2.2 Confined LNAPL

While groundwater becomes confined due to a confining layer with low vertical hydraulic conductivity that limits the flow of all liquids, LNAPL is classified as confined when the pore entry pressure of the overlying layer is higher than the LNAPL capillary pressure (H2A, 2011c). Since LNAPL typically exists in soils as the non-wetting fluid, confined LNAPL is a capillary limitation that generally does not inhibit the flow of groundwater (H2A, 2011c). The presence of confined LNAPL is not concurrent with confined groundwater and often results from minor soil heterogeneities in unconfined aquifers.

In contrast to unconfined LNAPL, confined LNAPL will rise in a monitoring well in proportion to the potentiometric surface elevation. Adamski et al. (2005) explained that since no new LNAPL is being added or removed from the system, conservation of mass in this scenario is achieved with bottom filling of the monitoring well by LNAPL. Since confined LNAPL is under pressure, a monitoring well that is screened across the LNAPL interval will act as a “pressure relief valve” (H2A, 2011c). The degree to which LNAPL will rise in a well is proportional to the potentiometric surface, or pressure head, in the confined LNAPL layer. Confined LNAPL conditions have been known to exaggerate ANT in a monitoring well by several to tens of feet relative to FNT (H2A, 2011c). Figure 6 illustrates ANT for unconfined LNAPL at vertical equilibrium and for confined LNAPL exhibiting bottom filling of the well.

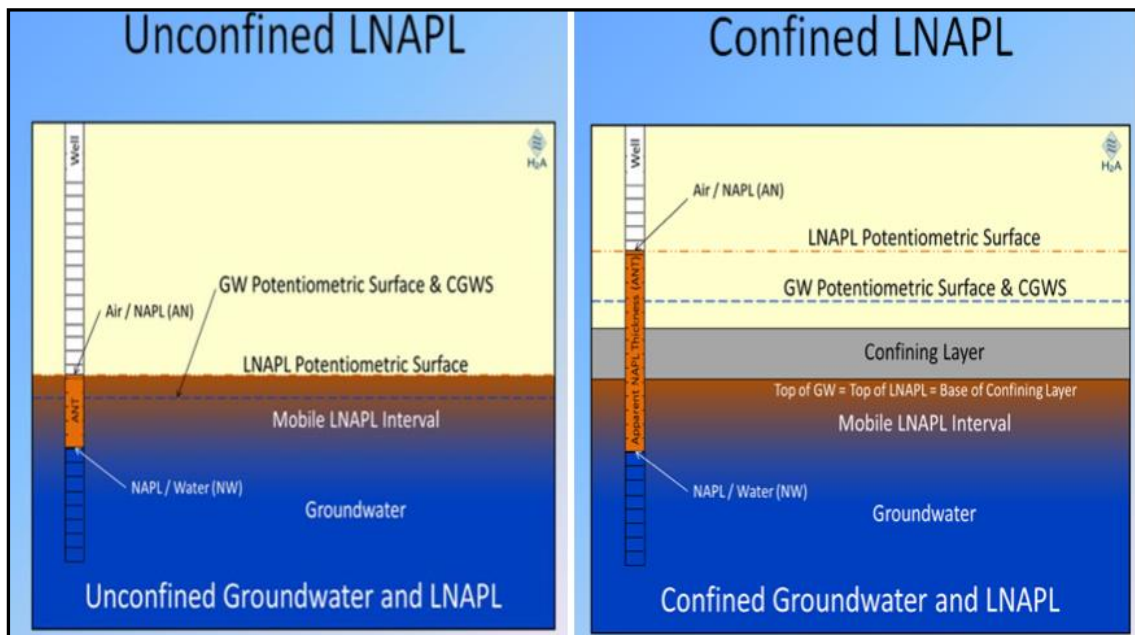


Figure 6. Conceptualized cross-sections displaying unconfined and confined LNAPL (Hawthorne, 2012).

It is important to note the distinction between confined LNAPL from soil heterogeneities and LNAPL that is trapped below the groundwater table. Adamski et al. (2005) investigated several instances of LNAPL migrating several meters below the groundwater surface within fine-grained soils (FGS). Historic water table fluctuations were precluded as a source for such occurrences. Additionally, relatively low LNAPL saturations were found in the adjacent formation with several feet of LNAPL observed in monitoring wells.

Fine-grained soil typically consists of matrix blocks with high capillary pore entry pressures, and interconnected macropores with low capillary pore entry pressures. As an LNAPL mass accumulates and displaces water within the capillary zone and groundwater surface, it often exhibits a pressure gradient with the macropore network that is sufficient to allow downward migration through the saturated zone. Similar to that of the

previously discussed confined LNAPL near the groundwater surface interface, if a monitoring well is screened across a macropore network, bottom filling can occur resulting in exaggerated ANT. Figure 7 is a sand tank experiment exhibiting confined LNAPL below the water table. Note the “monitoring well” at the right edge of the confined plume that has an ANT that extends up to the water table. Figure 8 is a photograph of FGS showing matrix blocks (lighter) and a dendritic macropore network.

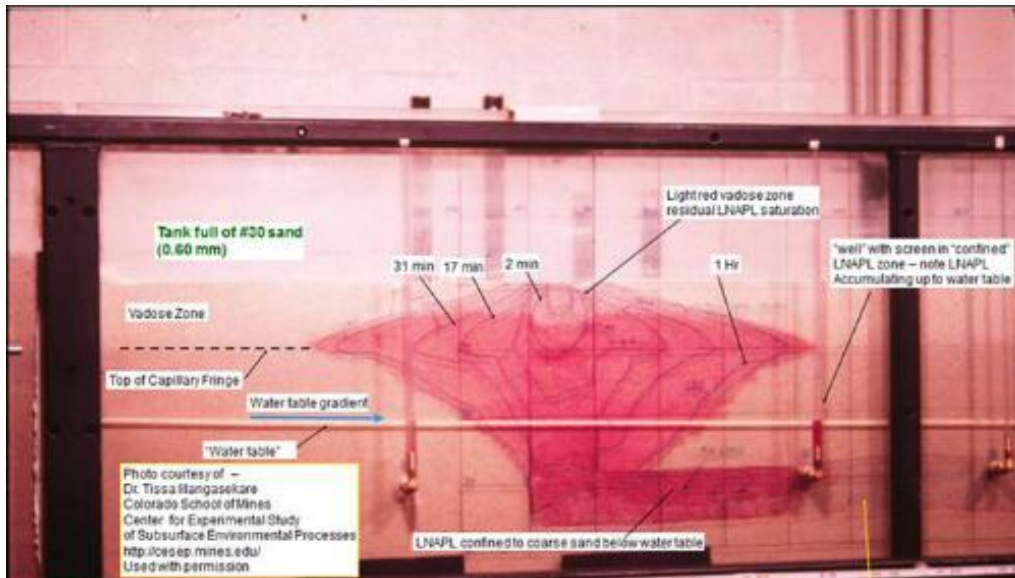


Figure 7. Sand tank exhibiting confined LNAPL and exaggerated apparent NAPL thickness (Illangasekare, 1995).



Figure 8. Photograph of fine-grained soil with matrix blocks and dendritic macropore network (Colin Johnston via ITRC, 2013a).

2.2.3 Perched LNAPL

The inverse of the above example explains why perched LNAPL will also result in an exaggerated ANT during decreasing groundwater elevations. Assuming that the LNAPL layer is underlain by a confining layer, when the groundwater elevation falls below the top of the confining layer, the monitoring well acts as a conduit and LNAPL will migrate to, and fill the well, in accordance with capillary pressure gradients. Figure 9 illustrates this process where the pore entry pressure (P_{PE}) of the confining layer exceeds the LNAPL capillary pressure (P_{cn}).

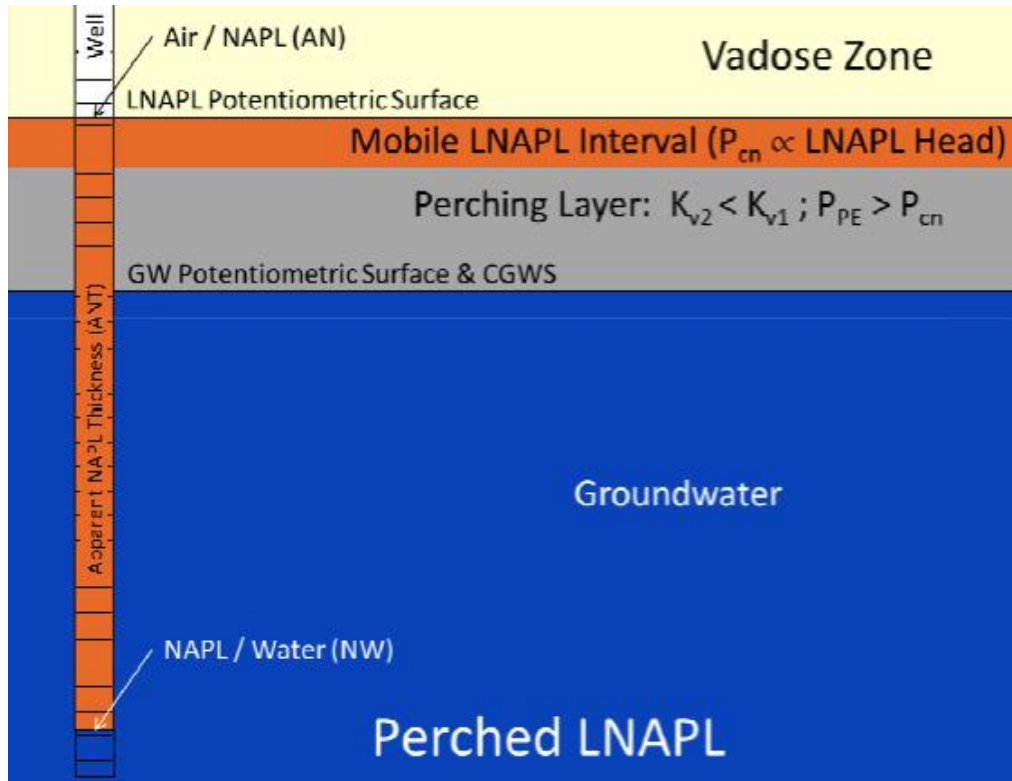


Figure 9. Conceptualized cross-section illustrating perched LNAPL (H2A, 2011d).

2.3 GRAPHICAL DETERMINATION OF LNAPL HYDROGEOLOGIC CONDITION

Based on empirical observations of LNAPL under various conditions, including with the use of laser-induced fluorescence and soil core photography, several graphical methods have been developed to determine LNAPL hydrogeologic condition. Despite generally limited information regarding LNAPL behavior within this context, H2A's Applied NAPL Science Review (H2A) and Kirkman et al. (2012) provide detailed explanations for estimating LNAPL hydrogeologic condition. Two such methods include diagnostic gauge plots (DGPs) and hydrostratigraphs (HSGs), which at a minimum require depth-to-water and depth-to-product measurements from a monitoring well. A major caveat to DGPs and HSGs is that reliable trend analysis is dependent on the degree to which vertical equilibrium is present within the formation. Non-vertical equilibrium conditions that can result from aquifer recharge, tidal – or in the case of the research sites, canal – fluctuations, manually bailing free-product from wells, hydraulic pumping, and other factors can decrease the reliability of such methods. H2A (2011b) recommends that multiple lines of evidence should be used when determining LNAPL hydrogeologic condition. Additional evidence includes, but is not limited to, grain-size distribution, stratigraphic data, photoionization (volatile) readings, analytical data, laser-induced fluorescence and soil core photography.

2.3.1 Diagnostic Gauge Plots

A diagnostic gauge plot (DGP) illustrates the trend in the air-NAPL (AN) interface, NAPL-water (NW) interface, and corrected groundwater surface (CGWS) as a function of apparent NAPL thickness (ANT) (H2A, 2011b). Figures 10, 11, and 12 display ideal DGPs for unconfined, confined, and perched LNAPL, respectively.

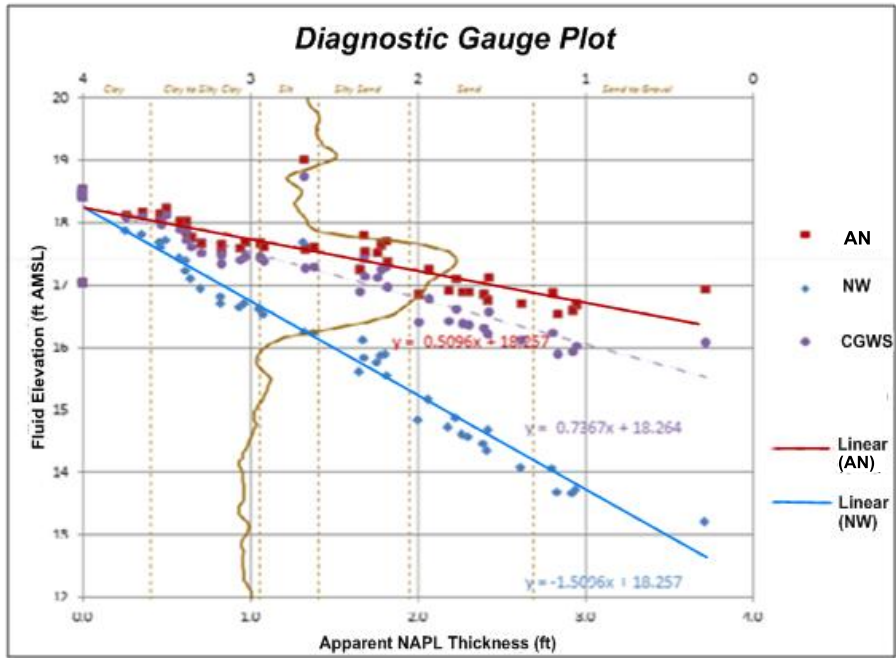


Figure 10. Unconfined LNAPL diagnostic gauge plot trend (adapted from Hawthorne, 2012).

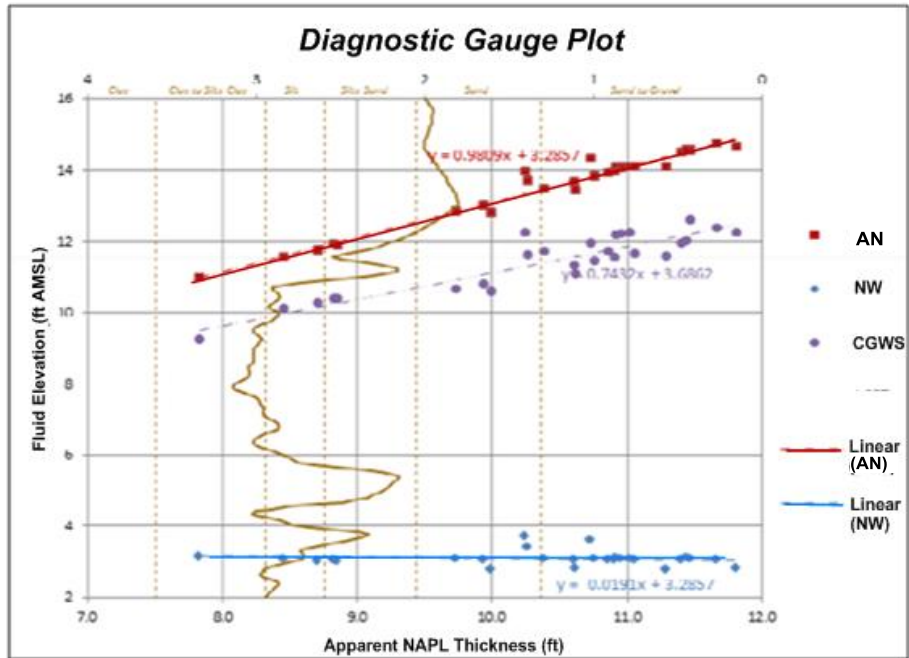


Figure 11. Confined LNAPL diagnostic gauge plot trend (adapted from Hawthorne, 2012).

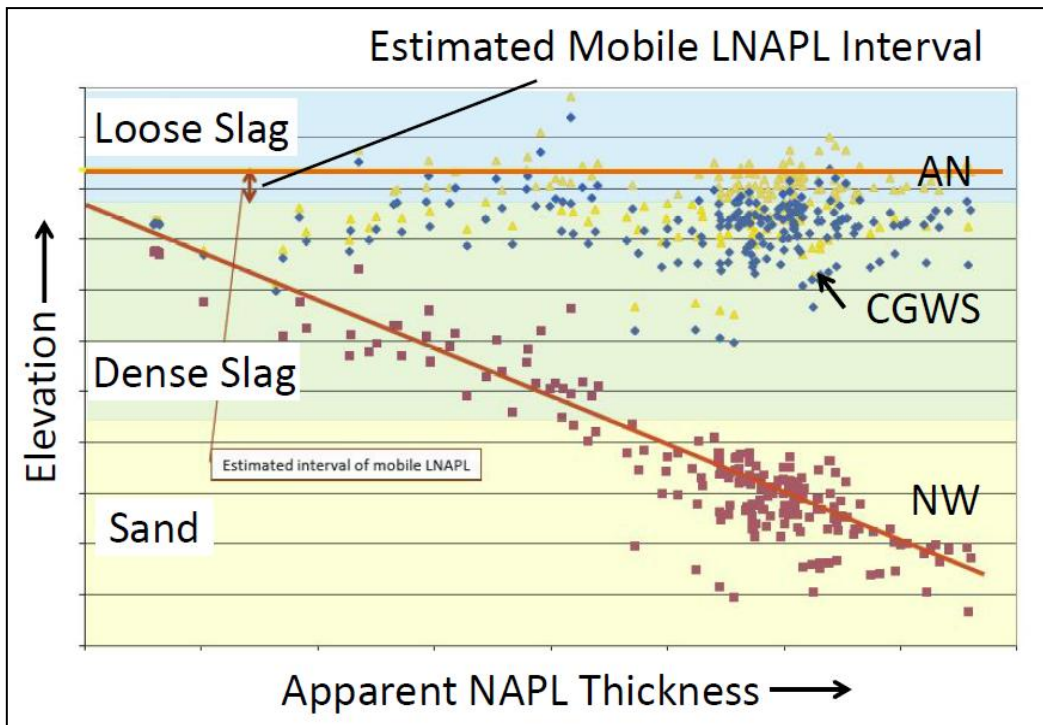


Figure 12. Perched LNAPL diagnostic gauge plot trend in an example setting composed of slag and sand (Hawthorne et al., 2011).

The general diagnostic trend for each condition is summarized as follows:

- Unconfined LNAPL: The air-NAPL interface trend line (red) and NAPL-water interface trend line (blue) both point downward.
- Confined LNAPL: The air-NAPL trend line (red) points upward while the NAPL-water interface trend line (blue) remains horizontal.
- Perched LNAPL: The air-NAPL trend line (orange) remains horizontal while the NAPL-water interface trend line (red) points downward.

Figure 13 on the following page summarizes these trends under rising and falling water levels.

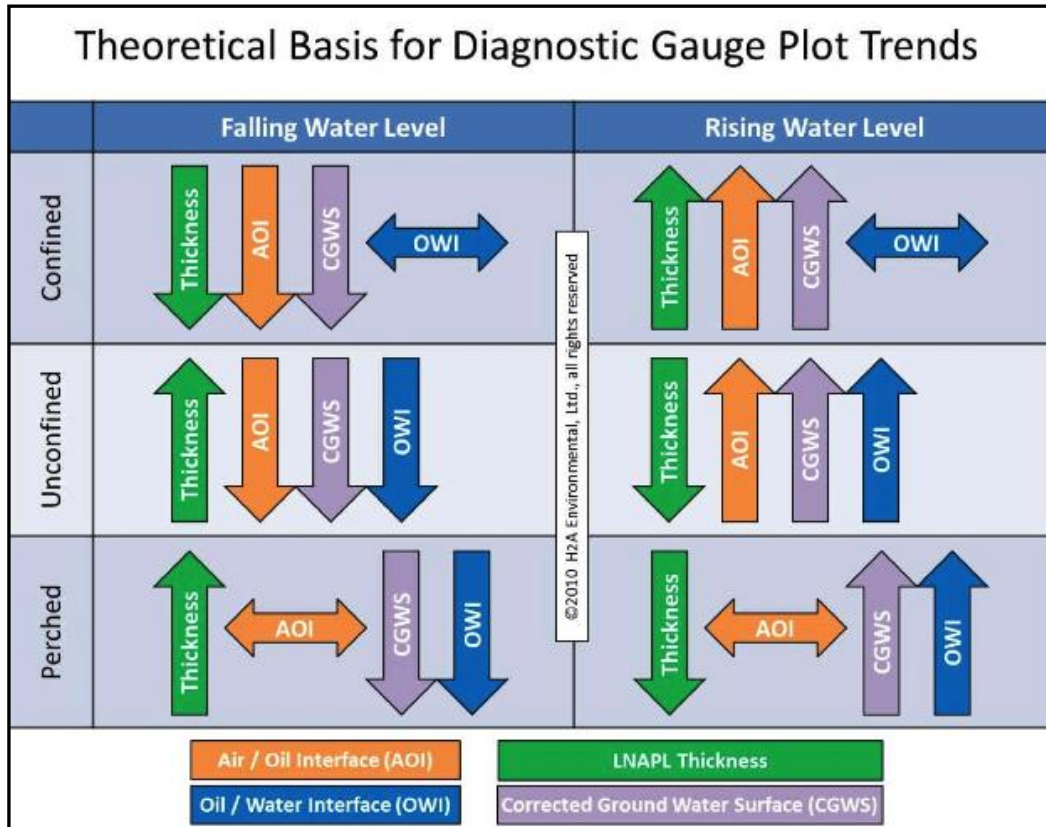


Figure 13. Theoretical basis for diagnostic gauge plot trends (H2A, 2011b).

Number of data points and regression analysis are important components in determining the accuracy of DGPs. For example, Figure 11 contains over 20 measurements over the course of several years and has an R^2 value of 0.9 for the air-NAPL trend line, which indicates a strong linear correlation. While there is no specific cutoff in terms of data density and scatter, a hypothetical DGP containing only four data points and an R^2 of 0.08 should be viewed skeptically. In order to increase the accuracy of DGP analysis, additional data should be incorporated. DGPs for both research sites are presented in further detail throughout Chapter 5 and Appendix B.

2.3.2 Hydrostratigraphs

A hydrostratigraph (HSG) is time-series plot of groundwater and LNAPL elevation data overlain with stratigraphy (H2A, 2011c). Figure 14 and 15 display HSGs for unconfined LNAPL at Site B, and both confined and perched LNAPL at Site A, respectively. In Figure 14, the air-LNAPL interface (pink), LNAPL-water interface (navy blue), and potentiometric surface, or corrected groundwater surface (royal blue), are plotted as a function of time as measured from depth below ground surface (left y-axis).

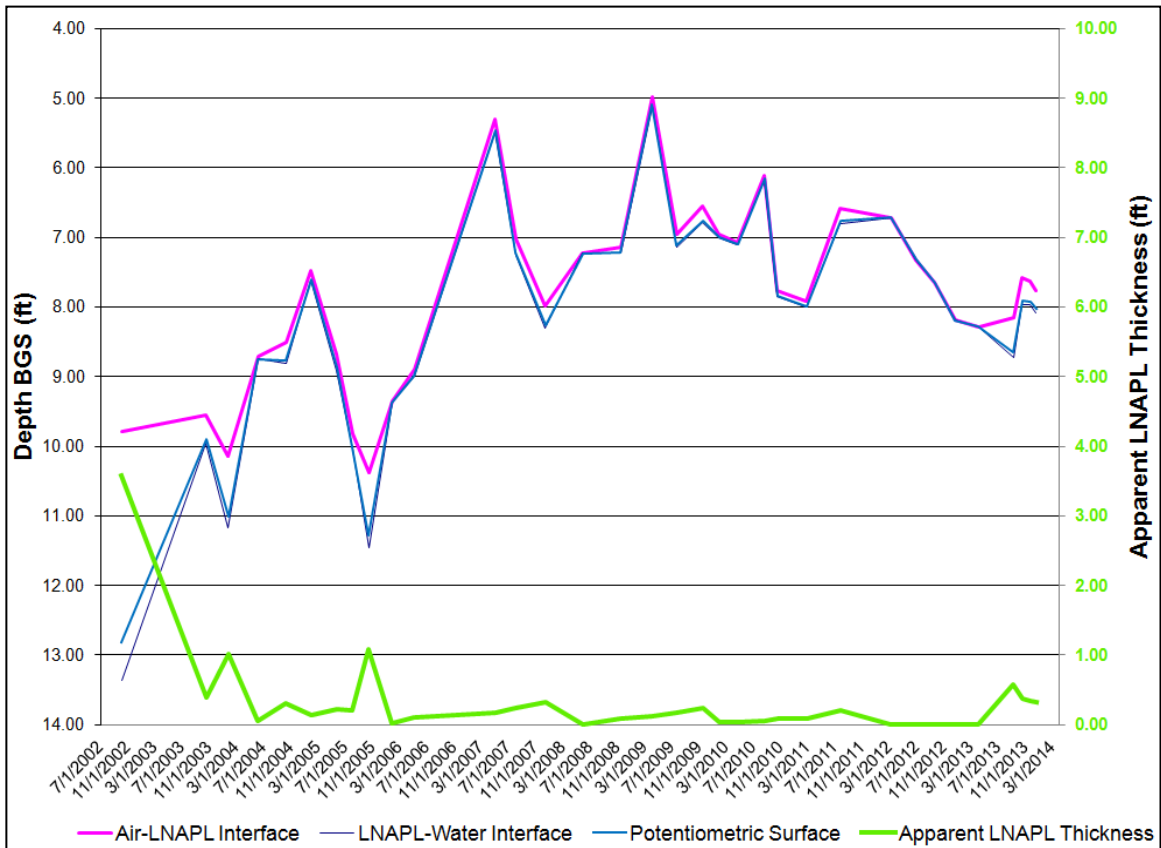


Figure 14. Hydrostratigraph exhibiting unconfined LNAPL at Site B.

Corresponding ANT values (green) are plotted and relate to the ANT scale (right y-axis). Figure 14 exhibits the characteristic unconfined trend observed throughout Site B, which from this depth interval is a result of the relatively homogenous well-graded sand. The ANT (green) has an inverse relationship with the LNAPL-water interface (navy blue) and potentiometric surface (royal blue), which is consistent with unconfined LNAPL conditions. As the groundwater surface elevation decreases, previously trapped LNAPL within the saturated zone overcomes the pore entry pressure in adjacent soil pores and remobilizes. This trend is highlighted particularly well from July 2002 to March 2004, and again in late 2005. Also note that during unconfined conditions, the ANT is inversely proportional to groundwater surface elevation.

Figure 15 exhibits a more complex HSG that would be difficult to interpret without additional data. The corresponding DGP for this monitoring well indicates a perched trend as illustrated in Figure 12. When the stratigraphy and PID data are considered, Figure 15 appears to exhibit perched *and* confined conditions. If the groundwater surface (blue) drops below the silty sand layer, the monitoring well acts as a conduit and fills with LNAPL (perched). If the groundwater surface rises above the silty sand layer, bottom filling of the monitoring well occurs, resulting in increased LNAPL thickness (confined). Despite the relative muted quality of bottom filling during higher groundwater elevations in Figure 15, it is still apparent as ANT is essentially 0 feet as the groundwater surface rises through the sandy silt layer prior to reaching the silt layer.

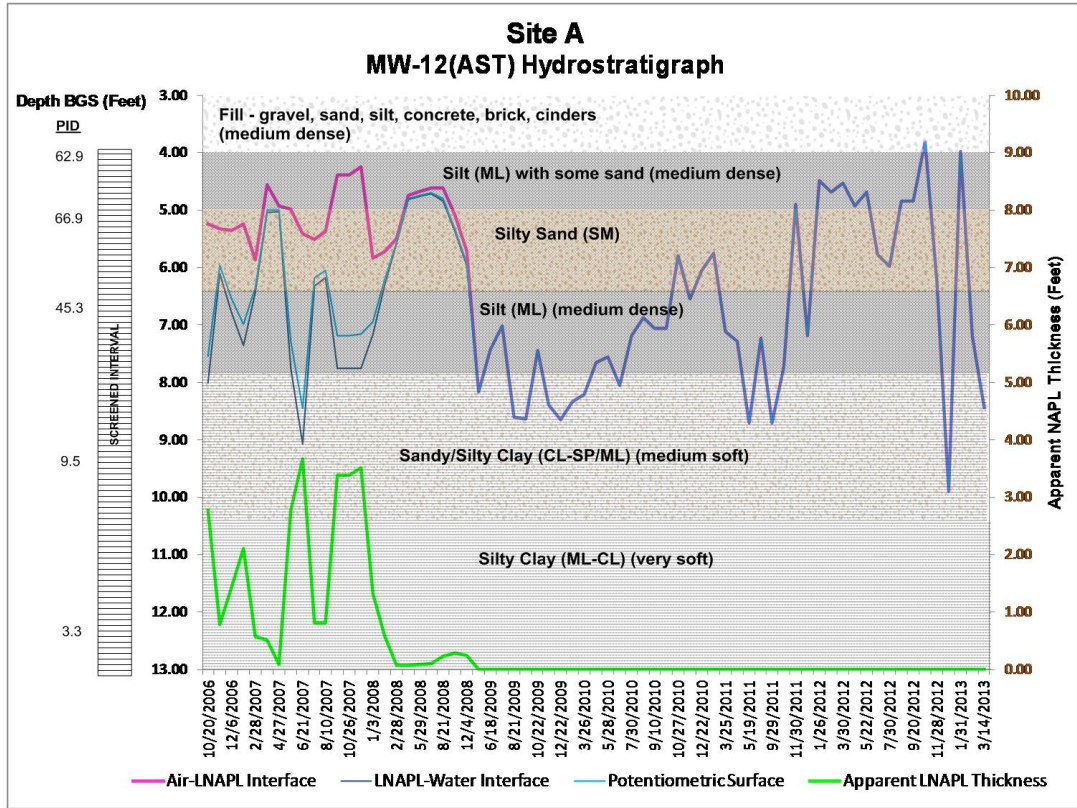


Figure 15. Hydrostratigraph exhibiting confined and perched LNAPL at Site A.

In order to more clearly illustrate confined LNAPL in an HSG, Figure 16 is presented below. Despite the prevalence of unconfined LNAPL at Site B, monitoring well P-02-010 (Figure 16) clearly exhibits confined LNAPL. The air-LNAPL interface (pink) and corresponding ANT (green) clearly increase as a result of an increase in the potentiometric surface. Unlike the unconfined example, the ANT is directly proportional to the groundwater surface elevation, which is consistent with bottom filling of a monitoring well under increasing pressure head. Hydrostratigraphs for both research sites are presented in further detail throughout Chapter 5 and Appendix C.

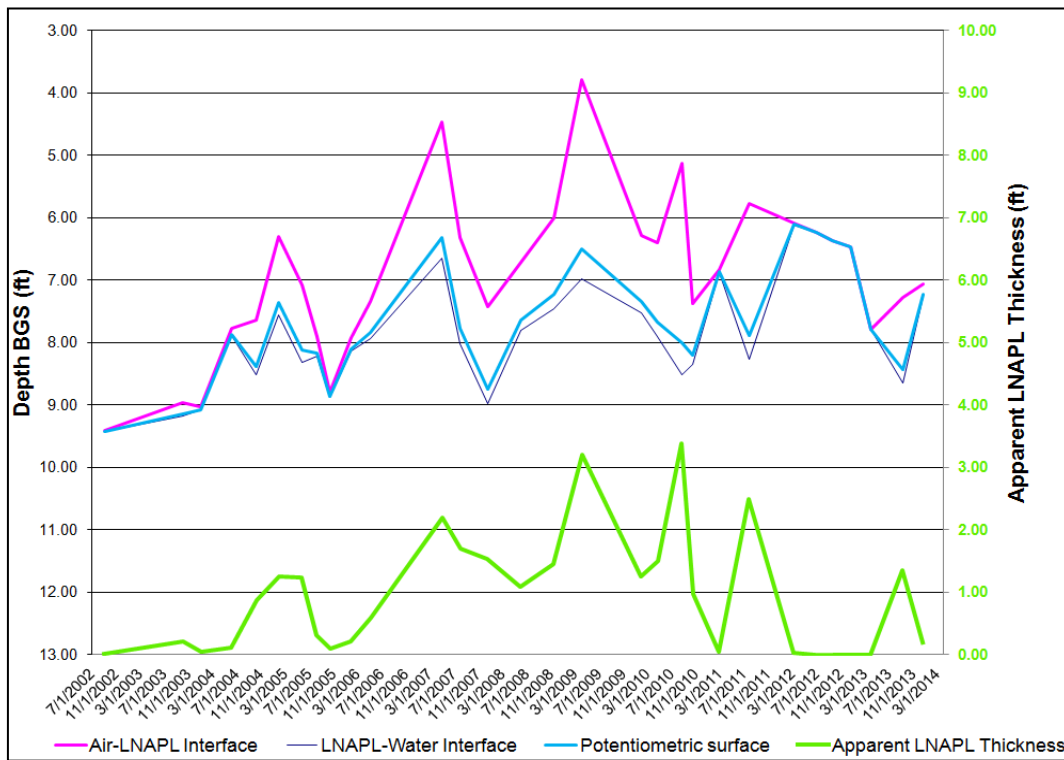


Figure 16. Hydrostratigraph exhibiting confined LNAPL at Site B.

2.3.3 Discharge versus Drawdown Graphs

Perhaps the most reliable graphical method for determining LNAPL hydrogeologic condition is a discharge versus drawdown (DvD) graph. DvD graphs require the input of more advanced monitoring well data that are collected during LNAPL baildown tests. An LNAPL baildown test is conducted by removing a measured volume of LNAPL from a monitoring or recovery well and recording LNAPL recharge as a function of time. The test is typically performed with a peristaltic pump and an oil-water interface probe. A static depth-to-water (DTW) and depth-to-product (DTP) measurement is taken prior to removing LNAPL. Upon completion of LNAPL pumping, subsequent DTW and DTP measurements are taken at a specified time interval. The baildown data are used to produce a scatter plot of LNAPL discharge as a function of LNAPL drawdown as illustrated in Figure 17.

The typical goal of a baildown test is to determine the LNAPL transmissivity, which is a reliable indicator for LNAPL mobility and recoverability. The data from such tests can be plotted and compared with idealized type curves that indicate LNAPL hydrogeologic condition. While non-vertical equilibrium conditions can still negatively impact the accuracy of LNAPL baildown tests, the results theoretically account for exaggerated ANT that can occur under confined and perched conditions. For example, a baildown test for exaggerated ANT under confined conditions will highlight the difference between filter pack LNAPL discharge and formation LNAPL discharge. Under this scenario, filter pack discharge will be significantly higher than formation discharge.

Figure 17 displays DvD graphs for unconfined LNAPL (left) and confined LNAPL (right). Confined LNAPL exhibits significant filter pack discharge with minimal and relatively constant formation discharge.

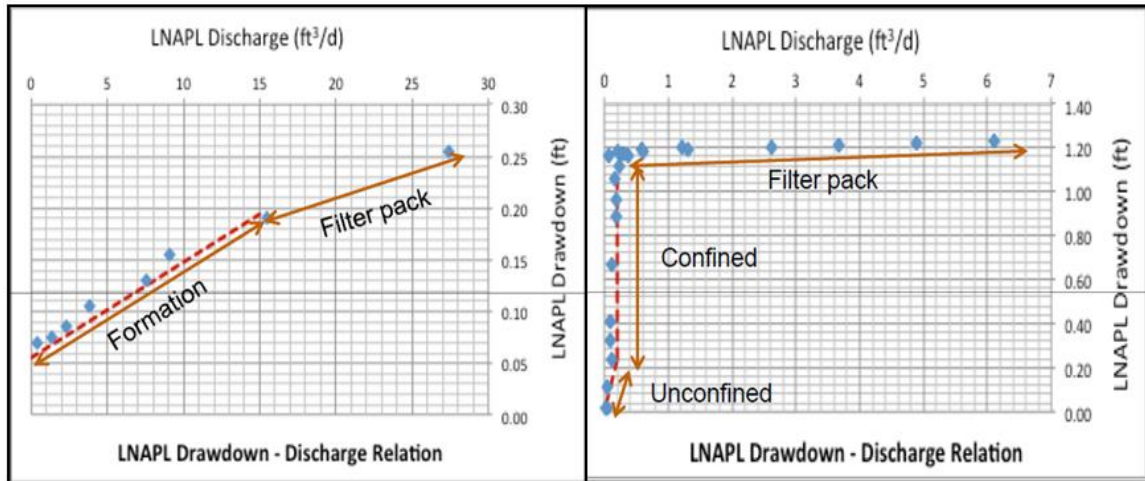


Figure 17. Discharge versus drawdown graphs for unconfined and confined LNAPL (Muthu and Hawthorne, 2013).

2.4 LNAPL THICKNESS CORRECTIONS AND VOLUME ESTIMATES

Total LNAPL (free and residual) and recoverable LNAPL estimates are the basis for conceptual site models and remediation management. Gauged LNAPL thickness – as measured in monitoring wells – is the most common metric used to evaluate LNAPL conditions in the surrounding formation. The gauged, or apparent NAPL thickness (ANT), is frequently the basis for inferring formation NAPL thickness (FNT) under the incorrect assumption that ANT directly corresponds to FNT. As illustrated previously, even unconfined LNAPL at vertical equilibrium can present an ANT that is significantly less than the actual vertical saturation distribution. For example, if current groundwater elevations are significantly higher than historical elevations, it is likely that much of the LNAPL within the vertical saturation distribution interval has become trapped within the saturated zone. Estimates using ANT in this manner will underestimate total LNAPL volume and will not account for increased free and recoverable LNAPL in the event of groundwater elevations returning to historically lower levels.

Kirkman et al. (2012) describes ANT for unconfined LNAPL at vertical equilibrium as corresponding to “the interval in the formation where LNAPL exhibits capillary pressure above zero within the screened interval” (p. 87). In other words, ANT is not exactly describing FNT, but rather the vertical distribution of mobile LNAPL within this interval. ANT for unconfined conditions likely then underestimates the vertical smear zone interval, which represents the complete extent of vertical LNAPL saturation distribution. In this scenario, the saturation distribution will deviate from the ideal shark fin shape of the distribution profile. For this reason, the API LDRM requires

that the maximum observed ANT is used as a model input, which is discussed in Chapter 3.

The situation is further complicated when confined and perched LNAPL is considered. The following data and corresponding figures are based on results published in Kirkman et al. (2012). Figure 18 is a DGP clearly exhibiting trends that are consistent with perched LNAPL. When the LNAPL-water interface (uncorrected groundwater surface) is at 6 feet bgs, the ANT is approximately 3.0 feet. Yet when the LNAPL-water interface is at 16 feet bgs, the ANT is over 11 feet. Without context, the maximum observed ANT for this monitoring well – as required by the LDRM – is over 11 feet. However, using this value for the LDRM or other volume estimates would grossly overestimate total and recoverable LNAPL.

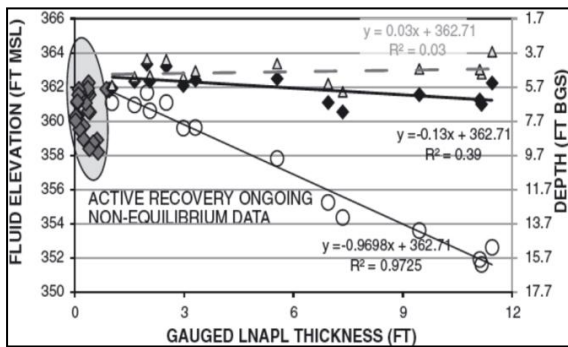


Figure 18. Diagnostic gauge plot exhibiting perched LNAPL (Kirkman et al., 2012).

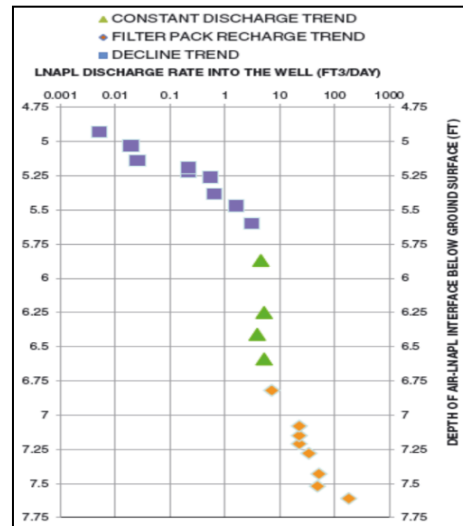


Figure 19. Corresponding discharge versus drawdown graph for conditions discussed in Figure 18 (Kirkman et al., 2012).

Figure 19 is a DvD graph compiled from LNAPL baildown data for the same monitoring well. Based on DvD results, Kirkman et al. (2012) estimates that the mobile LNAPL interval is actually only 0.8 feet, in significant contrast to the maximum observed

ANT of 11 feet. The mobile LNAPL interval is estimated from the DvD graph and equals the difference between the static air-LNAPL interface and the air-LNAPL interface that corresponds to the start of declining discharge (Kirkman et al., 2012). Similar techniques can be used to estimate the mobile interval for confined LNAPL.

In the above perched LNAPL example, the mobile interval of 0.8 feet is analogous to the mobile LNAPL layer for unconfined conditions at vertical equilibrium. The actual vertical saturation distribution for confined and perched LNAPL is more ambiguous. ANT for unconfined LNAPL frequently underestimates the smear zone extent since smear zone in this scenario is largely dependent on historical groundwater fluctuations. Perched conditions result from a decrease in groundwater elevation that effectively results in a monitoring well having a pore entry pressure of zero, thereby inducing LNAPL flow. Confined conditions result from an increase in groundwater elevation and increased pressure head, which increases LNAPL capillary pressure and induces lateral migration toward, and bottom filling of, the monitoring well. In both cases, the vertical saturation distribution is not represented by the ANT. In theory, whenever LNAPL exists within the screened interval of a monitoring well, it is capable of migrating into the surrounding formation if the pore entry pressure of the adjacent soil is exceeded by the LNAPL. However, while monitoring wells have been documented to act as conduits for LNAPL into the surrounding formation, under typical field conditions this process is prevented by exceedingly high capillary pressures in the saturated zone. Therefore, the mobile interval for confined and perched LNAPL is essentially the same as the vertical saturation distribution, which is frequently much less than the ANT in these cases.

If the vertical LNAPL saturation distribution is known, the ANT can be corrected and an LNAPL volume can be calculated. The concept of a corrected LNAPL thickness is somewhat erroneous since this confuses an LNAPL saturation distribution with the idea of a coherent LNAPL layer with saturations approaching 100%. However, the LNAPL volumetric content over an LNAPL planimetric lens can be calculated and simplified as a corrected LNAPL thickness. As shown in Figure 20 and 21, LNAPL specific volume is the vertically distributed LNAPL volume per unit planimetric area and represents total (free and residual) LNAPL (Charbeneau, 2007a). Specific volume has units of ft^3/ft^2 and is the hypothetical volume of LNAPL that would be present in a boring 1 ft^2 over the entire vertical saturation interval (ITRC, 2013a).

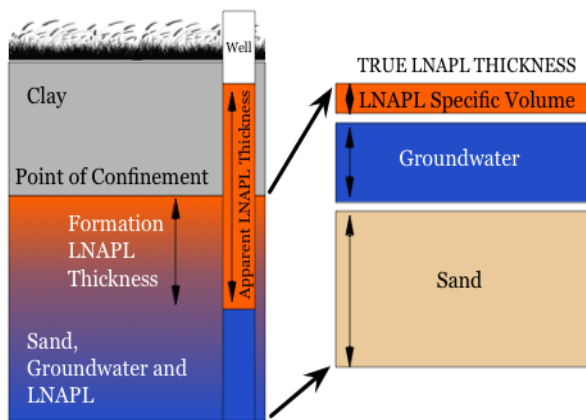


Figure 20. Cross-section depicting “true LNAPL thickness” for confined LNAPL (H2A, 2011a).

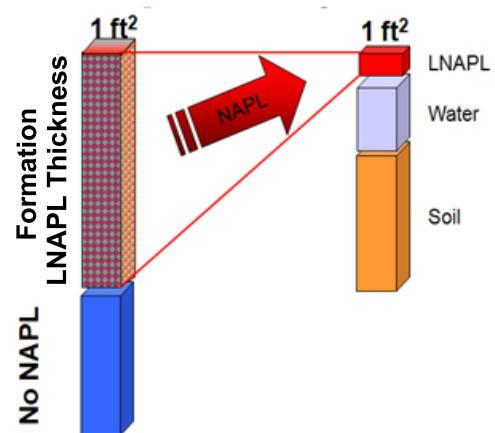


Figure 21. LNAPL specific volume (adapted from ITRC, 2013a).

The Interstate Technology and Regulatory Council (ITRC) (2013a) presents a volume estimation method that includes the following steps:

- 1) Measure or model vertical saturation distribution
- 2) Estimate LNAPL specific volume
- 3) Assign areas to each monitoring well

- 4) Calculate volume of each area (*specific volume* $ft^3/ft^2 * area\ ft^2 = volume\ ft^3$)
- 5) Integrate volumes across entire site.

However, this approach results in a volume that does not differentiate between free, residual, and recoverable product. The LDRM provides the means to model specific volume at each monitoring well while calculating the equivalent free and recoverable portions.

2.5 HYDRAULIC LNAPL RECOVERY

Hydraulic recovery of LNAPL involves the application of a pump or vacuum to a recovery well with the purpose of removing free-product and impacted groundwater and/or providing hydraulic control of the free- and dissolved-phase plume. Several variations of hydraulic recovery have been implemented for LNAPL recovery, which include skimming, groundwater pump-and-treat, and vacuum-enhanced recovery.

Skimming involves the use of an exterior vacuum pump and a recovery well skimmer that floats on the water table and in theory, only removes free-product floating on the water column. Groundwater pump-and-treat generally refers to the total-fluids (i.e., product and groundwater) extraction from a pumping well and the subsequent effluent treatment and disposal (EPA, 1999).

While water production wells generally have an in-well pump submerged beneath the water table, vacuum wells utilize an exterior pump to apply negative pressure to an extraction well. Vacuum-enhanced extraction, or recovery, was originally described by Blake and Gates (1986) as involving the simultaneous removal of subsurface air, groundwater, and NAPL (Lundy, 2008). Vacuum-enhanced recovery, which is also known as multiphase extraction (MPE), is the application of a vacuum to a single or

multiple recovery wells via an aboveground pump or “blower” in order to remove soil vapor, groundwater, and product (EPA, 1999). The screened interval for an MPE well typically intersects the groundwater surface such that the vadose and saturated zones are both exposed to vacuum influence. The vacuum pressure is typically applied through a drop tube or “stinger” that is placed in the recovery well at or below the water table. MPE results in the “transient multiphase flow of subsurface air, mobile LNAPL, and groundwater (that) occurs in vertically stacked overlapping zones near the discharging MPE well” (Lundy, 2008, p. 14).

The applied vacuum extracts soil vapor and enhances groundwater recovery due to an increased pressure gradient (EPA, 1999). As air is pulled into the recovery well, a pressure gradient will be transmitted to the adjacent formation. The resulting cone of depression (i.e., capture region) increases hydraulic gradients, which results in preferential flow of groundwater and LNAPL to the recovery well (Charbeneau, 2007a). LNAPL and impacted groundwater is pumped from the recovery well through the stinger tube to a treatment component. This process is analogous to groundwater pump-and-treat; however, groundwater production wells are often not screened into the vadose zone and also contain an in-well pump. Figure 22 illustrates vacuum influence on the surrounding formation where Q_a is the air discharge from the recovery well and the arrows indicate air flow to the recovery well. Figure 23 is a standard recovery well shown as a construction diagram, which depicts the static fluid level and vacuum fluid level.

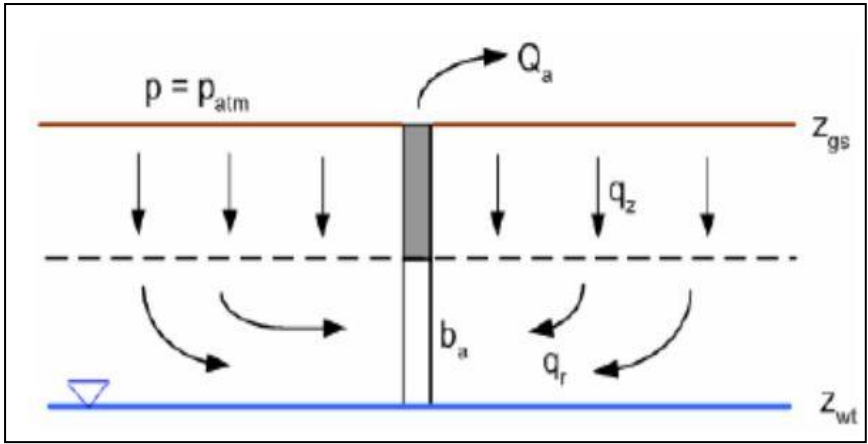


Figure 22. Diagrammatic depiction of vacuum influence on an aquifer (Charbeneau, 2007a).

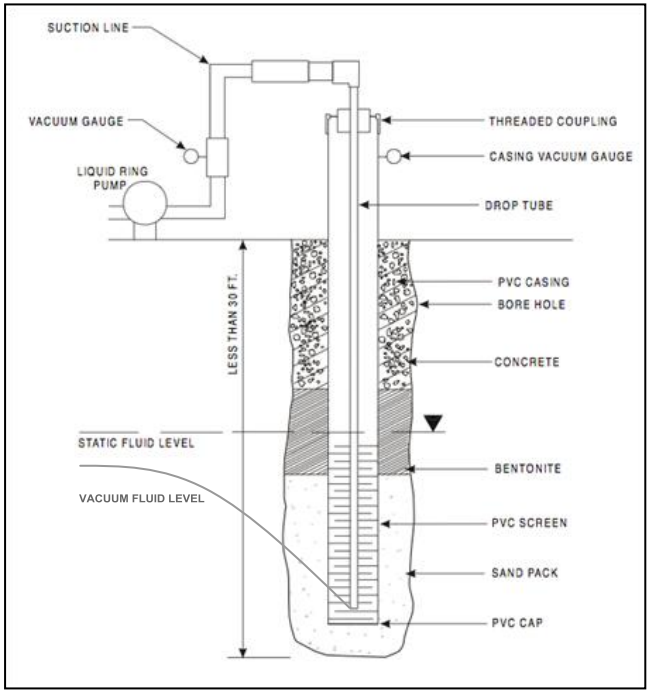


Figure 23. Recovery well construction diagram for a standard vacuum-enhanced well (adapted from EPA, 1999).

2.5.1 MPE Application

The mobility and recovery of impacted groundwater and LNAPL is primarily governed by hydraulic conductivity and formation transmissivity as described through Darcy's law (Charbeneau, 2007a). However, variability exists between the hydraulic conductivity of groundwater and LNAPL where one fluid may be more recoverable than the other. For example, high transmissivity formations will result in high rates of groundwater recovery with limited drawdown near the recovery well. In these cases, the recovery well is said to be flooded with groundwater and exhibits a negligible cone of depression. As a result, the hydraulic conductivity of LNAPL will not increase sufficiently enough to induce migration to the recovery well. Soil type frequently exhibits the strongest influence on the effectiveness of LNAPL recovery via MPE. Therefore, soil characterization is an important aspect in determining MPE applicability.

MPE is highly effective in fine- to medium-grained soils consistent with silty sand to fine-grained sand. MPE applicability can also be determined through the product of hydraulic conductivity and saturated thickness, which is known as transmissivity. The ideal transmissivity for effective MPE of LNAPL is generally less than 500 gpd/ft (67 ft²/day) (EPA, 1999). MPE is not only capable of overcoming the capillary forces that limit LNAPL mobility, but also results in slower drawdown and moderate gradients, both of which increase LNAPL recovery (EPA, 1999). MPE in high transmissivity formations consisting of, for example, sand and gravel, will result in limited groundwater drawdown at the recovery well. The resulting shallow gradients are insufficient to increase LNAPL conductivity enough to induce remobilization and migration to the recovery well.

2.5.2 MPE Advantages

MPE is typically preferred over groundwater production wells since the addition of vacuum often results in comparable drawdown while increasing total fluid discharge (EPA, 1999). MPE is known to reduce the drawdown necessary to obtain a given flow rate, thereby decreasing the smearing of LNAPL and reducing the total volume of contaminated soil. EPA (1999) reports the following benefits of MPE as compared to water production wells:

- 1) Recovery of shallow and floating product
- 2) Remediation of the capillary fringe and smear zone
- 3) Remediation of volatile residual LNAPL components in the vadose zone

MPE combines several individual components of LNAPL recovery – skimming, soil-vapor extraction, total fluids removal – at a single recovery well (Beckett and Huntley, 1998). Jeong and Charbeneau (2014) indicate that vacuum-enhanced recovery is effective for small formation LNAPL thicknesses and for treating residual LNAPL in the vadose zone. Perhaps the most significant advantage of MPE is its ability to expedite remediation resulting in a cost savings when compared to conventional pumping (EPA, 1996).

2.5.3 MPE Limitations

Despite the many documented benefits, MPE as an LNAPL remediation technology has several limitations. EPA (1999) indicates that the most significant technical limitation of MPE is the depth restrictions as typical vacuum pressures limit recovery to a depth of approximately 30 feet. Liquid ring vacuum pumps commonly implemented for the MPE of LNAPL are often rated to 26 inHg (0.67 atm). However,

these pressures are rarely achieved at individual recovery wells, particularly when considering a multi-year operation and standard efficiency losses.

Another limitation of MPE and hydraulic recovery in general is the exponential decline in LNAPL recovery rates. The mobility and recoverability of LNAPL in subsurface soils is a function of LNAPL saturation and transmissivity (Beckett and Lundegard, 1997; Charbeneau et al., 2000; Adamski et al., 2005; ITRC, 2013a). The mobility of an LNAPL plume will decrease through any process that results in an LNAPL mass spreading over larger areas, decreasing saturation (Beckett and Lundegard, 1997). Stated another way, the recoverability of LNAPL will decrease immediately upon the pumping of free-product from soil. As a result, LNAPL removal via hydraulic systems – including MPE – results in asymptotic recovery of free-product with time (Charbeneau et al., 2000; Charbeneau, 2007a; ITRC, 2013b). Figures 24 and 25 illustrate asymptotic LNAPL recovery rates for an undisclosed site and Site A, respectively.

Recovery endpoints are estimated by calculating LNAPL transmissivity, which can be modeled through the LDRM or determined by LNAPL baildown tests in monitoring wells. ITRC (2013b) reports that a reasonable LNAPL recovery endpoint ranges from 0.1 to 0.8 ft²/day. From a practical standpoint, however, if the MPE system is not recovering free-product on a daily basis, it is safe to assume very limited future recovery.

MPE is often implemented in part to reduce soluble constituents that have dissolved into groundwater from the LNAPL mass. However, contemporary research suggests that groundwater pumping through any means of hydraulic recovery is ineffective at significantly reducing dissolved phase concentrations (Huntley and Beckett,

2002; ITRC, 2013b). This limitation is largely a function of the LNAPL mass that remains in the subsurface during and after recovery efforts as either unrecovered mobile or residual LNAPL.

Tyler and Finley (1991) report that for even well-managed oil reservoirs, unrecovered mobile oil can range from 20 to 70% as compared to initial mobile oil in place. In oil production, unrecovered mobile LNAPL exists due to reservoir heterogeneities, hydraulic limitations, and time and cost factors (Charbeneau, 2007b). Oil production reservoirs can be used as an analog for LNAPL remediation in that it is uncommon to recover more than 60% of the initial mobile LNAPL. However, a comprehensive review of LNAPL remediation sites concluded that recovery of more than 30% of the original in place LNAPL volume is the exception; in finer-grained soils more than 15% recovery is rare (Charbeneau, 2007b).

In a post-recovery remediation setting, the unrecovered mobile LNAPL plume, while generally stable at the plume margins, has been known to continue migrating under varying groundwater conditions. The potential for continued migration after MPE has stopped can increase if the site setting includes tidal or canal fluctuations, which can affect hydraulic gradients at site and plume margins. Regardless of the continued threat of migration, the fact is that a significant portion of LNAPL remains in the subsurface after recovery efforts have ceased. The remaining LNAPL can act as a long term source of dissolved phase contaminants that will continue to threaten potential receptors.

Huntley and Beckett (2002) explain a hypothetical scenario whereby 50% of LNAPL is recovered from silty sand with a formation LNAPL thickness of 3 m. In this scenario, the dissolved phase plume will stabilize and even shrink; however, the residence time for

benzene at the site only decreases from 400 to 200 years. Therefore, even if MPE has rendered an LNAPL plume immobile, soluble constituents can pose a threat for decades to centuries.

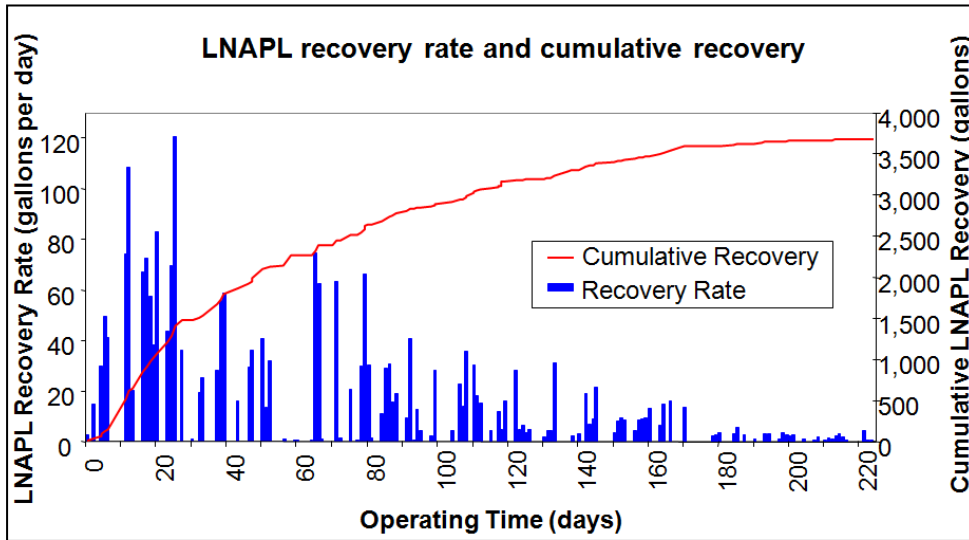


Figure 24. Typical recovery trend for hydraulic recovery of LNAPL (ITRC, 2013b).

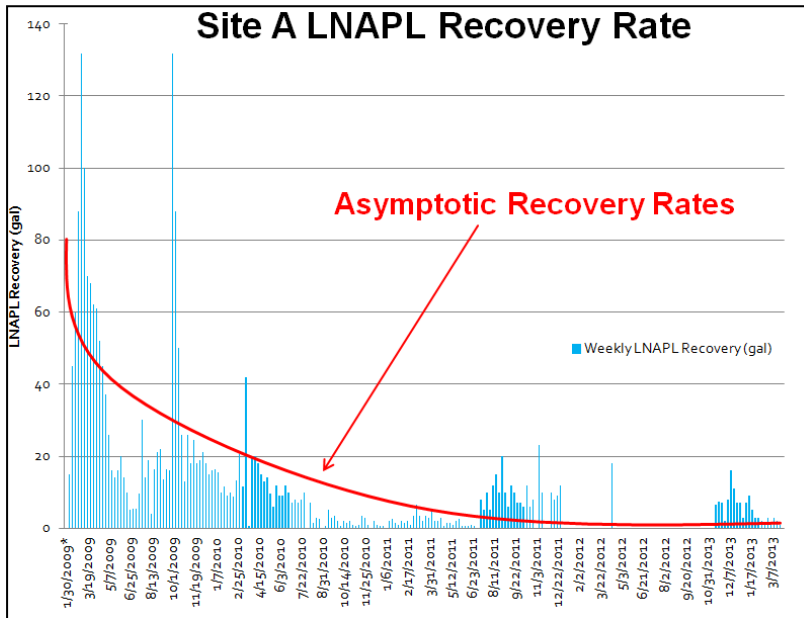


Figure 25. LNAPL recovery trend for Site A (AMEC 2013).

CHAPTER 3: THE LNAPL DISTRIBUTION AND RECOVERY MODEL

The American Petroleum Institute (API) LNAPL Distribution and Recovery Model (LDRM) is a downloadable modeling software program designed to assess the extent and recoverability of LNAPL in subsurface soils (Charbeneau, 2007a). Specifically, it is a physically based, semi-analytical model used to estimate LNAPL saturation distribution and recovery for conventional remediation technologies (Charbeneau, 2007a; Charbeneau and Adamski, 2008a). The LDRM domain is based on radial flow to a single recovery well (i.e., radius of recovery) and requires four field-measured parameters: 1) LNAPL thickness, 2) ground surface elevation, 3) water table elevation, and 4) soil facies interface elevation (Charbeneau and Adamski, 2008a). Additional soil and fluid parameters are also required to run the model. However, if soil and fluid field data are not available, these parameters can be estimated through the use of empirically derived values for various soil and fluid types.

The LDRM has two primary modeling functions:

- 1) Characterizing the vertical saturation distribution of LNAPL near the groundwater table, and
- 2) Estimating the LNAPL recovery volume as a function of time with different hydraulic remediation technologies including single- or dual-pump extraction, vacuum-enhanced extraction, product skimmer wells, and trenches.

The saturation distribution at each modeling point can be used to calculate LNAPL specific volume, which is the vertical integration of LNAPL volume per unit area (Charbeneau, 2007; ITRC, 2013a). Since LNAPL specific volume is reported in ft^3/ft^2 , it can be thought of as a true LNAPL thickness (H2A, 2011a). Specific volume can be

integrated across the area of a monitoring well network to estimate total free and residual LNAPL at a site. Recovery modeling can be used in remediation system design and evaluation of existing operations to estimate total recoverable LNAPL.

3.1 LNAPL DISTRIBUTION

The modeled LNAPL saturation distribution comprises a vertical interval that is located near the water table and does not account for LNAPL potentially present several feet into the saturated zone. Groundwater and LNAPL elevations in monitoring wells, when combined with capillary pressure curves, provide the basis for LNAPL specific volume and recoverable LNAPL estimations.

3.1.1 Porous Media

The distribution of LNAPL in subsurface soils is controlled largely by *interfacial tension, wettability, and capillary pressure*. Charbeneau (2007a) refers to the sum of these pore-scale factors as capillarity in porous media. When LNAPL comes into contact with water – the two fluids being immiscible – a surface energy exists due to the differences in molecular attraction between the two fluids (Newell et al., 1995). This surface energy differential is known as *interfacial tension* and is a controlling factor in *wettability*. Figure 26 indicates that the wetting fluid has a smaller contact angle and covers greater surface area. For practical purposes, water is the wetting fluid observed under most field conditions within the presence of LNAPL. The wetting fluid forms a continuous layer (i.e., preferentially wets soil grains); the non-wetting fluid is found within soil pores and is surrounded by a film of water (EPA, 2005). Charbeneau (2007a) lists the *wettability* sequence as *water* → *LNAPL* → *air*. This sequence elaborates on the relative ease of an LNAPL body migrating through the vadose zone in the absence of

water as the wetting fluid. Figure 27 is a pore-scale photograph showing the wetting fluid (i.e., water) and non-wetting fluid (i.e., LNAPL) within the pore space of sand grains. Note the contact angle between the wetting fluid and non-wetting fluid is similar to that in Figure 26.

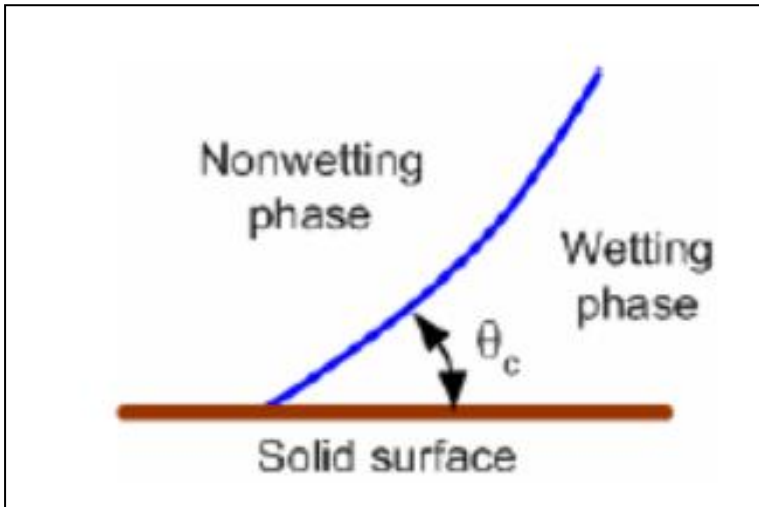


Figure 26. Wetting and non-wetting phase contact angle (Charbeneau, 2007a).

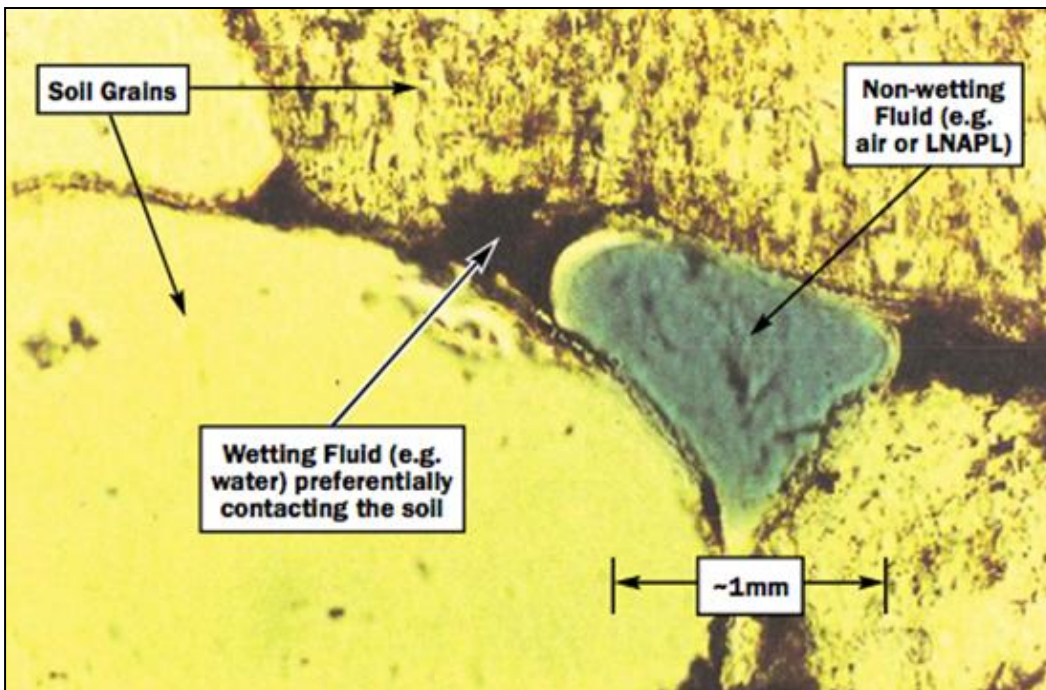


Figure 27. Pore-scale photo of wetting and non-wetting fluids (ITRC, 2013a).

The *capillary pressure* is a result of the curved interface between the wetting fluid (water) and non-wetting fluid (LNAPL), which creates a pressure differential. *Capillary pressure* indicates the relative cohesion between the two liquids and their adhesion to a solid surface (Newell et al., 1995; Charbeneau, 2007a). Bear (1972) described that *capillary pressure* is the propensity for a porous medium to attract the wetting fluid and repel the non-wetting fluid. Stated differently, a density differential exists between LNAPL and water, which results in different pressures within pore spaces (EPA, 2005). The difference in pressures between the two fluids is the *capillary pressure*, and ultimately controls the saturation distribution of LNAPL (EPA, 2005).

3.1.2 Capillary Pressure Curves

Capillary pressure tends to have an inverse relationship with pore size such that higher *capillary pressures* are typically observed in finer-grained soils. This relationship is a result of fine-grained soil exhibiting smaller pore sizes, which means lower water content and higher interfacial tension. Thus, LNAPL retention and capacity for transport is highly dependent on *capillary pressure*. Figure 28 is a *capillary pressure curve*, also known as the characteristic curve, which illustrates that increasing saturations of a non-wetting fluid in a porous medium – initially saturated with a wetting fluid – will force both fluids into smaller pore spaces. The result is a higher concentration of the non-wetting fluid and lower concentration of the wetting fluid. Conversely, decreasing the *capillary pressure* will result in the fluid interface to move into larger pore space, increasing the wetting saturation and decreasing the non-wetting saturation.

Capillary pressure curves have been developed through experimental observation by taking a soil completely saturated with a wetting fluid and slowly adding a non-wetting

fluid. As the non-wetting fluid is added, *capillary pressure* increases to a point where no further reduction in the wetting fluid saturation occurs. This point is known as the *wetting-phase residual saturation* and is a condition where no additional flow in the wetting fluid will occur (Charbeneau, 2007a). The specific path this follows within the *capillary pressure curve* is known as the *drainage curve*.

If this experiment is run in reverse, whereby the wetting fluid is now slowly added back into the soil, the resulting plot of *capillary pressure* as a function of saturation forms an *imbibition curve*. The difference between the *drainage and imbibitions curves* exhibits hysteresis, which means the *capillary pressure curve* is not a single function. Hysteresis in this setting is a result of variable drainage rates due to complex pore networks in a soil. As a result, the *capillary pressure curve* is dependent on the wetting *and* drainage history of the porous medium (Charbeneau, 2007a). Figure 28 illustrates a capillary pressure curve derived from this experiment. Note the higher saturations of the *drainage curve* and lower saturations of the *imbibition curve*, the difference of which demonstrates hysteresis. For practical applications, *capillary pressure curves* are used to identify displacement head, also referred to as pore entry pressure. Displacement head is the pressure LNAPL must overcome in order to migrate into an adjacent soil pore. As a result, fine-grained soil has higher displacement head, which suggests that LNAPL will not displace as much water when compared to coarse-grained soil, thus limiting mobility and migration.

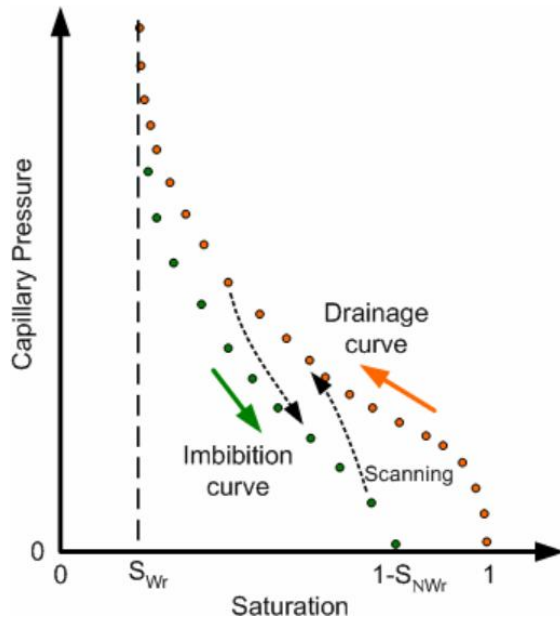


Figure 28. Lab produced capillary pressure curve showing the drainage and imbibition curves (Charbeneau, 2007a).

3.1.3 Permeability Models

Mathematical models are used to provide quantitative analysis of capillary pressure curve measurements (Charbeneau, 2007a). The van Genuchten (vG) model is most often used for soils that have been previously impacted by LNAPL. The vG model is expressed as:

$$S_e = (1 + (\alpha h^c)^N)^{-M}$$

where S_e is the *effective wetting-phase saturation* scaled from 0 to 1 and h^c is the *capillary pressure head* (van Genuchten, 1980, Charbeneau, 2007a). The vG model parameters required by the LDRM are α , N , and M . N and M are independent of α and based on one of two permeability models: Burdine (1953) and Mualem (1976). The mathematical relationship between the N and M can be described as:

$$\text{If } N > 2, \text{ then } M = 1 - 2/N \text{ (Burdine)}$$

If $N > 1$, then $M = 1 - 1/N$ (Mualem)

The parameters α and N are used to characterize soil texture where values of α (ft^{-1}) correspond to smaller pore sizes and values of N (unitless) correspond to a larger range in pore size (Charbeneau, 2007a). As such, the Mualem model is recommended for finer-grained soils, and the Burdine model is recommended for coarser soils. The LDRM corrects for potential error by requiring the Mualem model for N values greater than 2.

3.1.4 Saturation and Residual Saturation

The EPA defines LNAPL saturation as “the relative fraction of total pore space containing (LNAPL) in a representative volume of a porous medium” (Newell et al., 1995, p. 50). LNAPL saturation above the residual saturation is considered mobile and potentially recoverable through liquid recovery technologies such as MPE (Jeong and Charbeneau, 2014). Mobile and recoverable LNAPL is also known as free-product, which exists at saturations exceeding residual (Charbeneau, 2007a). However, mobile LNAPL is not always recoverable LNAPL, the former representing all free-product, and the latter representing free-product potentially recoverable given a specific remediation technology. Residual saturation is the theoretical endpoint of hydraulic LNAPL recovery that is rarely achieved on a field scale (EPA, 2005).

Residual saturation for LNAPL is a similar concept to the *wetting-phase residual saturation* described in the previous section. When LNAPL spreads through the formation, some fraction is left behind as residual. At residual saturations, an LNAPL mass becomes discontinuous and is rendered immobile due to capillary forces. However, LNAPL saturations observed in the field are significantly less than laboratory values indicated in Figure 29. In fact, LNAPL-water capillary pressures in the field are generally

too small to reproduce the *drainage curve* in Figure 28. Charbeneau (2007a) suggests that the maximum LNAPL saturations observed in the field are actually less than the residual LNAPL saturations as determined through experimental procedures indicated in Figure 28. As previously discussed, maximum LNAPL saturations in the field have been observed to range as low as 2% in fine-grained soils, and as high as 56% in coarse-grained soils (RTDF, 2006). Experimental evidence has shown that residual LNAPL saturation has a linear relationship with initial LNAPL saturation, as illustrated in Figure 29.

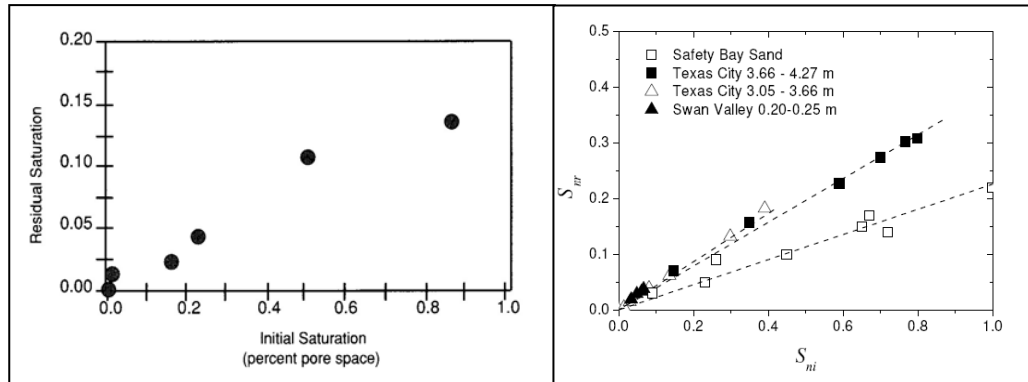


Figure 29. Residual LNAPL saturation as a function of pore size (Charbeneau, 2007a).

This has significance for LNAPL remediation at those sites exhibiting initial high saturations since a larger fraction will remain in the soil after recoverable LNAPL has been removed. Residual LNAPL is not recoverable through standard liquid recovery technologies (Jeong and Charbeneau, 2014). While generally immobile, residual LNAPL can become a long term source of dissolved phase contaminants in groundwater (Beckett and Lundegard, 1997). Figure 30 illustrates the characteristic saturation distribution curve while highlighting the residual and recoverable LNAPL fractions.

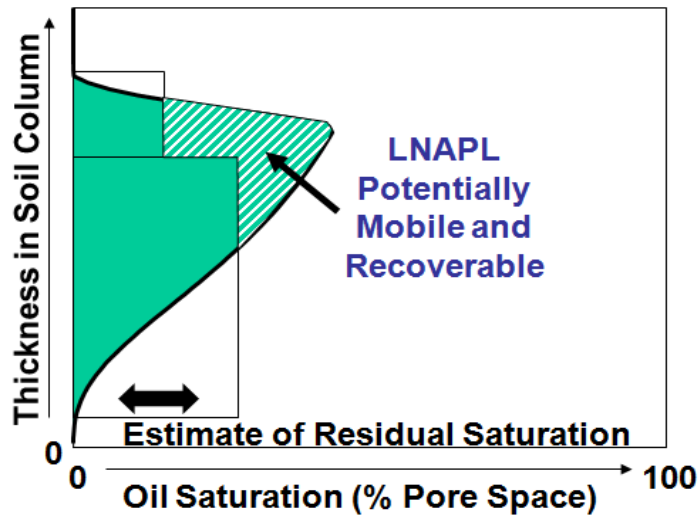


Figure 30. Characteristic LNAPL saturation distribution curve depicting residual and recoverable LNAPL (ITRC, 2013b).

3.2 LNAPL MOBILITY

The mobility and recoverability of LNAPL in subsurface soils is a function of LNAPL saturation (Beckett and Lundegard, 1997; Charbeneau et al., 2000; Adamski et al., 2005; ITRC, 2013b). In order for LNAPL to migrate as the non-wetting fluid, it must be present in sufficient saturations to overcome the capillary pressure in the adjacent pore space. In other words, it takes pressure for LNAPL to migrate into and out of soil pores (ITRC, 2013a). The minimum pressure required for LNAPL to enter a pore is called the pore entry pressure (Newell et al., 1995). The previous discussion on capillarity highlights the nature of LNAPL migration potential within a porous medium. The LNAPL (non-wetting) saturation must be sufficiently high to overcome the water (wetting) capillary pressure in order to migrate. Stated differently, if LNAPL saturation is sufficiently high, it can potentially overcome the displacement head or pore entry pressure in the adjacent soil pore, thus allowing for migration. In simplistic terms, a pressure differential has to exist between the LNAPL and water such that the LNAPL can “push”

the water out of a pore and take its place. Figure 31 is a simplified pore-scale illustration where P_{PE} is the pore entry pressure and P_{NC} is the NAPL capillary pressure. At the top of the image, P_{NC} is less than P_{PE} and therefore the non-wetting fluid (LNAPL) does not enter the pore. The bottom portion illustrates P_{NC} exceeding P_{PE} and the subsequent LNAPL migration through the pore throat and into the adjacent soil pore.

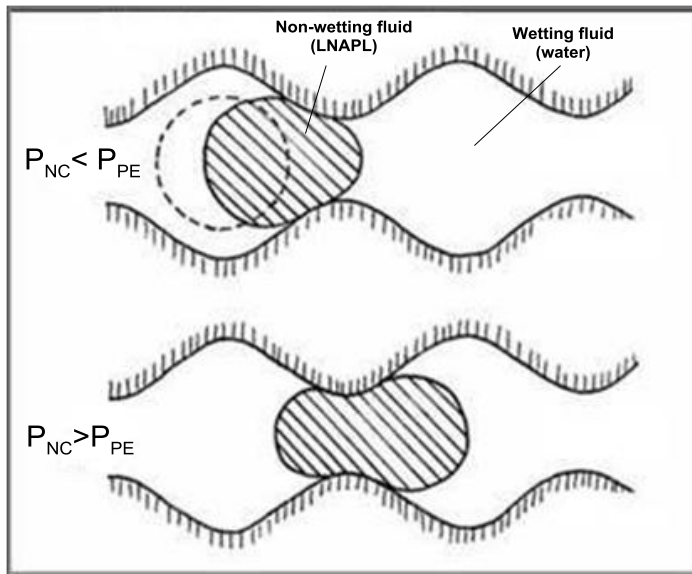


Figure 31. Illustration of LNAPL entering adjacent pore (adapted from ITRC, 2013b).

3.2.1 Darcy's Law

Fluid migration in porous media is described using Darcy's Law, which can also be used to describe LNAPL movement (Charbeneau, 2007a):

$$q_n = K_n i_n \quad (\text{Eq. 1})$$

where q_n is the NAPL flux (darcy velocity), K_n is the NAPL hydraulic conductivity, and i_n is the NAPL hydraulic gradient. The LNAPL hydraulic conductivity is a function of fluid density, viscosity, and intrinsic permeability. Charbeneau (2007a) introduces a variant to

Equation 1 that also factors water properties, effects of buoyancy, and capillary pressure gradient:

$$q_n = \frac{K_{ws}k_{rn}(S_w,S_n)}{\mu_r} \left[(1 - \rho_r)k - \frac{\nabla P_{c[nw]}}{\rho_w g} + J_w \right] \quad (\text{Eq. 2})$$

where K_{ws} is the water saturated hydraulic conductivity, k_{rn} is the LNAPL relative permeability, S_w, S_n are the water and LNAPL saturations, and μ_r is the viscosity ratio.

The right side of the equation represents the driving force for LNAPL migration where $(1 - \rho_r)$ is associated with buoyancy, $k - \frac{\nabla P_{c[nw]}}{\rho_w g}$ is associated with capillary pressure gradient, and J_w is related to the tendency for LNAPL to migrate in the direction of groundwater flow. Equation 2 essentially states that LNAPL will flow toward decreasing capillary pressure and generally in the same direction as groundwater flow.

Generally speaking, LNAPL mobility is inversely proportional to viscosity and dependent on the relative permeability of both LNAPL and water, which itself is a function of respective fluid saturations. In order for LNAPL as the non-wetting fluid to migrate, it has to overcome the pore entry pressure of the adjacent water-filled pore, thus displacing the wetting fluid. This process occurs predominantly in the saturated zone and typically requires a positive capillary pressure. However, in the vadose zone LNAPL is often present as the wetting fluid with respect to air, the non-wetting fluid. Due to gravitational forces and the surface energy found along the wettability interface (Figure 16 and 17), LNAPL will readily overcome the displacement entry pressure in air-filled pores and flow down through the formation. This process slows or stops as LNAPL contacts water-filled pores, which requires a much higher displacement entry pressure for LNAPL flow.

3.3 MODEL PARAMETERS

The LDRM requires four categories of parameters to run the full model simulation. The categories include 1) LNAPL thickness and elevations, 2) fluid characteristics, 3) capillary and petrophysical properties, and 4) recovery properties. Table 2 presents a detailed list of the parameters required by the LDRM to estimate LNAPL distribution as specific volume and LNAPL recovery as recoverable volume.

TABLE 2. PARAMETERS REQUIRED TO ESTIMATE LNAPL DISTRIBUTION AND RECOVERY

Thickness, Elevations, Vertical Gradient		Fluid Characteristics
Maximum monitoring well LNAPL thickness (ft)		LNAPL density (gm/cc)
Depth of ground surface (datum)		LNAPL viscosity (cp)
Water table depth (ft)		Air/water surface tension (dyne/cm)
Depth of soil facies interface (ft)		Air/LNAPL surface tension (dyne/cm)
Water vertical gradient		LNAPL/water interfacial tension (dyne/cm)
Capillary and Petrophysical (Soil) Properties		
Porosity		Hydraulic conductivity (ft/d)
van Genuchten N		van Genuchten α
Irreducible water saturation		Residual LNAPL saturation
Recovery Properties		
Recovery time (yr)	Radius of influence (ft)	Vacuum pressure (-atm)
Radius of recovery well (ft)	Water production rate (gpm)	Screen length (ft)
Radius of recovery (ft)	Water saturated thickness (ft)	Air radius of capture (ft)

3.4 MODEL ASSUMPTIONS

The basic assumption of the LDRM is that LNAPL is unconfined and at vertical equilibrium. Jeong and Charbeneau (2014) indicate that vertical equilibrium is essential so the LNAPL distribution can be estimated directly through measurements of air-LNAPL and LNAPL-water interfaces within a monitoring well. Charbeneau (2007b) and Jeong and Charbeneau (2014) list several key assumptions critical to the LDRM, which are provided below in order of relative importance:

- Uniform radial distribution of LNAPL adjacent to a recovery well
- Uniform drainage of LNAPL to a recovery well during recovery
- All LNAPL within the radius of recovery will be captured by the recovery well
- LNAPL recovery is estimated with steady-state radial flow equations
- Heterogeneity of soils and fluid properties is not considered
- Hydraulic gradient outside the radius of recovery is flat (i.e., zero)
- Groundwater and LNAPL gradients produced through vacuum are averaged across the recovery domain
- LNAPL conductivity is averaged across the vertical saturation distribution and radially uniform through the radius of recovery
- LNAPL is under vertical equilibrium and has been considered to be in place prior to recovery
- Interference from multiple recovery wells is not considered
- Hysteresis is not explicitly considered
- Recovery well efficiency is 100%

3.5 MODEL INTERFACE

The LDRM is a Windows-based program that is downloaded at no cost from the American Petroleum Institute's website (www.api.org). Once installed, the user has the option to open an existing simulation or start a new simulation. If "New Simulation" is chosen, the program opens the "Project Setup" window, as shown in Figure 32.

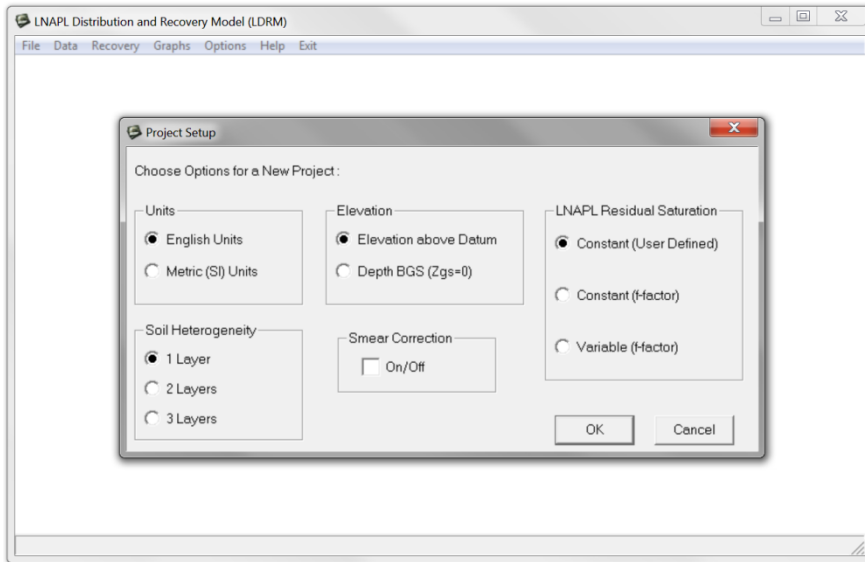


Figure 32. Project Setup window for the LDRM.

The "Project Setup" window displays options for units, number of soil layers, elevation datum, LNAPL smear correction, and LNAPL residual saturation.

After the setup has been completed, the user presses "OK" and progresses to the primary "Data Input" window as shown in Figure 33. The "Data Input" window requires all non-recovery parameters listed in Table 2, which are required to calculate the LNAPL specific volume.

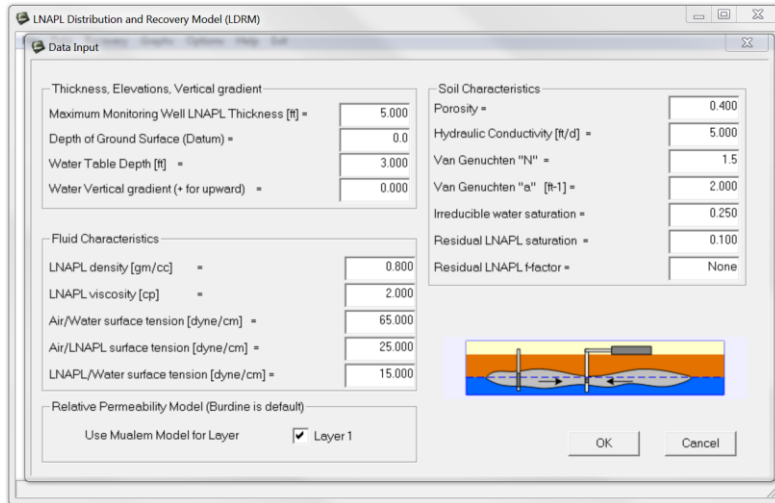


Figure 33. Primary “Data Input” window for the LDRM.

Once the “Data Input” window has been populated, the user presses “OK,” which results in the basic output window that includes the modeled LNAPL specific volume and LNAPL recoverable volume, which is displayed as Figure 35 in Section 3.5.1. At this point the user has the option to model LNAPL recoverable volume with various remediation technologies over a specified period of time. In order to accomplish this, “Recovery” is chosen from the Menu Bar and either “Well” or “Trench” is chosen. Figure 34 displays the “Well Recovery Systems” input window.

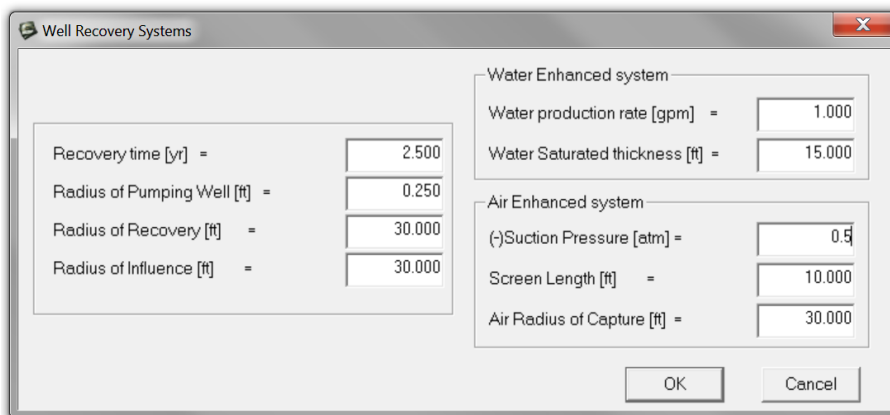


Figure 34. Well Recovery Systems window.

3.6 MODEL OUTPUT OPTIONS

Depending on input scenario, the LDRM will calculate several parameters including specific volume, recoverable volume, residual or non-recoverable volume, LNAPL transmissivity, and LNAPL discharge. The output values are expressed as a function of time (i.e., initial and after a chosen recovery period), and can be used to predict various recovery scenarios. Even though LDRM output values relate to a single monitoring or recovery well, values from multiple monitoring wells can be integrated across the area of a site to produce or refine a conceptual site model. Output options can be configured to include graphical and detailed tabular formats. The LDRM has options to model skimmer, trench, single- or dual-pumping, and vacuum-enhanced recovery systems. This study focuses on vacuum-enhanced recovery, which is a non-specific term for multiphase extraction (EPA, 1999).

3.6.1 Initial Output

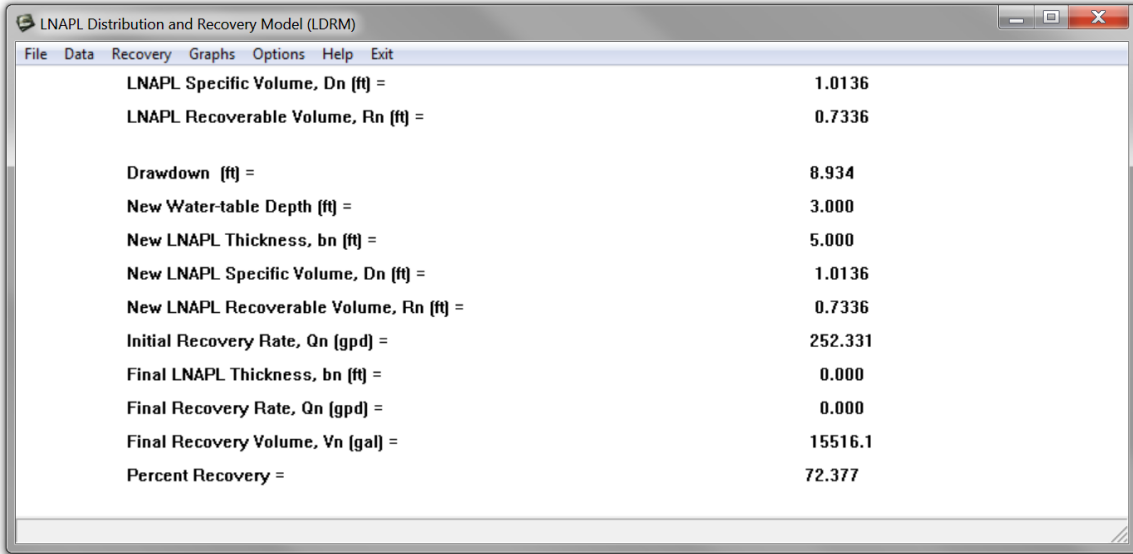
Figure 35 is the initial LDRM output window that appears once the “Data Input” window has been completed. Both specific volume and recoverable volume are given in units of feet, which as described previously is a simplification from ft^3/ft^2 .

LNAPL Specific Volume, Dn (ft) =	1.0136
LNAPL Recoverable Volume, Rn (ft) =	0.7336

Figure 35. Initial output window.

3.6.2 Recovery Output

Once the “Well Recovery Systems” window has been populated, as displayed in Figure 34, the LDRM will provide an advanced recovery output as presented in Figure 36 below. Several additional calculations are provided including drawdown, percent recovery, and final recovery volume. A .txt file can be saved upon completion of the “Well Recovery Systems” window and subsequent advanced recovery output. The .txt file contains all input values and detailed time-series data in tabular format.



The screenshot shows a window titled "LNAPL Distribution and Recovery Model (LDRM)" with a menu bar containing "File", "Data", "Recovery", "Graphs", "Options", "Help", and "Exit". The main area displays a list of calculated parameters and their values:

LNAPL Specific Volume, Dn (ft) =	1.0136
LNAPL Recoverable Volume, Rn (ft) =	0.7336
Drawdown (ft) =	8.934
New Water-table Depth (ft) =	3.000
New LNAPL Thickness, bn (ft) =	5.000
New LNAPL Specific Volume, Dn (ft) =	1.0136
New LNAPL Recoverable Volume, Rn (ft) =	0.7336
Initial Recovery Rate, Qn (gpd) =	252.331
Final LNAPL Thickness, bn (ft) =	0.000
Final Recovery Rate, Qn (gpd) =	0.000
Final Recovery Volume, Vn (gal) =	15516.1
Percent Recovery =	72.377

Figure 36. Advanced LDRM recovery output window.

3.6.3 Graphical Output

The LDRM provides additional graphical output options based on the tabular data provided in the .txt file. Primary options include specific volume, recovery, and transmissivity; saturation; and recovery rate, which are presented in Figures 37, 38, and 39, respectively.

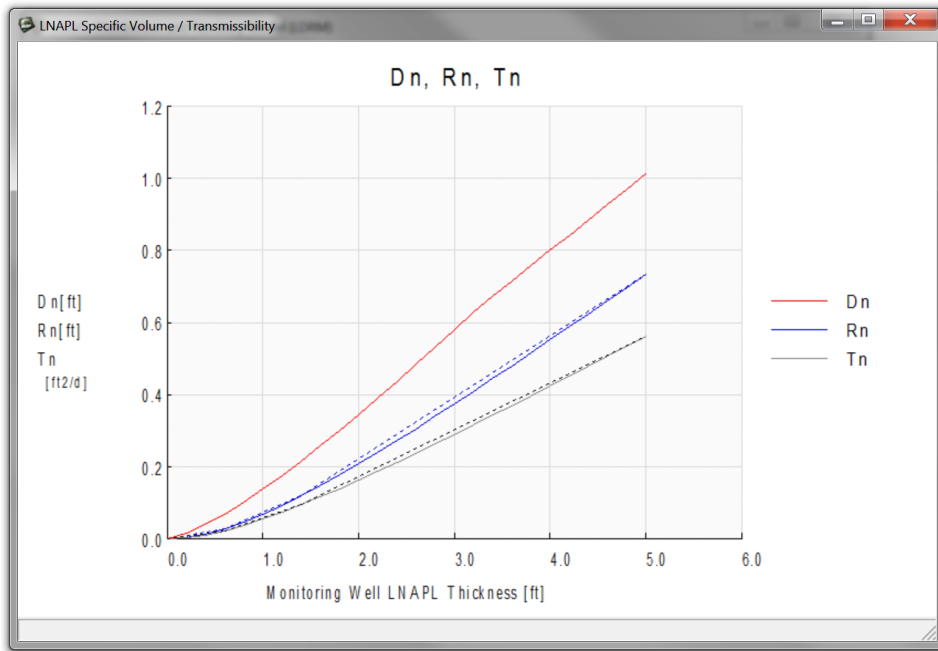


Figure 37. LDRM graphical output: specific volume, recovery, transmissivity.

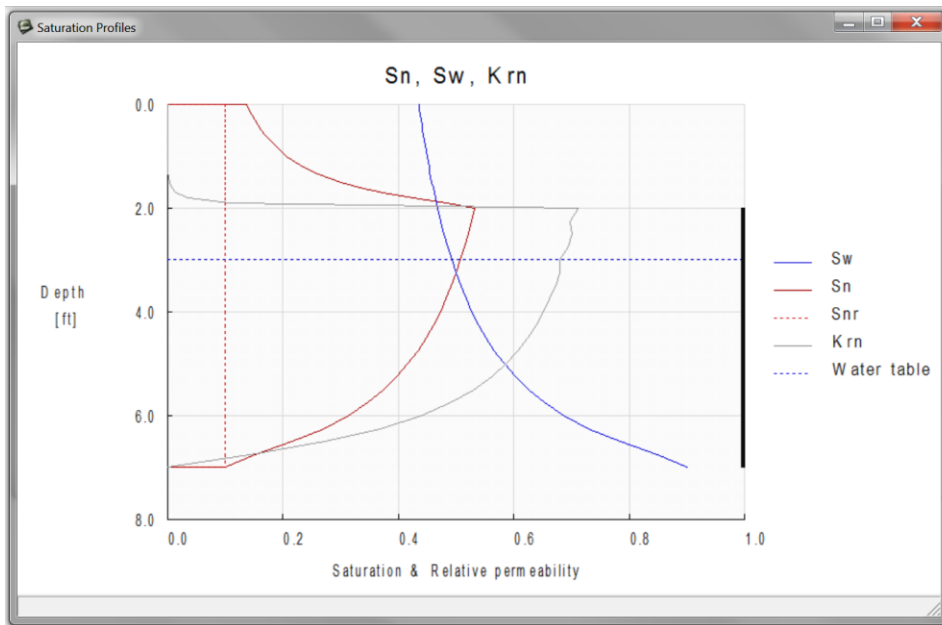


Figure 38. LDRM graphical output: saturation profiles.

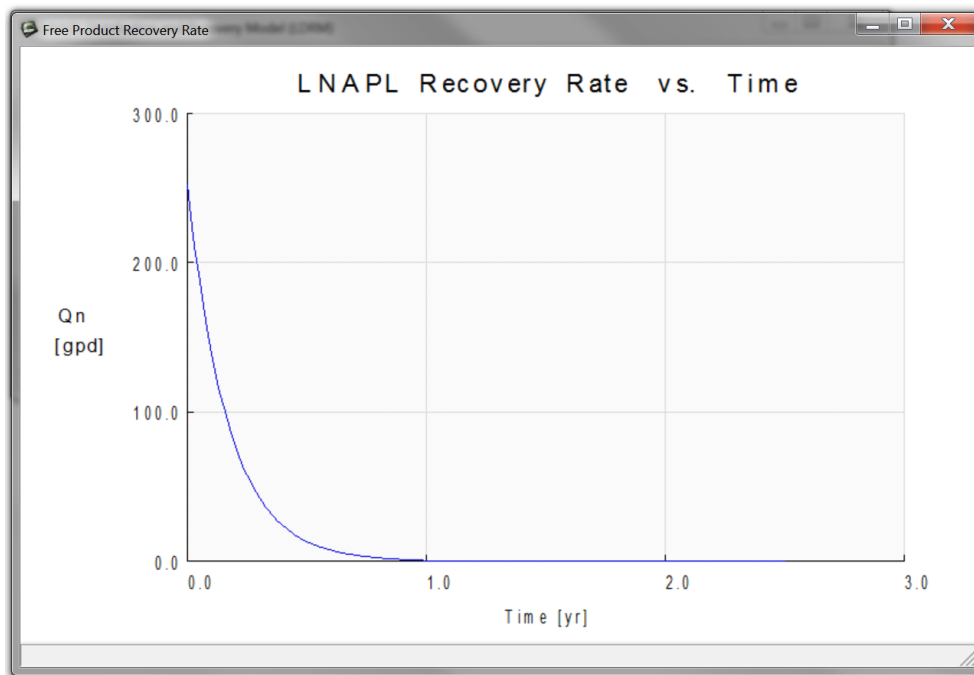


Figure 39. LDRM graphical output: LNAPL recovery rate.

CHAPTER 4: RESEARCH SITES

The research sites were chosen based on several factors including: 1) the author's intermittent field experience at each site, 2) the availability of data through the author's previous and current site experience, site representatives, and the public domain, 3) similarities in remediation technology, and 4) the large discrepancy between initial LNAPL estimates and actual recovery at both sites. Additionally, the heterogeneous soil of Site A as compared with the relative homogenous sand of Site B can assist in highlighting the nature of LNAPL contamination and recovery in these settings.

Each site is under a state and federal consent order to prevent LNAPL discharge to surface water, remove free-phase LNAPL (i.e., free-product) in subsurface soils to the "maximum extent practicable," and reduce dissolved-phase contaminants below regulatory limits. Per the consent orders, each site shall continuously operate a remediation system to achieve regulatory requirements. However, while both sites have approached asymptotic recovery rates of free-product, both continue to experience regular LNAPL seeps and sheen on adjacent canals. Additionally, each site continues to exhibit gauged product thicknesses that range from 0.01 feet to over 1.0 foot, as well as dissolved-phase contaminant concentrations that exceed regulatory limits.

4.1 SITE A

Site A is an active 50-acre railroad maintenance yard that is located in an industrial/commercially-zoned urban environment and bound to an engineered canal by vertical steel sheet pilings (Figure 40). The site was constructed in the early 20th century and has operated as a railroad maintenance yard for the duration of its existence. Prior to the 21st century, the site received diesel shipments from barges via a fuel unloading dock

along the sheet piling. The diesel was held in two, 2.5-million gallon aboveground storage tanks (ASTs) adjacent to the dock. The ASTs were eventually removed and replaced with one, 450-thousand gallon AST (AMEC, 2010).

Site investigations discovered weathered diesel contamination of subsurface soils, which was observed predominantly in the area of the former ASTs. In 2005 an approximate 0.5-mile long sheen was observed on the adjacent canal and subsequently traced back to the site. The site was placed under a consent order in 2006 requiring the prevention of additional discharges and the remediation of the petroleum hydrocarbon contamination (AMEC, 2010). A detailed site map that includes monitoring and recovery well designations and locations is presented in Appendix A.

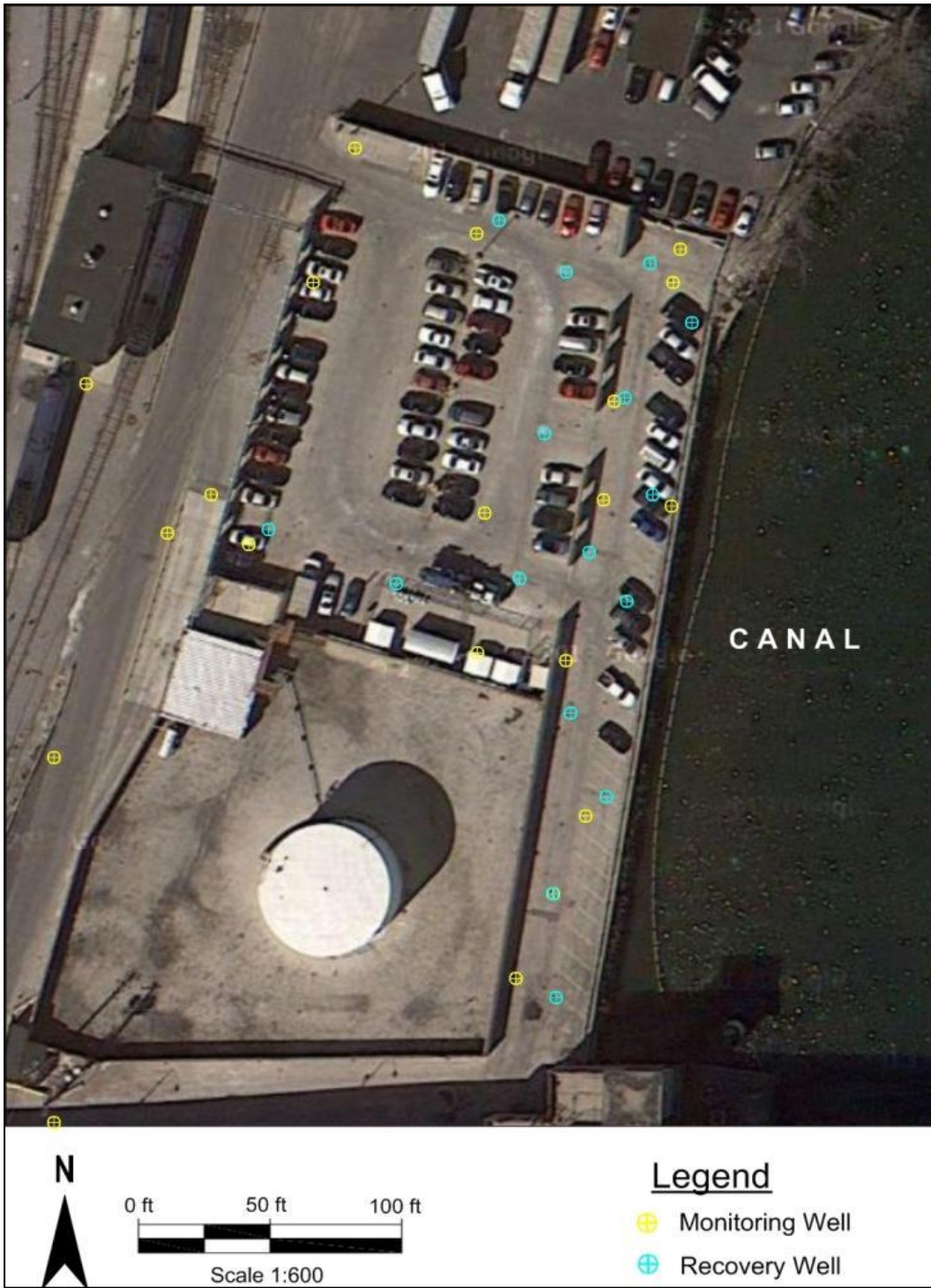


Figure 40. Site A remediation area.

4.1.1 Geology

Site A surface features generally consist of limestone ballast, concrete and weathered bituminous asphalt underlain by heterogeneous fill material associated with late 19th century fire and demolition debris. The site exhibits surface gradients typically less than 2%, consistent with urban railroad operations in the United States.

The remediation area is located within the containment area associated with the former northernmost 2.5-million gallon AST. This area is now a parking lot consisting of cracked and weathered asphalt underlain by a limestone sand and gravel sub-base. The sub-base is underlain by heterogeneous fill material exhibiting a grain-size distribution similar to till, with the exception of coarse gravel as defined by the Unified Soil Classification System. The fill material is associated with century-old fire and demolition debris and contains brick, wood, clinkers and slag.

The fill layer within the remediation area extends to approximately four feet below ground surface (bgs), grading into a silty clay of indeterminate origin (i.e., native or non-native). The silty clay exhibits varying degrees of fine- to coarse-grained sand and fine gravel and is frequently classified as sandy clay in historical soil boring logs. The sandy, silty clay layer terminates at approximately 10 to 12 feet bgs where it is underlain by a native, lean silty clay to clay confining layer. Based on regional investigations and drilling activities in other areas of Site A, the native clay is underlain at approximately 100 feet bgs by Silurian dolomite.

Groundwater within the remediation area is encountered at approximately 6 feet bgs to the west and 10 feet bgs to the east along the canal. Hydraulic conductivities measured through slug and baildown tests range from 0.060 to 0.200 ft/day. For purposes

of modeling, the native clay layer beginning at approximately 12 feet bgs is assumed to be confining, thus resulting in hydraulic head that ranges from approximately 6 feet to the west and 2 feet to the east. Soil boring logs are presented in Appendix D.

4.1.2 Nature and Extent of Contamination

Site A has a free-product plume footprint of approximately three acres with the remediation area covering an area of approximately 1.2 acres, which is defined by the approximate extents of recovery well radius of recovery. The majority of the LNAPL appears to be weathered diesel several decades old, but fingerprinting analysis has indicated the presence of less-weathered low sulfur diesel and trace amounts of kerosene.

Historical records indicate that the failure of two, 2.5-million gallon ASTs and underground fuel transfer lines resulted in diesel discharges to the underlying soils, groundwater, and adjacent canal (AMEC, 2010). Historical records do not indicate a volume estimate for total LNAPL in the subsurface. However, it is apparent that contamination at the site is not a result of catastrophic failure, but of periodic minor spills and long-term intermittent leaking from ASTs and fuel transfer lines.

4.1.3 Remediation System

In order to comply with consent order requirements, an MPE system, consisting of a liquid ring vacuum pump and 16 recovery wells, was installed in 2008. The recovery wells consist of 6-inch diameter, schedule 40 PVC with 0.002 inch slots through the screened interval. The well lengths extend approximately 15 to 17 feet bgs and consist of 10-foot screens. Within each recovery well is a one-inch PVC drop-tube or “stinger,” which is connected to the vacuum through underground recovery piping.

Typical operation of the MPE system consists of only two recovery wells operating concurrently for approximately one hour. Each recovery well pair is connected to one of eight solenoid valves that control the application of vacuum to each recovery well. The vacuum pump is rated at 26 inHg (0.87 atm), but initial vacuum ranged between 20-24 inHg (0.67-0.80 atm). Initial vacuum pressure at each recovery well ranged from 18-20 inHg (0.60-0.67 atm) and had decreased to approximately 10-15 inHg (0.33-0.55 atm) after three years of operation.

4.1.4 LNAPL Estimates and Recovery

Total free-product in the subsurface does not appear to have been estimated at Site A. Recoverable product through the remediation system was estimated at 15,000 gallons with asymptotic recovery rates projected after two to three years of operation. Between initial start-up in January 2009 and March 2013, the remediation system recovered a reported 2,700 gallons of product and 991,000 gallons of impacted groundwater. Based on the MPE system cycling at two recovery wells per hour for the duration of operation, each recovery well had an average runtime of 0.19 years and an approximate groundwater discharge rate of 1 gal/min.

While reported product recovery from start-up through March 2013 was approximately 2,700 gallons, a review of historical records and interviews with site personnel indicated that the MPE system actually only removed an estimated 1,500 gallons of product. The 2,700 gallon estimate is based on additional product manually removed from monitoring wells and significant volumes of sludge accumulation at the bottom of process tanks. Inefficient skimming of recovered product from the oil-water separator also resulted in overestimation of LNAPL recovery by the MPE system.

4.2 SITE B

Site B is an approximately 95-acre active bulk oil storage facility located in an area of mixed-used zoning and bound to an engineered canal to the north and east by vertical steel sheet pilings (Figure 41). The site was first developed in the early 20th century as a petroleum refinery and continued in this manner until it was dismantled in the 1980s. It has remained an oil storage operation since the refinery decommissioning. State and federal officials observed free-product on both stretches of canal (i.e., north and east), which was traced back to the site. A 2001 federal administrative order required the prevention of additional discharges and the remediation of the petroleum hydrocarbon contamination (Parsons, 2002). A detailed site map that includes monitoring and recovery well designations and locations is presented in Appendix A.



Figure 41. Site B site map.

4.2.1 Geology

Site B surfaces generally range from areas of non-vegetated sandy fill to relatively dense brush and trees. Compacted limestone gravel road surfaces are found throughout the site and serve as vehicular access to the various ASTs and respective containment dykes. Topographic gradient across the site is generally less than 2%.

The geology within the remediation areas (north and southeast) consist of well-graded sandy fill with fine- to medium-grained gravel. The fill layer terminates at approximately 4 feet bgs and is underlain by native well-graded sand deposits of glacio-lacustrine origin. The well-graded sand is underlain by a lean clay confining layer at approximately 30 feet bgs with a coefficient of permeability that ranges from 4.5×10^{-3} to 7.9×10^{-5} ft/d (1.6×10^{-6} cm/s to 2.8×10^{-8} cm/s) (Parsons, 2009). Detailed soil characterization and grain-size distribution is presented in Appendix D.

Groundwater throughout the site is encountered from approximately 4 to 6 feet bgs to 8 to 10 feet bgs near the canal. Groundwater flow is generally toward the canal. However, past groundwater contouring by hand and current contouring through digital kriging interpolation indicates a more complex flow regime. This does not pose major concern for purposes of this research, but does have significance for plume management. Aquifer tests conducted in the mid 1990s indicated that transmissivity ranged from 650 to 1,050 ft²/day (Groundwater Technology, 1993).

4.2.2 Nature and Extent of Contamination

Historical records indicate subsurface investigations at Site B took place as early as 1993. A 1995 site investigation indicated the presence of gauged LNAPL throughout most of the site from 0.01 feet to over 4 feet thick. Based on LNAPL thickness

contouring of historical gauging events at Site B, the LNAPL plume (free and residual) footprint covers the majority of the site. However, based on a lack of data and a complex groundwater flow regime, the dissolved-phase plume has not been accurately delineated. Contaminant sources at the site consist of historical spills and the leaking of ASTs and underground pipeline (Parsons, 2002). The LNAPL ranges from highly weathered diesel and gasoline dating back to the mid 1900s to less-weathered diesel released within the last decade. The June 1995 gauging event is believed to present the greatest apparent LNAPL thicknesses, which is significant for purposes of running the LDRM.

4.2.3 Remediation System

In order to comply with the federal administrative order, an MPE system was commissioned in June 2001 and continues to operate during the present day. The MPE system consists of a north and southeast remediation area, each area operated by a separate vacuum pump. The north remediation area consists of 11 recovery wells running east-west along the canal and another seven branching to the east-southeast. The southeast remediation consists of 12 recovery wells, eight of which run north-south along the canal.

MPE system operation consists of the vacuum application to all 30 recovery wells concurrently. The vacuum pumps are rated at 26 inHg (0.87 atm), but current vacuum at each pump ranges between 10-22 inHg (0.33-0.74 atm). Current vacuum at each recovery well ranges from 0-15 inHg (0.00-0.55 atm). Typical mechanical efficiency losses and clogged filter packs and well screens have substantially reduced vacuum rates from system commission in June 2001 through June 2013, which represents the recovery timeline reported in this research.

4.2.4 LNAPL Estimates and Recovery

Between June 2001 and June 2013, approximately 65,000 gallons of free-product and 838,000,000 gallons of impacted water were reportedly recovered by the MPE system. However, product volume is believed to be an overestimation by over a factor of four. As presented previously, Figures 24, 25, and 39 exhibit the typical asymptotic recovery trend as theorized by multiphase theory and demonstrated through field data. However, Figure 41, which represents the recovery rate at Site B, remains relatively constant over the 12 year period.

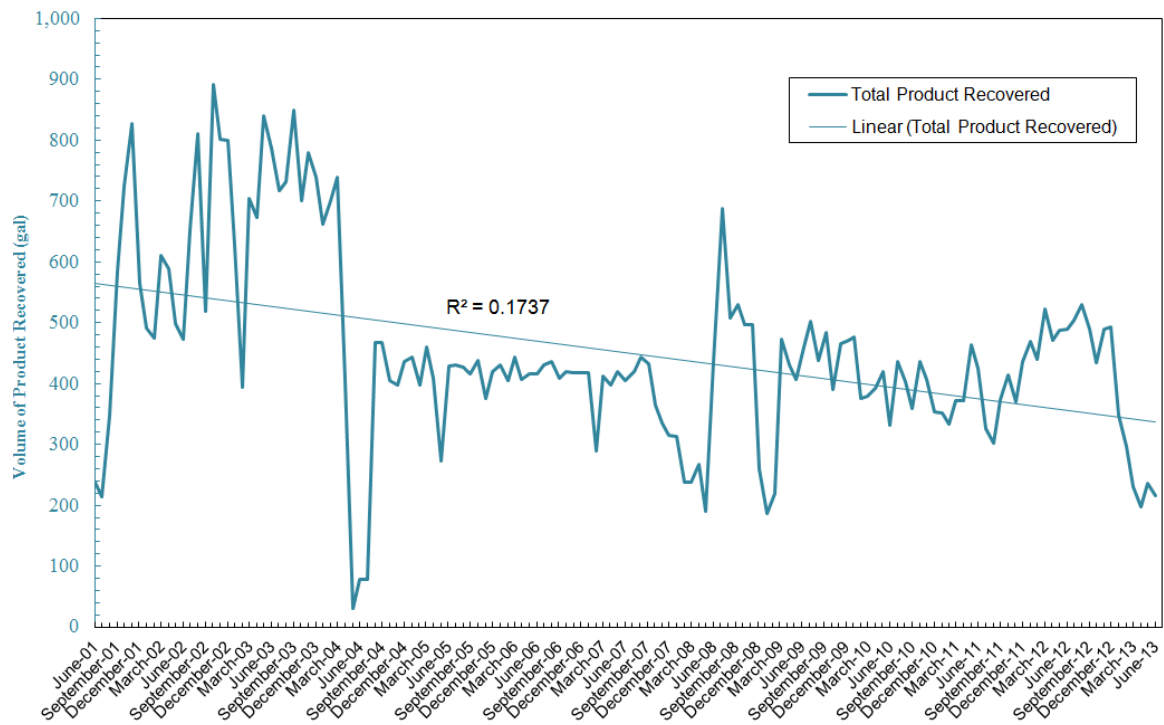


Figure 42. Site B LNAPL recovery rate from June 2001 to January 2014.

After reviewing recovery data, it appears the equation used to calculate product recovery contained flawed data. Product recovery at the site has historically been calculated by the following equation (Parsons, 2014):

$$Product\ Volume = \frac{\left(\frac{Treated}{Water\ Volume} \right) \times 3.78 \left(\frac{Influent - Effluent}{Oil\ and\ Grease\ Concentration} \right) \times 0.8}{1000 \times 454 \times 8.34} \quad (Eq. 3)$$

The effluent oil and grease concentration is sampled once per month as required by the discharge permit. However, influent oil and grease concentration has not been sampled regularly or possibly at all in over a decade. Despite the inherent accuracy problems in estimating recovered product volume with Equation 3 – such that it assumes a homogeneous emulsification of the grab sample – the influent concentration does not appear to have been sampled between December 2001 and July 2013. Through that period, the influent oil and grease concentration is reported as 100 mg/L every month. Influent oil and grease was sampled twice in late 2013 as part of an updated site investigation. Both samples resulted in non-detectable concentrations of oil and grease with a laboratory detection limit less than 4 mg/L. Visual observations of influent from July 2013 through March 2014 also confirm that no free-product is being recovered by the system. Additionally, the on-site operation and maintenance manager for the last 11 years has indicated that he has no recollection of the 20,000 gallon recovered product AST being emptied during this time. This AST currently has less than 15,000 gallons of product and water. Based on this information, the recovery of product at Site B (north and southeast remediation areas) likely reached asymptotic rates one to two years after

start-up in June 2001. Thus, an estimated 15,000 gallons of recovered product between June 2001 and June 2013 is used as a basis for LDRM comparison.

Pre-remedial free-product was estimated at 82,000 gallons, which was based on historical gauging data. However, this estimate was calculated with the Gruszczenski model previously discredited by Farr et al. (1990) and Lenhard and Parker (1990). The estimated 82,000 gallons of free-product is based on the incorrect assumption that FNT is only 10% of ANT. It is unlikely that pre-remedial free-product corresponded with an “uncorrected” estimate of 820,000 gallons; rather, the volume likely lied between those two extremes. Estimating pre-remedial free-product is not the objective of this thesis. However, for comparative purposes, the “uncorrected” estimate of 820,000 gallons of free-product at the site is used as a reference for estimated recoverable product.

Recoverable product generally refers to the portion of total free-product that is potentially recoverable through a given remediation technology or recovery well. As such, the “uncorrected” estimate factored over the approximate area covered by all recovery wells was used as the pre-remedial recoverable product estimate. The remediation areas cover approximately 15% of Site B, which translates to a pre-remedial recoverable product estimate of 123,000 gallons

CHAPTER 5: LDRM METHODS

The objective of this thesis is to determine if pre-remedial modeling at the two research sites could have prevented approximate order-of-magnitude errors in recoverable product. Therefore, historical records from each site were reviewed to determine if adequate data were available to run and calibrate the LDRM while providing a thorough defense of LDRM input values. Through this process it is the intention to gain an insight on the general utility of the LDRM as a cost-effective and accurate alternative to expensive and complex site investigations and numerical models. A general procedural outline for the LDRM at each research site is listed below:

- 1) Review of available site data
- 2) Estimation of LDRM input values from existing site data and empirically based comparisons
- 3) LDRM simulation with nominal values based on initial estimates
- 4) Sensitivity analysis
- 5) Model calibration and correction of maximum LNAPL thickness
- 6) Determination of input value range that corresponds to maximum and minimum LNAPL distribution and recovery scenarios
- 7) LDRM output for maximum and minimum scenarios

5.1 INPUT PARAMETER VALUES

5.1.1 Available Data

Abundant multi-year data exists for each research site, which was collected from initial site investigations to ongoing remediation system operation and maintenance, and continued through active site monitoring. Table 3 is a summary of available data from each site as determined through a review of historical records.

TABLE 3. SUMMARY OF AVAILABLE SITE DATA

Data Category	Site A	Site B
Monitoring well gauging	Depth-to-water and depth-to-product measurements; monthly from 2006 to present	Depth-to-water and depth-to-product measurements ; semi-annual to quarterly from 1993
Soil boring logs	Monitoring wells	Monitoring/recovery wells
Geotechnical	Approximately 5 locations outside remediation area	Approximately 15 locations along remediation areas; grain-size distribution, Atterberg limits, unconfined compressive strength, coefficient of permeability
Recovery wells	Construction diagrams	Construction diagrams
LNAPL properties	Fluid type	Fluid type and specific gravity
Aquifer testing	Slug and baildown	72-hour pump test, slug
Site Figures	Georeferenced figure of monitoring and recovery well network	Georeferenced figure of monitoring and recovery well network
MPE system	Groundwater discharge, recovered product, run-time, vacuum gauging, drawdown,	Groundwater discharge, recovered product, run-time, vacuum gauging, drawdown
Analytical	Semi-annual for VOC, SVOC, and RCRA metals	Annual for BTEX and MTBE
Reports	Monthly, semi-annual, and remediation program	Quarterly compliance update

Based on the available data, the LDRM input parameters that are known with relative certainty at each site are presented in Table 4.

TABLE 4. LDRM INPUT PARAMETERS KNOWN WITH A HIGH DEGREE OF ACCURACY

Max. LNAPL thickness (uncorrected)	Recovery time
Depth of ground surface	Radius of pumping well
Water table depth	Water production rate
Depth of soil facies	Water saturated thickness
LNAPL density	Suction (Vac) pressure
Hydraulic conductivity	Screen Length

5.1.2 Estimated Data

The remaining LDRM input parameters that require estimation are presented in Table 5. The exact method of estimation is dependent on the specific parameter and availability of related site data. For example, *maximum LNAPL thickness* is known at each research site as determined by monitoring well gauging. However, as discussed

previously, ANT under non-vertical equilibrium and varying LNAPL hydrogeologic conditions can greatly misrepresent ANT relative to the FNT. Therefore, a corrected *maximum LNAPL thickness* is estimated at each monitoring well by analyzing ANT with respect to DGPs and HSGs.

TABLE 5. LDRM INPUT PARAMETERS THAT REQUIRE ESTIMATION

Max LNAPL thickness (corrected)	van Genuchten “N”
Water vertical gradient	van Genuchten “ α ”
LNAPL viscosity	Irreducible water saturation
Air/water surface tension	Residual LNAPL saturation
LNAPL surface tension	Radius of recovery
LNAPL interfacial tension	Radius of Influence
Porosity	Air radius of capture

Alternatively, capillary characteristics including *van Genuchten N and α* , and *irreducible water saturation* are estimated by matching site-specific soil conditions with empirically derived capillary values for similar soils. Abundant data for soil and fluid properties have been collected and compiled into the API Parameter Database for use in estimating unknown input values. Additionally, the API Interactive LNAPL Guide also provides look-up tables for empirically derived values of required LDRM parameters, which are determined based on soil classification (e.g., silty clay or well-graded sand) or fluid type (e.g., diesel, gasoline, fuel oil #5). From Charbeneau (2007a), the API Database and API Guide contain the following information:

- Capillary parameters and associated raw data
- Petrophysical data such as porosity, hydraulic conductivity, water and LNAPL saturations

- Grain-size data presented in various formats including cumulative weight percentiles and percent grain-size fraction
- Fluid properties including density, viscosity, and interfacial tension

Remaining LDRM parameters that require estimation are *radius of recovery*, *radius of influence*, and *air radius of capture*. *Radius of recovery* is the areal extent of groundwater capture by a recovery well and is the basis for modeling recovery. As such, *radius of recovery* exhibits a high degree of sensitivity and accurate estimation is critical for predicting realistic LNAPL recovery. However, for MPE recovery wells utilizing vacuum pressure, the situation is simplified as compared to typical groundwater production wells. Production wells can exhibit a *radius of influence* that extends beyond a distance of 1000 feet with the corresponding *radius of capture* reaching only several hundred feet (Charbeneau, 2006). In this scenario, the *radius of influence* should always extend beyond the *radius of recovery* (Charbeneau, 2006). However, for vacuum-enhanced wells, *radius of recovery* equals the *radius of influence* and *air radius of capture* (Charbeneau, 2006). In other words, the *radius of influence* for a vacuum-enhanced recovery well limits the *radius of recovery*. In contrast to production wells, the *radius of recovery* for a vacuum well can extend to the *radius of influence*, which is typically on the order of 30 to 40 feet (Charbeneau, 2007a; Charbeneau, 2007b). Therefore, *radius of recovery* is estimated at each site on the basis that 1) *radius of recovery, influence, and air capture* are similar values, and 2) the maximum *radius of recovery* will only extend beyond 40 feet under theoretical best-case scenarios. Additionally, while recovery wells at Site B operated concurrently (i.e., vacuum applied to all wells during operation), recovery wells at Site A were cycled at two recovery wells

per hour. This cyclical recovery schedule at Site A provides a more apparent delineation of *radius of recovery* through the analysis of groundwater contours during vacuum application. More specific LDRM input estimation methodology is described in section 5.3.

5.1.3 Nominal Input Values

Nominal input values were established for each parameter based on uncorrected maximum LNAPL thicknesses, known values as determined through site-specific data, average values of published results for soils and LNAPLs, and basic estimations. Nominal input values were meant to provide a benchmark for additional LDRM simulations, as well as the basis for a detailed sensitivity analysis of every LDRM parameter. Nominal input values were determined for each research site based on the following information:

- 1) Known input values
- 2) Estimated values based on soil and fluid-matched samples in the API Database and API Guide
- 3) LDRM default values
- 4) Uncorrected *maximum LNAPL thickness*
- 5) Assumed moderate values for *radius of recovery*

The nominal LDRM input values for Site A and Site B are presented in Table 6 and Table 7, respectively.

TABLE 6. NOMINAL LDRM INPUT VALUES FOR SITE A

Site A – Railroad Maintenance Yard			
Parameter	Value	Source	Notes
Max Monitoring Well LNAPL Thickness (ft)	Variable, uncorrected	Historical gauging data	Specific to each modeling point (i.e., recovery well)
Depth Surface Datum (ft)	0	Historical gauging data	
Water Table Depth (ft)	Variable	Historical gauging data	Feet below ground surface
Water Vertical Gradient	0	LDRM default	
Depth of Soil Facies Interface (ft)	Variable	Soil boring logs, cross-sections, geotechnical data	
LNAPL Density (g/mL)	0.83	API Guide	Average for diesel
LNAPL Viscosity (cp)	2	API Guide	Average for diesel
Air/Water Surface Tension (dyne/cm)	65	LDRM Default	
Air/LNAPL Surface Tension (dyne/cm)	26	API Guide	Average for diesel
LNAPL/Water Surface Tension (dyne/cm)	26	API Guide	Average for diesel
Soil Characteristics for Fill Layer			
Porosity	0.32	API Database	Gravelly SW with silt; sample #162
Hydraulic Conductivity (ft/d)	4.2	API Database	Gravelly SW with silt; sample #162
van Genuchten “N”	1.55	API Database	Gravelly SW with silt; sample #162
van Genuchten “ α ” (ft ⁻¹)	2.38	API Database	Gravelly SW with silt; sample #162
Irreducible Water Saturation	0.29	API Database	Gravelly SW with silt; sample #162
Residual LNAPL Saturation	0.03	API Guide	Sand and Gravel
Permeability Model (Burdine/Mualem)	Mualem	LDRM Default	Dependent on “N” value. Mualem required for N<2
Soil Characteristics for varying sandy/silty clay			
Porosity	0.44	API Guide	Silty clay loam
Hydraulic Conductivity (ft/d)	0.625	API Guide	Silty clay loam
van Genuchten “N”	1.35	API Guide	Silty clay loam
van Genuchten “ α ” (ft ⁻¹)	0.46	API Guide	Silty clay loam
Irreducible Water Saturation	0.1	API Guide	Silty clay loam
Residual LNAPL Saturation	.21	API Guide	Silty clay loam
Permeability Model (Burdine/Mualem)	Mualem	LDRM Default	Dependent on “N” value. Mualem required for N<2
Recovery Characteristics			

Recovery Time (yr)	0.19	Historical records	Based on system runtime and 2 RW per hour cycle
Radius of Recovery Well (ft)	0.25	Historical records, well construction diagrams	6-inch diameter recovery wells
Radius of Recovery (ft)	35	Assumed moderate value	Review of pumping groundwater contours
Radius of Influence (ft)	35	Assumed moderate value	Review of pumping groundwater contours
Water Production Rate (gpm)	1	Historical Records	System runtime versus total recovered groundwater per recovery well
Water Saturated Thickness (ft)	Variable	Soil boring logs, cross-sections, geotechnical	
Vacuum Pressure (-atm)	0.67	Historical records	Average gauged vacuum at recovery wells
Screen Length (ft)	10	Historical records, well construction diagrams	
Air Radius of Capture	35	Assumed moderate value	Review of pumping groundwater contours

TABLE 7. NOMINAL LDRM INPUT VALUES FOR SITE B

Site B – Bulk Oil Storage Facility			
Parameter	Value	Source	Notes
Max Monitoring Well LNAPL Thickness (ft)	Variable, uncorrected	Historical gauging data	Specific to each modeling point (i.e., recovery well)
Depth Surface Datum (ft)	0	Historical gauging data	
Water Table Depth (ft)	Variable	Historical gauging data	Feet below ground surface
Water Vertical Gradient	0	LDRM default	
Depth of Soil Facies Interface (ft)	Variable	Soil boring logs, cross-sections, geotechnical data	
LNAPL Density (g/mL)	0.75	API Guide	Diesel and gasoline
LNAPL Viscosity (cp)	2	API Guide	Diesel and gasoline
Air/Water Surface Tension (dyne/cm)	65	LDRM Default	
Air/LNAPL Surface Tension (dyne/cm)	26	API Guide	Diesel and gasoline
LNAPL/Water Surface Tension (dyne/cm)	28	API Guide	Diesel and gasoline
Soil Characteristics for Well-graded Sandy Fill Layer (0-5 feet bgs)			
Porosity	0.44	API Database	Gravelly SW; sample #108
Hydraulic Conductivity (ft/d)	5	API Database	Mean value from pump and slug testing

van Genuchten "N"	4.05	API Database	SW; sample #108
van Genuchten "α" (ft-1)	1.22	API Database	SW; sample #108
Irreducible Water Saturation	0.25	API Database	SW; sample #108
Residual LNAPL Saturation	0.3	API Database	SW; sample #108
Permeability Model (Burdine/Mualem)	Mualem	LDRM Default	Dependent on "N" value. Mualem required for N<2
Soil Characteristics for Well-graded Sand Layer			
Porosity	0.44	API Database	SW; sample #108
Hydraulic Conductivity (ft/d)	5	API Database	SW; sample #108
van Genuchten "N"	4.05	API Database	SW; sample #108
van Genuchten "α" (ft-1)	1.22	API Database	SW; sample #108
Irreducible Water Saturation	0.25	API Database	SW; sample #108
Residual LNAPL Saturation	0.3	API Database	SW; sample #108
Permeability Model (Burdine/Mualem)	Mualem	LDRM Default	Dependent on "N" value. Mualem required for N<2
Recovery Characteristics			
Recovery Time (yr)	12.5	Historical records	13 years of operation with combined 6 months down time
Radius of Recovery Well (ft)	0.167	Historical records, well construction diagrams	4 inch diameter recovery wells
Radius of Recovery (ft)	35	Assumed moderate value	Review of pumping groundwater contours
Radius of Influence (ft)	35	Assumed moderate value	Review of pumping groundwater contours
Water Production Rate (gpm)	4.5	Historical Records	System runtime of 12.5 years between June 2001 and June 2014
Water Saturated Thickness (ft)	Variable	Soil boring logs, cross-sections, geotechnical	
Vacuum Pressure (-atm)	0.67	Historical records	Vacuum capacity of blower
Screen Length (ft)	20	Historical records, well construction diagrams	
Air Radius of Capture	35	Assumed moderate value	Review of pumping groundwater contours

5.2 SENSITIVITY ANALYSIS

Parameter sensitivity was determined by reviewing results published in Charbeneau (2007a), Jeong and Charbeneau (2014) and through trial-and-error model simulations using variations of nominal input values. A specific sensitivity analysis was also conducted in order to corroborate published sensitivity analyses. Sensitivity analysis results are presented in Table 8 and 9 and relate only to the change in the modeled recoverable LNAPL volume as a function of input value increase. The nominal values presented in Table 8 are based on RW-1 at Site A.

The sensitivity analysis was conducted by increasing an individual nominal value by 20% while maintaining original nominal values for all other parameters. The LDRM was executed for each parameter in this manner and the resulting affect on the volume of recoverable LNAPL was observed. All parameters were increased by 20% with the exception of LNAPL density, air/water surface tension, and hydraulic conductivity. The LNAPL density (specific gravity) of diesel and gasoline will rarely exceed that of 0.90, which is a 9% increase from the nominal value of 0.83. Air/water surface tension is a relatively universal value with an LDRM default of 65, and a value higher than 66 was not identified in the literature review. Finally, hydraulic conductivity was increased by an order-of-magnitude due to typical field-measured variability.

TABLE 8. EFFECT OF INCREASING NOMINAL VALUE BY 20% ON MODELED LNAPL RECOVERY

Parameter Site A: RW-1	Nominal	Recoverable LNAPL Volume	Nominal Increased 20%	Adjusted Recoverable LNAPL Volume	Percent Change
Max LNAPL (ft)	3.36	1953 gal	4.03	2836 gal	+42%
Water Table Depth (ft)	8.46	1953 gal	10.15	1953 gal	0%
Depth of Soil Facies Interface (ft)	2.0	1953 gal	2.4	1953 gal	0%
LNAPL Density (gm/cm) ¹	0.83	1953 gal	0.90	936 gal	-52%
LNAPL Viscosity (cp)	2.0	1953 gal	2.4	1953 gal	0%
Air/Water Surface Tension (dyne/cm) ²	65	1953 gal	66	1985 gal	+2%
LNAPL Surface Tension (dyne/cm)	26	1953 gal	31.2	2066 gal	+6%
LNAPL Interfacial Tension (dyne/cm)	26	1953 gal	31.2	1525 gal	-22%
Porosity	0.44	1953 gal	0.53	2352 gal	+2%
Hydraulic Conductivity (ft/d) ³	0.625	1953 gal	6.25	1953 gal	0%
van Genuchten <i>N</i>	1.35	1953 gal	1.62	2423 gal	+24%
van Genuchten α (ft ⁻¹)	0.46	1953 gal	0.55	2356 gal	+20%
Irreducible Water Saturation	0.10	1953 gal	0.12	1896 gal	-3%
Residual LNAPL Saturation	0.21	1953 gal	0.25	1840 gal	-6%
Recovery Time (yr)	0.19	1953 gal	0.23	1953 gal	0%
Radius of Recovery (ft)	35	1953 gal	42	2812 gal	+44%
Radius of Influence (ft)	35	1953 gal	42	1953 gal	0%
Water Production Rate (gpm)	1.0	1953 gal	1.2	1953 gal	0%
Water Saturated Thickness (ft)	6.54	1953 gal	7.85	1953 gal	0%
Vacuum Pressure (-atm)	0.67	1953 gal	0.80	1953 gal	0%
Air Radius of Capture (ft)	35	1953 gal	42	1953 gal	0%

¹ LNAPL density increased by 9% since a 20% increase would result in a density greater than water

² Air/water surface tension increased by 1 dyne/cm consistent with published values

³ Hydraulic conductivity increased by three orders-of-magnitude, consistent with field variability

Based on the sensitivity analysis, the following parameters exhibit a high degree of sensitivity: maximum LNAPL thickness, LNAPL density, LNAPL interfacial tension, van Genuchten N and α , and radius of recovery. The following parameters exhibit a moderate degree of sensitivity: air/water surface tension, LNAPL surface tension, porosity, irreducible water saturation, and LNAPL residual saturation. All remaining parameters exhibit low or no sensitivity. Parameter sensitivity and parameter relationship to modeled recoverable LNAPL is presented in Table 9.

TABLE 9. PARAMETER SENSITIVITY AND RELATIONSHIP TO RECOVERABLE LNAPL

Parameter	Sensitivity	Relationship to Recoverable LNAPL Volume
Max Monitoring Well LNAPL Thickness	High	Positive
LNAPL Density	High	Negative
LNAPL Interfacial Tension	High	Positive
van Genuchten N	High	Positive
van Genuchten α	High	Positive
Radius of Recovery	High	Positive
Air/Water Surface Tension	Moderate	Positive
Air/LNAPL Surface Tension	Moderate	Positive
LNAPL Interfacial Tension	Moderate	Negative
Porosity	Moderate	Positive
Irreducible Water Saturation	Moderate	Negative
Residual LNAPL Saturation	Moderate	Negative
Water Table Depth	None	NA
Depth of Soil Facies Interface	None	NA
Recovery Time	None	NA
Radius of Influence	None	NA
Water Production Rate	None	NA
Water Saturated Thickness	None	NA
Vacuum Pressure	None	NA
Radius of Influence	None	NA
Screen Length	None	NA
Air Radius of Capture	None	NA

Appendix A of Charbeneau (2007b) includes a sensitivity analysis conducted by AQUI-VER (2006) that investigates parameter value on recoverable LNAPL volume. While the sensitivity analysis outlined in Table 8 and 9 only investigates model output relative to an increase in parameter, Charbeneau (2007b) uses a low, base, and high input value. The results of AQUI-VER (2006) as presented in Charbeneau (2007b) corroborate Table 8 and 9 in that parameter sensitivity in absolute terms is the same regardless of an increased or decreased input value adjustment, and the relationship (i.e., inverse or direct) to recoverable LNAPL volume is the same in both sensitivity analyses.

5.3 DETERMINATION OF INPUT VALUE RANGE

The objective this thesis is to determine if pre-remedial modeling would have prevented an approximate order-of-magnitude overestimation in recoverable LNAPL. The nature of this objective precludes the use of actual recovery data as a means for calibration while requiring defensible model inputs based on pre-remedial site data. As such and wherever possible, site data obtained after start-up of the MPE system were not used in input determination. However, since some parameters, such as radius of capture, exhibit a high degree of sensitivity and are difficult to accurately estimate without site-specific recovery data, these values were partially estimated with post start-up data. While these data were not identified within historical records for Site A, aquifer testing and limited pilot studies are common as part of full-scale LNAPL recovery efforts. It is reasonably assumed that using this pumping data – in order to accurately determine radius of recovery – does not adversely impact the validity of the original hypothesis.

Due to the nature of the thesis, presenting a credible defense for input values is critical for testing the hypothesis. The methodology of such determination focuses on

those parameters that exhibit a moderate to high degree of sensitivity, and is presented in the following subsections.

5.3.1 Maximum LNAPL Thickness

At each research site, monitoring well gauging records were reviewed to determine the maximum LNAPL thickness as gauged in a monitoring well. This measurement has been previously referred to as the apparent NAPL thickness (ANT), which at vertical equilibrium for unconfined LNAPL can be used to infer the vertical interval of LNAPL saturation distribution. However, if gauging took place during non-vertical equilibrium conditions or if LNAPL is confined or perched, ANT can deviate greatly from the actual vertical saturation distribution and mobile LNAPL interval. The LDRM calculates LNAPL recovery based on the principals of vertical LNAPL saturation distribution, which can be thought of as encompassing the mobile LNAPL interval.

Site A

In order to determine maximum LNAPL thickness for each recovery well, monthly monitoring well gauging records between 2005 and 2009 were reviewed. Since recovery wells were not installed until MPE system installation in late 2008, maximum ANT in recovery wells was determined by monitoring well proxy. Maximum ANT in each monitoring well was contoured on a georeferenced aerial photograph using Surfer software and kriging as a means for geostatistical interpolation (Golden Software, 2013). The z-value, or ANT, was determined at individual recovery wells by digitizing the recovery well location into the Surfer figure. Figure 43 – a plume map displaying contours based on maximum ANT for monitoring wells – illustrates this process. Figure

43a displays uncorrected maximum ANT, and Figure 43b displays corrected maximum ANT.

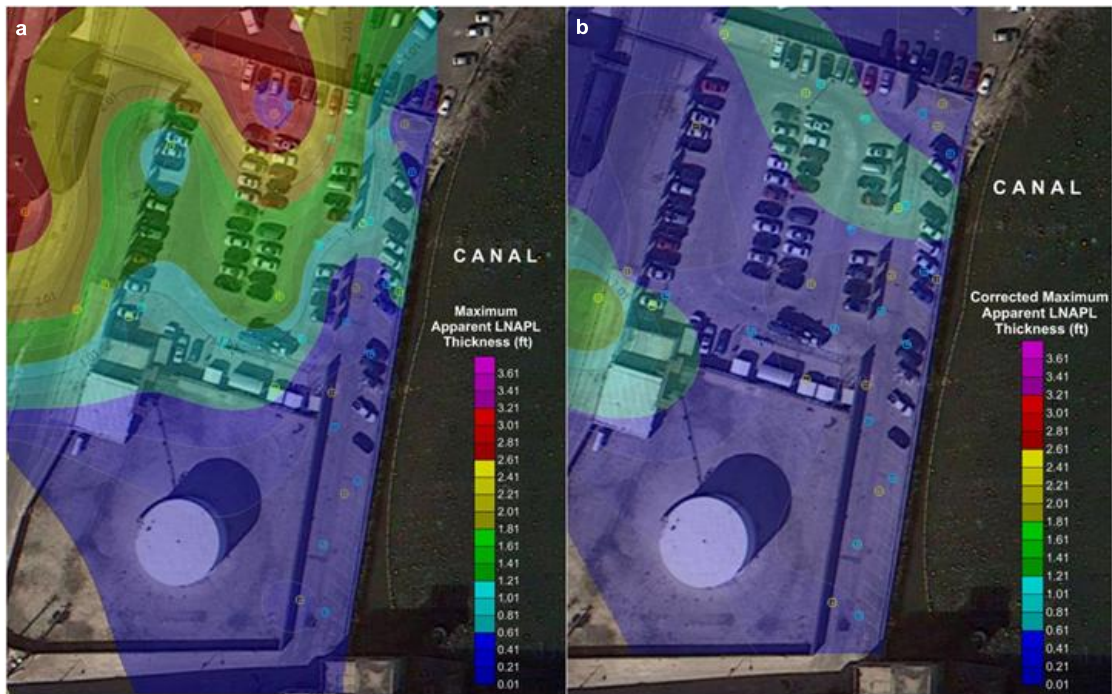


Figure 43. Site A maximum LNAPL thickness plume map with (a) uncorrected and (b) corrected maximum apparent NAPL thickness.

In order to identify LNAPL hydrogeologic condition, diagnostic gauge plots (DGPs) and hydrostratigraphs (HSGs) were created for all monitoring wells within the remediation area that contained free-product. DGPs were processed and analyzed to observe general trends for each monitoring well. In order to reduce statistical noise and erroneous values, only LNAPL thicknesses greater than 0.10 feet that were gauged prior to MPE system start-up were plotted. Linear regression and data density were factored into DGP analysis. Representative DGPs are presented as Figure 44 and 45, which display confined and perched LNAPL, respectively. All DGPs and HSGs that were determined to be statistically significant at Site A are presented in Appendix B and C, respectively. Statistical significance for DGPs is based on number of data points with an ANT greater than 0.10 feet (generally more than five). The HSGs presented in Appendix C are those that display observable trends in ANT as a function of LNAPL-water interface and potentiometric surface elevation.

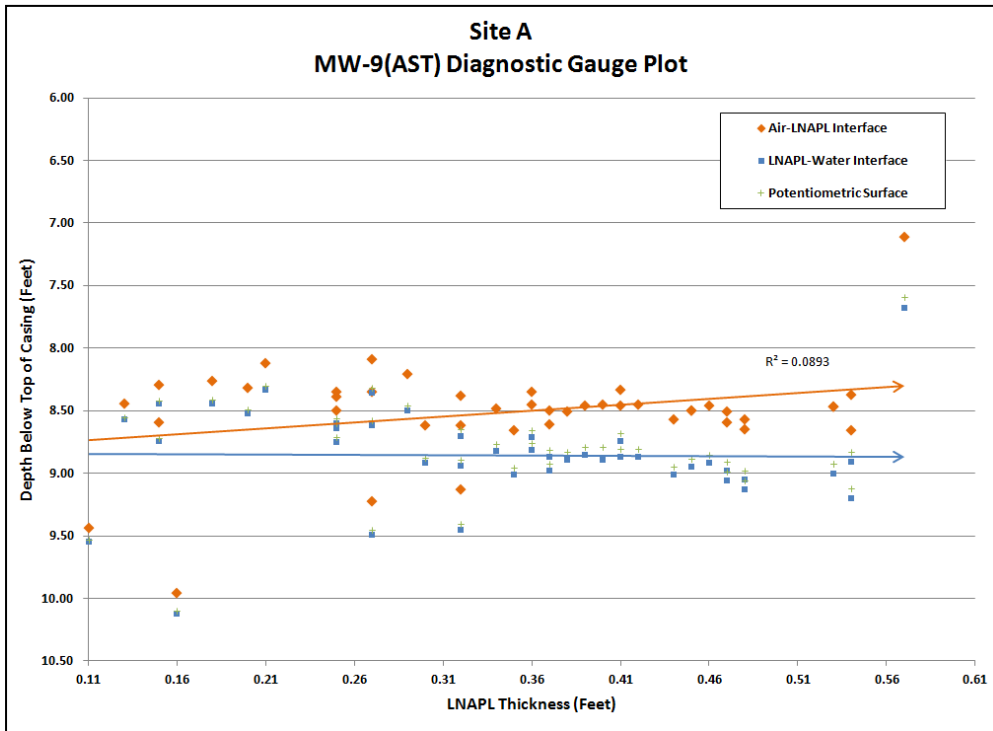


Figure 44. Representative diagnostic gauge plot at Site A exhibiting confined LNAPL trend.

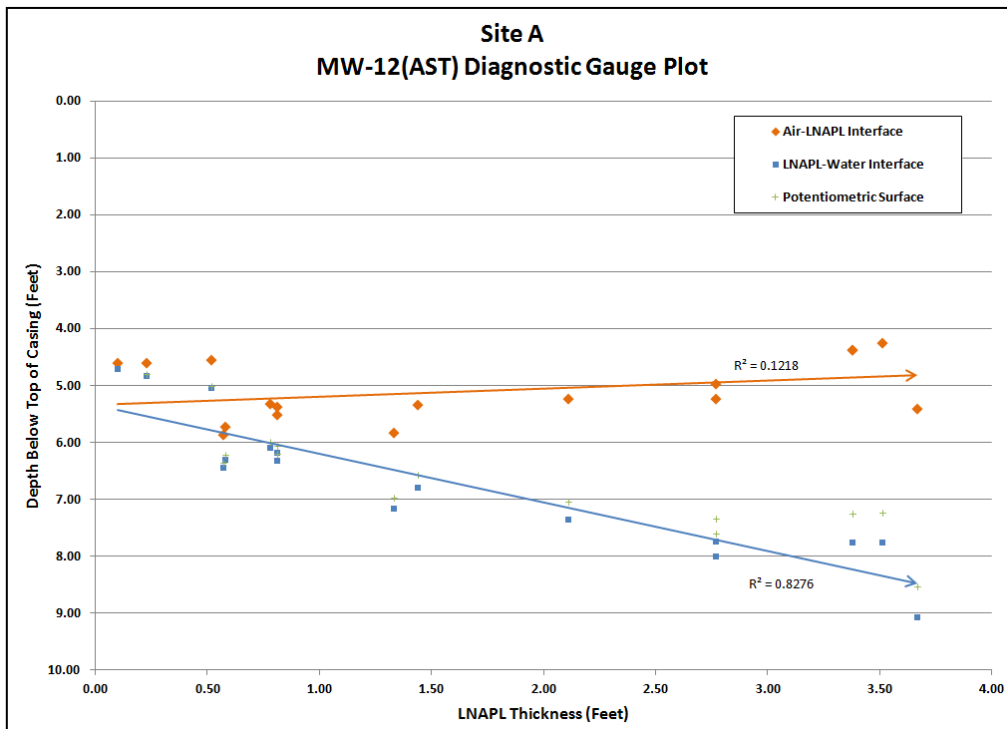


Figure 45. Representative diagnostic gauge plot at Site A exhibiting perched LNAPL trend.

Despite low to moderate R^2 values, most DGPs exhibit clear trends of confined or perched conditions. These trends were compared with HSGs for respective monitoring wells. Figure 46 and 47 display HSGs for MW-9 (AST) and MW-12 (AST), which had DGP classifications of confined and perched, respectively. The soil boring log for MW-9 (AST) does not indicate significant observable variation from 7-12 feet bgs. However, from approximately 8.5-9.0 feet bgs, the HSG (Figure 46) indicates confined LNAPL. As groundwater surface decreases, the air-LNAPL interface and ANT increases. The three largest groundwater surface fluctuations (March 2007, March 2009, and December 2013), point to confined LNAPL since an inverse relationship is observed between groundwater surface and ANT. The MW-12 (AST) HSG (Figure 47) exhibits trends consistent with perched *and* confined features. A confined trend is observed whenever the groundwater surface increases above 6 feet bgs. Perched conditions predominate when groundwater surface drops below 6 feet bgs. Without the context of the DGP indicating perched conditions, these same trends could be confused for unconfined LNAPL. The stratigraphic and PID data, while not correlating perfectly, provide additional evidence for perched *and* confined conditions. A silty sand layer, bound above and below by medium dense silt, corresponds with the ANT interval and elevated PID readings.

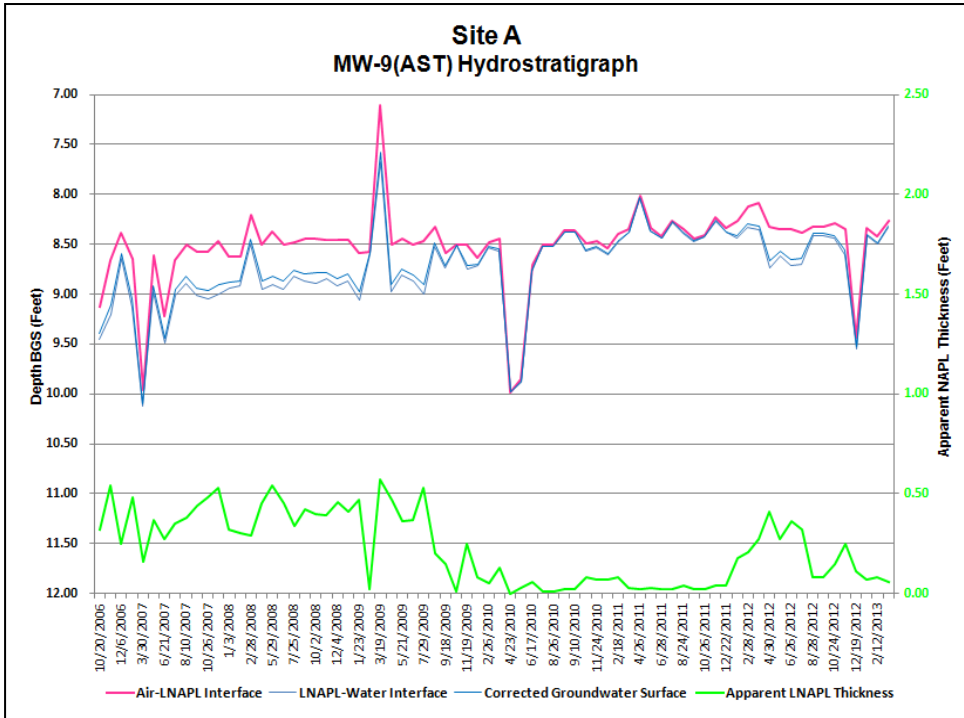


Figure 46. Hydrostratigraph for confined LNAPL at Site A.

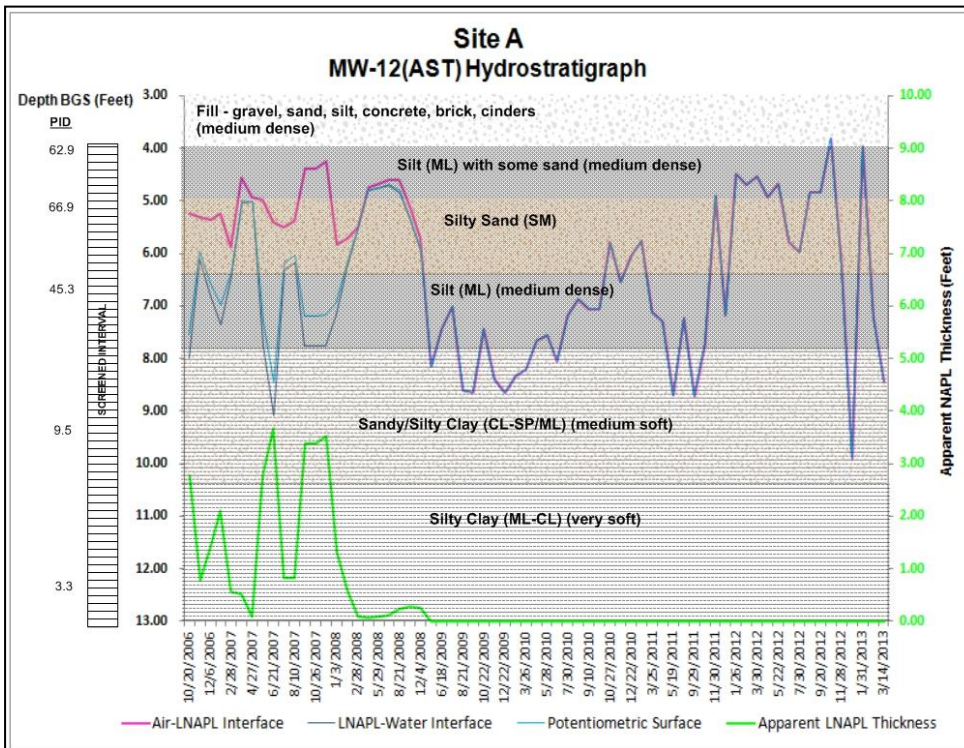


Figure 47. Hydrostratigraph for perched LNAPL at Site A.

The heterogeneous soils of Site A, fluctuating canal elevations, and rail traffic (aquifer compression and vibration) are likely responsible for the statistically noisy DGPs and HSGs. However, based on stratigraphic data and observed trends, most LNAPL at Site A appears to be confined and/or perched. As discussed in Section 2.3.3, an LNAPL baildown test can be conducted to identify the zone of mobile LNAPL, which is consistent with the maximum LNAPL thickness as required by the LDRM. These data are not available for Site A, but it is apparent that the ANT in most monitoring wells does not reflect the FNT or vertical saturation distribution. Therefore, the zone of mobile LNAPL – corrected ANT or LDRM maximum LNAPL thickness – is estimated from the median ANT value for monitoring wells exhibiting confined and/or perched LNAPL using a similar method presented in Kahraman (2013). In order to avoid erroneous values, all gauged thicknesses less than 0.10 feet were not considered. Uncorrected and corrected ANT for the monitoring wells is provided in Table 10. Corrected ANT for individual recovery wells was estimated by similar contouring methods discussed previously and is provided in Table 11.

TABLE 10. UNCORRECTED AND CORRECTED MONITORING WELL MAXIMUM ANT

Monitoring Well	Uncorrected	Corrected
MW-1 (AST)	0.01	0.01
MW-2 (AST)	0.00	0.00
MW-3 (AST)	0.76	0.33
MW-4 (AST)	3.06	0.58
MW-6 (AST)	1.64	0.34
MW-7 (AST)	0.10	0.10
MW-8 (AST)	0.81	0.48
MW-9 (AST)	0.54	0.36
MW-10 (AST)	2.68	0.62
MW-11 (AST)	0.15	0.15
MW-12 (AST)	3.67	0.81
MW-13 (AST)	0.00	0.00
MW-14 (AST)	0.73	0.38
OTMW-1	0.75	0.75
OTMW-2	1.39	0.35
OTMW-3	1.86	1.86
T-1	1.02	1.02
T-2	0.05	0.05
T-3	0.28	0.28

TABLE 11. UNCORRECTED AND CORRECTED RECOVERY WELL MAXIMUM ANT

Recovery Well	Uncorrected	Corrected
RW-1	3.36	0.80
RW-2	1.98	0.65
RW-3	1.22	0.60
RW-4	0.81	0.25
RW-5	1.03	0.50
RW-6	0.90	0.60
RW-7	0.18	0.22
RW-8	0.20	0.03
RW-9	0.08	0.08
RW-10	0.09	0.10
RW-11	0.24	0.15
RW-12	0.33	0.09
RW-13	0.60	0.50
RW-14	0.95	1.00
RW-15	0.54	0.50
RW-16	0.80	0.40

Site B

Maximum LNAPL thickness for each recovery well was determined by a review of quarterly gauging data between 1992 and 2001. Since gauging data are not available for recovery wells, maximum ANT in recovery wells was determined by monitoring well proxy. Maximum ANT in each monitoring well was contoured on a georeferenced aerial photograph using Surfer software and kriging as a means for geostatistical interpolation (Golden Software, 2013).

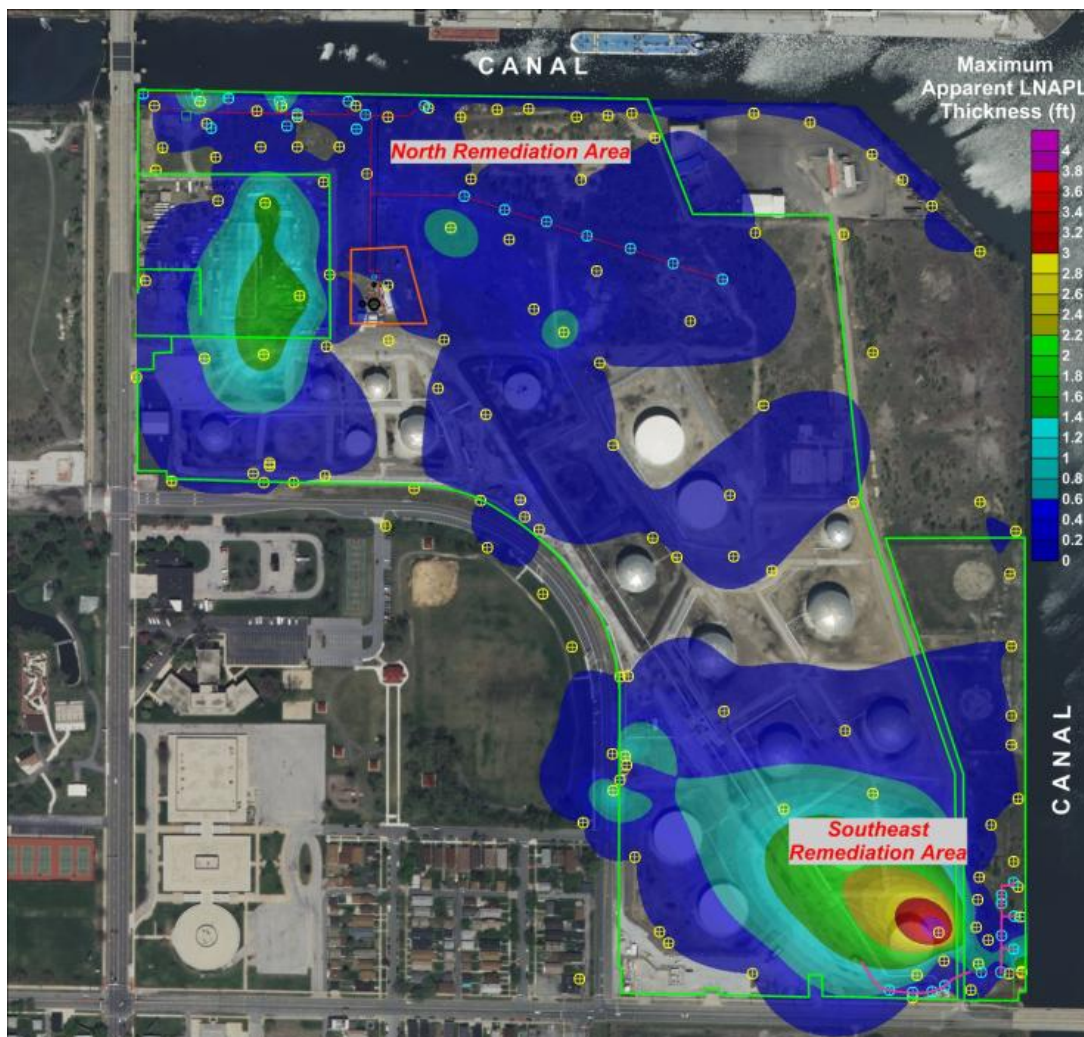


Figure 48. Plume map of monitoring well maximum apparent NAPL thickness at Site B.

The z-value, or ANT, was estimated for individual recovery wells by digitizing the recovery well location in the Surfer figure. Figure 48, a plume map displaying contours based on maximum ANT for monitoring wells, illustrates this process.

DGPs and HSGs were created for all monitoring wells exhibiting ANT greater than 0.10 feet. Figure 49 displays the characteristic trends at Site B indicating unconfined LNAPL. Unconfined LNAPL is consistent with the general stratigraphy throughout the site, which consists of relatively homogenous well-graded sand becoming increasingly fine-grained and dense with depth.

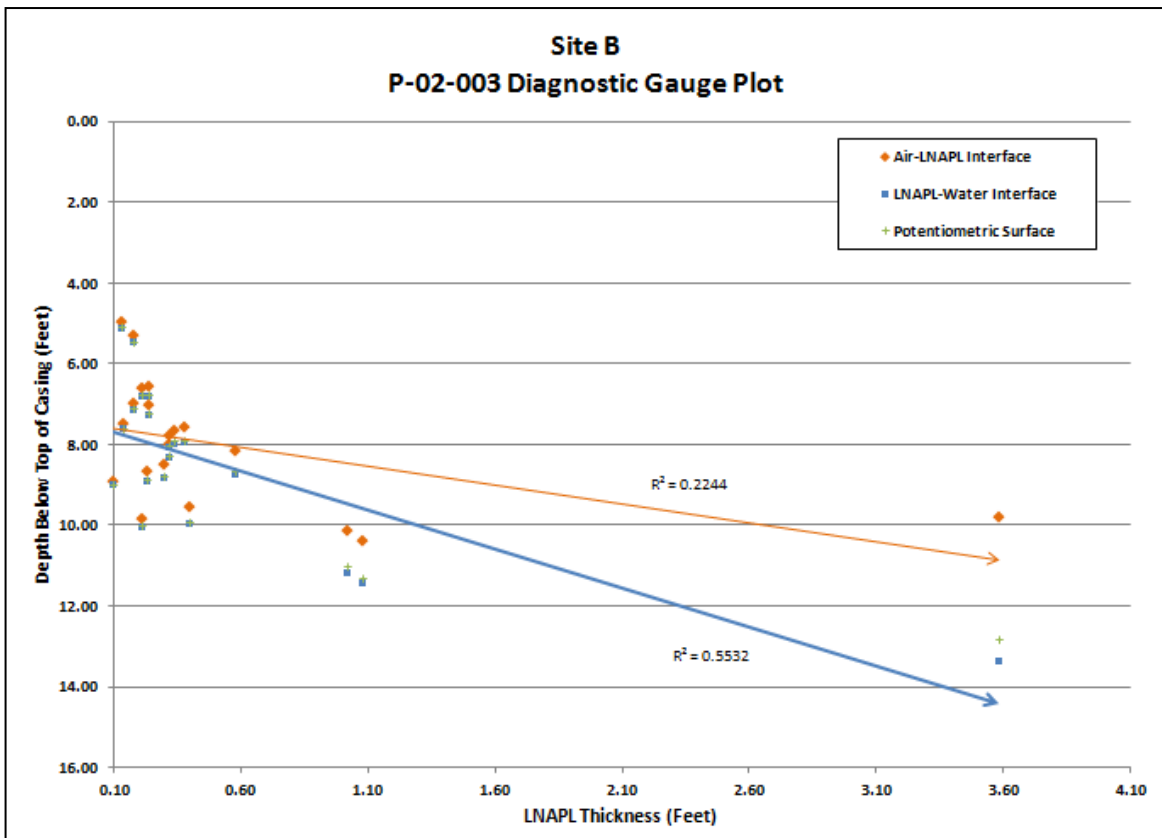


Figure 49. Characteristic diagnostic gauge plot at Site B exhibiting unconfined LNAPL trend

Figure 50 displays the HSG for the same monitoring well adding further evidence for unconfined LNAPL. Note how ANT (green) is inversely proportional to the LNAPL-water interface (navy blue) and potentiometric surface (royal blue), which is particularly apparent between July 2002 and July 2004.

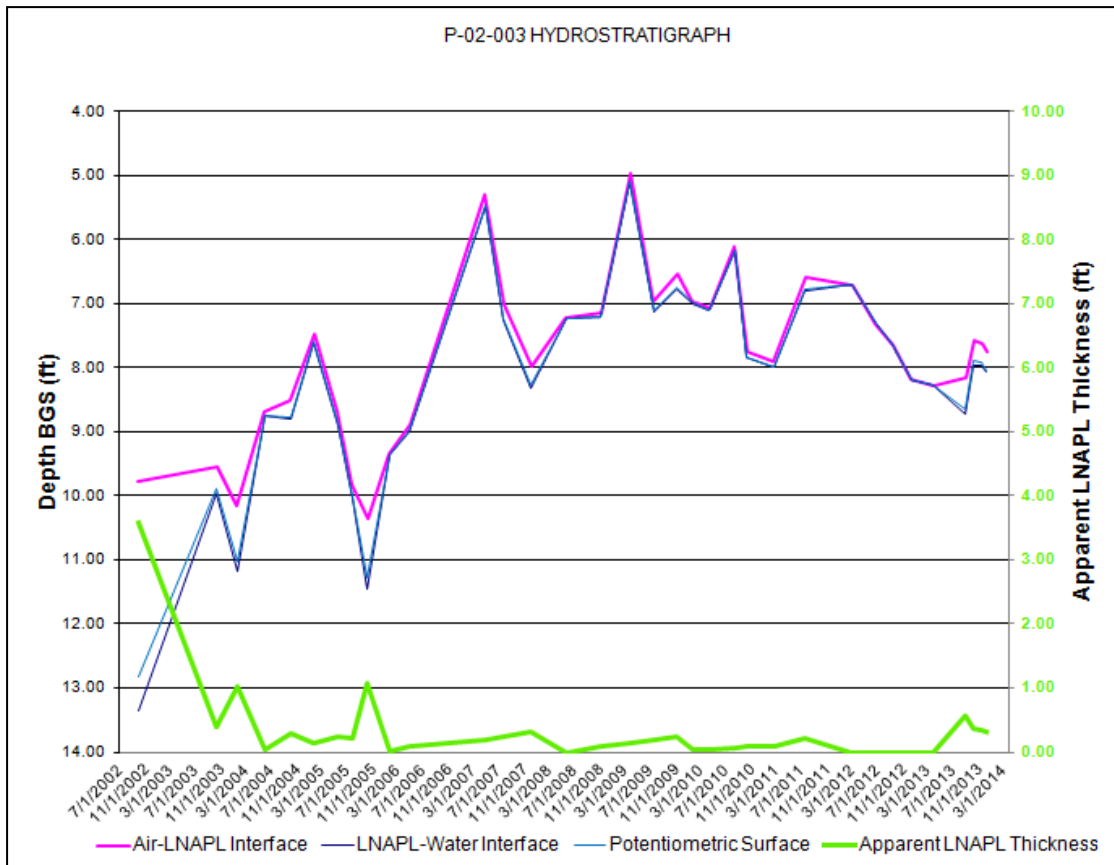


Figure 50. Characteristic hydrostratigraph at Site B exhibiting unconfined LNAPL trend.

Several DGPs and HSGs exhibited trends consistent with confined and/or perched LNAPL. Most of these had very low R^2 values (0.01-0.10) and low ANTs (0.01-0.50 feet). DGPs and HSGs with lower LNAPL thickness are susceptible to statistical noise and subsequent misinterpretation of LNAPL hydrogeologic condition. Therefore, 1) based the general stratigraphic and LNAPL hydrogeologic trends throughout the site, and 2) due to the unreliability of these DGPs and HSGs, the maximum ANT in these monitoring wells is used in the LDRM without a correction.

Two monitoring wells did however exhibit clear and statistically significant confined and perched LNAPL trends. Figures 51-54 display the DGPs and HSGs for these two wells. Figure 51 and 52 exhibit clear trends of confined LNAPL. The DGP displays a relatively flat LNAPL-water interface (blue) with an increasing air-LNAPL interface (orange). The corresponding HSG clearly exhibits an ANT (green) that is directly proportional to the LNAPL-water interface (blue). Figure 53 and 54 exhibit trends consistent with perched LNAPL. For example, the DGP (Figure 53) displays a relatively flat air-LNAPL interface (orange) with a decreasing LNAPL-water interface (blue).

A corrected ANT was calculated for these two wells using the median ANT value in the same procedure used for Site A. Maximum ANT was re-contoured in Surfer to reflect corrected ANT in these two wells. However, the wells are approximately 500 feet from the north remediation area and 2,900 feet from the southeast remediation area and therefore did not impact previously estimated recovery well maximum ANT.

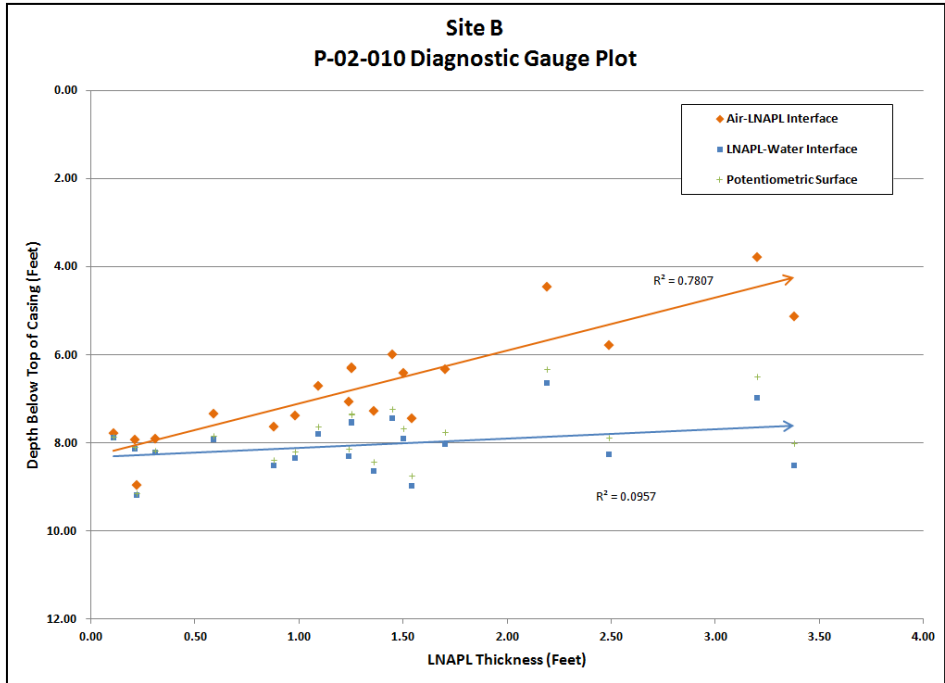


Figure 51. Diagnostic gauge plot exhibiting confined LNAPL trend at Site B.

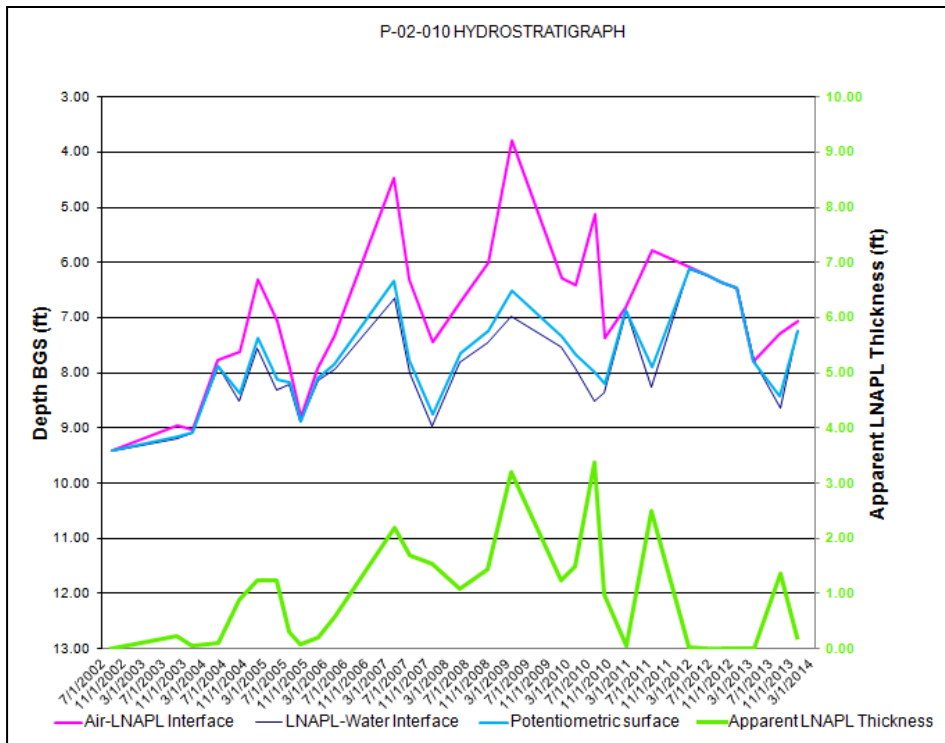


Figure 52. Hydrostratigraph exhibiting confined LNAPL at Site B.

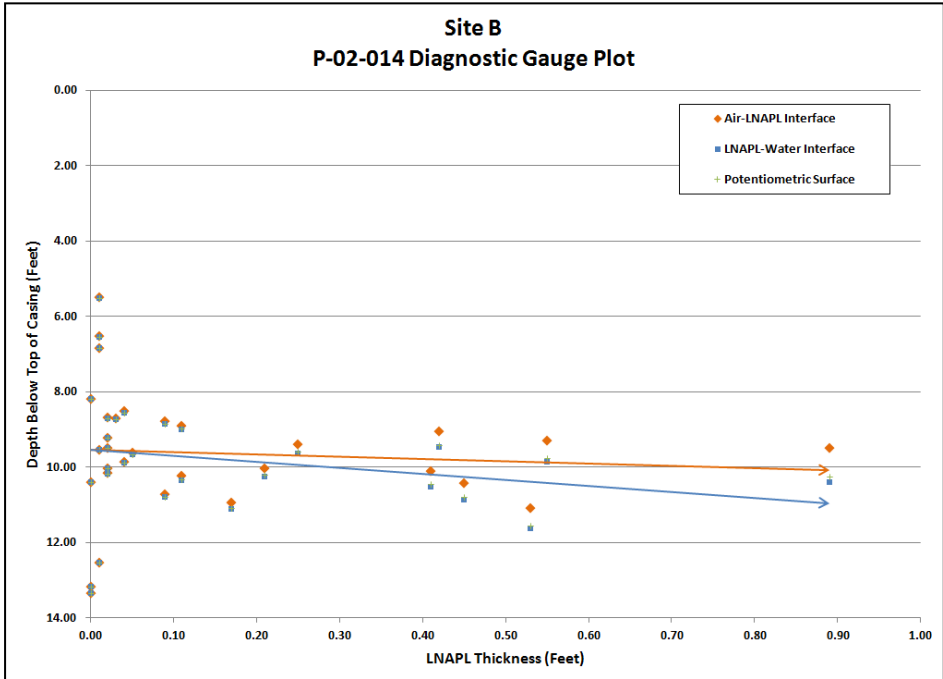


Figure 53. Hydrostratigraph exhibiting perched LNAPL trend at Site B.

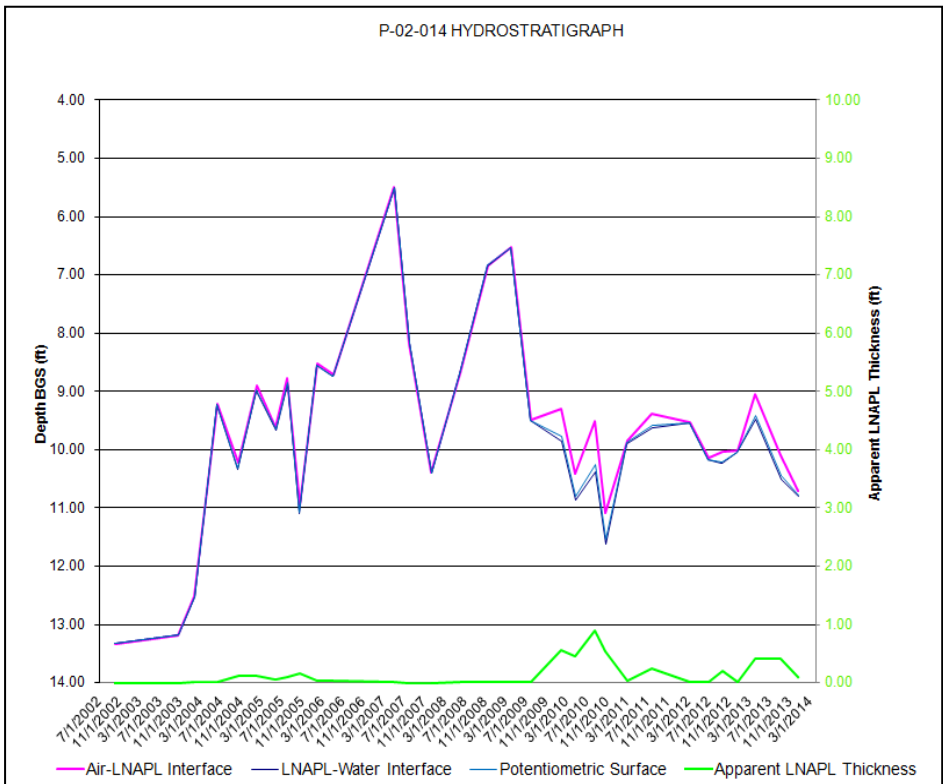


Figure 54. Diagnostic gauge plot exhibiting perched LNAPL at Site B.

All DGPs and HSGs that were determined to be statistically significant at Site B are presented in Appendix B and C, respectively. Statistical significance for DGPs is based on number of data points with an ANT greater than 0.10 feet (generally more than five). The HSGs presented in Appendix B are those that display observable trends in ANT as a function of LNAPL-water interface and potentiometric surface elevation. Due to the relative homogeneity of the soil at Site B, and the general downward fining of grain-size, all DGPs and HSGs that have been omitted from Appendix B are those that were concluded to represent unconfined LNAPL or did not contain an ANT in extent or frequency that was statistically significant.

5.3.2 Radius of Recovery

The radius of recovery for a vacuum well can extend to the radius of influence, which is typically on the order of 30 to 40 feet (Charbeneau, 2007a). Therefore, radius of recovery is estimated at each site on the basis that 1) radius of recovery, influence, and air capture are similar values, and 2) the maximum radius of recovery will only extend beyond 40 feet under theoretical best-case scenarios. Additionally, while recovery wells at Site B operated concurrently (i.e., vacuum applied to all wells during operation), recovery wells at Site A were cycled at two recovery wells per hour. This cyclical recovery schedule at Site A provides a more apparent delineation of radius of recovery through the analysis of groundwater contours during vacuum application.

Site A

Figure 55 and 56 display groundwater contours for static and pumping (i.e., vacuum) conditions, respectively. The only recovery wells displayed on Figure 56a and 56b are those under the influence of vacuum. By comparing the static and pumping

groundwater contours, it is possible to estimate the radius of recovery. It is apparent that soil heterogeneity, but more likely subsurface structures and proximity to the canal, negatively impact radius of recovery. In Figure 56a, RW-1 displays an apparent capture zone while RW-9 appears to have little influence on groundwater. Figure 56b shows vacuum operation of RW-7 and RW-11. RW-7 displays an apparent, if somewhat limited, radius of recovery while RW-11 appears to have limited influence on groundwater conditions. Measurements were conducted on georeferenced aerial photographs in Surfer in order to estimate a maximum and minimum range for radius of capture. The radius of recovery range includes a maximum value of 35 feet and a minimum value of 10 feet. The range of 10 to 35 feet is designed to model minimum and maximum LNAPL recovery scenarios, respectively.

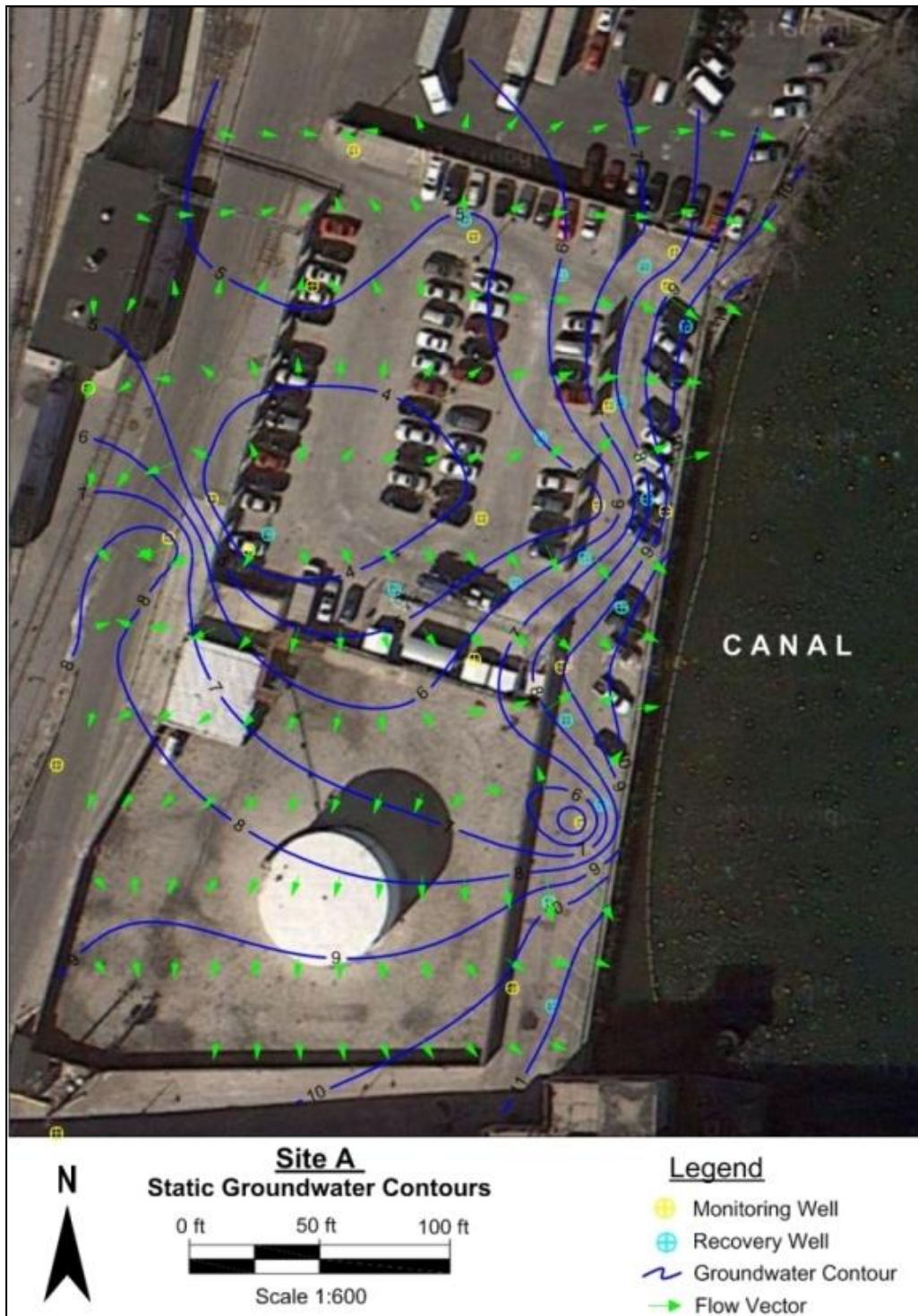


Figure 55. Water table map displaying 1-foot contour intervals for Site A.

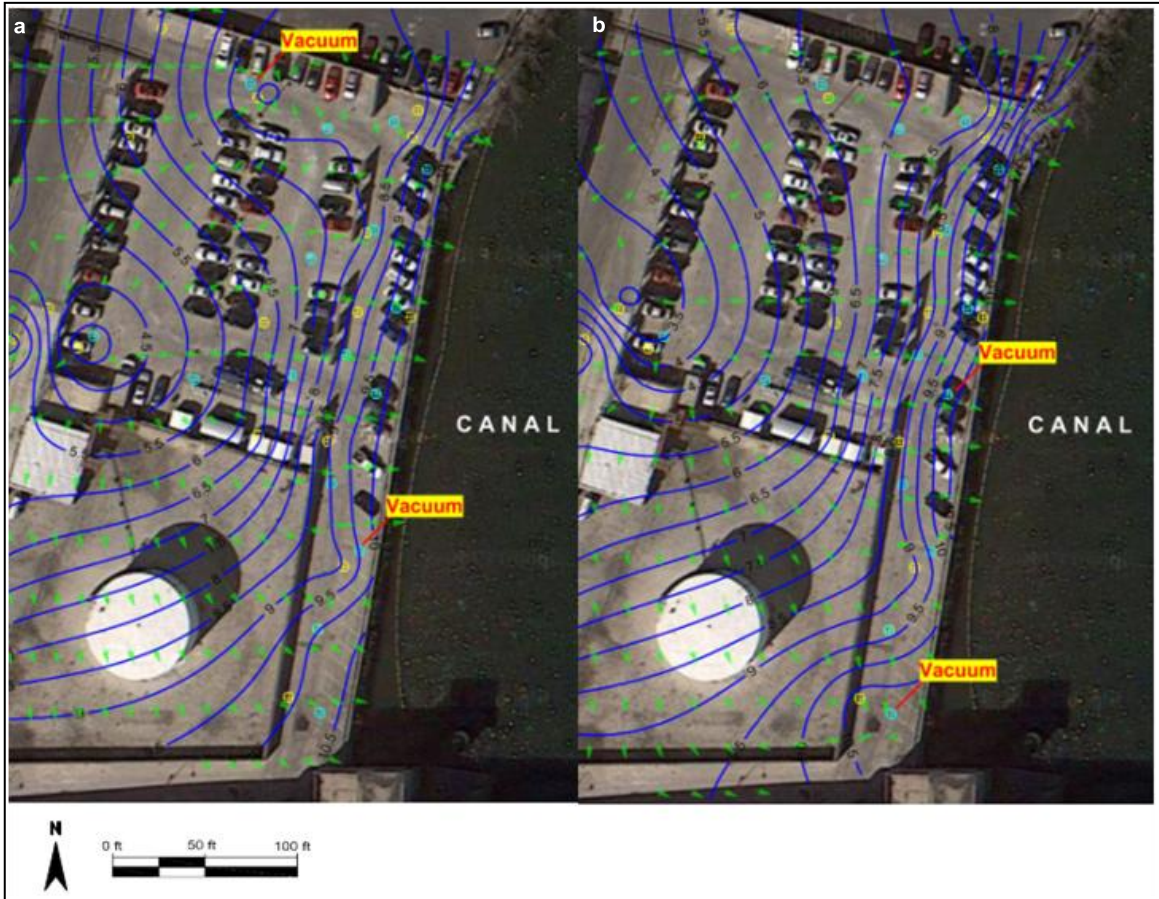


Figure 56. Water table map for Site A during vacuum operation.

Site B

Due to vacuum being applied to all recovery wells concurrently, the groundwater contours do not exhibit clear signs of individual capture zones. Recovery well proximity to the canal, which acts as a recharge boundary during operation, and high aquifer transmissivity, likely inhibits drawdown and corresponding radius of recovery for groundwater within the aquifer. Regardless, it remains difficult to accurately delineate a radius of recovery for individual recovery wells. Therefore, radius of recovery estimation is based on maximum values reported in literature. The radius of recovery range includes a maximum value of 45 feet, which exceeds maximum reported capture for vacuum wells by 5 feet, and a minimum value of 30 feet. The range of 30 to 45 feet is designed to model minimum and maximum LNAPL recovery scenarios, respectively.

5.3.3 Fluid Parameters

Fluid parameters at both research sites are based on LNAPL type reported in historical records and analytical data collected from free-product and impacted groundwater. Based on this information, the LNAPL at Site A is classified as diesel fuel, and a mixture of gasoline and diesel at Site B. In order to account for unknown variations in LNAPL characteristics, a value range was determined for each fluid parameter to account for maximum and minimum LNAPL recovery scenarios. The API Guide was used to lookup empirically derived LNAPL characteristics for each scenario. Many of the following fluid characteristics are temperature dependent. Based on field-measured groundwater temperatures at the research sites, LNAPL is assumed to be within a

temperature range of 10 to 15°C. Therefore, respective value ranges were chosen to most closely match fluid type and temperature conditions.

LNAPL Density

LNAPL density at Site A is based on the on the minimum and maximum observed density for diesel fuel of 0.80-0.85 gm/cc. LNAPL density at Site B is based on the minimum and maximum observed density for gasoline and diesel fuel of 0.75-0.85 gm/cc.

Air/Water Surface Tension

Air/water surface tension is based on the default value of 65 dyne/cm and the maximum value of 66 dyne/cm, as observed in other LDRM studies. This range is used for both research sites.

LNAPL/Water Surface Tension

LNAPL/water surface tension at Site A is based on the range of values for diesel fuel of 26.5-29.0 dyne/cm. Site B values are based on a mixture of gasoline and diesel fuel, which at 15°C is approximately 22.0-26.0 dyne/cm.

LNAPL Interfacial Tension

LNAPL interfacial tension at Site A is based on minimum and maximum observed values at 15°C, which are 24-35 dyne/cm. Site B values are based on a mixture of gasoline and diesel fuel, which at 15°C comprises a range of approximately 18-23 dyne/cm.

5.3.4 Capillary and Petrophysical Parameters

Site specific soil values were estimated by using available soil data, which were matched to similar soil samples and types in the API Database and API Guide that

included empirically derived capillary and petrophysical properties. The most precise method for estimating these properties in this manner was based on grain-size distributions for various depth intervals, which were only available at Site B. Soil classification based on soil boring logs at Site A was used as a means for comparison to listed soils with empirically derived capillary and petrophysical properties. Therefore, estimated soil properties at Site B are inherently more accurate than Site A. As a result, the chosen value range for capillary and petrophysical parameters at Site A reflects this uncertainty through an increased value range for the minimum and maximum recovery scenarios.

The API Database was opened in Microsoft Access and used to match soil type and grain-size distribution at each research site with the samples reported in the database. For example, at Site B 15 geotechnical samples were collected along the north and southeast remediation areas to depths exceeding 30 feet bgs (Parsons, 2009). Grain-size analysis was performed from approximately 1-3 feet bgs, 11-15 feet bgs, 25-29 bgs, and 31-35 bgs. Undisturbed samples were collected in Shelby tubes from the clay confining layer at approximately 30 feet bgs and submitted for Atterberg limits, unconfined compressive strength, and coefficient of permeability. Table 12 summarizes the grain-size distribution results for five of the samples that correspond to RW-1N through RW-11N in the north remediation area. Soil characterization and grain-size distribution is presented in Appendix D.

TABLE 12. GRAIN-SIZE DISTRIBUTION FROM SAMPLES COLLECTED AT SITE B

1-3 Feet BGS			
Sample	Gravel	Sand	Fines
NW1	18	75	7
NW2	24	71	5
NW3	21	39	40
NW4	7	81	12
NW5	20	66	14
Average	18	66	16

25-29 Feet BGS			
Sample	Gravel	Sand	Fines
NW1	0	76	24
NW2	0	4	96
NW3	0	7	93
NW4	0	61	39
NW5	4	4	92
Average	1	30	69

11-15 Feet BGS			
Sample	Gravel	Sand	Fines
NW1	5	87	8
NW2	1	91	8
NW3	1	94	5
NW4	1	94	5
NW5	2	93	5
Average	2	93	5

31-35 Feet BGS			
Sample	Gravel	Sand	Fines
NW1	0	4	96
NW2	0	61	39
NW3	4	3	93
NW4	1	4	95
NW5	NA	NA	NA
Average	1	18	81

Once average grain-size distribution was determined for each sample interval, a query was made in the database to match these results with database samples. A total of 11 well-graded sand samples were retrieved from the API Database, each exhibiting slightly different grain-size distributions and respective capillary and petrophysical properties. Figure 57 is a database sample that closely matches the averages for the depth interval of 1-3 feet bgs. The most important parameters contained within the output are the van Genuchten Alpha (α) and Beta (N), and residual (irreducible) water saturation. Additional geotechnical samples correlate with the remaining recovery well locations at Site B.

<i>Database summary of samples for given soil type</i>															
<i>Sample ID</i>	162	<i>Permeability (mD)</i>		2.865E+03											
Soil Description of Sample															
<i>Folk Sample Description</i>	gravelly sand			<i>Folk Ternary Diagram Symbol</i>	gS										
<i>Folk Sorting Description</i>	well sorted			<i>USCS_symbol</i>	SW										
Capillary Parameters Summary															
<i>VanGenuchten Alpha (/cm)</i>	7.83E-02	<i>Brooks-Corey Bubbling Pres (cm water)</i>		5.82E+00											
<i>VanGenuchten Beta</i>	1.55	<i>Brooks-Corey lambda</i>		0.44											
<i>Fit R squared</i>	0.98	<i>Brooks-Corey Fit R squared</i>		0.99											
<i>Residual Saturation</i>	29.0%														
Petrophysical Parameter Summary															
<i>Permeability (mD)</i>	2.865E+03	<i>depth (feet)</i>	25.5												
<i>Conductivity (cm/s)</i>	1.560E-03	<i>Sampling Zone</i>	Aquifer Zone												
<i>Sample Orientation (V or H)</i>	V		<i>Bulk Density (g/cc)</i>	1.79											
<i>Effective Porosity (%Vb)</i>	0.3282	<i>Grain Density (g/cc)</i>	2.66												
<i>Air Filled Porosity (%Vb)</i>	0.0584	<i>Testing Fluid</i>	Inert Oil												
<i>Water Saturation (%Pv)</i>	0.822	<i>Testing State</i>	Intrinsic												
<i>Hydrocarbon Saturation (%Pv)</i>	0	<i>Confining Pressure (psi)</i>	25												
<i>Moisture Content (%Wt)</i>	15.1														
Grain Sizes as Percentage of Total Sample															
<i>Total Sand</i>	79.68%	<i>Total Fines</i>	4.32%	<i>Gravel</i>	16.00%	<i>Coarse Sand</i>	29.59%	<i>Medium Sand</i>	31.22%	<i>Fine Sand</i>	18.87%	<i>Silt</i>	4.32%	<i>Clay</i>	0.00%

Figure 57. API Parameter Database summary for well-graded sand sample #162.

Geotechnical data were not available within the remediation area at Site A. However, soil boring logs provide general soil and stratigraphic characterizations. Geotechnical data several hundred feet north of the remediation area presents corroborating evidence to the general stratigraphic sequence observed throughout the remediation area. Despite developing accurate cross-sections for the remediation area, without grain-size data from the heterogeneous fill and underlying silty clay layer, an accurate match to a sample in the API Database is questionable. In order to compensate for indeterminate grain-size distribution within the two soil layers at Site A, multiple scenarios have been designed to account for varying soil conditions.

Three distinct soil layers have been identified in the remediation area at Site A that generally consist of heterogeneous fill underlain by sandy, silty clay underlain by clay.

The clay confining layer ranges from 9-12 feet bgs and is not required by or considered for the LDRM. The sandy, silty clay is observed from approximately 4-12 feet bgs and ranges from silty clay to sandy, silty clay with occasional sand seams. The fill layer is observed from approximately 0-4 feet bgs and consists of varying combinations of silt, sand, and gravel. The soil-specific minimum and maximum LNAPL recovery scenarios at Site B are as follows:

- Minimum: Gravelly well-graded sand with silt underlain by silty clay loam
- Maximum: Gravel and sand underlain by sandy clay loam

Porosity, van Genuchten N and α , irreducible water saturation, and residual LNAPL saturation were estimated in this manner by matching site-specific soil data to related soil samples and types provided in the API Database and API Guide. Soil boring logs for Site A are presented in Appendix D.

5.4 MODEL CALIBRATION

Presenting a thorough defense of input values – those that would likely have been chosen during pre-remedial modeling – while adequately calibrating the model is imperative in testing the hypothesis. The exact method of calibration depends on the desired model output. If the intention is to determine if an existing remediation system has reached asymptotic recovery, it would be best to use observed recovery volume and current LNAPL transmissivity values collected through baildown testing. Once these values are obtained, model input values are adjusted until actual recovery volume and transmissivity values match model output values. At this point a graphical analysis of LNAPL recovery rate can be analyzed to estimate future recovery. As discussed in the previous section, recovered LNAPL volume was not used for calibration since the model

objective is to match this value, thus confirming that pre-remedial modeling would have prevented recoverable volume estimation errors. Therefore, the LDRM was calibrated with available data at each site that was known with a relatively high degree of certainty.

In a typical setting, LDRM execution would be performed using limited or no site-specific field data. Subsequent to this initial run, field data would be collected to calibrate the model. Limited calibration could consist of basic site data such as monitoring well gauging and soil boring logs. Extensive calibration through the use of pump or vacuum tests, LNAPL baildown tests, analytical data, and geotechnical analysis would refine the model for more accurate results. For purposes of this research, the LDRM can be thought of as pre-calibrated since site-specific data was used for each model simulation. For example, the LDRM for Site A was calibrated through monitoring well gauging, aquifer testing, product fingerprinting, soil boring logs, and MPE data including applied vacuum, groundwater production rate, recovery time, well schematics, and even radius of recovery. Site B calibration is similar, but the model is further refined with grain-size distribution at various locations and depth intervals.

5.5 SPECIFIC MODEL SIMULATIONS

Three primary LDRM simulations are reported in this thesis:

- 1) Nominal input values
- 2) Maximum LNAPL recovery
- 3) Minimum LNAPL recovery

The initial simulation using nominal values was designed to obtain a general understanding of LDRM capabilities with basic input estimates. The maximum and minimum simulations were not necessarily designed to produce an LNAPL recovery

volume range that encompassed the nominal modeled recovery. However, this was the end result and likely reflects nominal inputs based largely on site-specific data and average values for fluid, capillary, and petrophysical properties. Regardless, the maximum and minimum simulations represent refined calibration through the analysis of LNAPL hydrogeologic condition (both sites), and detailed grain-size distributions at Site B. Table 13 presents the LDRM input values for the three model simulations. The value range and associated maximum and minimum recovery simulations are designed to correct for potential uncertainty inherent in many of the estimated values.

TABLE 13. LDRM INPUT VALUES FOR SITE A

Site A – Railroad Maintenance Yard			
Parameter	Nominal Value – Uncorrected ANT	Maximum Recovery Scenario	Minimum Recovery Scenario
Max Monitoring Well LNAPL Thickness (ft)	Well specific, uncorrected	Well specific, corrected	Well specific, corrected
Depth Surface Datum (ft)	0	0	0
Water Table Depth (ft)	Well specific	Well specific	Well specific
Water Vertical Gradient	0	0	-0.1
Depth of Soil Facies Interface (ft)	Well specific	Well specific	Well specific
LNAPL Density (g/mL)	0.83	0.80	0.85
LNAPL Viscosity (cp)	2	2	2
Air/Water Surface Tension (dyne/cm)	65	65	65
Air/LNAPL Surface Tension (dyne/cm)	26.0	29.0	26.5
LNAPL/Water Surface Tension (dyne/cm)	26	24	35
Soil Characteristics for Heterogeneous Fill Layer			
Porosity	0.32	0.35	0.33
Hydraulic Conductivity (ft/d)	4.2	0.2	0.2
van Genuchten N	1.55	2.2	1.2
van Genuchten α (ft ⁻¹)	2.38	5.00	0.25
Irreducible Water Saturation	0.29	0.29	0.45
Residual LNAPL	0.03	0.03	0.2

Saturation			
Permeability Model (Burdine/Mualem)	Mualem	Mualem	Mualem
Soil Characteristics for Sandy, Silty clay			
Porosity	0.44	0.48	0.3
Hydraulic Conductivity (ft/d)	0.625	0.200	0.2
van Genuchten <i>N</i>	1.35	1.48	1.8
van Genuchten α (ft ⁻¹)	0.46	1.80	0.96
Irreducible Water Saturation	0.10	0.10	0.05
Residual LNAPL Saturation	0.21	0.19	0.15
Permeability Model (Burdine/Mualem)	Mualem	Mualem	Mualem
Recovery Characteristics			
Recovery Time (yr)	0.19	0.19	0.16
Radius of Recovery Well (ft)	0.25	0.25	0.25
Radius of Recovery (ft)	20	35	10
Radius of Influence (ft)	20	35	10
Water Production Rate (gpm)	1	1	1
Water Saturated Thickness (ft)	Well specific	Well specific	Well specific
Vacuum Pressure (atm)	0.50	0.67	0.34
Screen Length (ft)	10	10	10
Air Radius of Capture	20	35	10

TABLE 14. LDRM INPUT VALUES FOR SITE B

Site B – Bulk Oil Storage Facility			
Parameter	Nominal Value	Maximum Recovery Scenario	Minimum Recovery Scenario
Max Monitoring Well LNAPL Thickness (ft)	Well specific, uncorrected	Well specific, corrected	Well specific, corrected
Depth Surface Datum (ft)	0	0	0
Water Table Depth (ft)	Well specific	Well specific	Well specific
Water Vertical Gradient	0	0	0
Depth of Soil Facies Interface (ft)	Well specific	Well specific	Well specific
LNAPL Density (g/mL)	0.75	0.75	0.85
LNAPL Viscosity (cp)	2	2	2

Air/Water Surface Tension (dyne/cm)	65	65	65
Air/LNAPL Surface Tension (dyne/cm)	26	26	22
LNAPL/Water Surface Tension (dyne/cm)	18	18	23
Soil Characteristics for Sandy Fill Layer			
Porosity	0.44	0.44	0.33
Hydraulic Conductivity (ft/d)	5	5	5
van Genuchten N	4.05	4.05	1.55
van Genuchten α (ft ⁻¹)	1.22	1.22	2.36
Irreducible Water Saturation	0.25	0.12	0.20
Residual LNAPL Saturation	0.3	0.1	0.3
Permeability Model (Burdine/Mualem)	Mualem	Mualem	Mualem
Soil Characteristics Well-graded Sand Layer			
Porosity	0.44	0.44	0.49
Hydraulic Conductivity (ft/d)	5	5	5
van Genuchten N	4.05	3.45	3.50
van Genuchten α (ft ⁻¹)	1.22	0.50	0.50
Irreducible Water Saturation	0.12	0.12	0.15
Residual LNAPL Saturation	0.3	0.1	0.3
Permeability Model (Burdine/Mualem)	Mualem	Mualem	Mualem
Recovery Characteristics			
Recovery Time (yr)	12.5	12.5	12
Radius of Recovery Well (ft)	0.167	0.167	0.167
Radius of Recovery (ft)	35	45	30
Radius of Influence (ft)	35	45	30
Water Production Rate (gpm)	4.5	4.5	4.5
Water Saturated Thickness (ft)	Well specific	Well specific	Well specific
Vacuum Pressure (atm)	0.67	0.67	0.5
Screen Length (ft)	20	20	30
Air Radius of Capture	35	45	30

CHAPTER 6: MODEL RESULTS

In this thesis, retrospective pre-remedial LNAPL recovery was modeled at the two active remediation research sites – Site A and B. Three model simulations were executed for each research site that included 1) nominal input values, and an input value range designed to simulate 2) maximum LNAPL recovery and 3) minimum LNAPL recovery. LDRM output text files with detailed input values and recovery results for each recovery well are provided in Appendix C. The LDRM results are summarized in the subsequent sections.

6.1 NOMINAL RESULTS

Nominal values were used to execute an initial model simulation at each research site for the purposes of determining model capabilities and performing a sensitivity analysis. The nominal values were determined largely through uncorrected site data and average published values for fluid and soil properties as provided in the API Parameter Database and API Interactive LNAPL guide.

6.1.1 Site A

Nominal results for Site A are presented in Table 15. The nominal simulation for Site A resulted in a final LNAPL recovery volume of 3,889 gallons, which is 2,389 gallons more than the actual recovered volume and represents an error factor of approximately 2.59.

TABLE 15. NOMINAL RESULTS FOR SITE A

Recovery Well	Specific Volume (ft)	Recoverable Volume (ft)	Final Recovery Volume (gal)	Percent Recovery
RW-1	0.46	0.07	1953	15
RW-2	0.25	0.02	632	9
RW-3	0.15	0.01	215	5
RW-4	0.10	0.00	85	3
RW-5	0.10	0.02	595	22
RW-6	0.11	0.00	108	3
RW-7	0.02	0.00	3	0
RW-8	0.02	0.00	3	0
RW-9	0.01	0.00	0	0
RW-10	0.01	0.00	1	0
RW-11	0.03	0.00	5	1
RW-12	0.04	0.00	11	1
RW-13	0.07	0.00	42	2
RW-14	0.11	0.00	122	4
RW-15	0.06	0.00	33	2
RW-16	0.10	0.00	82	3
Total			3889	

6.1.2 Site B

Nominal results for Site B are presented in Table 16. The nominal simulation for Site B resulted in a final LNAPL recovery volume of 9,183 gallons, which is 5,817 gallons less than the actual recovered volume and represents an error factor of approximately 1.64.

TABLE 16. NOMINAL RESULTS FOR SITE B

Recovery Well	Specific Volume (ft)	Recoverable Volume (ft)	Final Recovery Volume (gal)	Percent Recovery
RW-1N	0.03	0.00	0	0
RW-2N	0.33	0.08	2312	25
RW-3N	0.06	0.00	8	0
RW-4N	0.17	0.02	461	10
RW-5N	0.25	0.04	1208	17
RW-6N	0.04	0.00	1	0
RW-7N	0.06	0.00	8	0
RW-8N	0.04	0.00	1	0
RW-9N	0.20	0.02	691	12
RW-10N	0.23	0.04	1021	16
RW-11N	0.00	0.00	0	0
RW-12N	0.08	0.00	20	1

RW-13N	0.06	0.00	8	0
RW-14N	0.05	0.00	3	0
RW-15N	0.04	0.00	1	0
RW-16N	0.03	0.00	0	0
RW-17N	0.02	0.00	0	0
RW-18N	0.06	0.00	8	0
RW-1S	0.00	0.00	0	0
RW-2S	0.00	0.00	0	0
RW-3S	0.00	0.00	0	0
RW-4S	0.01	0.00	0	0
RW-5S	0.09	0.00	34	1
RW-6S	0.26	0.05	1407	19
RW-7S	0.09	0.00	35	1
RW-8S	0.16	0.01	418	9
RW-9S	0.01	0.00	0	0
RW-10S	0.03	0.00	0	0
RW-11S	0.08	0.00	38	2
RW-12S	0.26	0.05	1499	20
Total			9183	

6.2 MAXIMUM RECOVERY SIMULATION

Maximum LNAPL recovery was simulated at each research site to estimate a best case recovery scenario. Input values for the maximum recovery simulations were determined by the corrected maximum LNAPL thickness, and through the value that represented the extreme range of published values for fluid and soil properties resulting in a best case recovery scenario. These values are presented in Chapter 5.

6.2.1 Site A

Maximum results for Site A are provided in Table 17. The maximum recovery simulation for Site A resulted in a final recovery volume of 4,923 gallons, which is 3,423 gallons more than the actual recovered volume and represents an error factor of approximately 3.28.

TABLE 17. MAXIMUM RESULTS FOR SITE A

Recovery Well	Specific Volume (ft)	Recoverable Volume (ft)	Final Recovery Volume (gal)	Percent Recovery
RW-1	0.14	0.03	824	21
RW-2	0.10	0.02	560	19
RW-3	0.10	0.02	462	17
RW-4	0.03	0.00	65	6
RW-5	0.08	0.01	301	14
RW-6	0.10	0.02	448	16
RW-7	0.03	0.00	48	6
RW-8	0.00	0.00	0	0
RW-9	0.01	0.00	4	1
RW-10	0.01	0.00	7	2
RW-11	0.02	0.00	19	3
RW-12	0.01	0.00	6	2
RW-13	0.08	0.01	320	15
RW-14	0.18	0.05	1349	26
RW-15	0.08	0.01	318	15
RW-16	0.06	0.01	192	11
Total			4923	

6.2.2 Site B

Maximum results for Site B are provided in Table 18. The maximum recovery simulation for Site B resulted in a final recovery volume of 22,892 gallons, which is 3,423 gallons more than the actual recovered volume and represents an error factor of approximately 1.53.

TABLE 18. MAXIMUM RESULTS FOR SITE B

Recovery Well	Specific Volume (ft)	Recoverable Volume (ft)	Final Recovery Volume (gal)	Percent Recovery
RW-1N	0.02	0.00	0	0
RW-2N	0.29	0.12	5775	42
RW-3N	0.04	0.00	18	1
RW-4N	0.12	0.02	1151	19
RW-5N	0.20	0.06	3016	32
RW-6N	0.03	0.00	2	0
RW-7N	0.04	0.00	18	1
RW-8N	0.03	0.00	2	0
RW-9N	0.15	0.04	1726	25
RW-10N	0.18	0.05	2549	29
RW-11N	0.00	0.00	0	0
RW-12N	0.05	0.00	47	2

RW-13N	0.00	0.00	0	0
RW-14N	0.04	0.00	7	0
RW-15N	0.03	0.00	2	0
RW-16N	0.02	0.00	0	0
RW-17N	0.01	0.00	0	0
RW-18N	0.04	0.00	18	1
RW-1S	0.00	0.00	0	0
RW-2S	0.00	0.00	0	0
RW-3S	0.00	0.00	0	0
RW-4S	0.00	0.00	0	0
RW-5S	0.06	0.00	81	3
RW-6S	0.22	0.07	3515	34
RW-7S	0.06	0.00	85	3
RW-8S	0.12	0.02	1044	18
RW-9S	0.01	0.00	0	0
RW-10S	0.02	0.00	0	0
RW-11S	0.05	0.00	92	4
RW-12S	0.21	0.08	3744	37
Total			22892	

6.3 MINIMUM RECOVERY SIMULATION

Minimum LNAPL recovery was simulated at each research site to estimate a worst case recovery scenario. Input values for the minimum recovery simulations were determined by the corrected maximum LNAPL thickness, and through the value that represented the extreme range of published values for fluid and soil properties resulting in a worst case recovery scenario.

6.3.1 Site A

Minimum results for Site A are provided in Table 19. The minimum recovery simulation for Site A resulted in a final recovery volume of 391 gallons, which is 1,109 gallons less than the actual recovered volume and represents an error factor of approximately 3.84.

TABLE 19. MINIMUM RESULTS FOR SITE A

Recovery Well	Specific Volume (ft)	Recoverable Volume (ft)	Final Recovery Volume (gal)	Percent Recovery
RW-1	0.08	0.01	74	9
RW-2	0.07	0.00	43	7
RW-3	0.06	0.00	34	6
RW-4	0.02	0.00	3	1
RW-5	0.05	0.00	20	4
RW-6	0.06	0.00	33	6
RW-7	0.02	0.00	2	1
RW-8	0.00	0.00	0	0
RW-9	0.01	0.00	0	0
RW-10	0.01	0.00	0	0
RW-11	0.01	0.00	1	1
RW-12	0.01	0.00	0	0
RW-13	0.05	0.00	22	5
RW-14	0.01	0.01	126	12
RW-15	0.05	0.00	21	5
RW-16	0.04	0.00	12	3
Total			391	

6.3.2 Site B

Minimum results for Site B are provided in Table 20. The minimum recovery simulation for Site B resulted in a final recovery volume of 3,349 gallons, which is 11,651 gallons less than the actual recovered volume and represents an error factor of approximately 4.48.

TABLE 20. MINIMUM RESULTS FOR SITE B

Recovery Well	Specific Volume (ft)	Recoverable Volume (ft)	Final Recovery Volume (gal)	Percent Recovery
RW-1N	0.19	0.00	0	0
RW-2N	0.20	0.02	412	10
RW-3N	0.04	0.00	47	5
RW-4N	0.12	0.01	144	6
RW-5N	0.16	0.03	554	17
RW-6N	0.03	0.00	18	3
RW-7N	0.04	0.00	47	5
RW-8N	0.03	0.00	18	3
RW-9N	0.13	0.02	346	12
RW-10N	0.15	0.02	496	16
RW-11N	0.00	0.00	0	0
RW-12N	0.05	0.00	72	7
RW-13N	0.04	0.00	47	5
RW-14N	0.03	0.00	30	4
RW-15N	0.03	0.00	18	3
RW-16N	0.02	0.00	9	2
RW-17N	0.01	0.00	3	1
RW-18N	0.04	0.00	47	5
RW-1S	0.00	0.00	0	0
RW-2S	0.00	0.00	0	0
RW-3S	0.00	0.00	0	0
RW-4S	0.00	0.00	0	0
RW-5S	0.06	0.00	92	8
RW-6S	0.17	0.03	595	17
RW-7S	0.07	0.00	57	4
RW-8S	0.11	0.01	291	12
RW-9S	0.01	0.00	0	0
RW-10S	0.02	0.00	0	0
RW-11S	0.05	0.00	0	0
RW-12S	0.14	0.00	9	0
Total			3349	

6.4 GRAPHICAL RECOVERY RESULTS

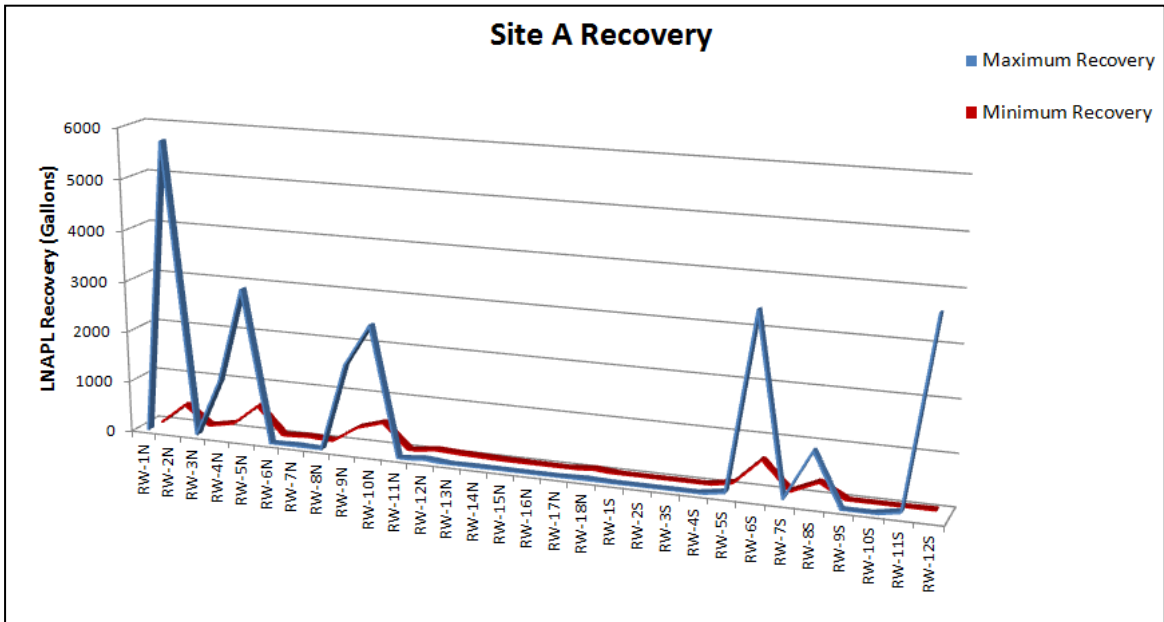


Figure 58. Graphical recovery results for Site A.

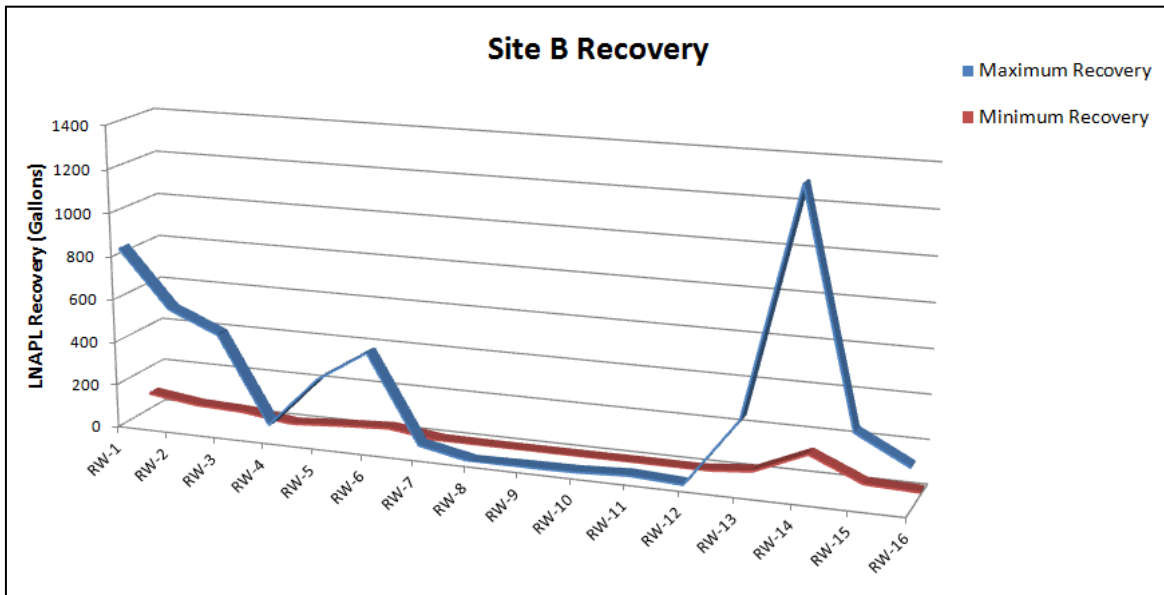


Figure 59. Graphical recovery results for Site B.

CHAPTER 7: ANALYSIS AND DISCUSSION

7.1 LDRM ESTIMATIONS

The LDRM results are summarized in Table 21 and compared with pre-remedial estimates and actual recovery at each research site. The error in modeled recovery is presented in Table 22. A total of three LDRM simulations are reported below, which include an initial simulation using nominal values, and a maximum and minimum recovery simulation using a refined input value range. The input value range was designed to factor variability within estimated parameters exhibiting a high degree of sensitivity. Therefore, the results are intended to represent an LNAPL recovery range that corresponds to the best-and worst-case recovery scenario.

TABLE 21. LDRM RESULTS AS COMPARED TO PRE-REMEDIAL ESTIMATES AND ACTUAL RECOVERY

	Non-Modeled Recovery		Modeled Recovery		
	Pre-remedial Estimate (gal)	Actual (gal)	Nominal (gal)	Maximum (gal)	Minimum (gal)
Site A	15,000	1,500	3,889	4,923	391
Site B	123,000	15,000	9,182	22,892	3,349

TABLE 22. ERROR FACTOR IN MODELED RECOVERY VERSUS ACTUAL RECOVERY

	Maximum Recovery Simulation	Minimum Recovery Simulation
Site A	+3.3	-3.8
Site B	+1.5	-4.5

7.1.1 Site A

The LDRM simulations for maximum and minimum LNAPL recovery scenarios at Site A resulted in 4,923 gallons and 331 gallons, respectively. The maximum modeled recovery of 4,923 gallons is within actual recovery of 1,500 gallons by a factor of 3.3. The minimum modeled recovery of 331 gallons is within actual recovery of 1,500 gallons by a factor of 4.5. The pre-remedial estimate of recoverable LNAPL volume at Site A was 15,000 gallons and is more than 10,000 gallons of the maximum modeled recovery. Based on both scenarios resulting in recoverable LNAPL within an error factor of five, the hypothesis is supported for Site A.

7.1.2 Site B

The LDRM simulations for maximum and minimum LNAPL recovery scenarios at Site B resulted in 22,892 gallons and 3,349 gallons, respectively. The maximum modeled recovery is within the actual recovery of 15,000 gallons by a factor of 1.5. The minimum modeled recovery of 3,349 gallons is within actual recovery of 15,000 gallons by a factor of 4.5. The pre-remedial estimate of recoverable LNAPL volume at Site A was 123,000 gallons and is more than 100,000 gallons of the maximum modeled recovery. Based on both scenarios resulting in recoverable LNAPL within an error factor of five, the hypothesis is supported for Site B.

7.2 ERROR AND UNCERTAINTY

Several potential sources of error have been identified to determine the effect on LDRM results and overall validity of the hypothesis. The greatest obstacle to overcome in this method of testing is to provide a thorough defense of LDRM input values. If there is variability within input values other than what is presented in this research then the

estimated value range provided through the maximum and minimum simulations does not encompass all possible error.

7.2.1 Actual Recovery Volume

Actual recovery volume at each research site, which is independent of the LDRM, provides the greatest non-model source of error. Based on a review of historical records and interviews with site personnel, reported LNAPL recovery at both research sites has been overestimated, significantly so at Site B. The reported LNAPL recovery at Site A – approximately 2,700 gallons between January 2009 and March 2013 – is actually closer to 1,500 gallons. At Site B, approximately 65,000 gallons of LNAPL were reportedly recovered between June 2001 and June 2013. However, actual recovered LNAPL is closer to 15,000 gallons. The rationale for using revised recovery volume is explained in detail in Chapter 5.

Despite the potential uncertainty in using an estimated recovery volume as basis for testing the hypothesis, if the reported volumes were used, which are believed to be overestimated, research results would not vary significantly. For example, the uncorrected reported LNAPL recovery at Site A is 2,700 gallons, which is within the nominal and maximum LDRM outputs by a factor of 1.4 and 3.3, respectively. Additionally, if 65,000 gallons was used at Site B, the maximum LDRM output remains within an error factor of 2.8. Furthermore, the LDRM results provide additional evidence for the accuracy of the estimated (i.e., corrected) actual recovered LNAPL at each site. This is particularly evident at Site B due to the drastic overestimation and the abundance of grain-size distribution data, which was used as a basis for determining capillary and petrophysical parameters.

7.2.2 LNAPL Hydrogeologic Condition

The actual method of gauging LNAPL thickness at both research sites was conducted with an oil-water interface probe accurate to 0.01 feet. Despite the relative accuracy of determining LNAPL thickness in this manner, it is difficult to determine if LNAPL is at vertical equilibrium. The LDRM not only assumes vertical equilibrium, but it also assumes unconfined conditions, which is the basis for requiring maximum monitoring well LNAPL thickness. Without further context on LNAPL hydrogeologic condition, the maximum LNAPL thickness can introduce significant error into LDRM estimates.

Using an uncorrected LNAPL thickness will only underestimate modeled volumes during a high water table stand under unconfined conditions. However, using multi-year gauging data and analyzing historical groundwater elevations at or near the site will typically mitigate this problem. Identifying the maximum LNAPL thickness through multi-year data for unconfined LNAPL will ensure an accurate vertical saturation distribution resulting in increasingly accurate LDRM estimates. Alternatively, confined and perched LNAPL will frequently result in the overestimation of recoverable volume unless the specific LNAPL hydrogeologic condition is identified and corrected. This suggests that simply using long-term gauging data without further context is not adequate to accurately define maximum LNAPL thickness at individual recovery wells.

At a minimum, graphical analysis through DGPs and HSGs should be used in conjunction with documented site activities and conditions to determine LNAPL hydrogeologic condition and identify deviations from vertical equilibrium. If the presence of confined and/or perched LNAPL is confirmed, additional baildown testing

should be completed to estimate the mobile LNAPL interval, which is analogous to the maximum LNAPL thickness as required by the LDRM. In the case of this research, baildown test data was unavailable and therefore the mobile LNAPL interval was estimated by using the median LNAPL thickness as a maximum LNAPL thickness equivalent. Due to the degree to which confined and/or perched LNAPL has been observed to exaggerate LNAPL thickness, this method could overestimate the mobile LNAPL interval relative to more refined techniques as those described in Kirkman et al. (2012).

7.2.3 Input Values Based on Published Results

Several fluid, capillary, and petrophysical LDRM parameters were unknown from site-specific field data at the two research sites. Many of these parameters are not typically determined during standard subsurface site investigations. Additionally, several unknown parameters exhibited a high degree of sensitivity, including LNAPL interfacial tension and van Genuchten N and α . API provides a means to estimate unknown parameters through its Parameter Database and Interactive LNAPL Guide. Fluid characteristics were matched by type and temperature, the latter of which was estimated at each site based on groundwater temperature. Capillary and petrophysical characteristics are grain-size dependent, indicating some variability within each soil type through differing grain-size distributions. These characteristics are listed for specific soil samples with known grain-size distributions (Parameter Database), and as average values by soil type (LNAPL Guide).

Geotechnical samples were collected along the north and southeast remediation areas at Site B and submitted for grain-size analysis. Therefore, matching site-specific

grain-size distributions with those provided in the Parameter Database are inherently more accurate than Site A. Site A was limited to general soil characterizations using the USCS and matched mostly with the average values listed in the LNAPL Guide. Despite the potential error in estimating fluid, capillary, and petrophysical LDRM parameters at both research sites, a value range was determined for maximum and minimum LNAPL recovery. Providing that the values listed in the Parameter Database and LNAPL Guide represent the full range of variability found in the field, the range in potential LNAPL recovery represented by maximum and minimum recovery simulations correct for error.

7.3 MODEL LIMITATIONS

The LDRM simulates steady-state radial flow for a single recovery well while assuming unconfined conditions at vertical equilibrium. As previously discussed, this requires a correction for LNAPL hydrogeologic condition other than assumed conditions in order to accurately delineate the vertical LNAPL saturation distribution and mobile LNAPL interval. Additionally, this implies that 1) the hydraulic gradient is zero, and 2) the groundwater elevation will remain constant. The significance is that the LDRM does not account for LNAPL migrating into the radius of recovery or future groundwater fluctuations that could result in trapping or releasing LNAPL. Therefore, the LDRM is most effective for stable LNAPL plumes and groundwater conditions.

At Site B in particular, petroleum hydrocarbon releases could date back to the early 1900s while gauging data only extends to the 1990s. It is possible for a significant amount of LNAPL to be present within the saturated zone, unaccounted for by gauging data and hence, LDRM simulations. Additionally, while both research sites exhibit relatively stable LNAPL plumes, canal fluctuations and additional factors resulting in

non-vertical equilibrium conditions are capable of inducing LNAPL migration into and out of respective remediation areas.

7.4 FUTURE WORK

It is understood that a high-resolution LNAPL delineation was performed at Site A in early to mid 2014 through cone penetration testing (CPT) with laser induced fluorescence (LIF). However, data from the investigation have not yet been provided to the author, nor has the exact scope of the investigation been confirmed. Efforts are currently being made to obtain this data, which could validate the research findings and/or refine the LDRM simulations at the site.

Additional subsurface investigations are tentatively planned at Site B for later this year or into 2015. The exact methods of investigation are not yet confirmed, but possibilities range from soil borings and monitoring well installation to CPT with LIF. Based on current arrangements with Site B representatives, all additional data will be immediately available for further analysis by the author. These data will assist in refining the graphical methods used to determine LNAPL hydrogeologic condition and provide a means for additional LDRM calibration and ultimately produce more accurate estimates. Additionally, LNAPL baildown testing is planned during the spring and/or summer of 2014. Data from such testing will be used to construct DvD graphs in order to corroborate LNAPL hydrogeologic condition and refine the mobile LNAPL interval. However, limited ANT in monitoring wells (i.e., <0.5 feet) is expected to limit the scope and accuracy of the testing and data.

CHAPTER 8: SUMMARY AND CONCLUSION

The objective of this research was to demonstrate that the LDRM could be used as an accurate recovery estimation tool for vacuum-enhanced recovery of LNAPL with basic site data. Therefore, the hypothesis was designed to test the effectiveness of pre-remedial modeling using the LDRM to estimate recoverable LNAPL with vacuum-enhanced extraction. Retrospective pre-remedial modeling was conducted at two active remediation sites that have approximate order-of-magnitude recovery errors and have reached asymptotic LNAPL recovery. The hypothesis was tested by comparing modeled recovery with actual recovery at both sites.

In order to account for potential error associated with choosing values based on limited site-specific data, an input value range was established for each LDRM parameter, which was designed to simulate maximum and minimum LNAPL recovery. The value range for each parameter was based either on the variability observed in site data (e.g., radius of recovery at Site A) or the maximum and minimum values observed in published literature. If a given parameter was unknown through site-specific data, the API Parameter Database and API Interactive LNAPL Guide was used to estimate values based on soil type or grain-size distribution and fluid type. Site-specific soil and fluid data were matched to corresponding data in the API Database and API LNAPL Guide, which included unknown parameter values such as LNAPL interfacial tension and van Genuchten N .

The maximum monitoring well LNAPL thickness was determined through monitoring well gauging records and corrected through the analysis of diagnostic gauge plots and hydrostratigraphs. Previous site investigations and conceptual site models did

not account for confined and/or perched LNAPL, which can result in the overestimation of LNAPL recovery volume and MPE system capabilities. Despite the confirmation of confined and perched LNAPL at both research sites, baildown data was not available. Therefore, a corrected maximum LNAPL thickness at each site was calculated based on the median value of ANT at a given monitoring well.

The model was calibrated with site-specific data at each site known with relative certainty including hydraulic conductivity, water production rate, LNAPL density, and vacuum pressure. Additional calibration through soil and fluid-matched data within the API Database and API LNAPL Guide, such as interfacial tension and van Genuchten values, was also conducted. However, despite using maximum and minimum values, matched values may contain variability that does not encompass actual variability at each site. Therefore, a refined calibration could be conducted by taking undisturbed soil samples at each research site and conducting laboratory testing to confirm capillary and petrophysical properties.

The results of the maximum and minimum LDRM simulations were compared with actual LNAPL recovered at each research site. The results for each of the four simulations are within an error factor of five of the actual recovered LNAPL. Since the pre-remedial estimates exaggerated recoverable LNAPL by an approximate order-of-magnitude at each site, and the modeled estimates are within an error factor of 5, the LDRM could have been utilized at each site to avoid such errors. More specifically, the hypothesis is supported at each research site suggesting that the pre-remedial estimation of recoverable LNAPL within a factor of five of actual recovered LNAPL is plausible. Based on these results, the LDRM can be utilized at future vacuum-enhanced recovery

operations that are limited to basic site data in order to avoid significant predictive errors in recoverable LNAPL volume.

REFERENCES

- Adamski, M., V. Kremesec, R. Kolhatkar, C. Pearson, and B. Rowan, 2005, LNAPL in fine-grained soils: Conceptualization of saturation, distribution, recovery, and their modeling: *Ground Water Monitoring and Remediation*, v. 25, no. 1, p. 100–112.
- AMEC Earth & Environmental, Inc., 2010, Remedial Action Plan, Submitted to the Illinois EPA: AMEC Project No. 277720016, p. 1-32.
- AMEC Environment & Infrastructure, Inc., 2013, 1st Quarter 2013 System Operation and Maintenance Report, Submitted to the Illinois EPA: AMEC Project No. 277720068, p. 1-72.
- American Petroleum Institute, 2003, API LNAPL Parameters Database, Version 2.0.
- American Petroleum Institute, 2006, API Interactive LNAPL Guide: Version 2.0.4.: A computer program for evaluating LNAPL mobility, stability, and recoverability.
- AQUI-VER, Inc., 2006, Appendix A: Review of the LNAPL distribution & recovery model mathematical verification, code fixes, & sensitivity, *in* LNAPL Distribution and Recovery Mode (LDRM), Volume 2: User and Parameter Selection Guide: API Publication Number 4760, Washington, DC: American Petroleum Institute, p. 9-19.

- Ballestero, T. P., Fiedler, F. R., & Kinner, N. E., 1994, An investigation of the relationship between actual and apparent gasoline thickness in a uniform sand aquifer: *Groundwater*, v. 32, no. 5, p. 708-718.
- Bear, J., 1972, *Dynamics of fluids in porous media*, American Elsevier Pub., New York, p. 441-457.
- Beckett, G. D., and P. Lundegard, 1997, Practically Impractical – The limits of LNAPL recovery and relationship to risk, *in* *Proceedings of Petroleum Hydrocarbons and Organic Chemicals in Ground Water: Prevention, Detection and Restoration*: Houston, Texas, p. 442-445
- Beckett, G. D., and D. Huntley, 1998, Soil properties and design factors influencing free-phase hydrocarbon cleanup, *Environmental Science & Technology*, v. 32, no. 2, p. 287-293.
- Blake, S.B. and M.M. Gates. 1986. Vacuum enhanced hydrocarbon recovery: A case study, *in* *Proceedings: Petroleum Hydrocarbons and Organic Chemicals in Groundwater*, 709-721.
- Charbeneau, R.J., 2007a, LNAPL Distribution and Recovery Model (LDRM), Volume 1: *Distribution and Recovery of Petroleum Hydrocarbon Liquids in Porous Media*: API Publication Number 4760, Washington, DC: American Petroleum Institute, p. 1-41.

Charbeneau, R.J., 2007b, LNAPL Distribution and Recovery Mode (LDRM), Volume 2: User and Parameter Selection Guide: API Publication Number 4760, Washington, DC: American Petroleum Institute, p. 1-79.

Charbeneau, R.J., 2000, Groundwater Hydraulics and Pollutant Transport, Long Grove, Illinois: Waveland Press, p. 527.

Charbeneau, R.J., R.T. Johns, L.W. Lake and M.J. McAdams III, 2000, Free-product recovery of petroleum hydrocarbon liquids: API Publication Number 4682, Washington D.C: American Petroleum Institute, p. 147-158.

Charbeneau, R.J. and M. Adamski, 2008a, LNAPL in the subsurface: LNAPL modeling recovery and endpoint example, San Diego Department of Environmental Health, Site Assessment and Mitigation Program (SAM) Forum: Developments in LNAPL Understanding
http://www.sdcounty.ca.gov/deh/water/sam_update_agenda.html#SAMFall2010Update2 (October 2013), p. 1-35.

Charbeneau, R.J. and M. Adamski, 2008b, LNAPL in the subsurface: LNAPL mobility and well thickness variations, San Diego Department of Environmental Health, Site Assessment and Mitigation Program (SAM) Forum: Developments in LNAPL Understanding

http://www.sdcounty.ca.gov/deh/water/sam_update_agenda.html#SAMFall2010Update2 (Accessed October 2013), p. 1-23.

Environmental Protection Agency (EPA), 1996, How to Effectively Recover Free-product at Leaking Underground Storage Tank Sites: A Guide for State Regulators. Office of Solid Waste and Emergency Response, EPA 510-R-96-001, p. 1-38.

Environmental Protection Agency (EPA), 1999, MPE state of the practice: Office of Solid Waste and Emergency Response, EPA 542-R-99-004, p. 1-70.

Environmental Protection Agency (EPA), 2004, Cleanup of the nation's waste sites: Office of Solid Waste and Emergency Management, EPA 542-R-04-015, Executive Summary.

Environmental Protection Agency (EPA), 2005, A Decision Making Framework for Cleanup of Sites Impacted with Light Non-Aqueous Phase Liquids (LNAPL): Office of Solid Waste and Emergency Response, EPA 542-R-04-011, p. 21-25.

Farr, A.M., R.J. Houghtalen, D.B. McWhorter, 1990, Volume estimation of light nonaqueous phase liquids in porous media: *Ground Water*, v. 28, no. 1, p. 48-56.

Groundwater Technology, Inc., 1993, Installation of Recovery Wells RW-2, RW-3, and RW-4, p. 1-15.

Gruszczenski, T.S, 1987, Determination of a realistic estimate of the actual formation product thickness using monitor wells: A field bailout test, *in* Proceedings of the NWWA/API Conference on Petroleum Hydrocarbons and Organic Chemicals in Ground Water: Prevention, Detection, and Restoration, p. 235-253.

Hawthorne, J.M, 2012, Advanced Diagnostic Gauge Plots: Pattern Recognition and Analysis of Light Non-Aqueous Phase Liquid Hydrogeologic Conditions, *in* Proceedings of the International Petroleum Environmental Conference (IPEC), Houston, Texas.
http://ipec.utulsa.edu/Conf2012/Papers_Presentations/Hawthorne_AdvDGPs.pdf
(January 2014), p. 1-17.

Hawthorne, J.M., A.J. Kirkman, and M. Adamski, 2011, Light Non-Aqueous Phase Liquids (LNAPL): It's Not Just Unconfined, *in* Proceedings of the International Petroleum Environmental Conference (IPEC), Houston, Texas.
http://ipec.utulsa.edu/Conf2011/Full%20Manuscripts%20&%20PP%20presentations/Hawthorne_43.pdf (December 2013), p. 1-20.

H2A Environmental, Ltd (H2A), 2011a, LNAPL Thickness Revitalized: Applied NAPL Science Review, v. 1, no. 1: <http://www.h2altd.com/ansr> (January 2014).

H2A Environmental, Ltd (H2A), 2011b, Diagnostic Gauge Plots: Applied NAPL Science Review, v. 1, no. 2: <http://www.h2altd.com/ansr> (January 2014).

H2A Environmental, Ltd (H2A), 2011c, Confined LNAPL: Applied NAPL Science Review, v. 1, no. 5: <http://www.h2altd.com/ansr> (January 2014).

H2A Environmental, Ltd (H2A), 2011d, Perched LNAPL: Applied NAPL Science Review, v. 1, no. 6: <http://www.h2altd.com/ansr> (January 2014).

Huntley, D., 2000, Analytic determination of hydrocarbon transmissivity from baildown tests, *Groundwater*, v. 38, no. 1, p. 46-52.

Huntley, D., J.W. Wallace, and R.N. Hawk, 1994, Nonaqueous phase hydrocarbon in a fine-grained sandstone: 2. Effect of local sediment variability on the estimation of hydrocarbon volumes, *Ground Water*, v. 32, no. 5, p. 778–783.

Huntley, D. and G.D. Beckett, 2002, Persistence of LNAPL sources: relationships between risk reduction and LNAPL recovery, *Journal of Contaminant Hydrology*, v. 59, no. 1, p. 3-26.

Illangasekare, T.H., J.L. Ramsey Jr, K.H. Jensen, and M.B. Butts, 1995, Experimental study of movement and distribution of dense organic contaminants in heterogeneous aquifers, *Journal of Contaminant Hydrology*, v. 20, no. 1, p. 1-25.

Interstate Technology and Regulatory Council (ITRC), 2013a, LNAPL Training Part 1:
An Improved Understanding of LNAPL Behavior in the Subsurface – State of
Science vs. State of Practice: Contaminated Site Clean-up Information (CLU-IN):
<http://clu.in.org/live/archive/default.cfm?display=all&group=itrc#> (January 2014), p.
1-81.

Interstate Technology and Regulatory Council (ITRC), 2013b, LNAPL Training Part 2:
LNAPL Characterization and Recoverability – An Improved Understanding:
Contaminated Site Clean-up Information (CLU-IN):
<http://clu.in.org/live/archive/default.cfm?display=all&group=itrc#> (January 2014), p.
1-88.

Jeong, J., and R.J. Charbeneau, 2014, An analytical model for predicting LNAPL
distribution and recovery from multi-layered soils, *Journal of Contaminant
Hydrology*, no. 156, p. 52-61.

Kahraman, I., 2013, Analysis of a LNAPL Recovery System Using LDRM in a South
Texas Facility [M.Sc. Thesis]: Austin, The University of Texas, p. 82.

Kirkman, A.J., M. Adamski, and J.M. Hawthorne, 2013, Identification and assessment of
confined and perched LNAPL conditions, *Groundwater Monitoring and
Remediation*, v. 33, no. 1, p. 75-86.

Lenhard, R.J., and J.C. Parker, 1990, Estimation of free hydrocarbon volume from fluid levels in monitoring wells, *Ground Water*, v. 28, no. 1, p. 57-67.

Lundy, D.A., 2008, A conceptual model and analytical solutions for multiphase extraction at a vacuum-enhanced LNAPL recovery well, *in the Proceedings of the NGWA Petroleum Hydrocarbons and Organic Chemicals in Ground Water: Prevention, Detection, and Remediation Conference*, Houston, TX, p. 1-16.

Munzar, S. and V. Hemmera, 2009, LNAPL Deep Below the Water Table – How Did It Get There? The Importance of Proper Site Characterization and Implications for Remediation., National Groundwater Association Online Archive: info.ngwa.org/GWOL/pdf/100684263.pdf (January 2014), p. 1-14

Muthu, R. and J.M. Hawthorne, 2013, Discharge vs. Drawdown: A Critical Tool for the API LNAPL Transmissivity Spreadsheet Tool, *in Proceedings of the International Petroleum Environmental Conference (IPEC)*, Houston, Texas: http://ipec.utulsa.edu/Conf2013/Manuscripts_pdfs/Muthu_DvD.pdf (February 2014), p. 1-16.

Newell, C.J., S.D. Acree, R.R. Ross, and S.G. Huling, 1995, Light Non-Aqueous Phase Liquids: Environmental Protection Agency, Groundwater Issue EPA/540/S-95/500, p. 1-28.

Parsons Engineering Science, Inc., 2002, Revised Work Plan for the Former Bulk Storage Facility, Prepared for the USEPA Region V: Parsons project no. 739418, p. 1-21.

Parsons Engineering Science, Inc., 2009, Geotechnical Investigation – Barrier Wall Design, Oil Bulk Storage Facility, p. 1-11.

Parsons Engineering Science, Inc., 2014, USEPA Quarterly Progress Report: 1st Quarter 2014, Prepared for the USEPA Region, p. 1-12.

Remediation Technologies Development Forum (RTDF), 2006, The Basics: Understanding the Behavior of Light Non-Aqueous Phase Liquids (LNAPLs) in the Subsurface: <http://www.rtdf.org/PUBLIC/napl/training/> (February 2014).

Golden Software, Inc., 2013, Surfer 12: Contouring and 3D Surface Mapping for Scientists and Engineers, User's Guide, Golden, Colorado, p. 1-620.

van Genuchten, M.T., 1980, A closed form equation for predicting the hydraulic conductivity of unsaturated soils, Soil Science Society of America Journal, v. 44 no. 5, p. 892-898.

APPENDIX A. MONITORING AND RECOVERY WELL LOCATION MAPS

FIGURE A.1. Site A Monitoring and Recovery Well Location Map

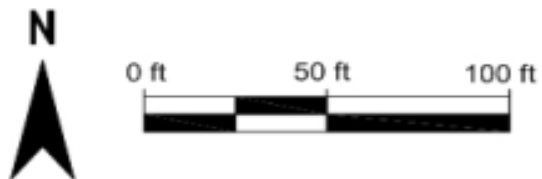


FIGURE A.2. Site B Monitoring Well Location Map

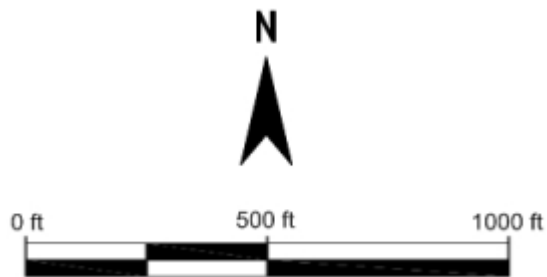
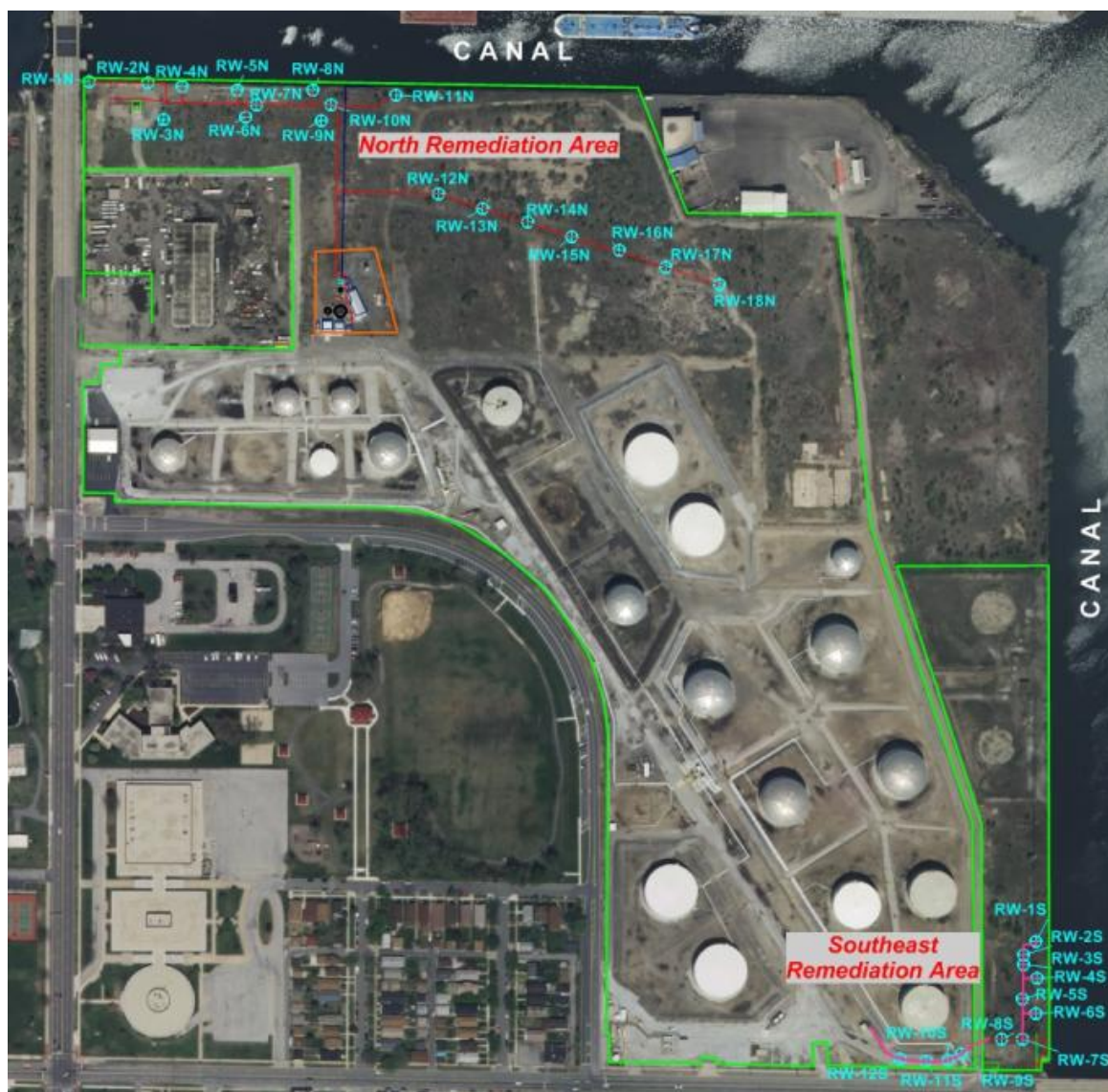
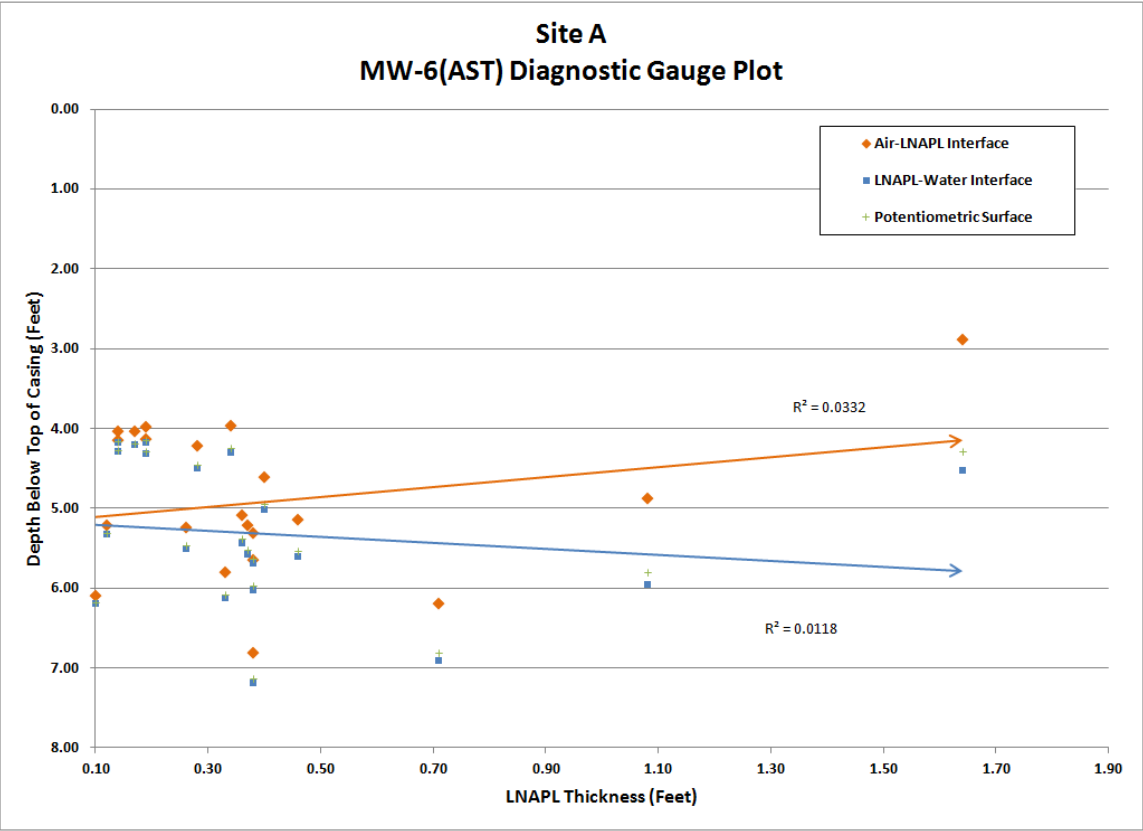
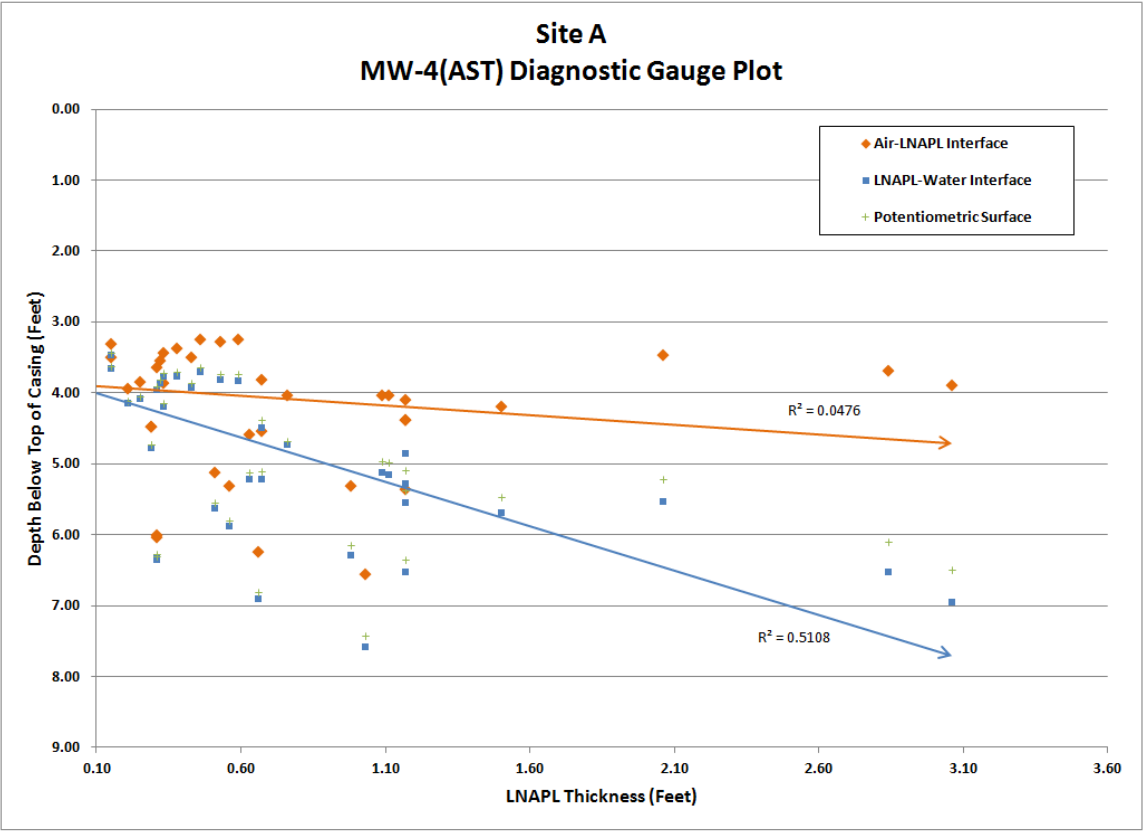
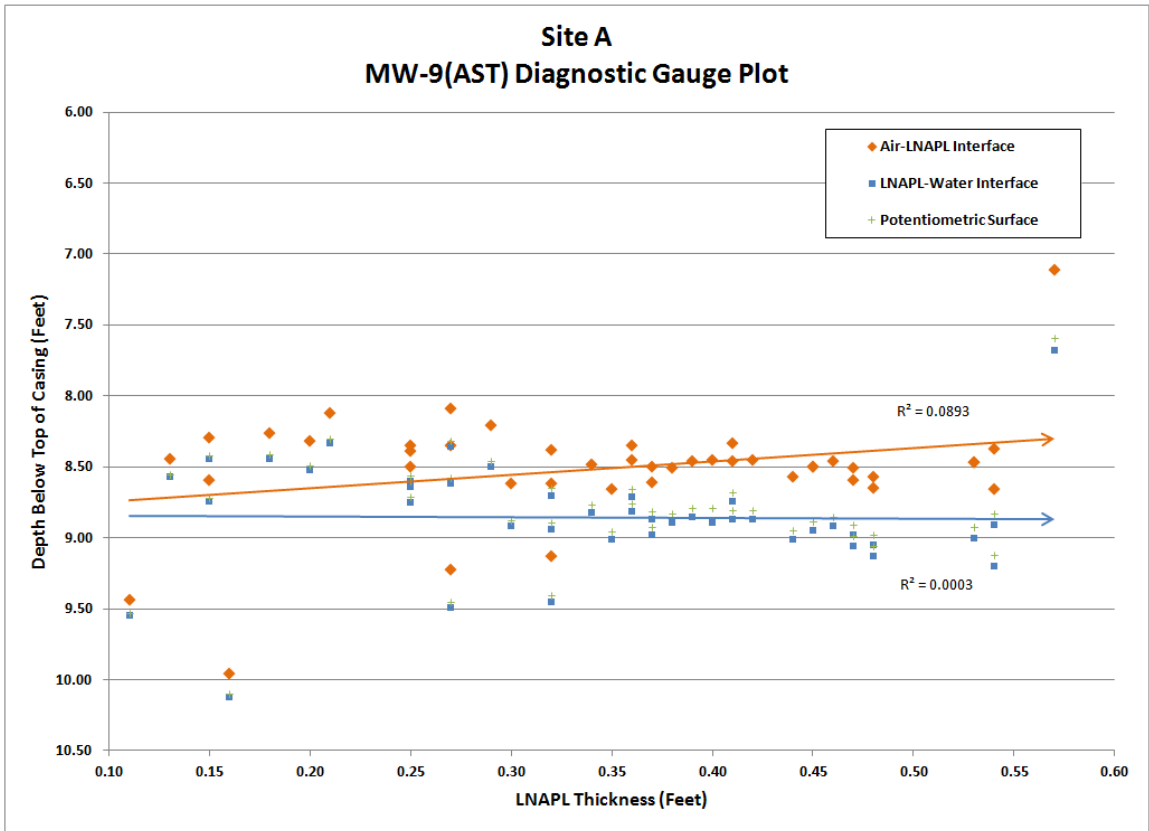
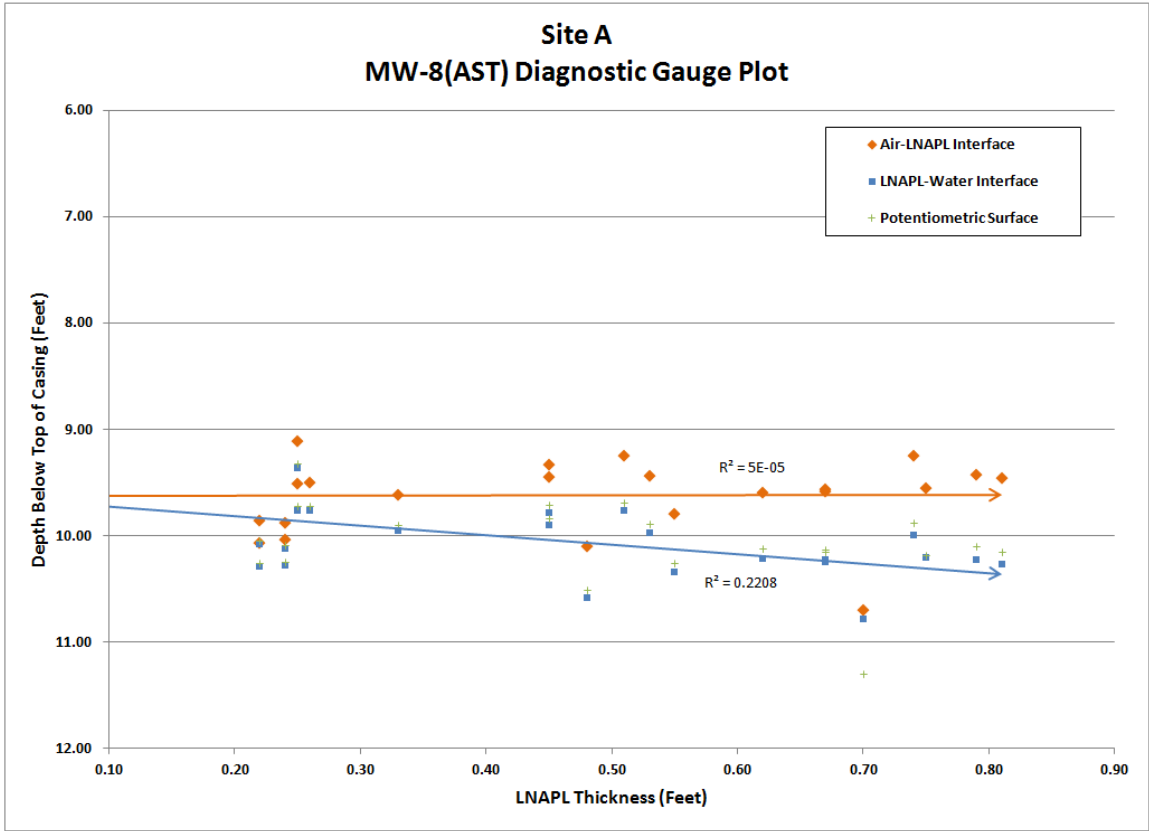


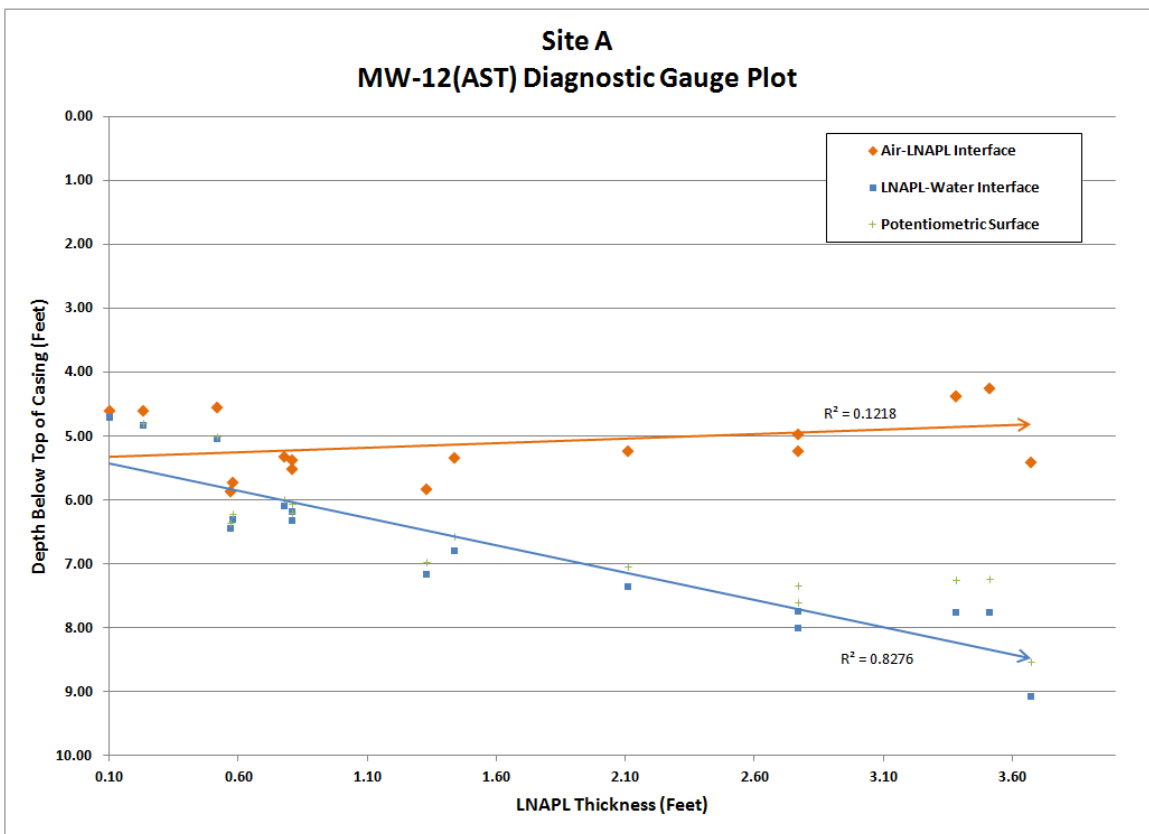
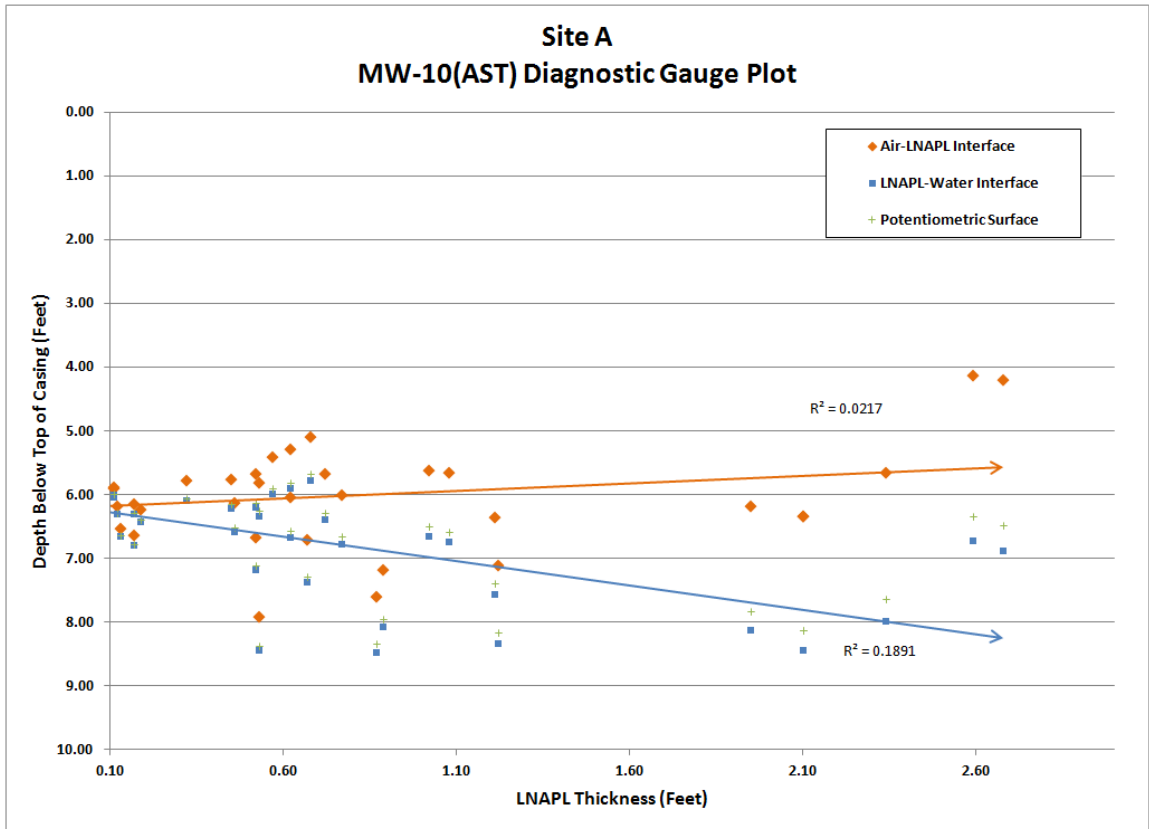
FIGURE A.3. Site B Recovery Well Location Map

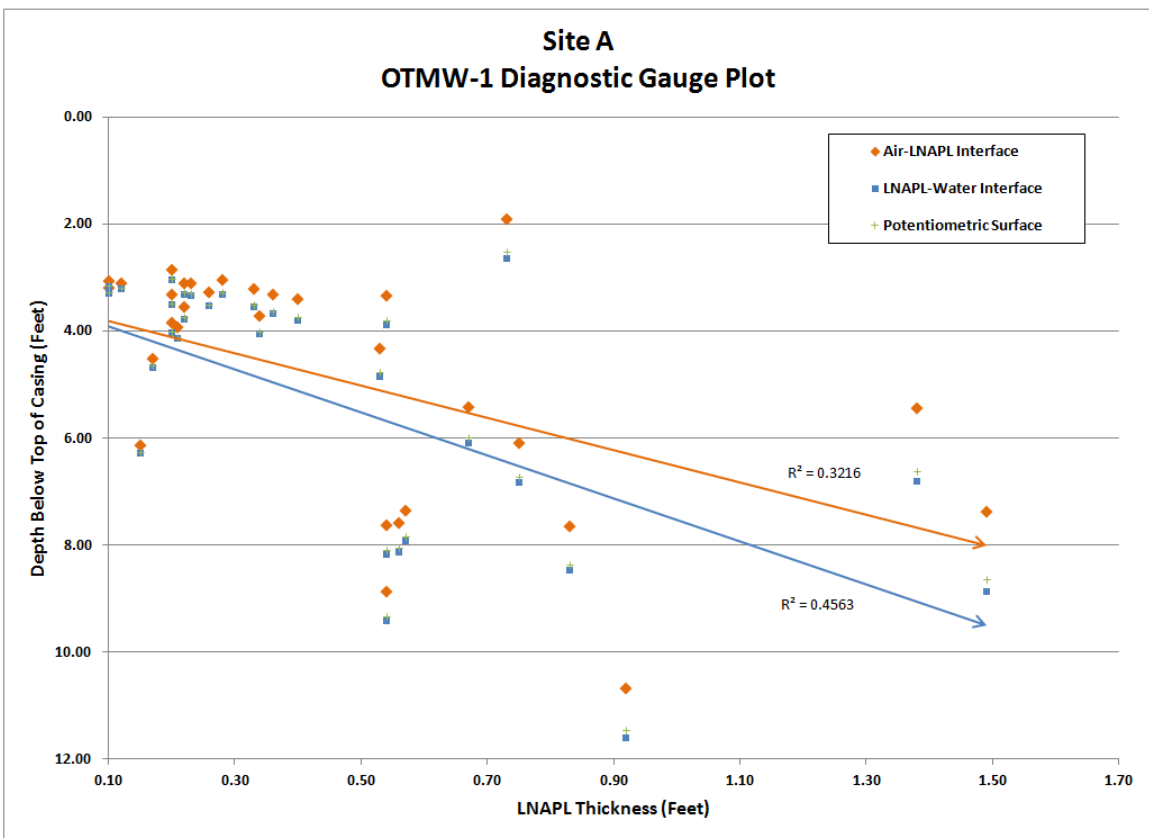
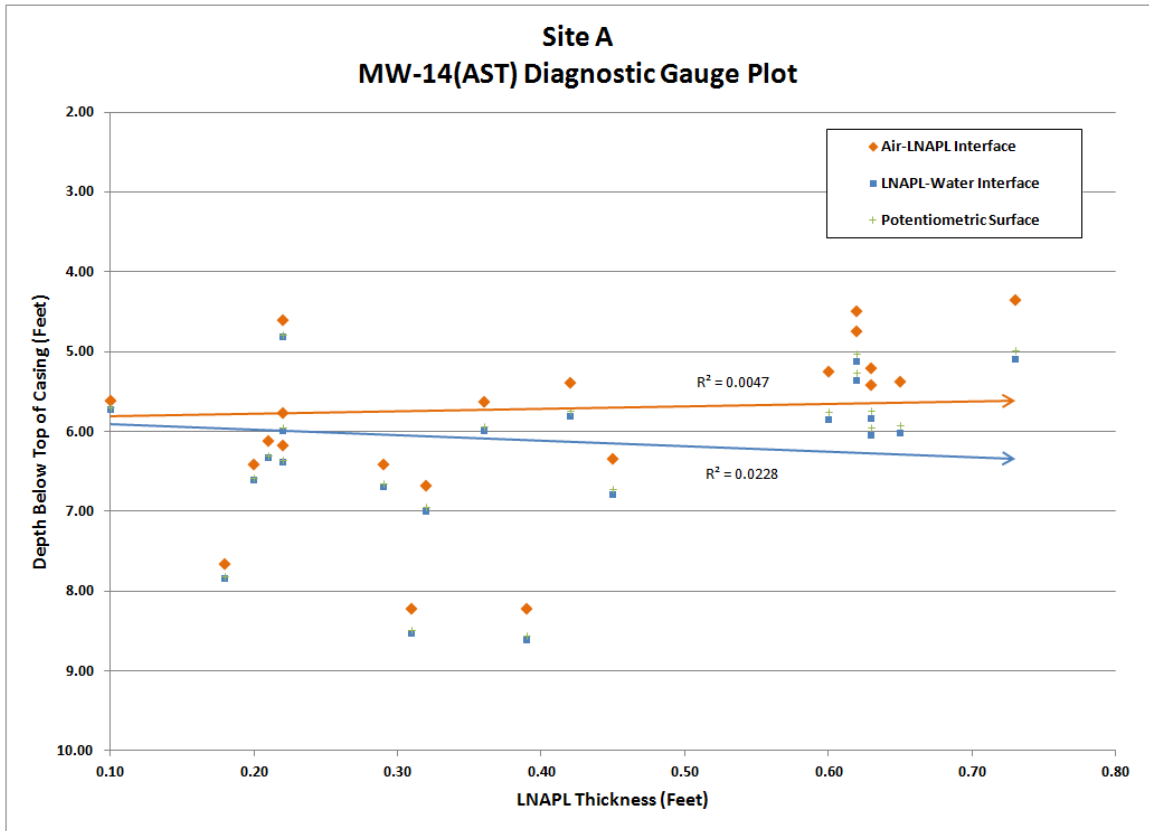


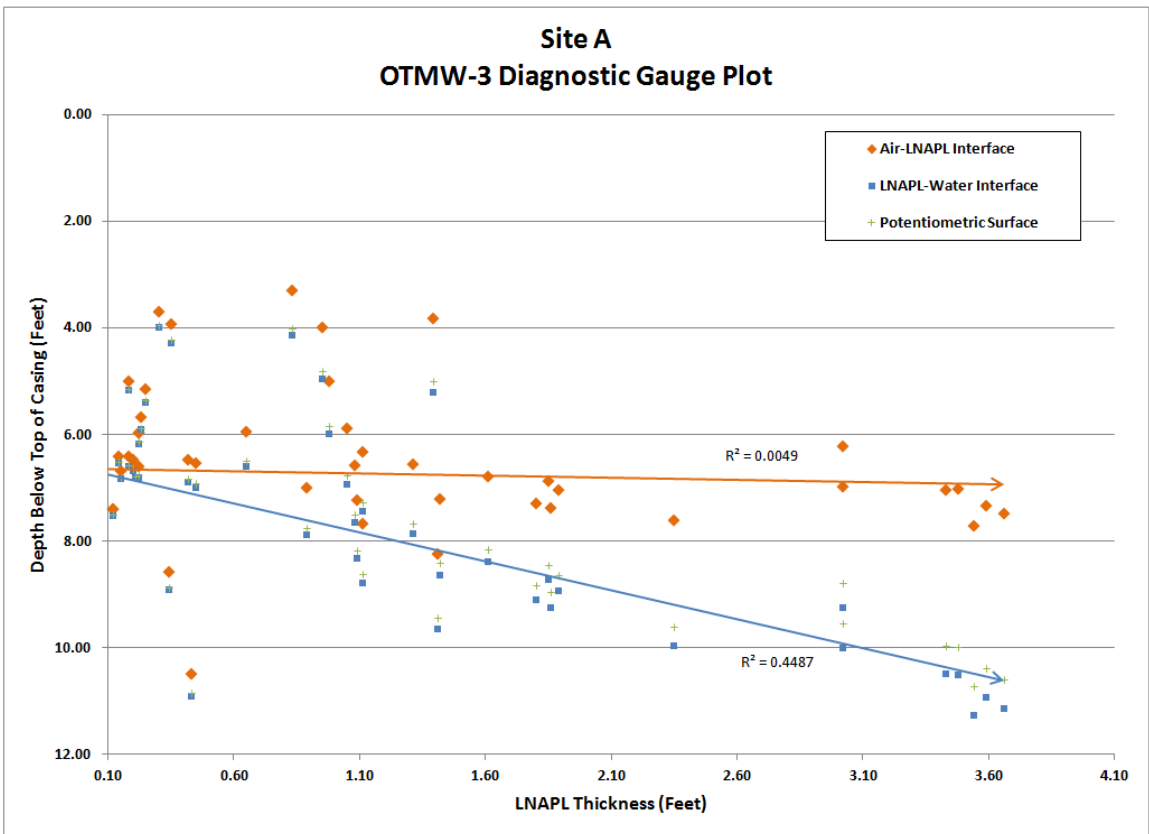
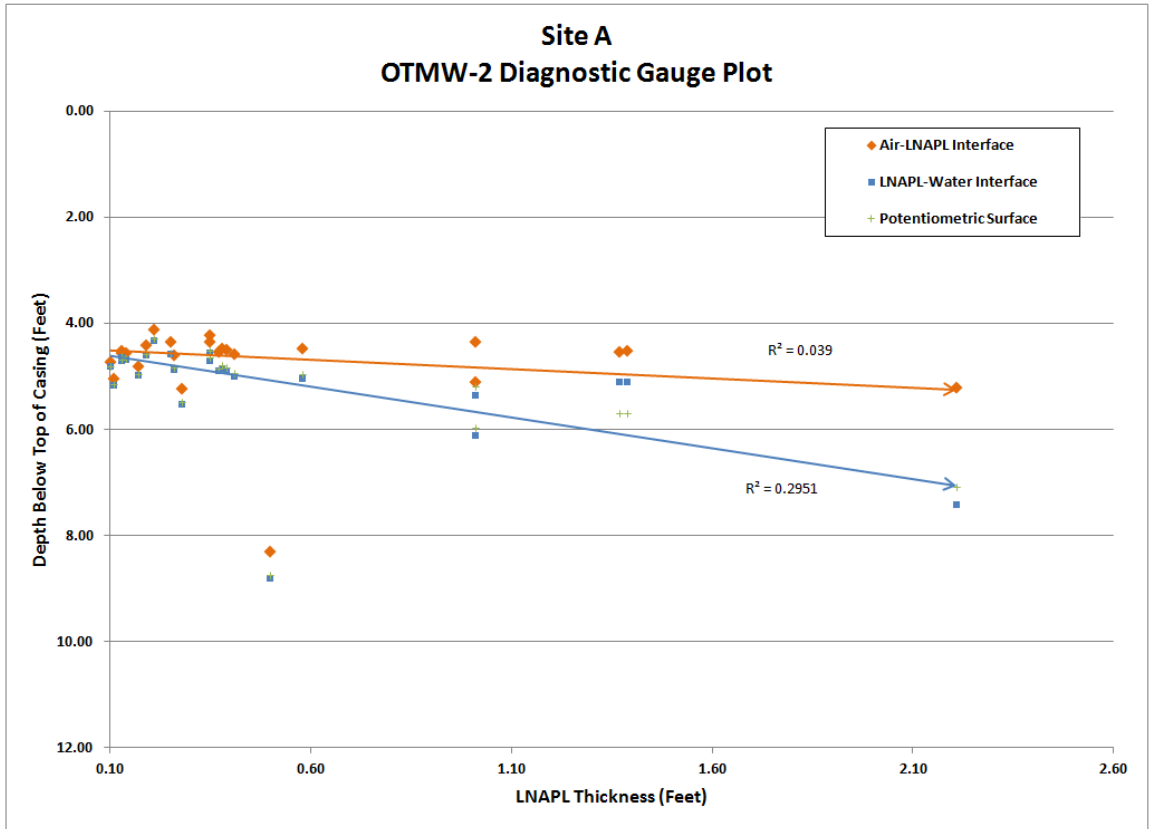
APPENDIX B. DIAGNOSTIC GAUGE PLOTS

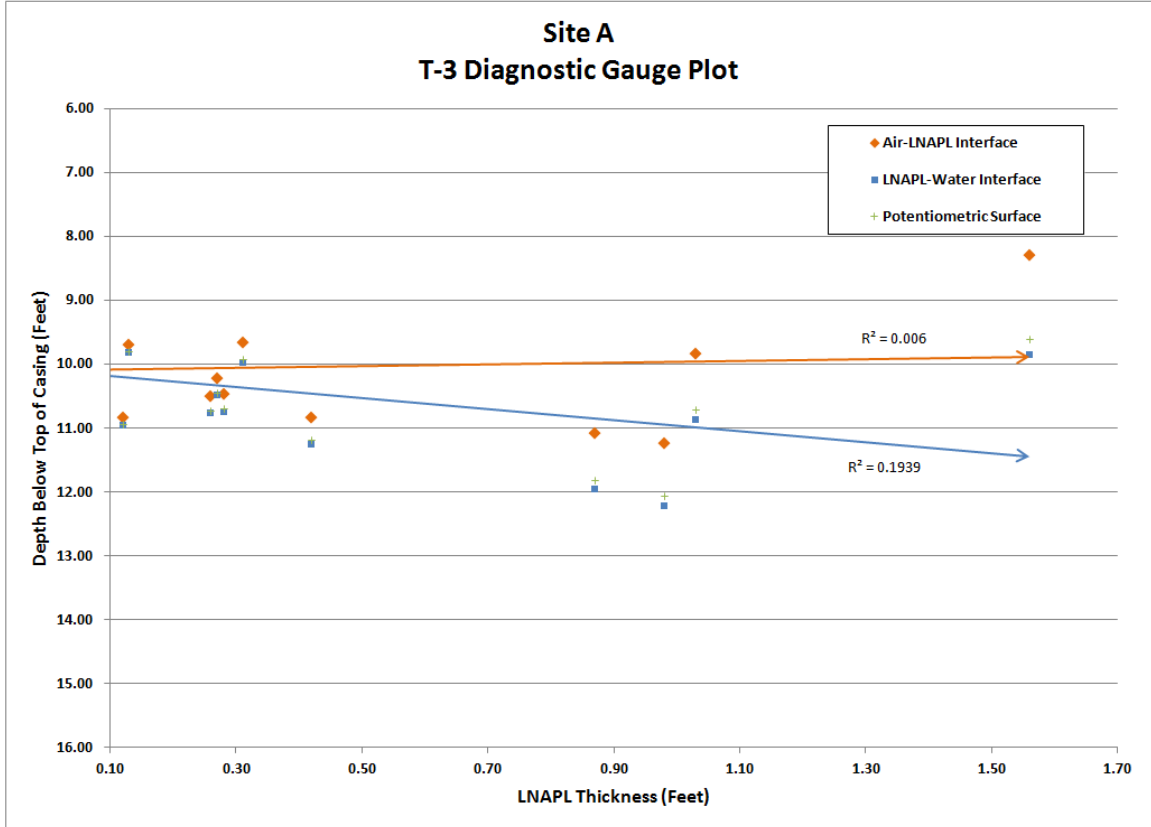
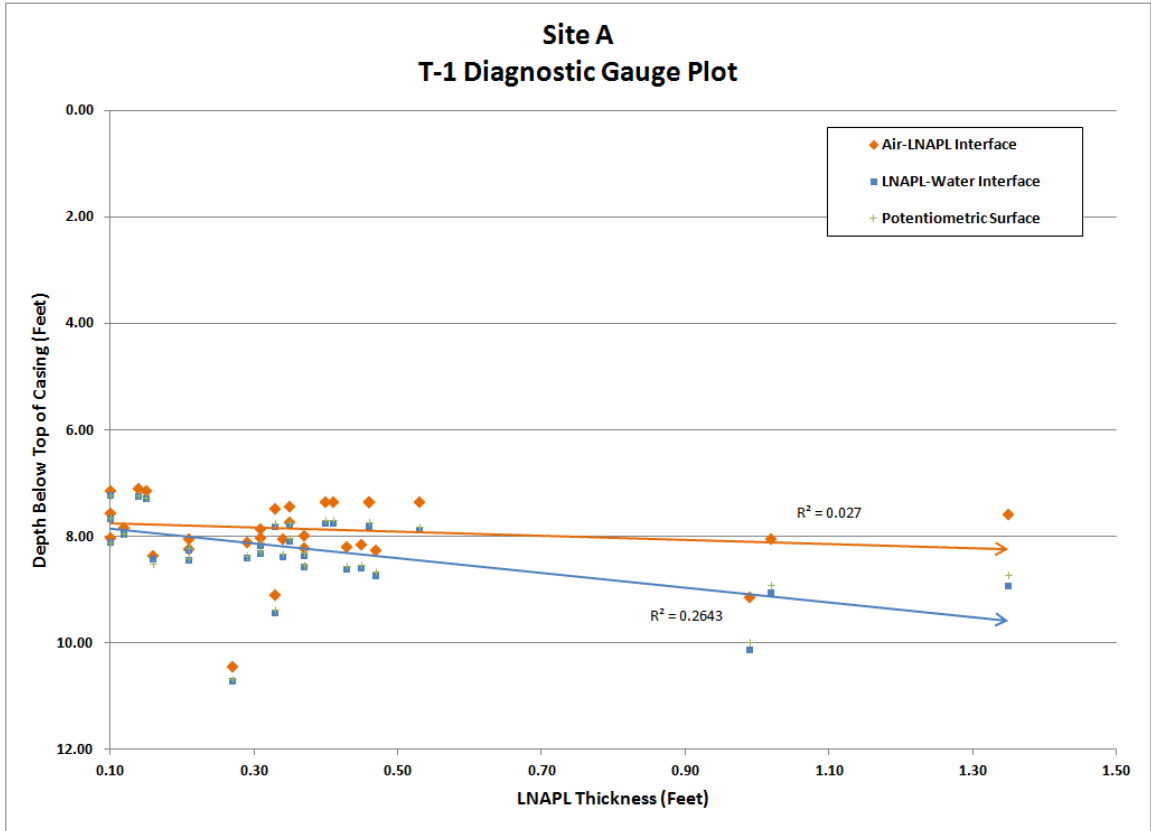


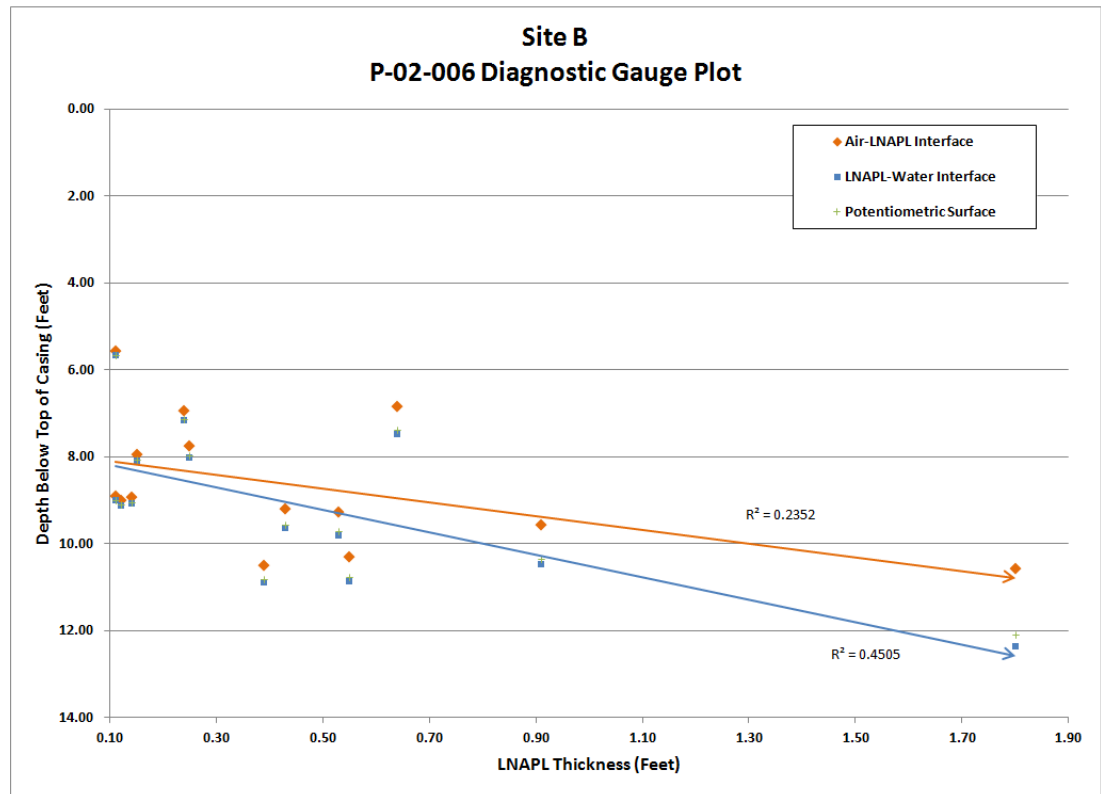
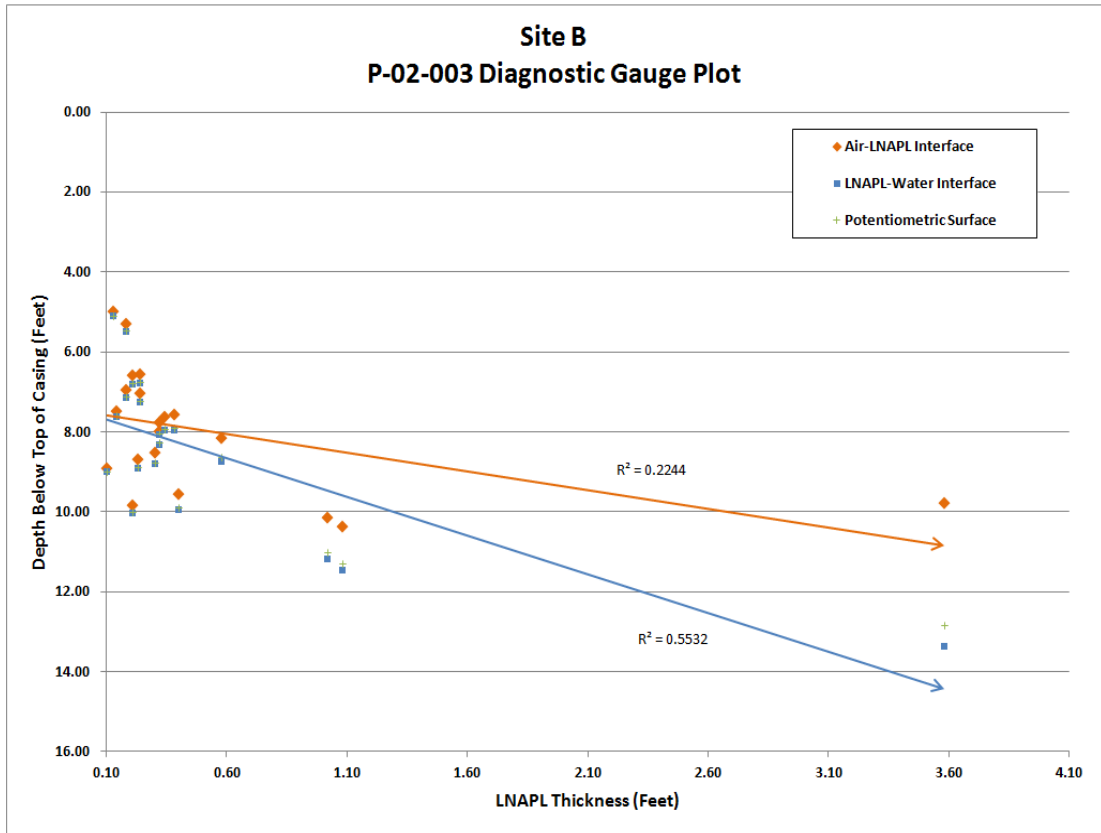


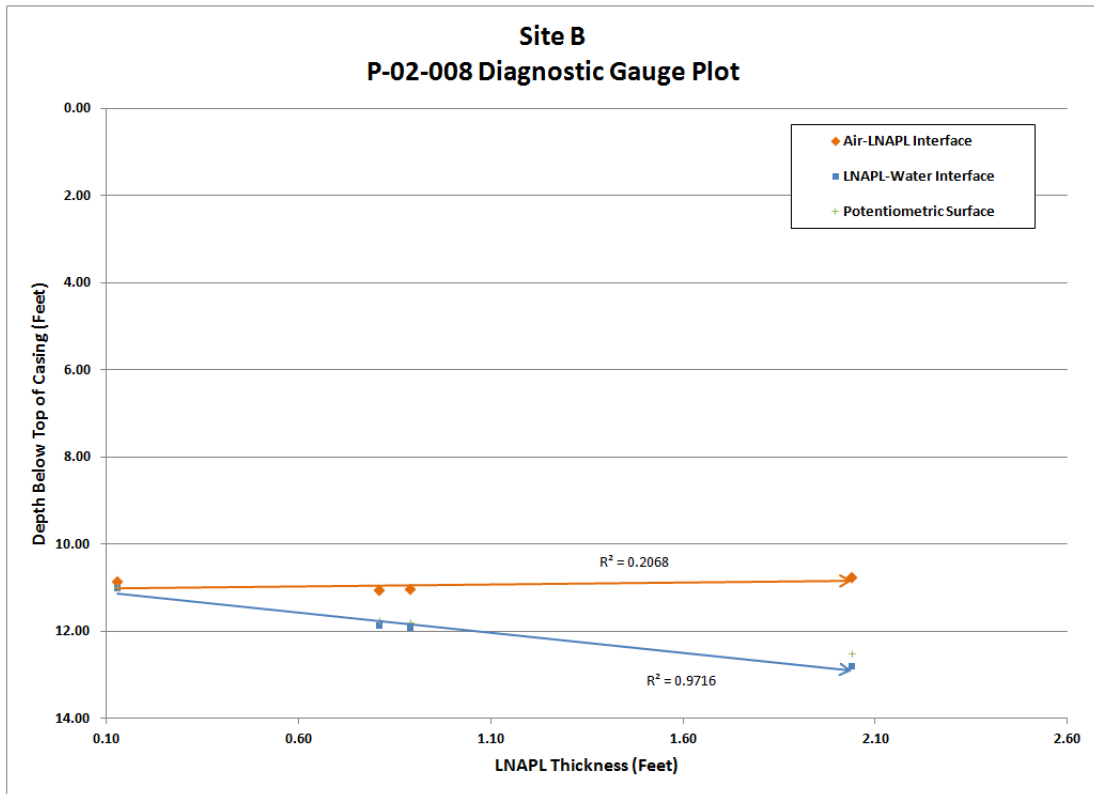
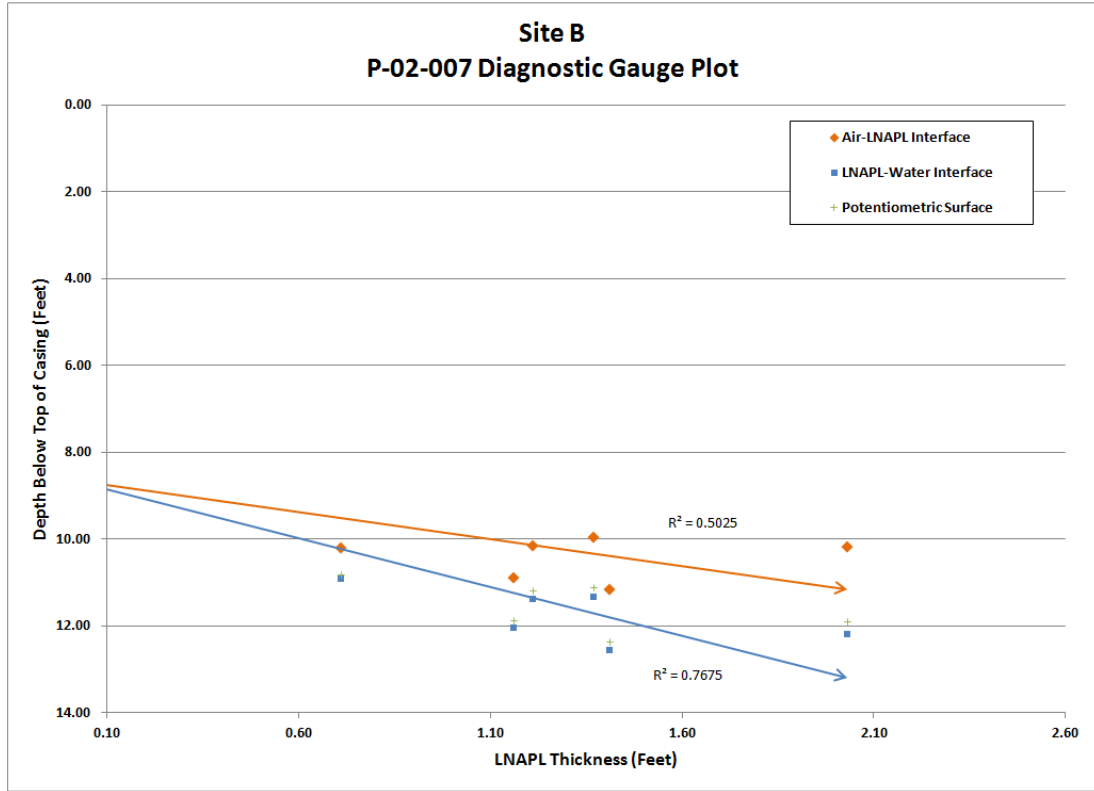


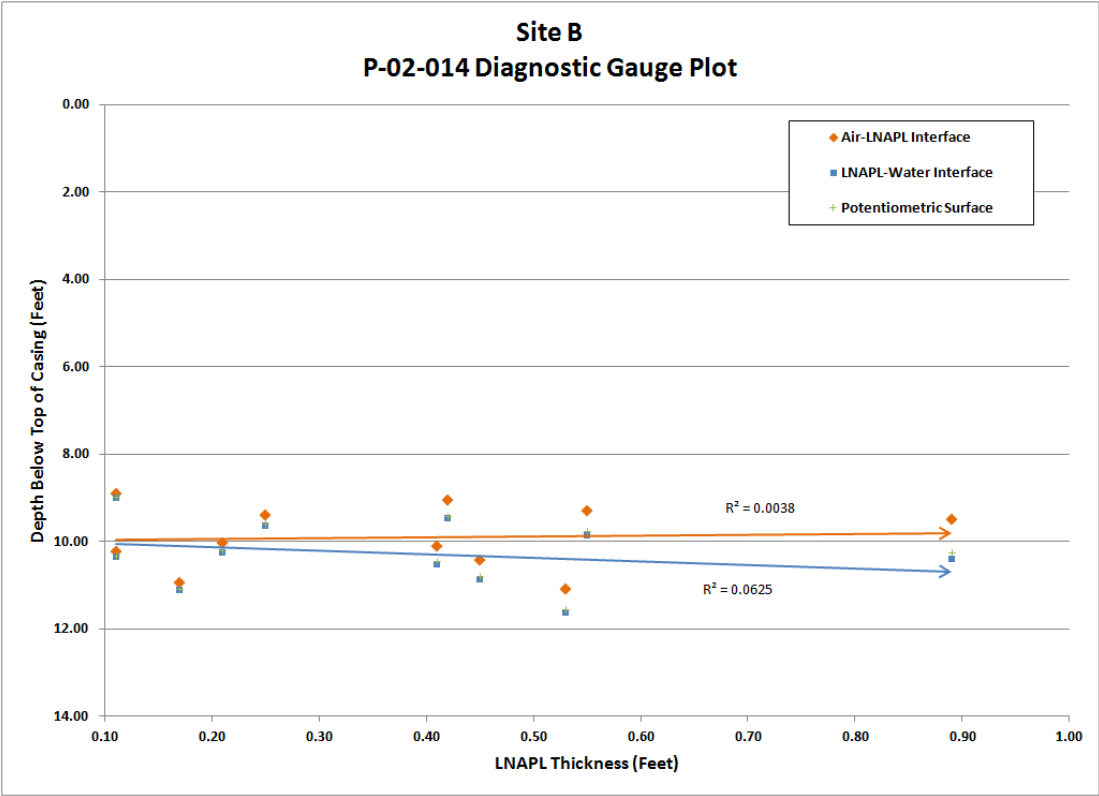
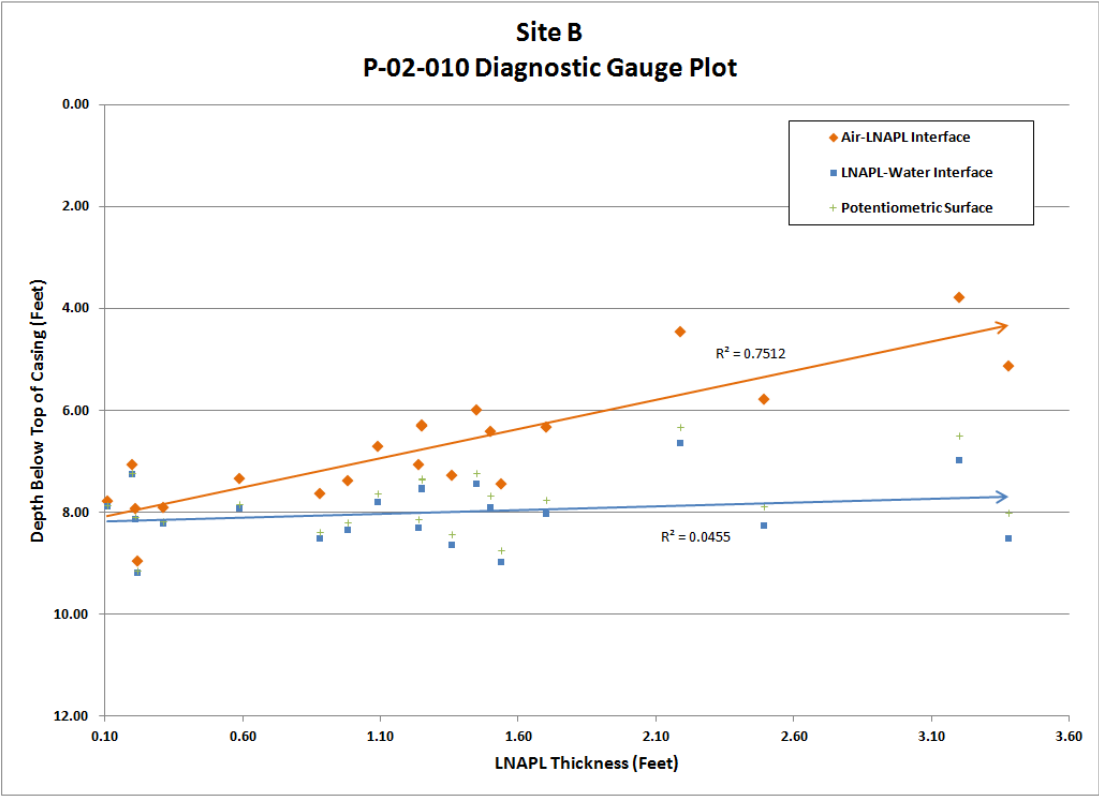


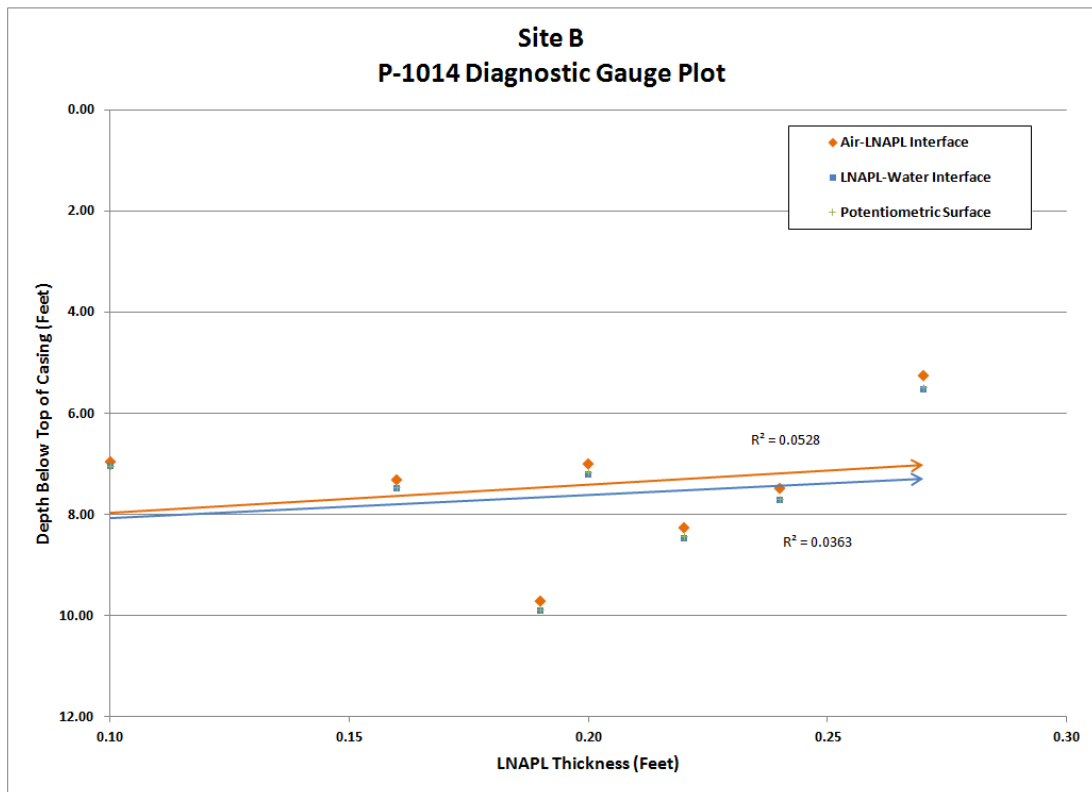
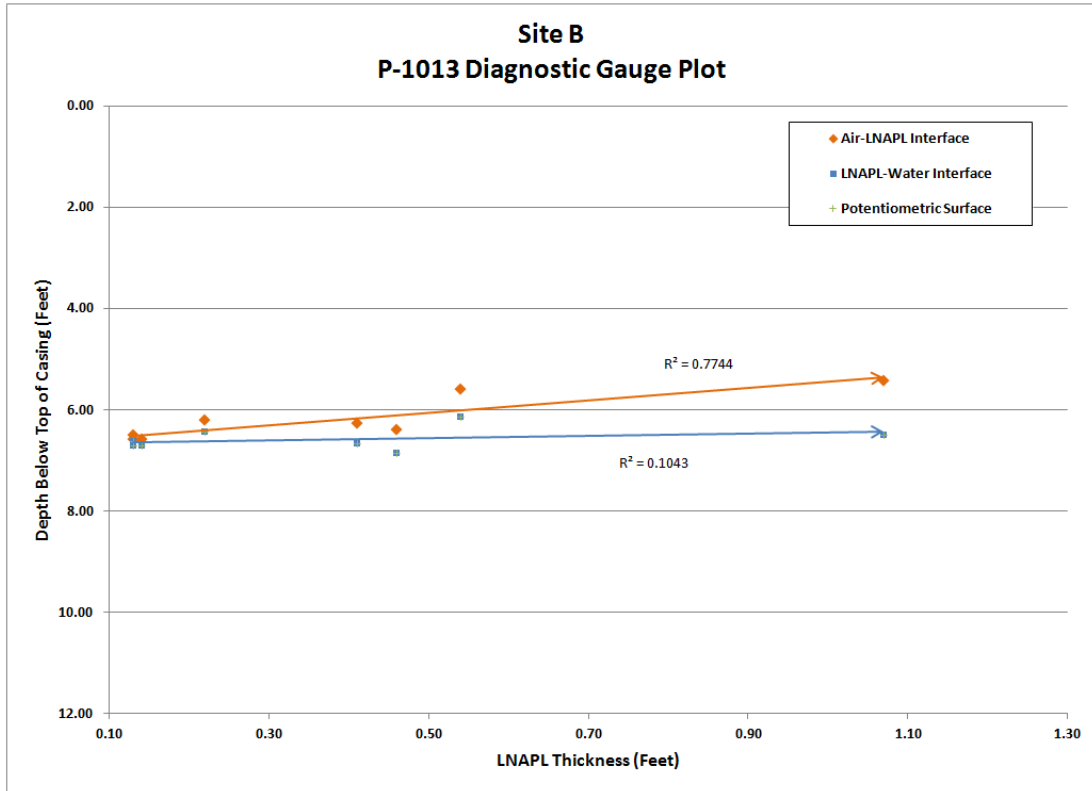


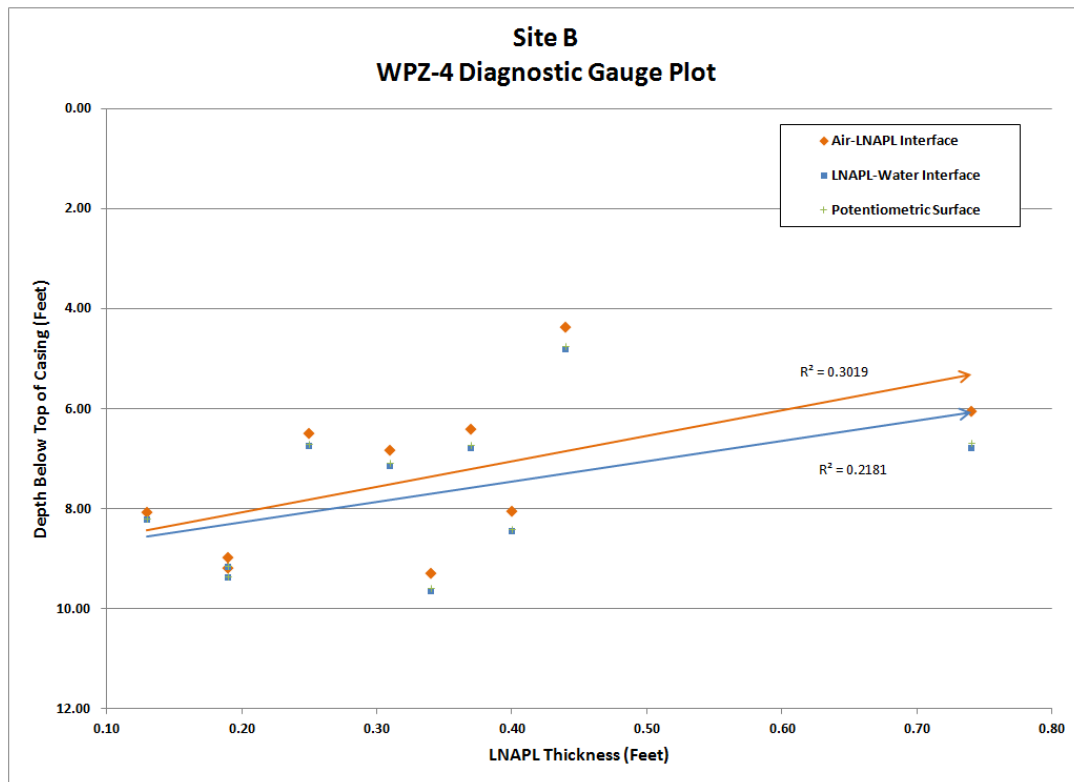
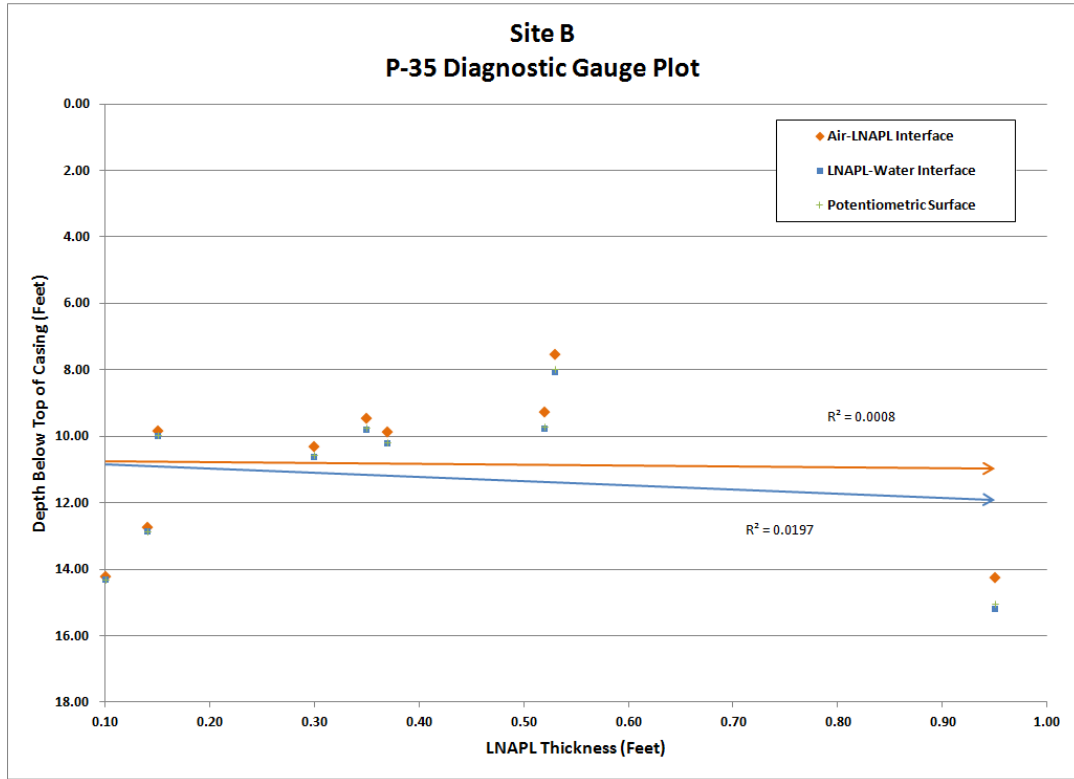


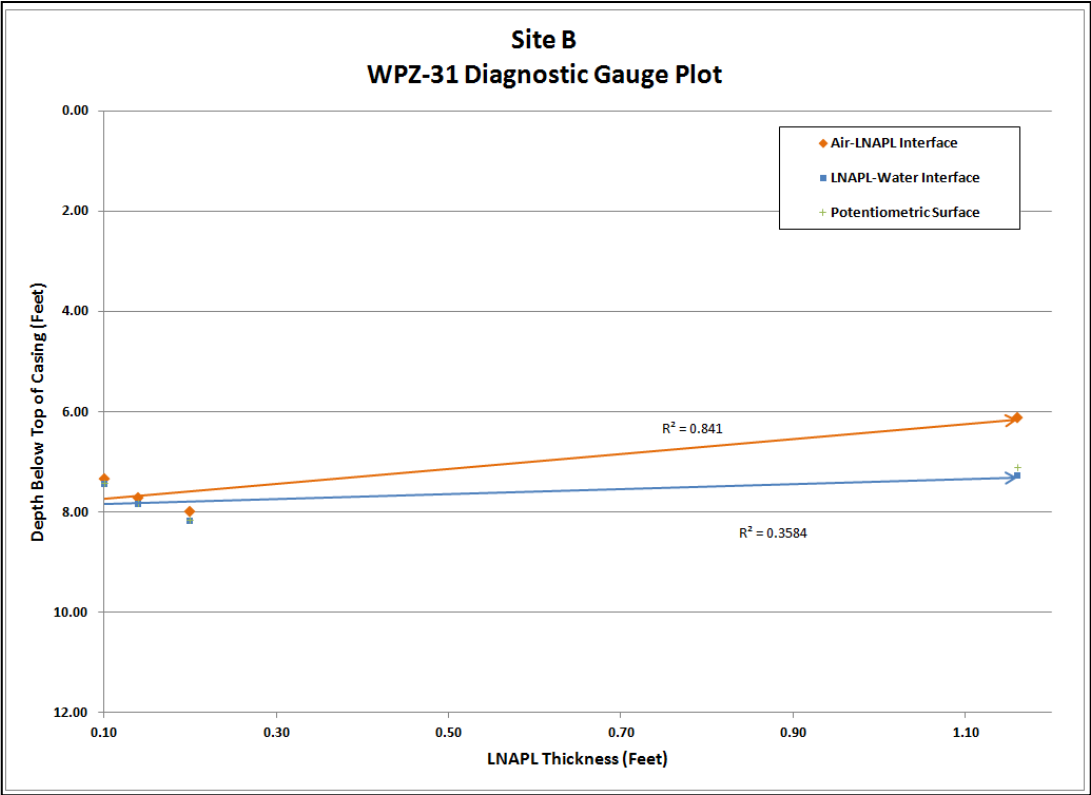




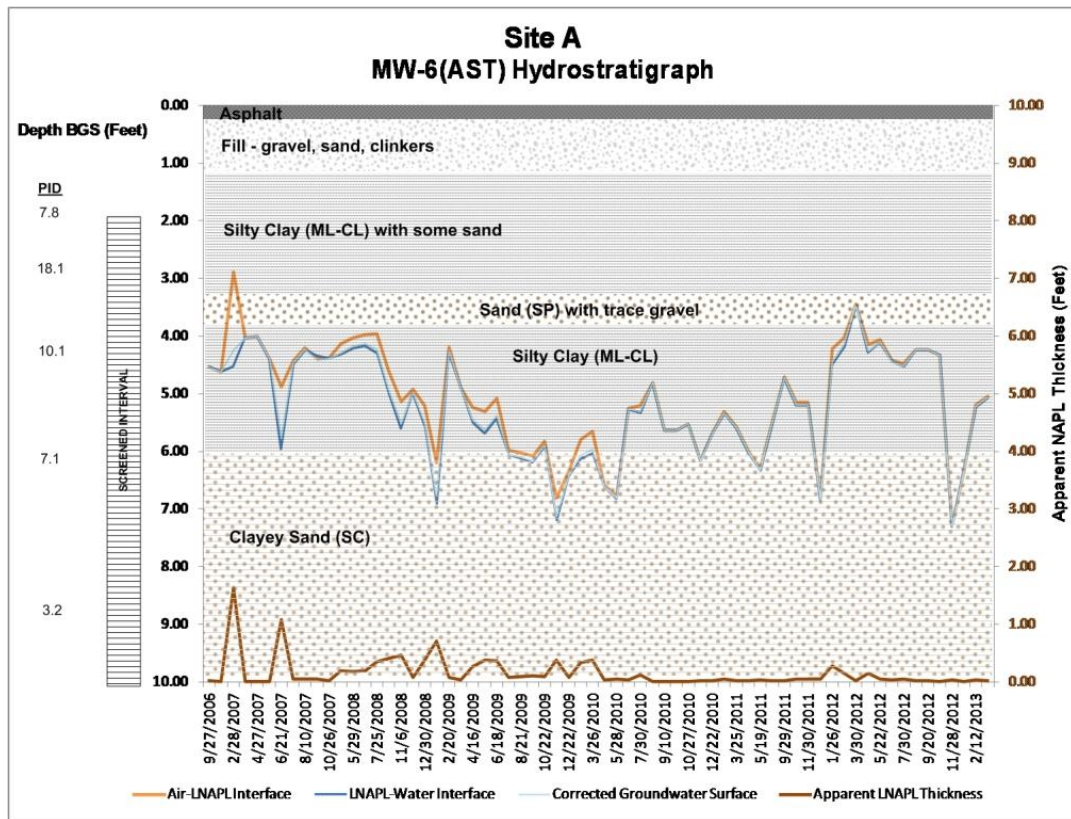
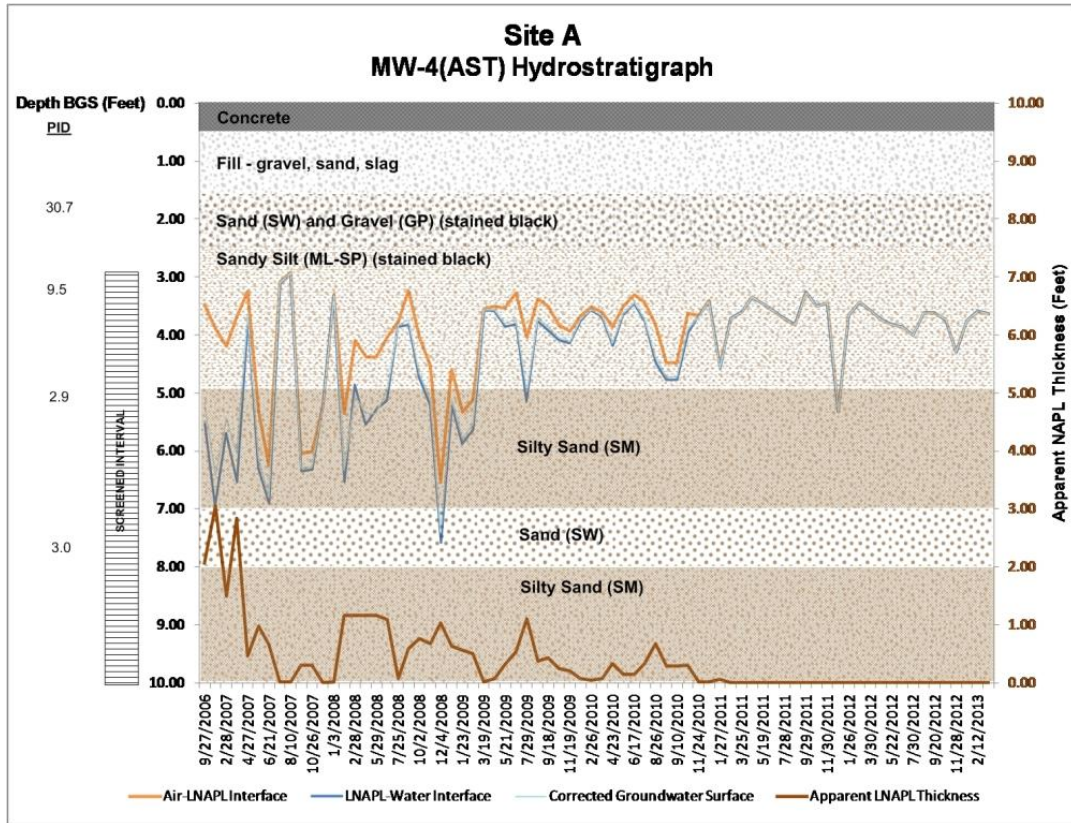


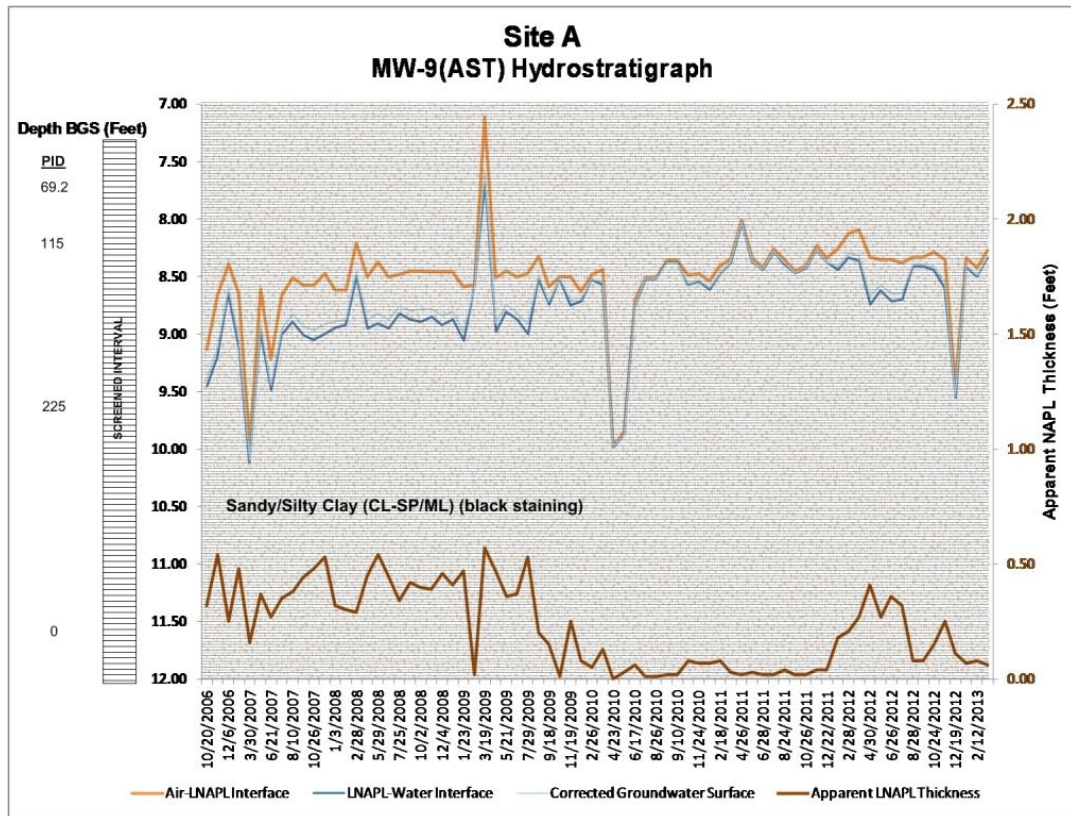
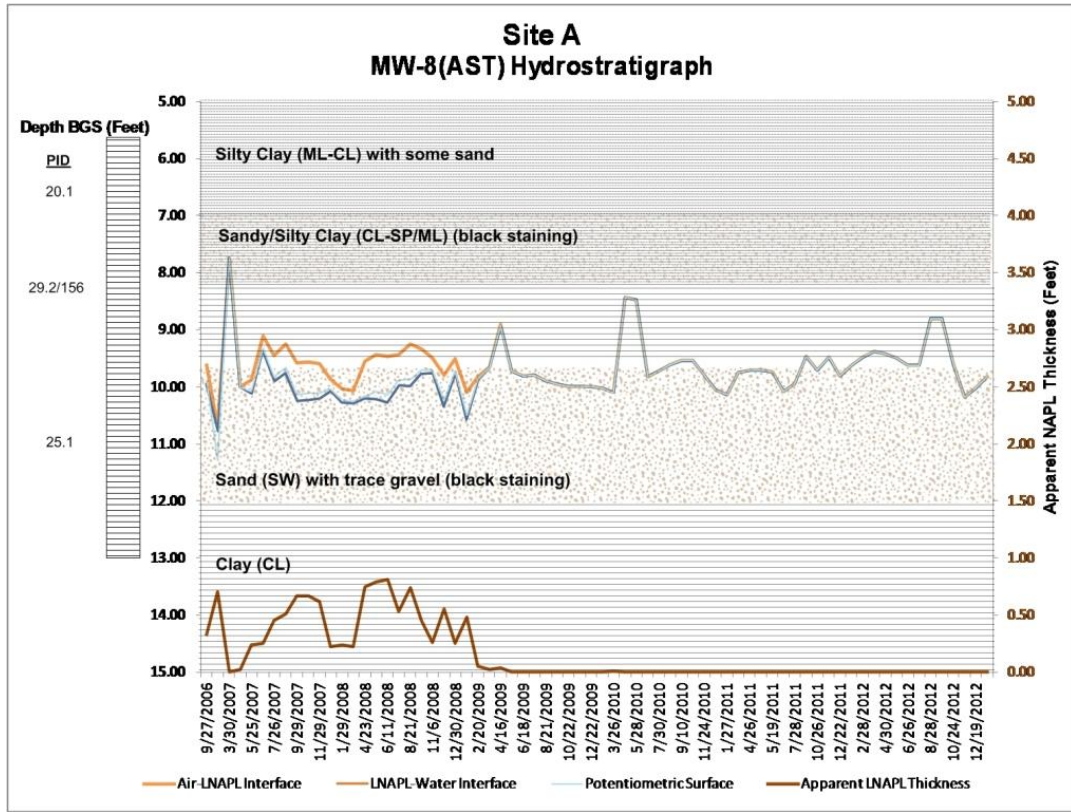


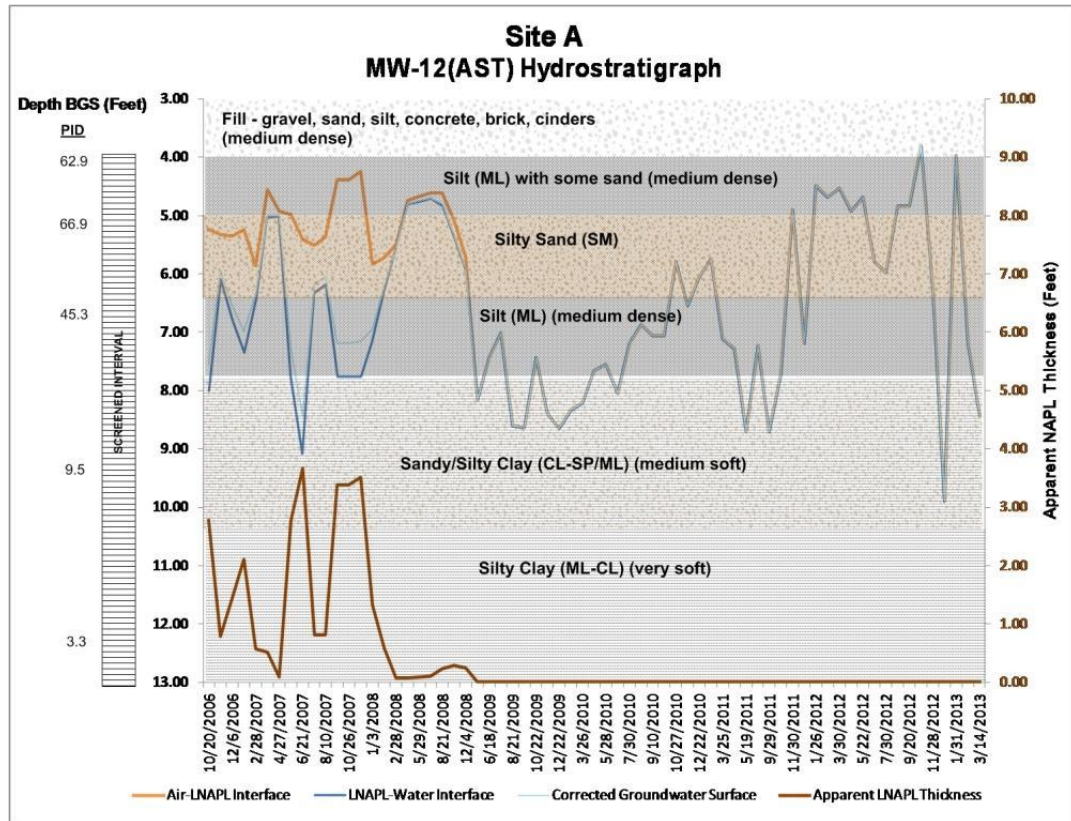
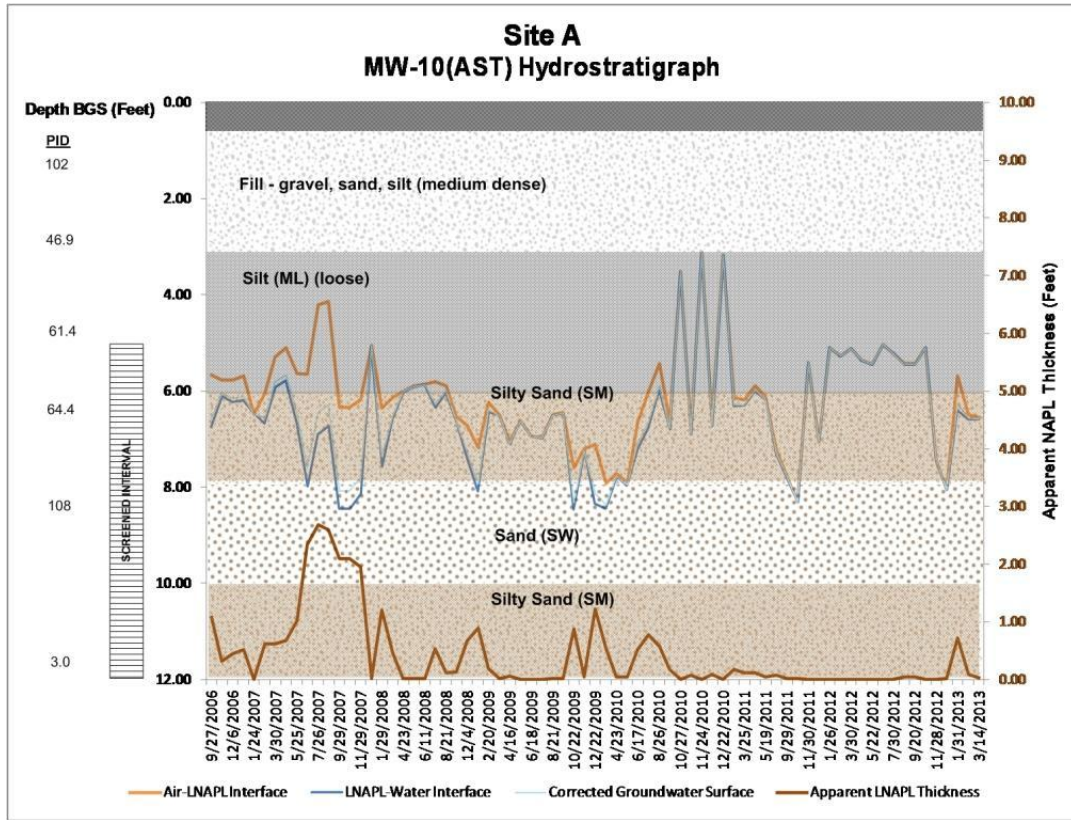


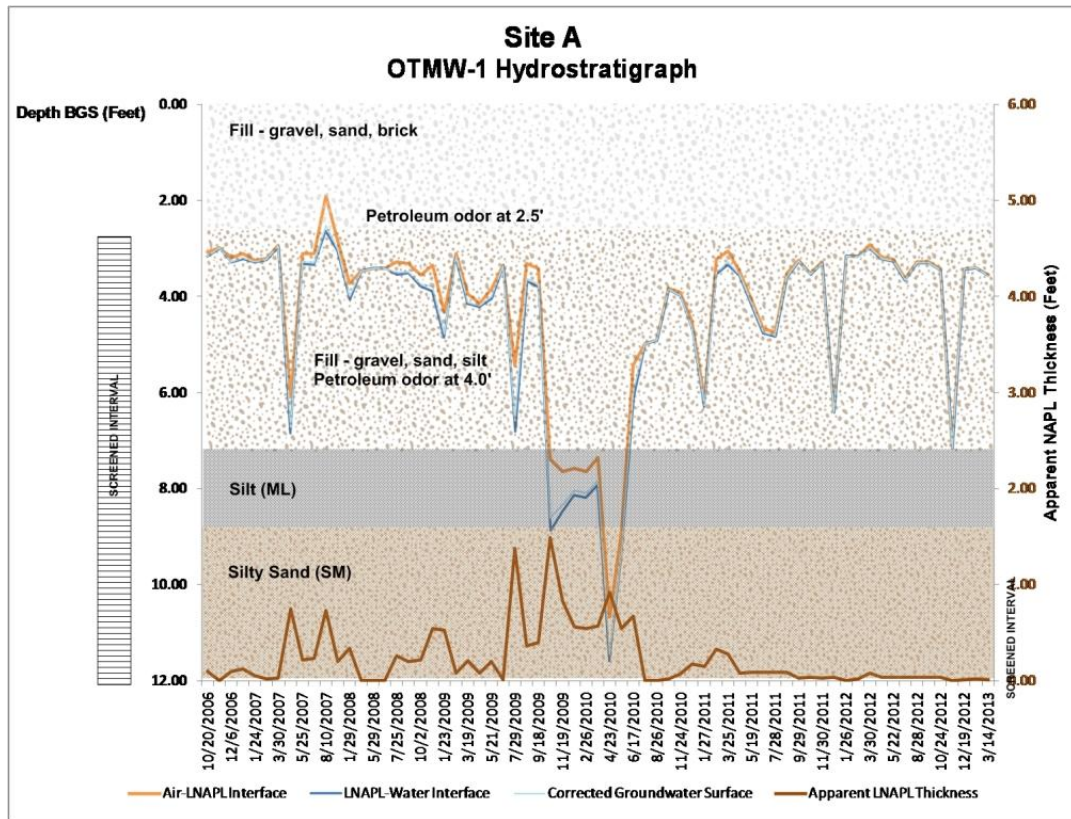
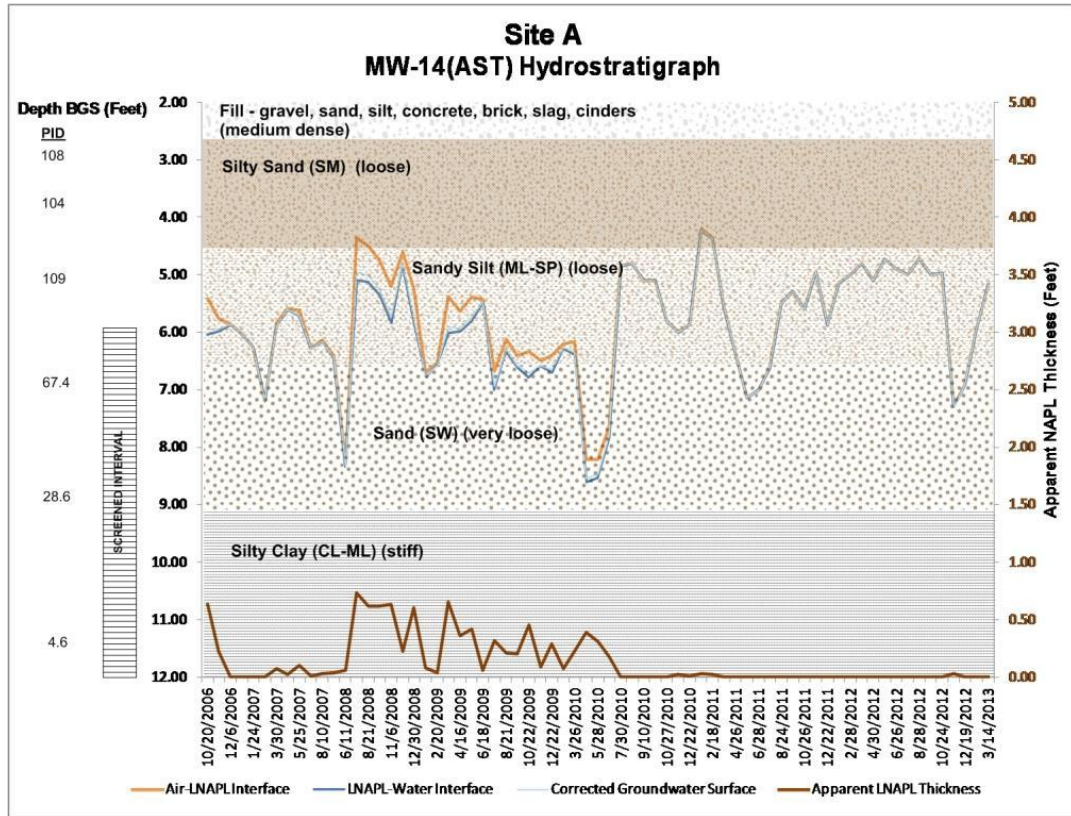


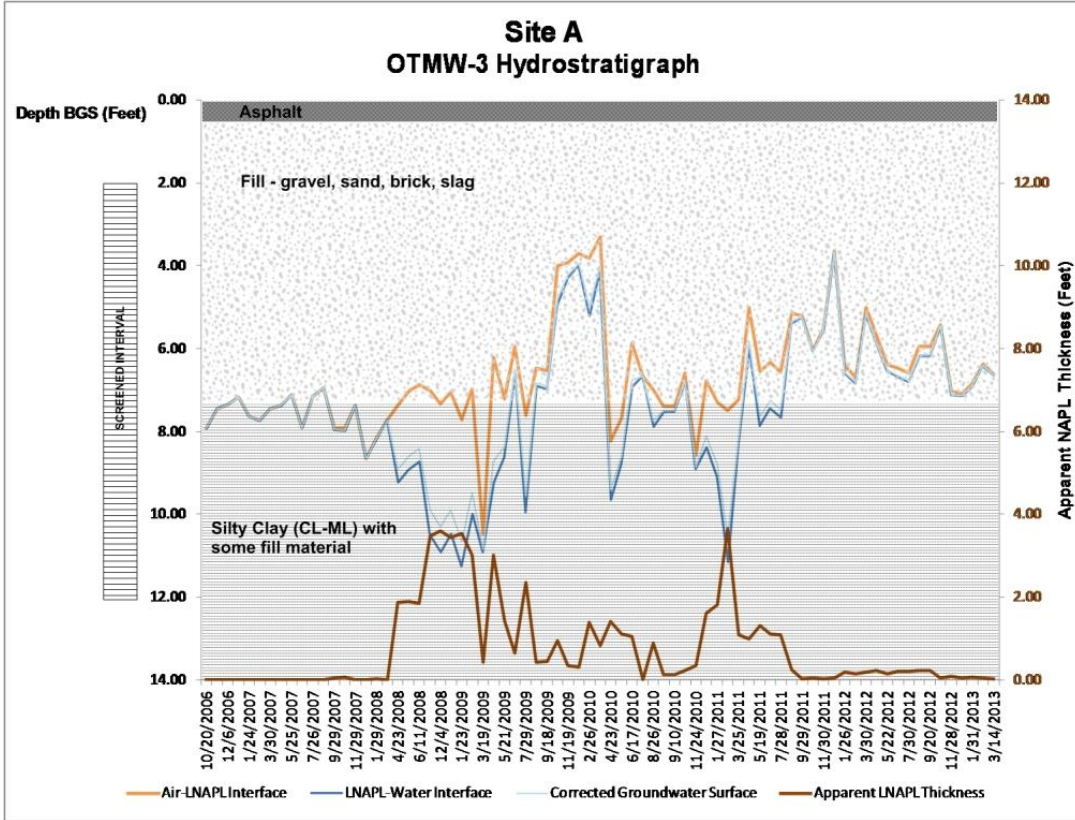
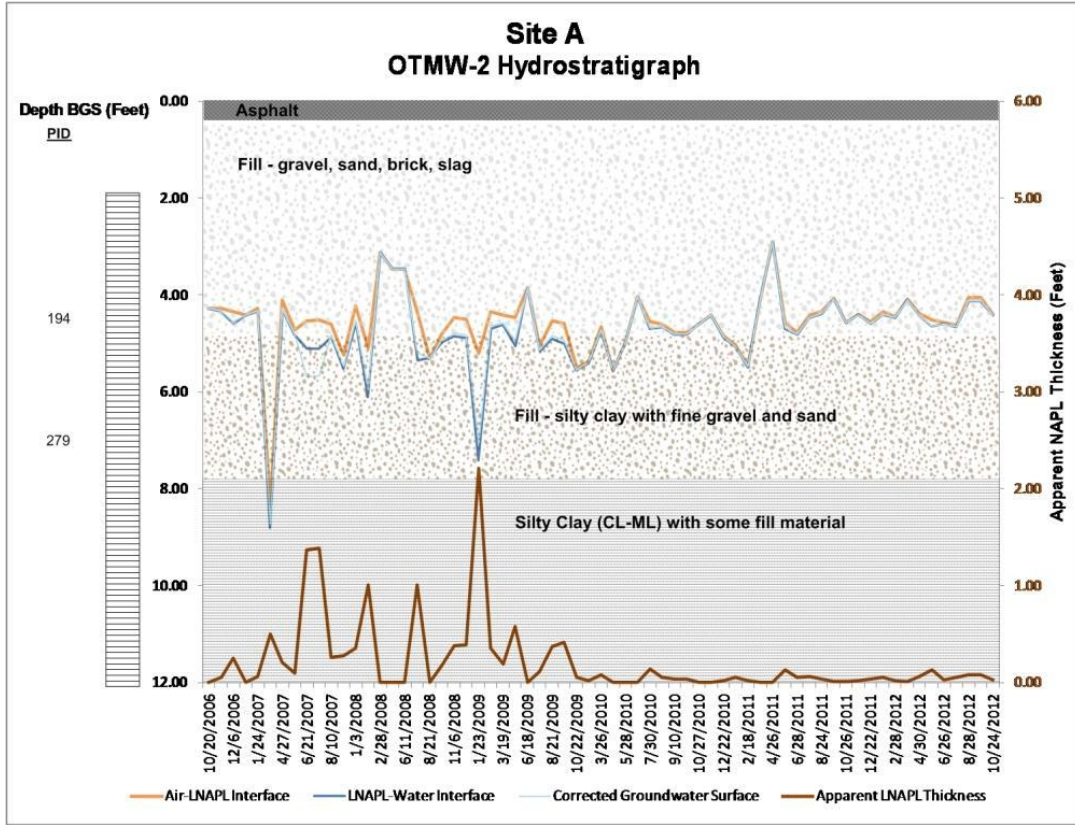
APPENDIX C. HYDROSTRATIGRAPHS



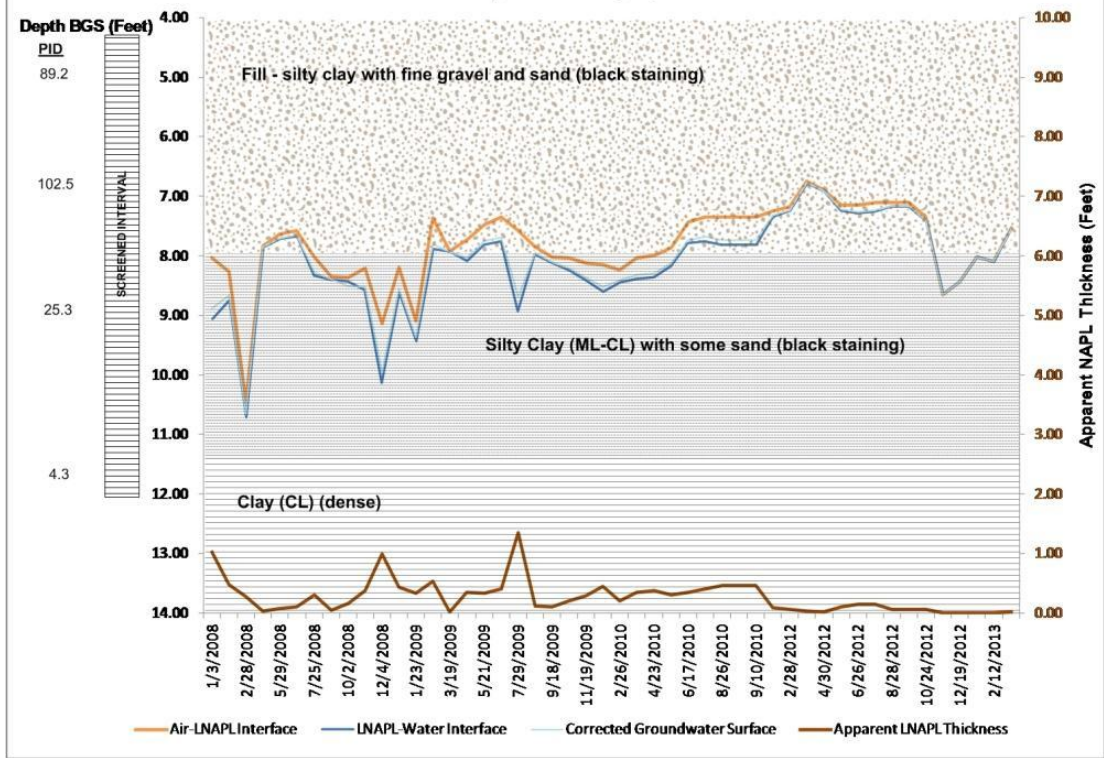


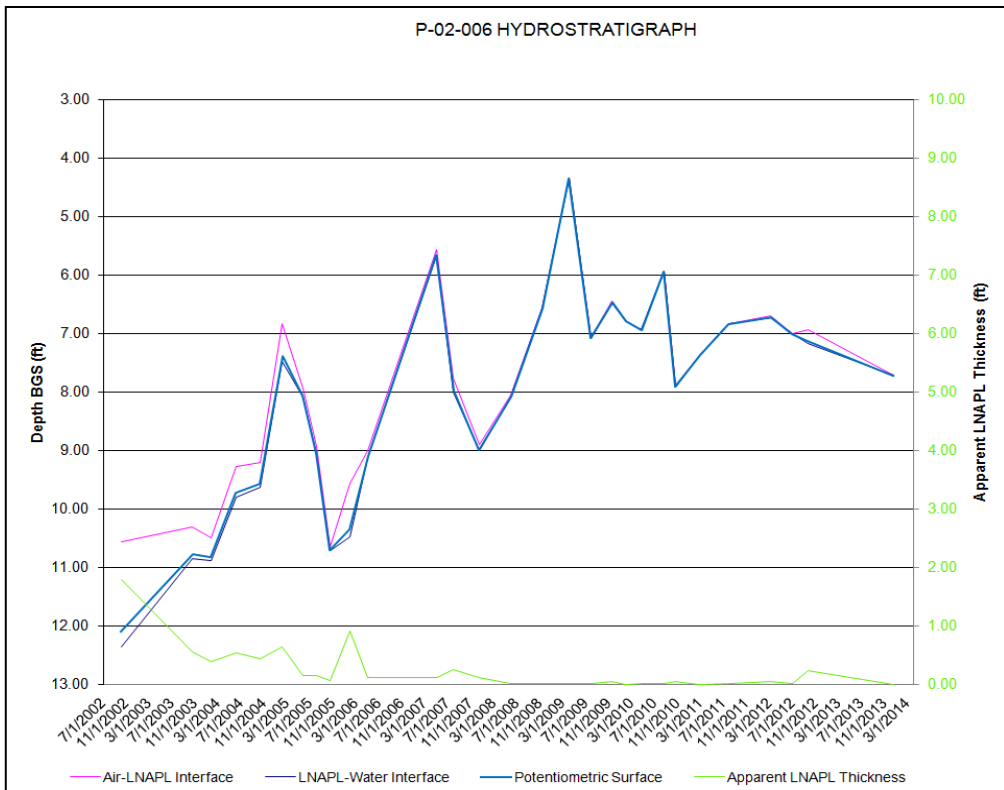
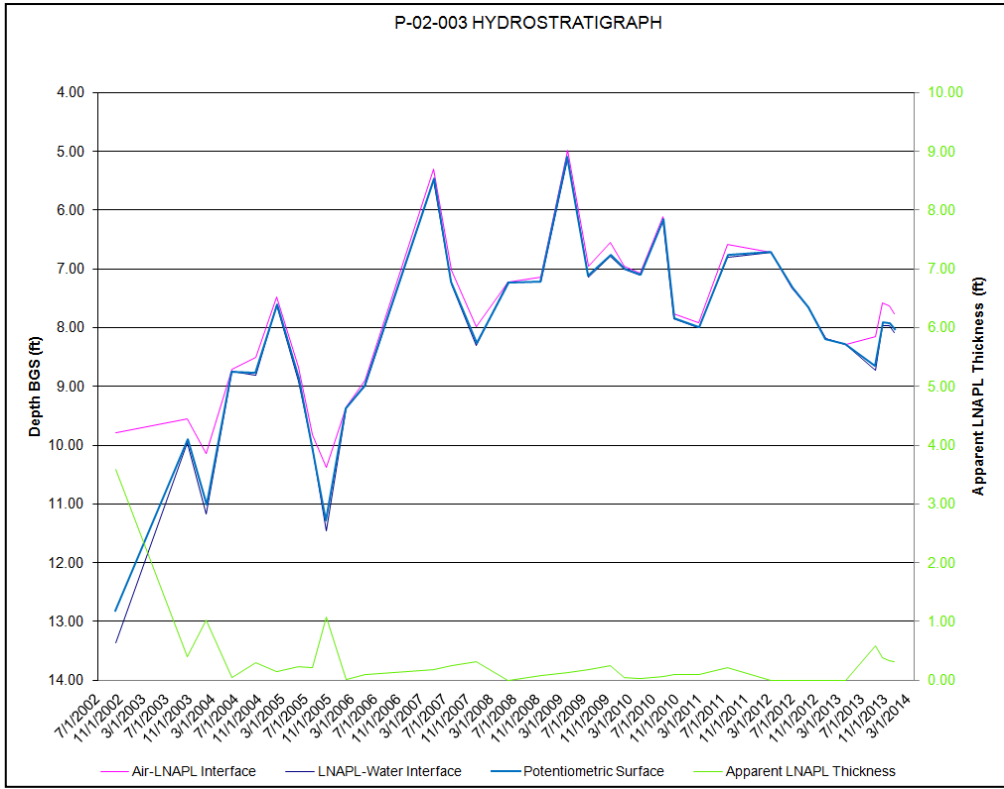


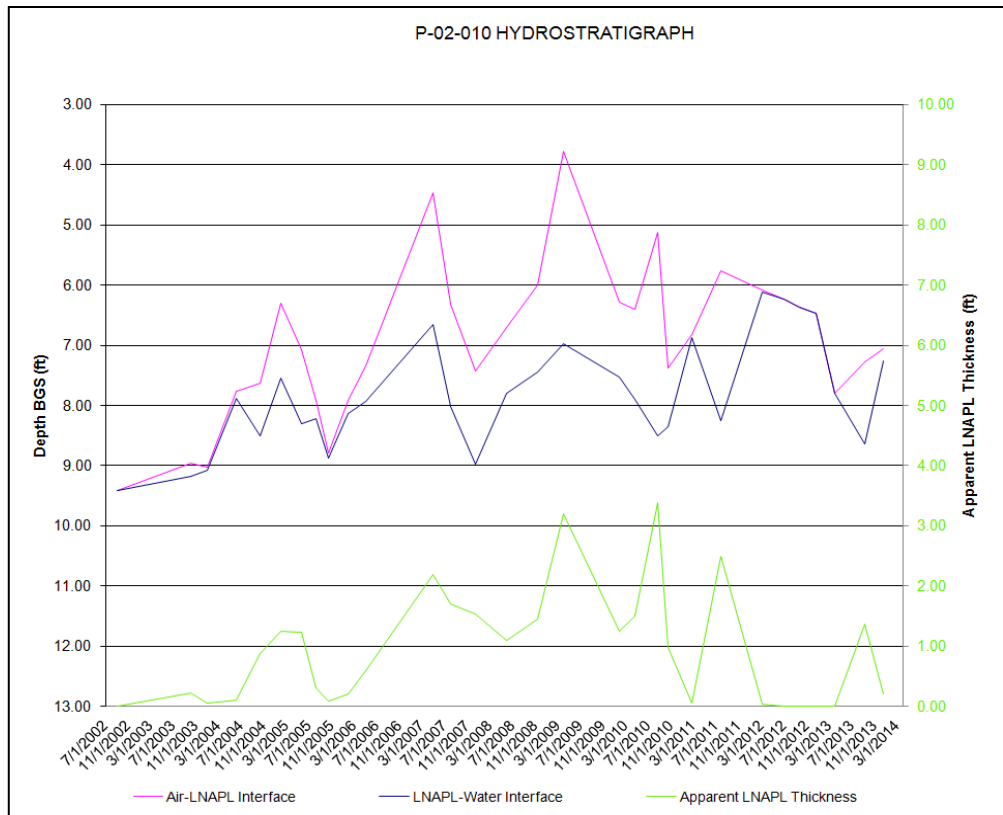
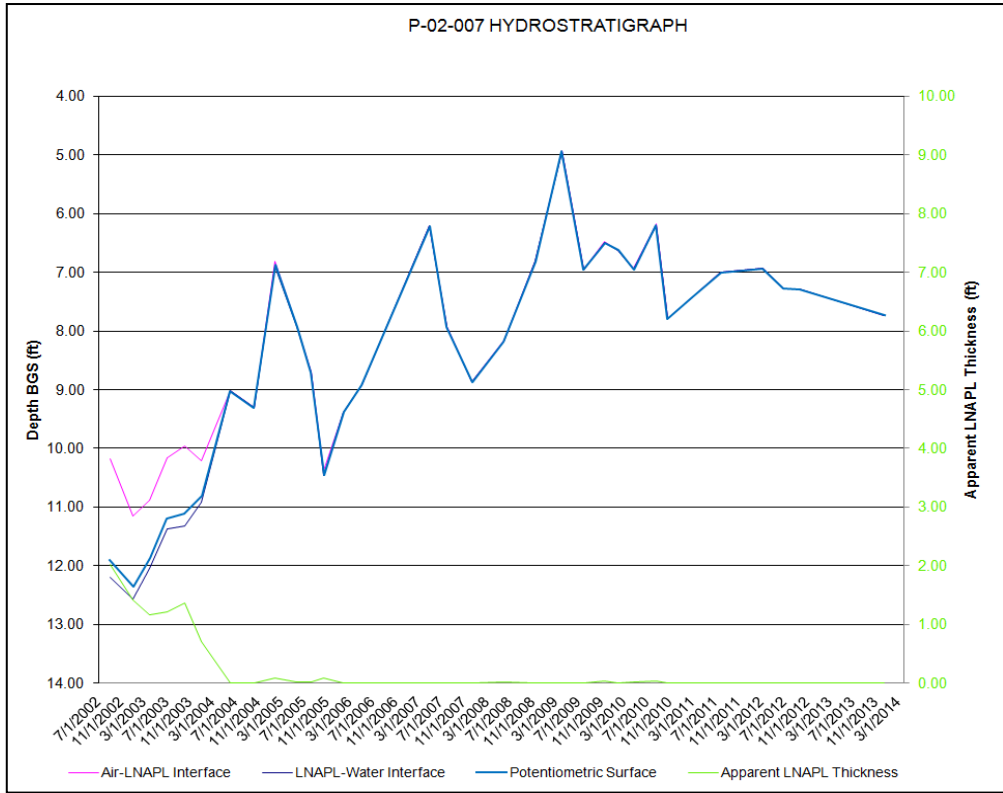


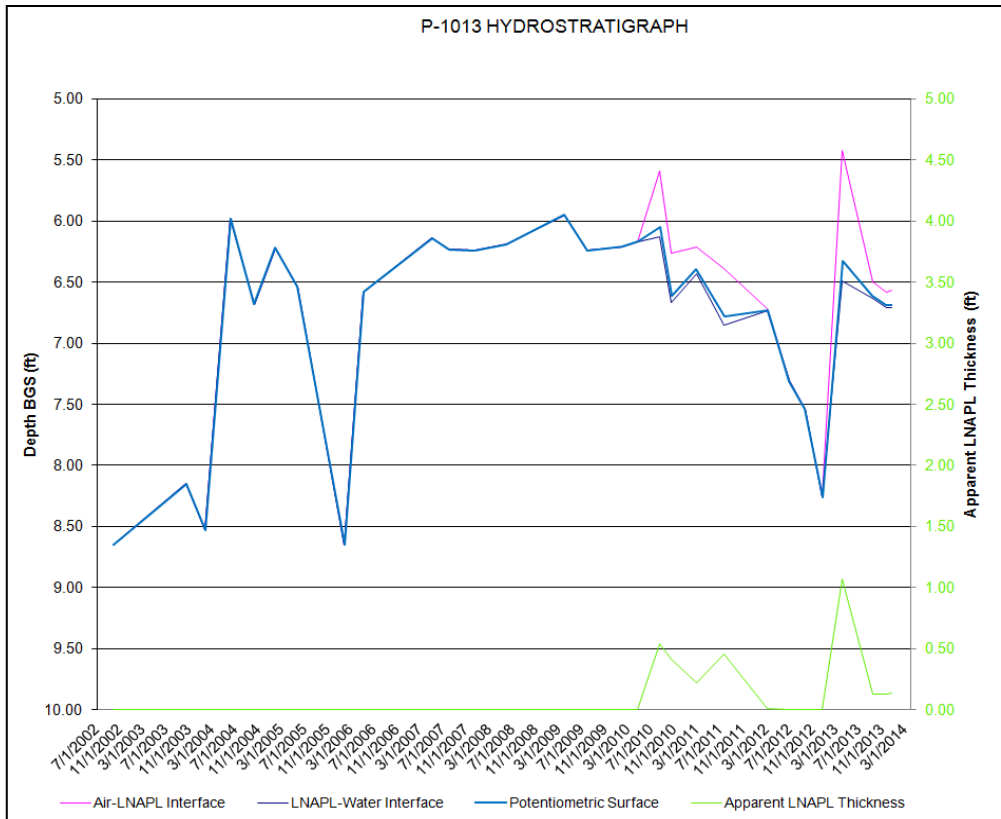
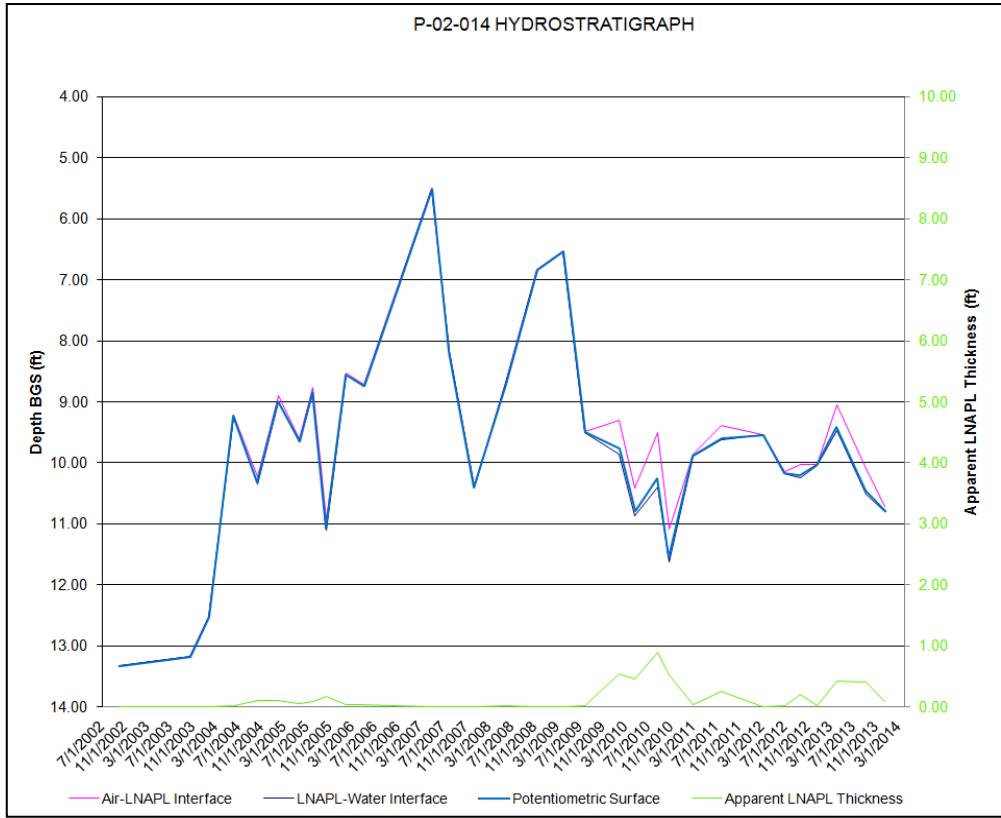


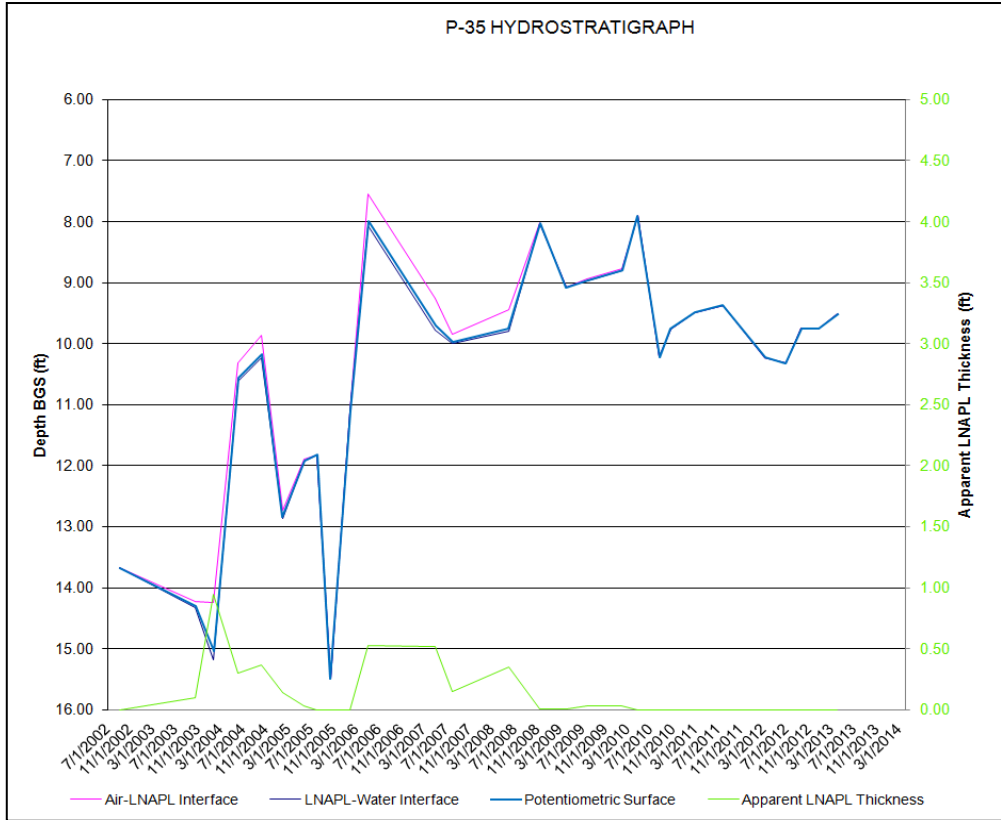
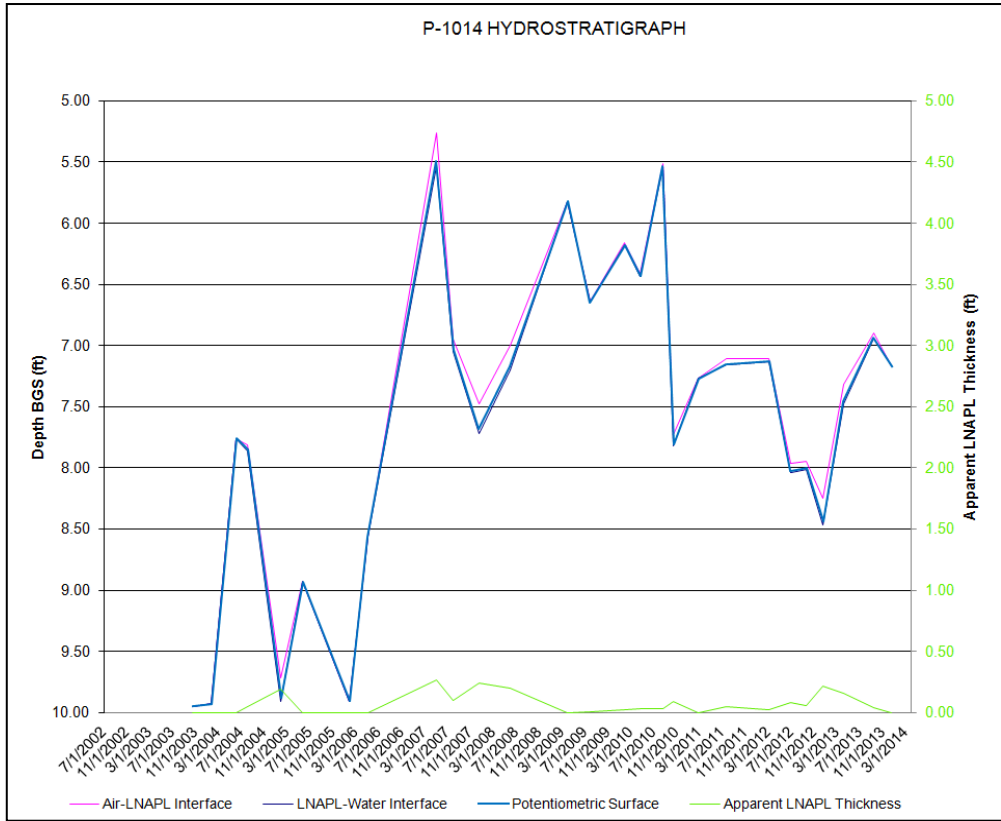
Site A T-1 Hydrostratigraph

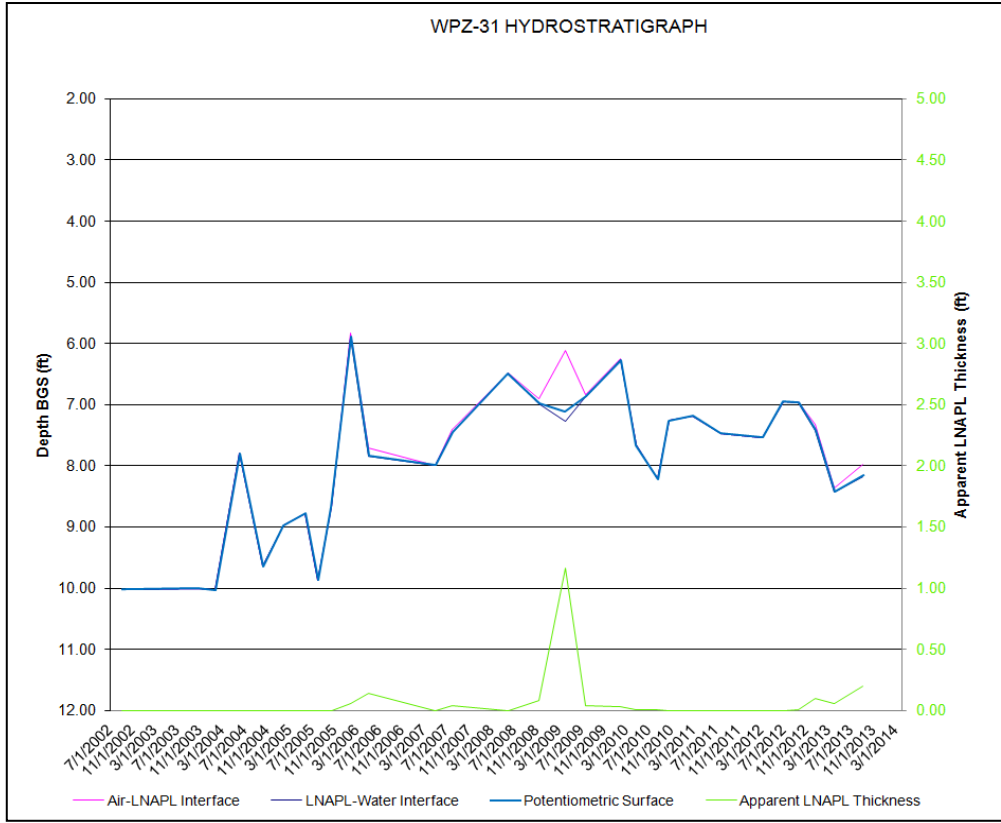
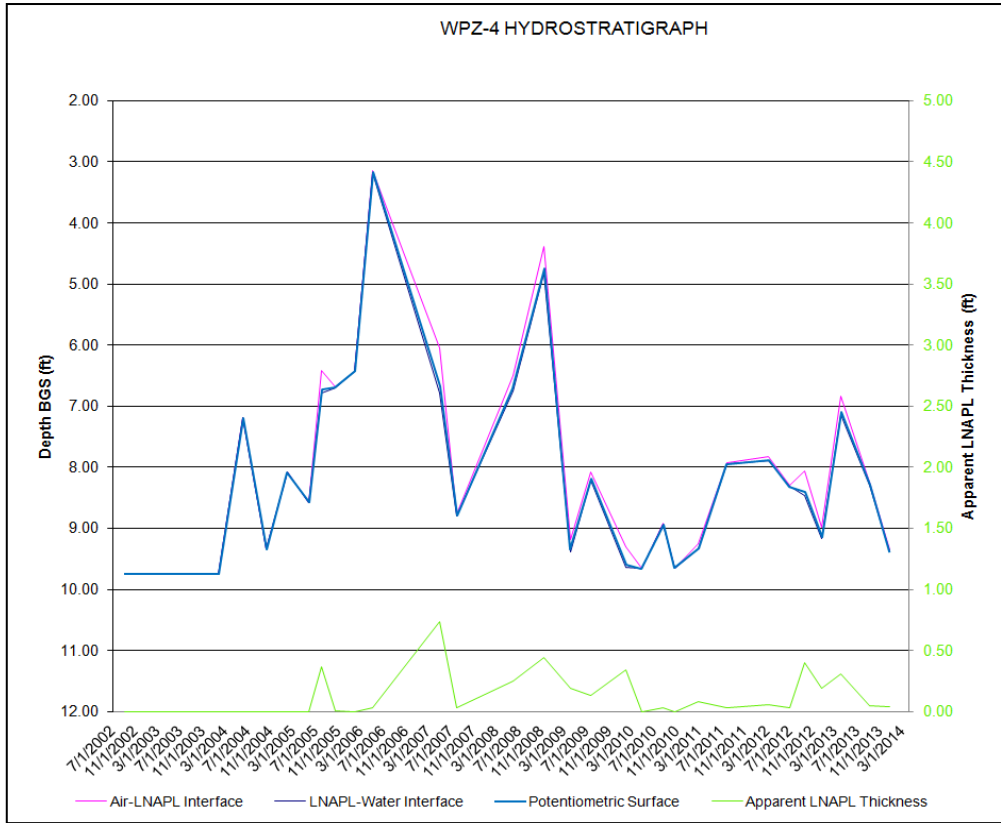






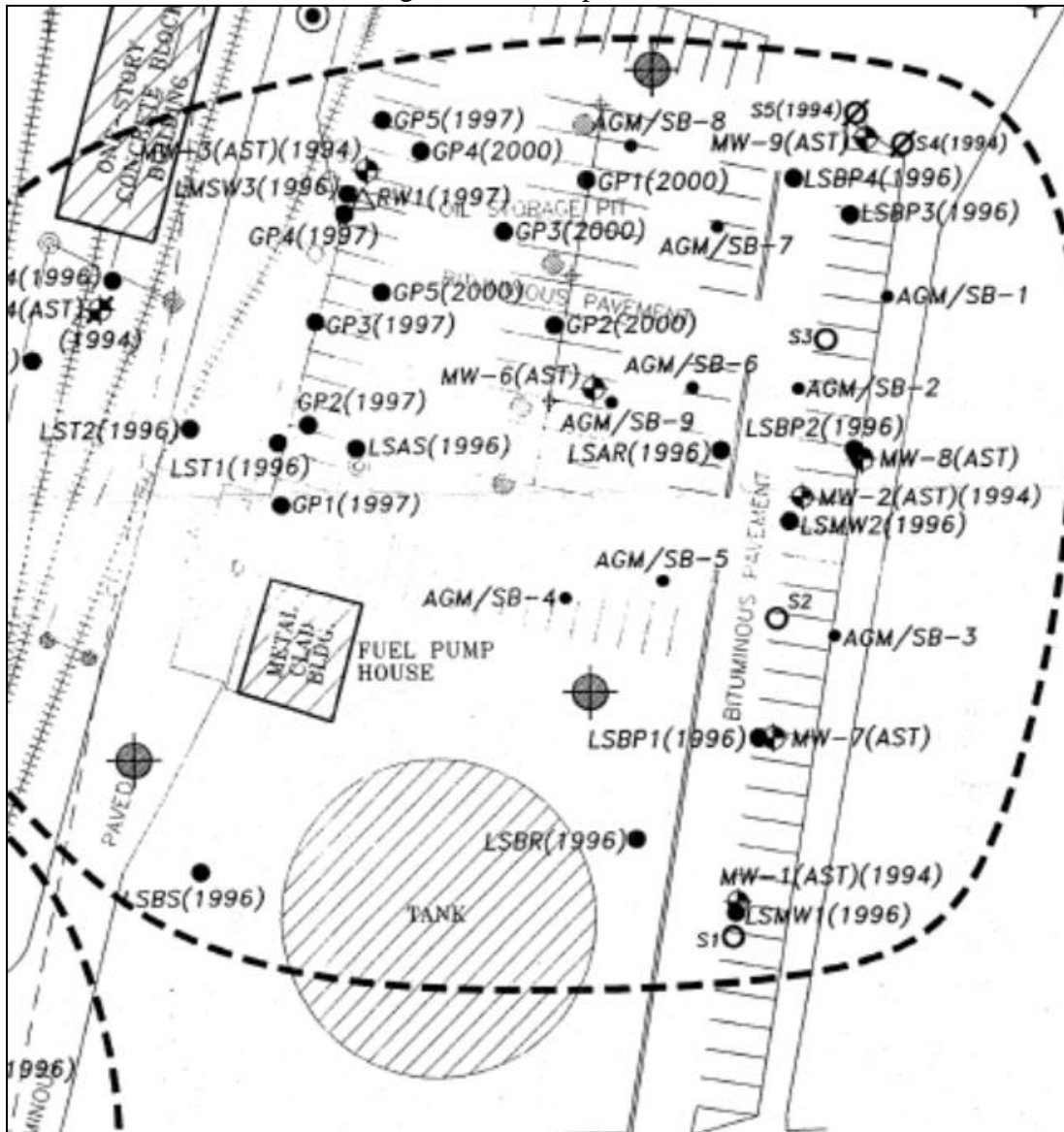






APPENDIX D. SOIL BORING LOGS AND GRAIN-SIZE DATA

FIGURE D.1. Site A Soil Boring Location Map



Boring Log: MW6(AST)

Project Name: _____ Date Started: 12/20/04 Logger: Keith
 Project Number: C1001243.0012 Date Completed: 12/20/04 Editor: Todd

Depth (feet)	Blows (6 in.)	Recovery (Inches)	Sample	PID (PPM)	Graphic Log	Soil Class.	Description
0		36				FILL	Asphalt. Fill, gravel, gray, dry.
				7.8		CL-ML	Silty clay, moist, dark brown, low plasticity.
				18.1		CL-ML	Silty clay, moist, dark brown, low plasticity.
3						SP	Sand, brown, well sorted, moist.
		48		10.1		CL-ML	Silty clay, moist, dark brown, low plasticity.
						CL-ML	Silty clay, moist to wet at 6', dark brown, low plasticity.
6				7.1		SC	Clayey, sand, gray, wet, fine.
		48		6.5		SC	Clayey, sand, gray, wet, fine.
9						SC	Clayey, sand, gray, wet, fine.
				3.2		SC	Clayey, sand, gray, wet, fine.
12		48		2.1		CL	Clay, gray, wet, low plasticity.
				0		CL	Clay, gray, wet, low plasticity.
15							End of boring.
18							

Composite Sample to Lab
 Grab Sample to Lab
 Sample Not Analyzed
 Page 1 of 1

Drilling Co.: Envirodynamics Sampling Method: Continuous
 Driller: Rob Mores Sampling Interval: 2'
 Drilling Method: Direct Push/Dual Tube (1.125" dia.)/Hollow Stem(7"ID) Water Level Start: _____
 Drilling Fluid: _____ Water Level Finish: _____

Project Name: _____ Date Started: 12/20/04 Logger: Keith
Project Number: C1001243.0012 Date Completed: 12/20/04 Editor: Todd

Depth (feet)	Blows (6 in.)	Recovery (inches)	Sample	PID (PPM)	Graphic Log	Soil Class.	Description
0		18				FILL	Asphalt. Fill, gravel, gray, dry.
1.5						CL-ML	Silty clay, dark brown, moist, brittle.
2.5						CL-ML	Silty clay, dark brown with black staining, moist, brittle.
3							
24				13.2		CL-ML	Silty clay, dark brown with black staining, moist, brittle.
6				7.1		CL-ML	Silty clay, dark brown with black staining, moist to wet at 7', brittle.
36				8.5		VC	Silty sandy clay, wet, black staining.
9				8.2		VC	Silty sandy clay, gray, wet, some black staining.
12				2.1		CL	Clay, gray, lean, wet, low plasticity.
15				0.4		CL	Clay, gray, lean, wet, low plasticity.
18							End of boring.

Composite Sample to Lab Grab Sample to Lab Sample Not Analyzed Page 1 of 1

Drilling Co.: Envirodynamics Sampling Method: Continuous
 Driller: Rob Mores Sampling Interval: 2'
 Drilling Method: Direct Push/Dual Tube (1.125" dia./Hollow Stem(7"ID)) Water Level Start: _____
 Drilling Fluid: _____ Water Level Finish: _____

Project Name: _____ Date Started: 12/20/04 Logger: Keith
 Project Number: CI001243.0012 Date Completed: 12/20/04 Editor: Todd

Depth (feet)	Blows (/6 in.)	Recovery (inches)	Sample	PID (PPM)	Graphic Log	Soil Class.	Description
0		6				FILL	Asphalt. Fill, gravel, gray, moist.
3				2.3		FILL	Fill, gravel, gray, moist.
6		30		17.3		CL-ML	Silty clay, gray, wet, low plasticity.
9				20.1		VC	Silty sandy clay, wet, black staining.
12		36		29.2		VC	Silty sandy clay, wet, black staining.
15				25.1		SW	Sand, poorly sorted, medium to coarse, trace gravel, gray, wet, black staining.
18		48		7.9		CL	Clay, gray, wet, low plasticity.
				2.5		CL	Clay, gray, wet, low plasticity.
							End of boring.

Composite Sample to Lab Grab Sample to Lab Sample Not Analyzed Page 1 of 1

Drilling Co.: Envirodynamics Sampling Method: Continuous
 Driller: Rob Mores Sampling Interval: 2'
 Drilling Method: Direct Push/Dual Tube (1.125" dia.)/Hollow Stem(7"ID) Water Level Start: _____
 Drilling Fluid: _____ Water Level Finish: _____

Project Name: _____ Date Started: 12/20/04 Logger: Keith
 Project Number: CI001243.0012 Date Completed: 12/20/04 Editor: Todd

Depth (feet)	Blows (6 in.)	Recovery (inches)	Sample	PID (PPM)	Graphic Log	Soil Class.	Description
0		36				FILL	Asphalt. Fill, gravel, dry.
				2.5		CL-ML	Silty clay with some coarse sand, dark brown, moist.
				13.1		CL-ML	Silty clay with some coarse sand, dark brown, moist.
3							
		48		10.2		SP	Sand, fine, tan, moist to wet at 5'.
6							
				69.2		VC	Silty sandy clay, dark brown, black staining, wet.
		48		115		VC	Silty sandy clay, dark brown, black staining, wet.
9							
				225		VC	Silty sandy clay, dark brown, black staining, wet.
12		48		0		CL	Clay, gray, lean, wet, low plasticity.
				0		CL	Clay, gray, lean, wet, low plasticity.
15							
							End of boring.
18							

Composite Sample to Lab Grab Sample to Lab Sample Not Analyzed Page 1 of 1

Drilling Co.: Envirodynamics Sampling Method: Continuous
 Driller: Rob Mores Sampling Interval: 2'
 Drilling Method: Direct Push/Dual Tube (1.125" dia.)/Hollow Stem(7"ID) Water Level Start: _____
 Drilling Fluid: _____ Water Level Finish: _____

Project Name: _____ Date Started: 12/20/04 Logger: Keith
 Project Number: C1001243.0012 Date Completed: 12/20/04 Editor: Todd

Depth (feet)	Blows (8 in.)	Recovery (inches)	Sample	PID (PPM)	Graphic Log	Soil Class.	Description
0		30		0		FILL	Asphalt. Fill, gravel, gray, dry.
3				0		FILL	Fill, gravel, gray, dry.
6		36		9.0		CL-ML	Silty clay, brown, moist, low plasticity.
9				0.2		CL-ML	Silty clay, brown, moist to wet at 7', low plasticity.
12		36		6.1		CL-ML	Silty clay, brown, wet, low plasticity.
15				25.1			Sandy gravelly clay, wet, black stained.
18		48		10.2		CL	Clay, gray, wet, lean, low plasticity.
21				0		CL	Clay, gray, wet, lean, low plasticity.
24							End of boring.

Composite Sample to Lab Grab Sample to Lab Sample Not Analyzed Page 1 of 1

Drilling Co.: Envirodynamics Sampling Method: Continuous
 Driller: Rob Mores Sampling Interval: 2'
 Drilling Method: Direct Push/Dual Tube (1.125" dia.) Water Level Start: _____
 Drilling Fluid: _____ Water Level Finish: _____

Boring Log: **AGM/SB-2**

Project Name: _____ Date Started: 12/20/04 Logger: Keith
 Project Number: C1001243.0012 Date Completed: 12/20/04 Editor: Todd

Depth (feet)	Blows (6 in.)	Recovery (inches)	Sample	PID (PPM)	Graphic Log	Soil Class.	Description
0		24		0		FILL	Asphalt. Fill, gravel, gray, dry.
3				0		FILL	Fill, gravel, gray, dry.
6		24		4.5		FILL	Fill, clay with some gravel, brown, moist.
9				4.1		FILL	Fill, gravel, gray, moist to wet at 7'.
12		24		15.3		FILL	Fill, gravel, gray, wet.
15				20.1		FILL	Fill, gravel, gray, wet.
18		36		13.1		CL-CH	Clay, gray, wet, low plasticity.
				3.1		CL-CH	Clay, gray, wet, low plasticity.
							End of boring.

Composite Sample to Lab Grab Sample to Lab Sample Not Analyzed Page 1 of 1

Drilling Co.: Envirodynamics Sampling Method: Continuous
 Driller: Rob Mores Sampling Interval: 2'
 Drilling Method: Direct Push/Dual Tube (1.125" dia.) Water Level Start: _____
 Drilling Fluid: _____ Water Level Finish: _____

Project Name: _____ Date Started: 12/21/04 Logger: Keith
 Project Number: CI001243.0012 Date Completed: 12/21/04 Editor: Todd

Depth (feet)	Blows (6 in.)	Recovery (inches)	Sample	PID (PPM)	Graphic Log	Soil Class.	Description
0		36		0		FILL	Asphalt. Fill, gravel, gray, dry.
3				0		FILL	Fill, gravel, gray, dry.
6		30		0		CL	Clay, brown, moist, firm, low plasticity.
9		36		33.2		CL	Clay, brown, wet, firm, low plasticity.
12		36		62.3		CL	Clay, gray with black staining, wet, low plasticity.
15		36		12.2		CL	Clay, gray with less staining, wet, low plasticity.
18				3.4		CL	Clay, gray, wet, low plasticity.
							End of boring.

Composite Sample to Lab Grab Sample to Lab Sample Not Analyzed Page 1 of 1

Drilling Co.: Envirodynamics Sampling Method: Continuous
 Driller: Rob Mores Sampling Interval: 2'
 Drilling Method: Direct Push/Dual Tube (1.125" dia.) Water Level Start: _____
 Drilling Fluid: _____ Water Level Finish: _____

Project Name: _____ Date Started: 12/21/04 Logger: Keith
 Project Number: C1001243.0012 Date Completed: 12/21/04 Editor: Todd

Depth (feet)	Blows (/6 in.)	Recovery (inches)	Sample	PLD (PPM)	Graphic Log	Soil Class.	Description
0		30				FILL	Asphalt.
				10.2		FILL	Fill, gravel, gray, dry.
				24.2		FILL	Fill, coarse sand and gravel, brown, moist.
3						FILL	Fill, coarse sand and gravel, brown, moist.
		36		14.5		CL-ML	Silty clay with some sand, brown, moist to wet at 5'.
6				10.9		CL-ML	Silty clay with some sand, brown, wet.
		48		20.5		CL	Clay, gray, wet, soft.
9				10.1		CL	Clay, gray, wet, soft.
12		36		9.5		CL	Clay, gray, wet, firm.
15				3.1		CL	Clay, gray, wet to moist, firm.
18							End of boring.

Composite Sample to Lab Grab Sample to Lab Sample Not Analyzed Page 1 of 1

Drilling Co.: Envirodynamics Sampling Method: Continuous
 Driller: Rob Mores Sampling Interval: 2'
 Drilling Method: Direct Push/Dual Tube (1.125" dia.) Water Level Start: _____
 Drilling Fluid: _____ Water Level Finish: _____

Project Name: _____ Date Started: 12/21/04 Logger: Keith
Project Number: C1001243.0012 Date Completed: 12/21/04 Editor: Todd

Depth (feet)	Blows (6 in.)	Recovery (Inches)	Sample	PID (PPM)	Graphic Log	Soil Class.	Description
0		18		0		FILL	Asphalt. Fill, gravel, gray, dry.
3				0		FILL	Fill, gravel, gray, dry.
6		36		32.3		VC	Sandy silty clay, brown, moist, some black staining.
						VC	Sandy silty clay, brown, wet, some black staining.
				25.3		VC	Sandy silty clay, brown, wet, some black staining.
9		36		15.3		CL	Clay, gray, firm, wet, low plasticity.
				9.6		CL	Clay, gray, firm, wet, low plasticity.
12		36		3.2		CL	Clay, gray, firm, wet, low plasticity.
				0		CL	Clay, gray, firm, wet to moist, low plasticity.
15							End of boring.
18							

Composite Sample to Lab Grab Sample to Lab Sample Not Analyzed Page 1 of 1

Drilling Co.: Envirodynamics Sampling Method: Continuous
Driller: Rob Mores Sampling Interval: 2'
Drilling Method: Direct Push/Dual Tube (1.125" dia.) Water Level Start: _____
Drilling Fluid: _____ Water Level Finish: _____

Boring Log: AGM/SB-6

Project Name: _____ Date Started: 12/21/04 Logger: Keith
 Project Number: CI001243.0012 Date Completed: 12/21/04 Editor: Todd

Depth (feet)	Blows (/5 in.)	Recovery (inches)	Sample	PID (PPM)	Graphic Log	Soil Class.	Description
0		24				FILL	Asphalt. Fill, gravel, gray, dry.
3				0		FILL	Fill, gravel, gray, dry.
6		48		25.2		CL-ML	Silty clay, dark brown, some black staining, moist.
				49.2		CL-ML	Silty clay, dark brown, some black staining, wet.
				40.1		CL-ML	Silty clay, dark brown/gray with black staining, wet.
9		48		28.1		CL-ML	Silty clay, some sand, gray, soft, wet.
				15.1		CL-ML	Silty clay, some sand, gray, soft, wet.
12		48		0		CL	Clay, gray, firm, wet, low plasticity.
				0		CL	Clay, gray, firm, wet, low plasticity.
15				0		CL	Clay, gray, firm, wet, low plasticity.
18							End of boring.

Composite Sample to Lab Grab Sample to Lab Sample Not Analyzed Page 1 of 1

Drilling Co.: Envirodynamics Sampling Method: Continuous
 Driller: Rob Mores Sampling Interval: 2'
 Drilling Method: Direct Push/Dual Tube (1.125" dia.) Water Level Start: _____
 Drilling Fluid: _____ Water Level Finish: _____

Project Name: _____ Date Started: 12/21/04 Logger: Keith
 Project Number: C1001243.0012 Date Completed: 12/21/04 Editor: Todd

Depth (feet)	Blows (6 in.)	Recovery (inches)	Sample	PID (PPM)	Graphic Log	Soil Class.	Description
0		42				FILL	Asphalt. Fill, gravel, gray, dry.
3				32.5		CL-ML	Silty clay with some sand and gravel, dark brown with some black staining, moist.
		48		89.2		CL-ML	Silty clay, some fine sand, brown/gray with some black staining, wet.
6				102.5		CL-ML	Silty clay, some fine sand, brown/gray with some black staining, wet.
9		48		25.3		VC	Sandy silty clay, brown, wet, soft.
				15.1		VC	Sandy silty clay, brown, wet, soft.
12		48		4.5		CL	Clay, gray, wet, firm, low plasticity.
15				0		CL	Clay, gray, wet, firm, low plasticity.
18							End of boring.

Composite Sample to Lab Grab Sample to Lab Sample Not Analyzed Page 1 of 1

Drilling Co.: Envirodynamics Sampling Method: Continuous
 Driller: Rob Mores Sampling Interval: 2'
 Drilling Method: Direct Push/Dual Tube (1.125" dia.) Water Level Start: _____
 Drilling Fluid: _____ Water Level Finish: _____

Project Name: _____ Date Started: 12/21/04 Logger: Keith
 Project Number: C1001243.0012 Date Completed: 12/21/04 Editor: Todd

Depth (feet)	Blows (6 in.)	Recovery (inches)	Sample	PID (PPM)	Graphic Log	Soil Class.	Description
0		30		0		FILL	Asphalt. Fill, gravel, gray, dry.
3				82.1		CL-ML	Silty clay with some sand and gravel, dark brown with some black staining, moist.
6		30		52.5		VC	Sandy silty clay, dark brown with black staining, wet, soft.
9				32.1		VC	Sandy silty clay, dark brown with black staining, wet, soft.
12		30		15.1		VC	Sandy silty clay, tan, brown, wet.
15				7.2		VC	Sandy silty clay, tan, brown, wet.
18		36		0		CL	Clay, gray, firm, wet, low plasticity.
				0		CL	Clay, gray, firm, wet, low plasticity.
							End of boring.

Composite Sample to Lab Grab Sample to Lab Sample Not Analyzed Page 1 of 1

Drilling Co.: Envirodynamics Sampling Method: Continuous
 Driller: Rob Mores Sampling Interval: 2'
 Drilling Method: Direct Push/Dual Tube (1.125" dia.) Water Level Start: _____
 Drilling Fluid: _____ Water Level Finish: _____

Boring Log: AGM/SB-9

Project Name: _____ Date Started: 12/21/04 Logger: Keith
 Project Number: CI001243.0012 Date Completed: 12/21/04 Editor: Todd

Depth (feet)	Blows (6 in.)	Recovery (inches)	Sample	PID (PPM)	Graphic Log	Soil Class.	Description
0						FILL	Asphalt. Fill, gravel, gray, dry.
3		36					Sample core submitted to lab for geotechnical analysis.
6		36					Sample core submitted to lab for geotechnical analysis.
9							End of boring.
12							
15							
18							

Composite Sample to Lab Grab Sample to Lab Sample Not Analyzed Page 1 of 1

Drilling Co.: Envirodynamics Sampling Method: Continuous
 Driller: Rob Mores Sampling Interval: 2'
 Drilling Method: Direct Push/Dual Tube (1.125" dia.) Water Level Start: _____
 Drilling Fluid: _____ Water Level Finish: _____

FIGURE D.2. Site B Soil Sample Location Map

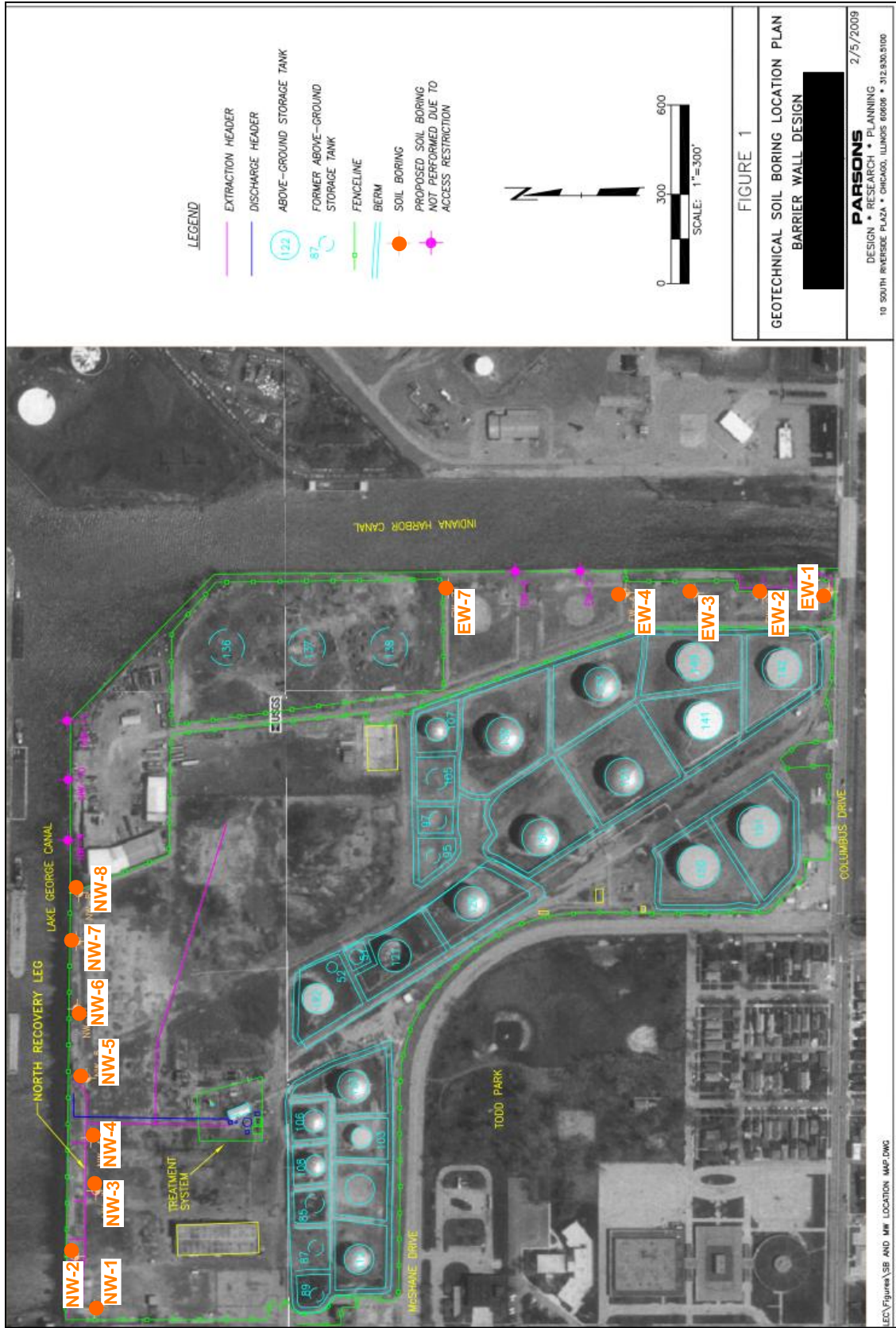


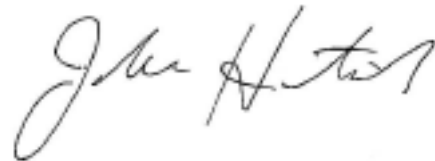
Table D.1. Site B North Remediation Area Soil Characterization and Grain-size Distributions

Sample ID	Sample Depth	USCS		Grain Size Distribution				
		Group Name	Group Symbol	#4	#10	#40	#100	#200
				From / To [ft/ft]	[%]	[%]	[%]	[%]
NW-1 (1-3)	1-3	SAND GRAVELLY	GP	82	70	60	18	7
NW-1 (11-15)	11-15	SILTY SAND	SM	95	92	87	12	8
NW-1 (25-27)	25-27	SILTY SAND	SM	100	100	100	96	24
NW-1 (31-33)	31-33	SILTY CLAY	CL	100	100	98	97	96
NW-2 (1-3)	1-3	SAND GRAVELLY	GP	76	68	60	19	5
NW-2 (11-15)	11-15	SAND	SW	99	98	97	18	8
NW-2 (27-29)	27-29	SAND	SM	99	100	100	93	31
NW-2 (30-31)	30-31	SILTY CLAY	CL	100	100	99	97	96
NW-3 (1-3)	1-3	SAND	SM	79	70	60	46	40
NW-3 (11-15)	11-15	SAND	SW	99	97	92	10	5
NW-3 (27-29)	27-29	SAND	SM	100	100	100	99	47
NW-3 (30-31)	30-31	SILTY CLAY	CL	97	95	94	92	90
NW-4 (1-3)	1-3	SAND	SM	93	90	88	45	12
NW-4 (11-15)	11-15	SAND	SW	99	98	96	12	5
NW-4 (27-29)	27-29	SAND	SM	100	100	100	99	39
NW-4 (32-33)	32-33	SILTY CLAY	CL	99	99	98	96	95
NW-5 (1-3)	1-3	SAND	GP	80	78	73	21	14
NW-5 (11-15)	11-13	SAND	SW	98	95	89	14	5
NW-5 (25-29)	25-29	SILT	SC	100	100	100	98	61
NW-5 (29-31)	29-31	SILTY CLAY	CL	96	95	94	93	92
NW-6 (1-3)	1-3	SAND	SM	99	99	94	50	27
NW-6 (11-13)	11-13	SAND	SW	100	99	98	9	3
NW-6 (29-31)	29-31	SAND	SM	100	100	100	89	40
NW-6 (31-33)	31-33	SILTY CLAY	CL	100	100	100	100	100
NW-7 (1-3)	1-3	SAND	GP	86	80	62	9	4
NW-7 (11-15)	11-15	SAND	SW	100	100	98	10	3
NW-7 (25-29)	25-29	SAND	SM	100	99	99	82	16
NW-7 (32-33)	32-33	SILTY CLAY	CL	98	97	96	94	91
NW-8 (1-3)	1-3	GRAVEL	GS	35	21	10	7	6
NW-8 (13-19)	13-19	SAND	SM	92	91	90	51	37
NW-8 (21-27)	21-27	SAND	SM	100	100	100	87	27
NW-8 (31-33)	31-33	SILTY CLAY	CL	100	100	99	97	97

Table D.2. Site B Southeast Remediation Area Soil Characterization Grain-size Distributions

Sample ID	Sample Depth From / To [ft / ft]	USCS		Grain Size Distribution					
		Group Name	Group Symbol	#4	#10	#40	#100	#200	
				[%]	[%]	[%]	[%]	[%]	
EW-1 (1-3)	1-3	SAND	SW	99	99	98	8	3	
EW-1 (10-15)	10-15	SAND	SW	93	88	81	19	5	
EW-1 (30-32)	30-32	SAND	SW	100	100	100	98	60	
EW-1 (36-37)	36-37	CLAY	CL	99	97	96	93	91	
EW-2 (1-3)	1-3	SAND	SW	99	98	94	20	4	
EW-2 (11-15)	11-15	SAND	SW	100	98	97	21	5	
EW-2 (27-31)	27-31	SAND	SM	99	98	96	94	36	
EW-2 (33-35)	33-35	SILTY CLAY	CL	95	91	87	87	84	
EW-3 (1-3)	1-3	SAND	SW	94	91	85	16	5	
EW-3 (11-15)	11-15	SAND	SW	100	99	97	25	5	
EW-3 (27-29)	27-29	SAND	SM	100	100	100	95	27	
EW-3 (32-33)	32-33	SILTY CLAY	CL	98	97	94	92	87	
EW-4 (1-3)	1-3	SAND	SW	100	100	85	4	3	
EW-4 (9-15)	9-15	SAND	SW	96	93	91	21	7	
EW-4 (29-31)	29-31	SAND	SM	100	100	99	95	38	
EW-4 (33-35)	33-35	SILTY CLAY	CH	100	100	99	96	90	
EW-7 (1-3)	1-3	SAND	SW	100	100	99	22	4	
EW-7 (9-13)	9-13	SAND	SM	99	98	98	43	35	
EW-7 (28.5-31)	28.5-31	SAND	SM	100	100	99	89	39	
EW-7 (31.5-33)	31.5-33	SILTY CLAY	CL	99	99	99	98	97	

I, Jacob M. Hartsock, hereby submit this thesis to Emporia State University as partial fulfillment of the requirements for an advanced degree. I agree that the Library of the University may make it available to use in accordance with its regulations governing materials of this type. I further agree that quoting, photocopying, digitizing or other reproduction of this document is allowed for private study, scholarship (including teaching) and research purposes of a nonprofit nature. No copying which involves potential financial gain will be allowed without written permission of the author. I also agree to permit the Graduate School at Emporia State University to digitize and place this thesis in the ESU institutional repository.



Signature of Author

5/19/2014

Date

Evaluating the Effectiveness of Pre-remedial LNAPL Recovery Modeling using the 'LNAPL Distribution and Recovery Model' at Two Active Remediation Sites

Title of Thesis

Signature of Graduate School Staff

Date Received